CHIRAL HOST/GUEST CATALYSIS: ENANTIOSELECTIVE EPOXIDATION OF UNFUNCTIONALIZED ALKENES

ZENGMIN LI

Chiral Host/Guest Catalysis: Enantioselective Epoxidation of Unfunctionalized Alkenes

by

Zengmin Li

B.Sc. (Hons.), ShanXi University, Taiyuan, China, 1983

M.Sc., Hubei Research Institute of Chemistry, Wuhan, China, 1986

A thesis submitted to the School of Graduate Studies

in partial fulfilment of the requirements for

the degree of Doctor of Philosophy

Department of Chemistry

Memorial University of Newfoundland

August 1999

St. John's Newfoundland

ABSTRACT

Catalytic asymmetric synthesis is the most effective and challenging approach to obtain enantiomerically enriched organic compounds. This research focussed on development of new chiral salen-based macrocyclic catalysts for catalytic asymmetric synthesis, particularly asymmetric epoxidation of unfunctionalized alkenes.

Template-directed reactions of dialdehydes and (*1R,2R*)- or (*1S,2S*)-cyclohexane-1,2-diamine gave three series of macrocyclic salen dimers. A single-crystal X-ray study of the first series, 26-membered macrocycles having $-CH_2-$ links, showed a novel calixarene-like structure with a 1,3-alternate conformation in the solid state. NMR studies revealed that a single conformer was maintained in solution for this series of macrocycles. However, the related 32-membered macrocyclic salen dimer containing longer $-(OCH_2)_2-$ links was flexible and showed four conformers in $CDCl_3$ at room temperature.

Sequentially, controlled complexation of the macrocyclic salen dimers afforded mononuclear (C_1 symmetric) and binuclear (C_2 symmetric) complexes. Host/guest interactions of the mononuclear complexes were demonstrated through ^1H NMR titration experiments. For the binuclear complexes, two cofacial salen units adopted a *syn-* or *anti-*conformation with respect to the cyclohexyl rings relative to a cavity defined by four benzene units. An intramolecular inclusion compound between a binuclear Ni(II)

macrocyclic complex and a non-aromatic guest, acetonitrile, was structurally determined by X-ray diffraction.

Electrocatalytic studies using the rotating ring-disk technique showed that the activity and selectivity of a binuclear calixsalen cobalt complex compared favourably with that of a face-to-face porphyrin catalyst reported by Collman for catalytic reduction of dioxygen at biological pH.

Catalytic epoxidation studies showed that binuclear Mn(III) complexes had moderate enantioselectivity. An ee of 72% was achieved in the epoxidation of styrene at ambient temperature. The new binuclear catalysts were size-selective and both X-ray and MMX modelling studies of a model complex supported the experimental observations. This research provided the first strong experimental evidence for host/guest catalysis in asymmetric epoxidation.

Acknowledgements

Without help from a number of people and organizations, this work would not have been possible.

First and foremost I am deeply grateful to my supervisor, Dr. Chet Jablonski, for his guidance, encouragement, and help. I have learned an enormous amount during my time in Chet's group and his enthusiasm for chemistry has left a deep impression with me. I also greatly appreciate his assistance and patience in the preparation of this thesis.

I would like to express my deep gratefulness to my defence committee members Dr. J. L. Atwood (University of Missouri), Dr. D. J. Burnell, and Dr. C. R. Lucas for their critical and insightful comments on the thesis. It is also a great honour for me to have a chance to discuss my research with them.

Many thanks to Dr. J. N. Bridson and Mr. D. Miller for the excellent X-ray crystallographic work. I also would like to thank my supervisory committee members Dr. R. Helleur and Dr. H. J. Clase for their comments regarding this thesis.

Much credit goes to Dr. P. Georghiou for kindly providing his HPLC and a sample of compound **11** in Chapter 2, Dr. M. L'Her (Université de Bretagne Occidentale, France) for electrochemistry experiments, Dr. M. McGlinchey (McMaster University) for 500

MHZ NMR. Dr. J. F. Britten (McMaster University) for low temperature CCD X-ray data. Dr. J. Chen (University of Waterloo) for ESMS analysis. Dr. B. Gregory and Ms. M. Baggs for MS analysis. and Mr. G. Bao (Dr. D. J. Burnell graduate student) for GC-MS data. Thanks also are extended to the faculty and staff of the Department of Chemistry as well as to my labmates for their support.

I extend my appreciation to SepraChem Canada Ltd. for generous donation of several chiral compounds. I am greatly indebted to Memorial University of Newfoundland for financial support.

Finally, I would like to thank my wife for all the years of support and sacrifice. and my son for allowing me being in the lab for many of the nights over the years.

To my wife Jihong Su

our parents

and of course our son Suqing

Table of Contents

List of Tables

List of Figures

List of Schemes

List of Abbreviations

AcAc	acetylacetonate
Anal.	analysed
aq	aqueous
BINAP	[2.2'-bis(diphenylphosphino)-1.1'-binaphthyl]
br	broad
°C	degrees (Celsius)
Calcd.	calculated
Cat.	catalyst
cm	centimetres
δ	chemical shift in parts per million
COSY	$^1H/^1H$ 2D correlation spectroscopy
CPK	Cory-Pauling-Koltun
d	doublet
dec.	decomposed
DET	(+) or (-)-diethyl tartrate
DMF	*N,N*-dimethylformamide
DMSO	dimethylsulfoxide
ee	enantiomeric excess
EPGE	edge-plane graphite electrode

equiv.	equivalent
ESMS	electron spray mass spectrum
FTF	face-to-face porphyrin
g	gram
GC-MS	gas chromatography-mass spectrometer
h	hour
HETCOR	^{1}H-^{13}C ^{1}J heterocorrelation
HOMO	highest occupied molecular orbital
HPLC	high performance liquid chromatography
Hz	hertz
I_d	disk current
i-Pr	isopropyl
I_r	ring current
IR	infrared
LUMO	lowest unoccupied molecular orbital
LAC	ligand acceleration catalysis
m	multiplet
*m*CPBA	*m*-chloroperoxybenzoic acid
Me	methyl
mL	millilitre
mp	melting point

NHE	normal hydrogen electrode
oxone	potassium peroxymonosulfate
OAc	acetate
Ph	phenyl
PhIO	iodosylbenzene
rpm	revolution per minute
RT	room temperature
s	singlet
SCE	saturated calomel electrode
t	triplet
TBHP	*tert*-butylhydroperoxide
t-Bu	*tert*-butyl
THF	tetrahydrofuran
TLC	thin layer chromatography
VT	variable temperature
R*, L*	optically active group or ligand

Chapter 1

Asymmetric Induction in Enantioselective Epoxidation

1.1 Introduction

1.1.1 Molecular chirality

Nature provides many examples of asymmetry. For instance, the shells of snails of the same species all spiral the same way. Climbing plants like honeysuckle and bindweed corkscrew around their vertical supports in one direction only. This kind of "handedness" is called chirality and is more fundamental than twirling garden plants in that chirality is directly related to the very molecules of life such as DNA, amino acids, and sugars.

Molecules are three-dimensional objects. If there are four different chemical groups attached to a tetrahedral central atom such as C, N, P, Si, or a metal in a molecule, then two and only two spatial arrangements, which are mirror images of each other (Figure 1.1), will be possible.[1] Like our right and left hands, it is impossible to

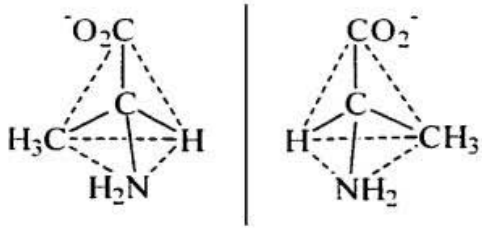

Figure 1.1 Optical isomers of alanine

overlay the two mirror image tetra-substituted tetrahedral carbons. They cannot be interconverted unless bonds are broken and reformed since the energy barrier to inversion via a planar intermediate would be too high.

The criteria which define molecular chirality are based on group theory. A molecule is chiral if it does not have any improper axis (S_n) of symmetry.[1,2,3] A chiral molecule may belong to any of the C_n, D_n, T, O or I point groups. Chiral molecules within the C_1 group are termed asymmetric, within C_n (n>1) are dissymmetric, within D_n are dihedral symmetric, and within T, O, I are polyhedral symmetric.

The first class[2] of chiral molecules contains at least one atom bound to four different substituents in a tetrahedral fashion with C_1 symmetry (Figure 1.2) such as glyceraldehyde **1**: phosphine oxide **2**: the organometallic complex **3**: and the cluster compound **4**. Other molecules lacking any symmetry elements are the Werner complex **5**: the ferrocene derivative **6**: and the biphenyl **7** whose chirality is due to restricted rotation about the Ph-Ph single bond. Restricted rotation is also responsible for the chirality of many molecules with C_2 symmetry like binaphtyl **8** and spirane **9**. Chiral molecules with C_3 or higher symmetry elements are scarce. One example is the bridged biphenyl **10** with D_3 symmetry which owes its chirality to restricted motion. Example **11**, another Werner complex, is chiral with D_3 symmetry.

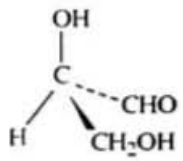

1

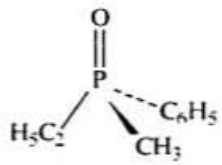

2

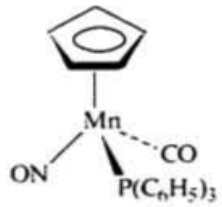

3

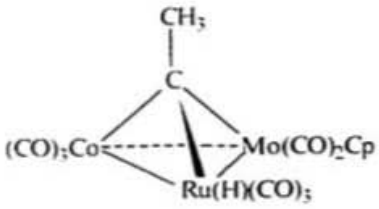

4

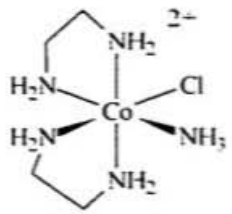

5

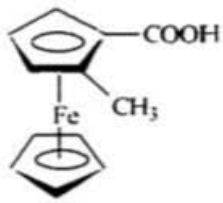

6

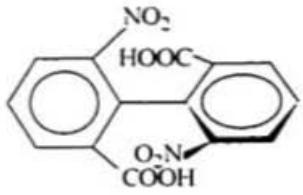

7

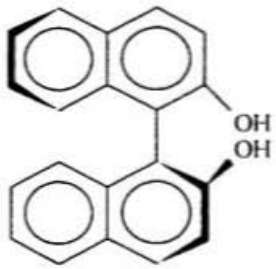

8

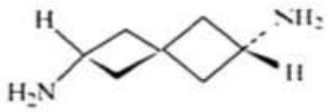

9

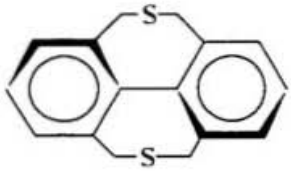

10

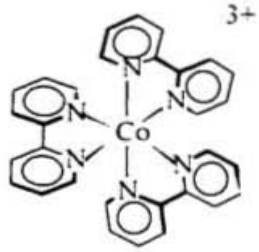

11

Figure 1.2 Examples of chiral molecules with C_n or D_n symmetry

For mobile molecules, if transient conformations cannot be brought into congruence with their mirror image by translation, rotation, or intramolecular motions that can occur under the observation conditions (temperature, timescale of experimental instrument, etc.), then the molecule is chiral.[1] This is why *cis*-cyclohexane-1,2-diamine **12**, containing two asymmetric carbons and Mislow's *L*-menthyl-*D*-menthyl-2,6,2',6'-tetranitro-4,4'-diphenate **13** containing chiral carbons (Figure 1.3), are achiral because in the former case at least one conformation with a symmetry plane (the high energy planar conformation) is accessible. In the latter case all possible conformations are chiral, but this compound is achiral because rotation about the unhindered phenyl-ester bonds allows interconversion between mirror-image conformations. Thus, **13** is chiral in all its conformations, but does not exist in stable enantiomeric forms: it is chemically achiral.

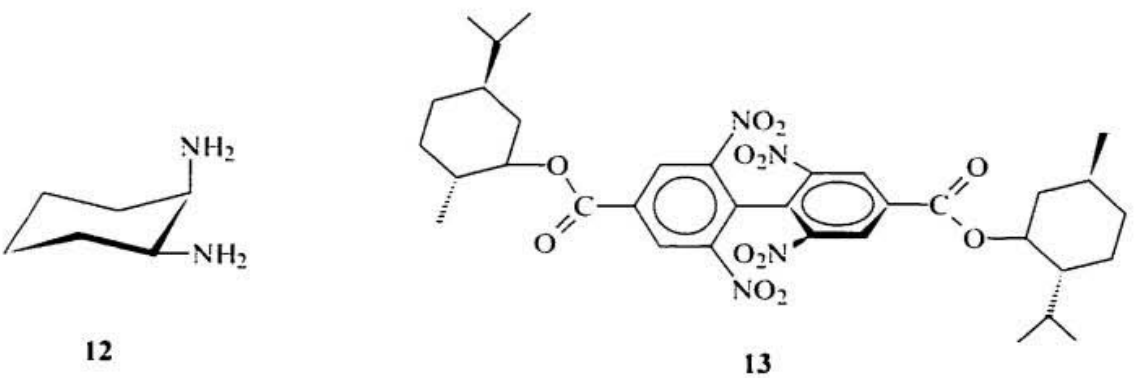

12 **13**

Figure 1.3 *cis*-Cyclohexane-1,2-diamine **12** and *L*-menthyl-*D*-menthyl-2,6,2',6'-tetranitro-4,4'-diphenate **13**

1.1.2 Synthetic strategies for new chiral molecules

Molecular chirality has very significant impacts on life because enantiomers in most cases demonstrate very different biological activity. For instance, the natural enantiomer (-)-physostigmine **14** (Figure 1.4) is 700 times stronger than its unnatural enantiomer as an inhibitor of cortex acetylcholinesterase.[4a] The recently developed (-)-Carbovir **15** (Figure 1.4) is a highly potent inhibitor of HIV reverse transcriptase whereas the antiviral activity of its enantiomer is negligible.[4b] Therefore, development of new synthetic methods to obtain new or naturally existing enantiopure compounds is highly desirable and also challenging. Three basic strategies have been developed: **(a) Resolution** Racemates with reactive functional groups such as -COOH or -NH_2 are transformed into two chemically different diastereomers by reaction with an enantiopure reagent. Diastereomer separation by crystallization is followed by cleavage of the resolving reagent, which releases the pure enantiomer: **(b) Transformation** An enantiopure molecule is stereospecifically converted into the desired chiral target via

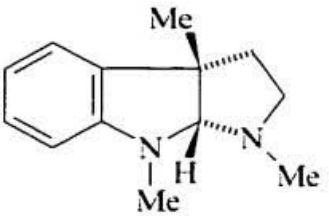

(-)-physostigmine

14

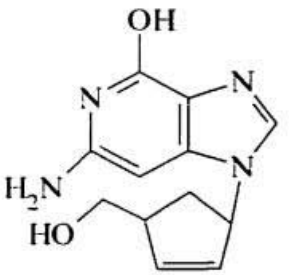

(-)-Carbovir

15

Figure 1.4 Two biologically active chiral molecules

stereoselective reaction(s): **(c) Asymmetric synthesis** A prochiral substrate is transformed into a chiral compound in the presence of a chiral auxiliary, reagent, or catalyst.

Asymmetric synthesis has many advantages over resolution and transformation in terms of accessibility to synthetic methodologies, potential substrates and thus new chiral molecules. As illustrated in Scheme 1.1, 1,2- addition of a reagent A-B to each enantioface of prochiral compounds such as alkenes, aldehydes, and ketones, affords enantiomers. The aim of asymmetric synthesis therefore is to find or synthesize a highly efficient chiral auxiliary, reagent, and/or catalyst to induce enantiofacial discrimination. An ideal case would be to develop an efficient chiral catalyst and thus chirality could be transferred and multiplied.[5,6]

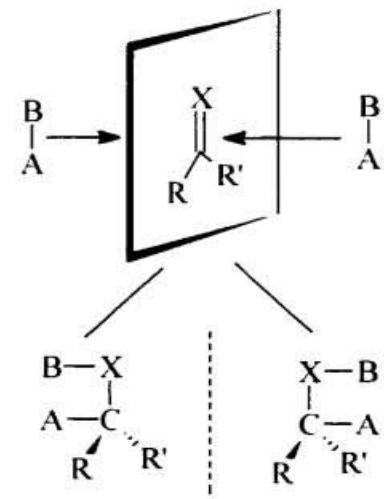

X = O, CH_2, N, etc.
A-B = H_2, $HSiR_3$, dienes, etc.

Scheme 1.1 Enantiofacial selective reactions

This research project focuses on the synthesis of chiral epoxides. The subject is reviewed in this chapter, and particular attention is paid to catalytic asymmetric epoxidation.

1.2 Asymmetric Epoxidation

1.2.1 General considerations

The importance of chiral molecules to life has spurred chemists to prepare enantiopure building blocks for the synthesis of biologically active compounds [7, 8] In this regard, chiral epoxides are extremely important.[9, 10]

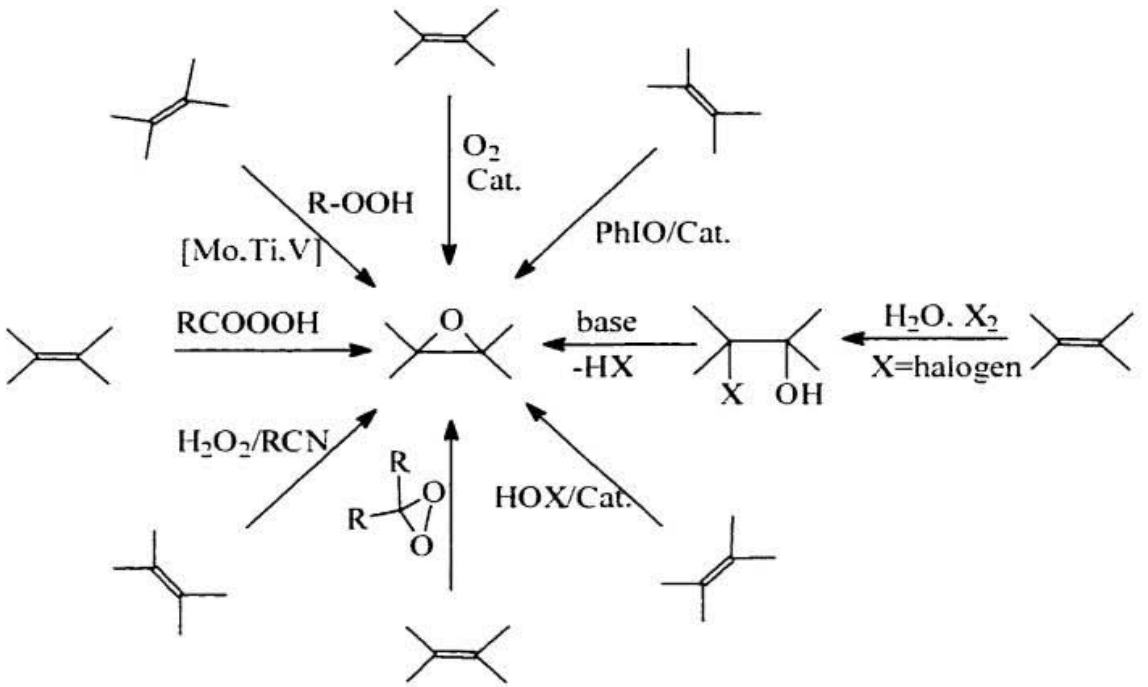

Scheme 1.2 Common methods for preparation of epoxides

Traditionally, chiral epoxides are obtained through resolution of racemates, which are prepared by several well-known methods[11] shown in Scheme 1.2. This approach however is time-consuming and not efficient. The enantioselective version (asymmetric epoxidation) of these reactions using chiral oxidizing agents such as chiral peroxides,

chiral auxiliaries with achiral oxidants, and chiral catalysts coupled with achiral oxidants provides new methods for obtaining enantiopure epoxides. In the asymmetric reactions, asymmetric induction, measured by enantiomeric excess (%ee), is the major issue. Asymmetric epoxidations may be broadly classified into two categories: epoxidations involving organic chiral peroxides and epoxidations involving chiral catalysts/achiral oxidants.

1.2.2 Enantioselective epoxidations with chiral organic oxidants

In asymmetric epoxidation, chiral information is present either in an optically pure substrate or in an oxidizing agent (Scheme 1.3). In case A, epoxidation of a chiral substrate with an achiral oxidant generates diastereomeric isomers, therefore further

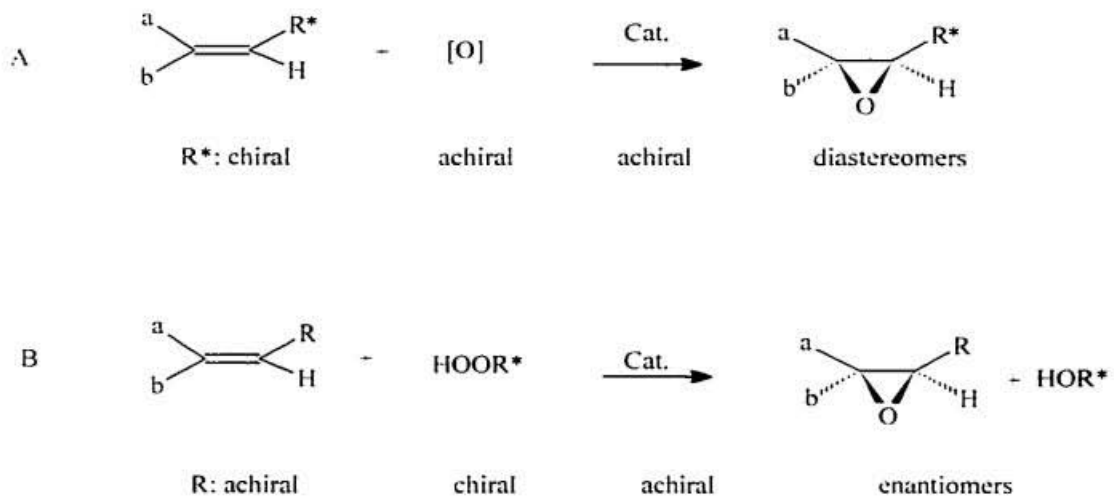

Scheme 1.3 Asymmetric epoxidation with oxidants

separation is needed. This approach obviously is impractical to obtain directly enantiopure epoxides. The use of optically pure organic chiral peroxides (case B) such as peroxy acids, hydroperoxides, or dioxiranes as both oxygen and chiral source, with or without a catalyst, for epoxidation of a prochiral alkene represents another approach that has attracted great attention since 1965. (+)-Peroxycamphoric acid **16** (Figure 1.5) showed a slight enantioselectivity (1-3% ee) with a variety of substrates.[12a] Subsequent work with the peroxy acids **17** and hydroperoxide **18** in different research groups also had limited success (< 10% ee) [12b, 12c] With chiral dioxiranes **19** and **20**[13] (Figure 1.5), generated by reaction of oxone (potassium peroxymonosulfate) with enantiomerically pure ketones, the enantiomeric excesses obtained were slightly higher than using peroxoacids. About 9-20% ee was obtained for the epoxidation of methylstyrene, 2-octene, and 1-methylcyclohexene. Surprisingly, with oxone and the C_2 symmetric chiral ketone **21** (Figure 1.5), up to 87% ee was achieved by Yang[14] for epoxidation of *trans*-stilbene derivatives. Recently, very promising work employing the chiral ketone **22** (Figure 1.5) was carried out in Shi's group. Epoxide product with > 90% ee was obtained for epoxidation of stilbene at -10°C.[15] Epoxidation of prochiral alkenes with chiral oxaziridine oxidants such as the *N*-sulfonyloxaziridine derivatives **23** (Figure 1.5) generated *in situ* from the corresponding nitrile was investigated by Davis.[16] *Trans*-methylstyrene epoxide was prepared with up to 64.7% ee using **23**. The notable feature of this type chiral reagent is that it may be recycled.

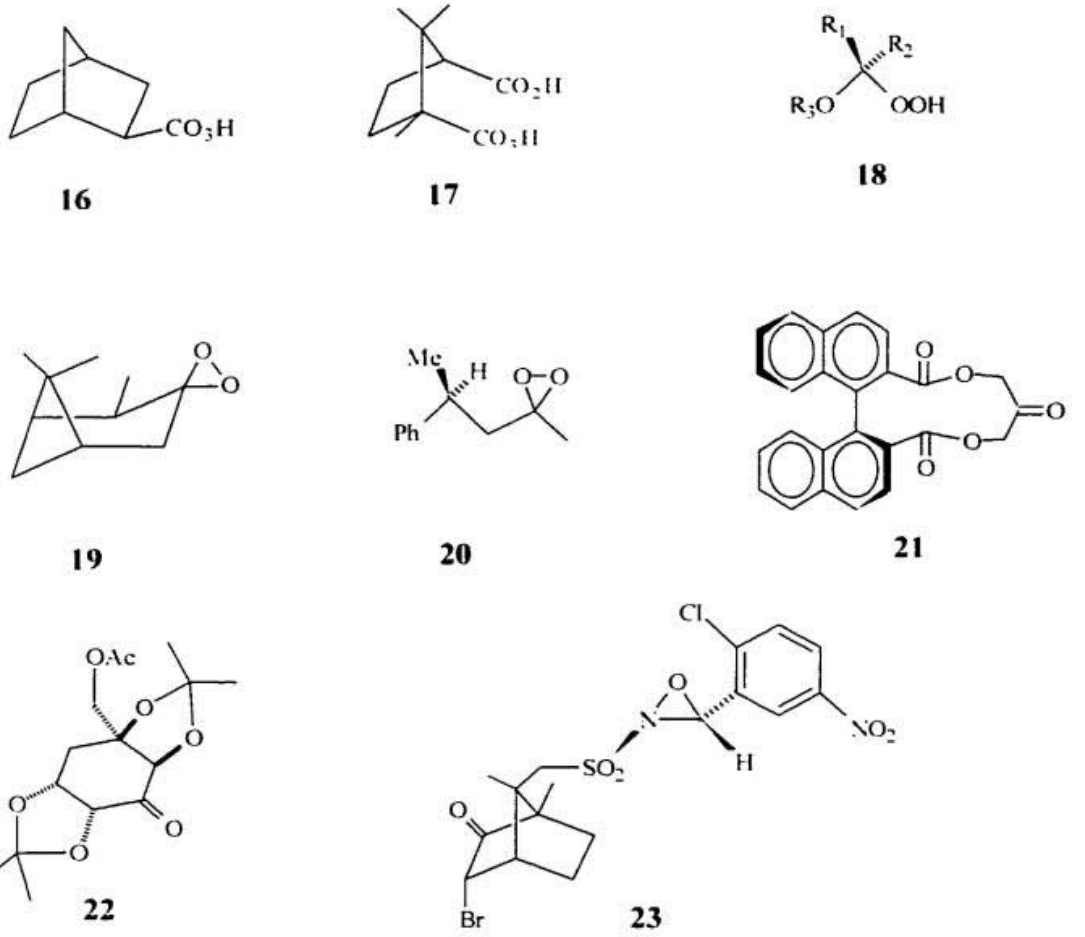

16 17 18

19 20 21

22 23

Figure 1.5 Chiral peroxy acids, hydroperoxides, dioxiranes, ketones, and oxaziridine

1.2.3 Mechanistic implications involving chiral oxidants

Correlation of the enantioselectivities and molecular structure of the chiral oxidants mentioned above suggests that sterically demanding oxidants such as **21** and **23** (Figure 1.5) and/or close proximity of the delivered oxygen to the chiral centre such as in **22** and **23** are necessary to accomplish effective asymmetric induction. Explanation of the

phenomena must rely on the understanding of the mechanism involved in the epoxidation reactions.

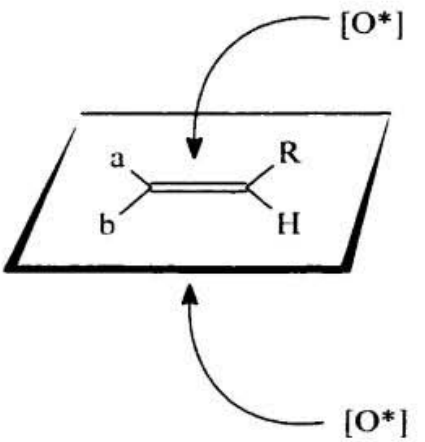

Figure 1.6 Approach of oxygen to the two faces of a prochiral alkene

Firstly, the two oxygen atoms in peroxy acids, hydroperoxides, and dioxiranes can be regarded as an oxygen dianion, O_2^{-2}. A theoretical investigation[15] has shown that the LUMO of O_2^{-2} serves effectively as an electron-accepting orbital for electron-donating alkenes even though it has a net negative charge. The reaction rates shown below for epoxidation of various alkylated alkenes follow the order of π-electron density[15] and support the theoretical argument.

alkene:	$CH_2=CH_2$	< $RCH=CH_2$	< $PhCH=CH_2$	< $RCH=CHR$	< $R_2C=CR_2$
relative reaction rate	1	25	60	500	6000

Thus, electrophilic attack of a chiral oxidant at either face of a prochiral alkene (Figure 1.6) gives epoxides. The preference for *R* or *S* epoxide logically depends on the rate of the formation of the two diastereomers in the transition states. Since both diastereoisomers have the same reactant and leaving groups, steric factors must play the major role in the asymmetric induction process. Since the transferred oxygen in the peroxy acids and hydroperoxides is directly bonded to a hydrogen and another oxygen,

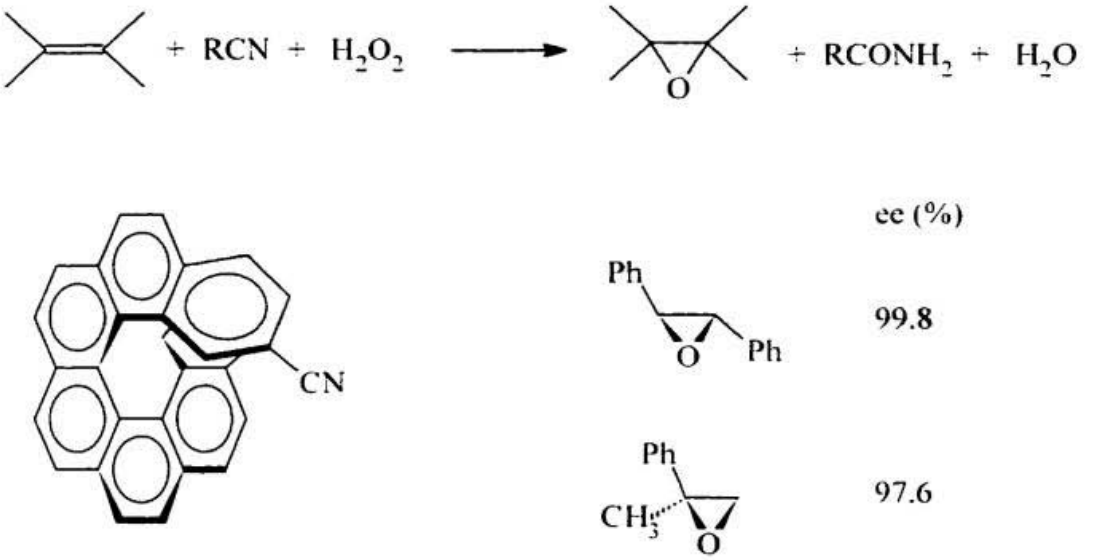

Figure 1.7 *In situ* asymmetric epoxidation of alkenes with a chiral oxaziridine

it follows that steric interactions between the nucleophile (alkene) and the electrophile (oxidant) in the transition state are not biassed toward either approach. Therefore, less than 3% ee was observed with chiral peroxoacids and hydroperoxides. On the other hand, the steric environment of the delivered oxygen in dioxiranes as well as oxaziridines can be adjusted to discriminate approaches, and thus higher enantioselectivity (> 65% ee) was achieved. Another example, the (+)-2-heptahelicenonitrile/H_2O_2 system[11] (Figure 1.7), further supports the argument. The chiral heptahelicene group close to the transferred oxygen enhanced the chiral communication via steric interactions between the bulky chiral residue and alkene. Therefore, it was very efficient for enantioselective epoxidation of unfunctionalized alkenes. Based on the analysis above, it follows that

development of a new oxo-transfer system in which the oxo site resides in the vicinity of a rigid and/or bulky stereogenic centre is required to achieve high enantiomeric excesses. This idea is further demonstrated in catalytic asymmetric epoxidation as discussed below.

1.2.4 Enantioselective epoxidation with chiral catalysts/achiral oxidants

The results obtained employing chiral peroxy oxidants, especially dioxiranes, are very promising. However, the fact that the required chiral ketone needs to be added in large amounts (30% mol) to a multi-solvent medium limits its potential application on large scale. New types of asymmetric epoxidation reactions are obviously required. In this respect, catalytic asymmetric epoxidation represents the most powerful synthetic tool since, with a small amount of chiral catalyst (< 5% mol), a large amount of chiral epoxide can be obtained.[5,6] Thus, chirality is "multiplied" in the presence of a chiral catalyst.

Three different cases for catalytic asymmetric epoxidation can be distinguished (Scheme 1.4). In case A, epoxidation of both enantiomers under kinetic control leads to improvement of the optical purity of both starting materials and products since one enantiomer may react faster than the other in the presence of a chiral catalyst. Such a strategy has been applied in the epoxidation of allylic alcohols,[18] hydrogenation,[19] as well as epoxide ring opening.[20] With regard to chemical yield, this approach is less efficient since the maximum yield is only 50%.

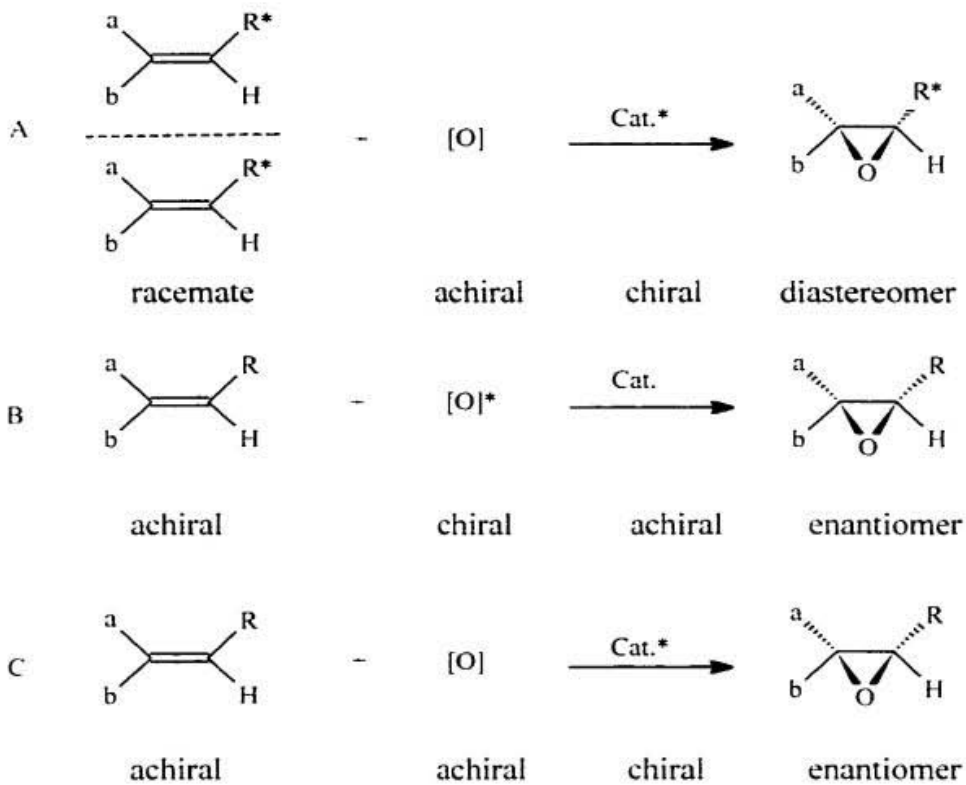

Scheme 1.4 Asymmetric epoxidation in the presence of a chiral or achiral catalyst

In case B, a chiral oxidant is used with an achiral catalyst and thus the reaction is catalytic, but chirality transfer is stoichiometric. In reality, the chiral oxidant may first react with the catalyst (normally an oxophilic transition metal) and subsequently this reaction generates a metal-oxo species[21] which then would react with the substrate. During the transfer, chirality is lost before reaching the substrate. Therefore, this strategy was not found in the literature.

Catalytic asymmetric epoxidation mainly deals with case C (Scheme 1.4). In this way, a large amount of optically active compound can be synthesized, even though only a comparatively small amount of a chiral catalyst is used. Naturally, a great deal of effort has been applied to develop such chiral catalysts which normally contain a transition metal bound by a chiral ligand. Papers published in 1991,[22] 1992,[23] 1993,[11, 24] 1994[25] and 1995[26] reviewed such efforts. To this end, some of the chiral catalysts are quite remarkable and give chiral epoxide with synthetically useful ee's (>90% ee). Based on the chiral ligands, three types of chiral catalysts are presented: i) chiral, tartrate-based Sharpless catalysts; ii) chiral, salen-based Jacobsen catalysts, and iii) chiral, porphyrin-based catalysts.

1.2.4.1 Sharpless catalysts involving chiral diethyl tartrate as the source of chirality

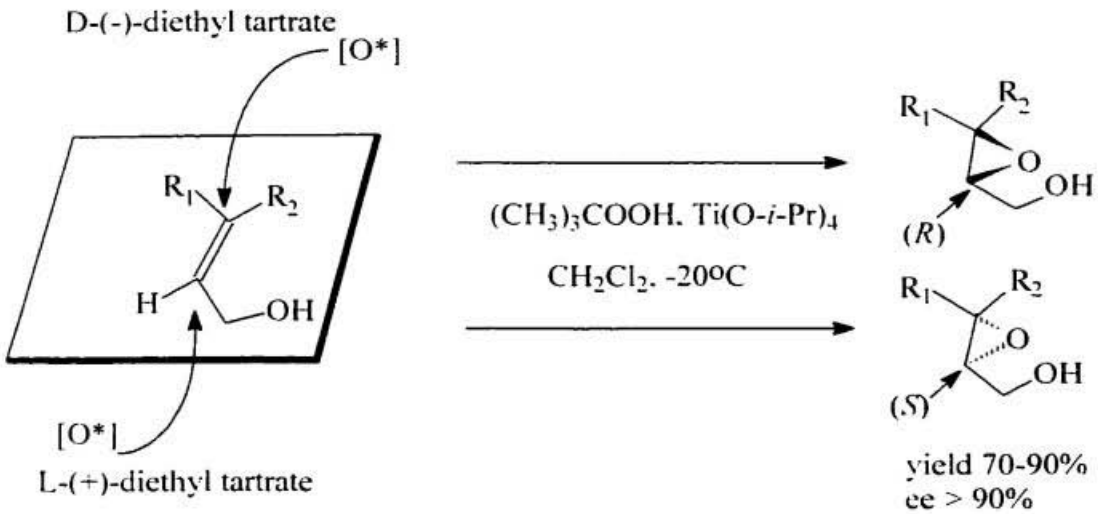

Figure 1.8 Sharpless epoxidation

In 1980, Sharpless first reported an asymmetric epoxidation system[27] composed of a mixture of commercially available titanium(IV) tetraisopropoxide, *t*-butylhydroperoxide (TBHP), and (+) or (-)-diethyl tartrate (DET). Five years later, this system was developed into a catalytic version through addition of Molecular Sieves.[28] With this system, efficient asymmetric induction was achieved for epoxidation of allylic alcohols (Figure 1.8).

With a given enantiomeric tartrate ester, the system is forced to deliver oxygen to one of the two faces of an alkene, regardless of its substitution pattern. When the olefinic unit is in the plane of the drawing, as shown in Figure 1.8, the use of (+)-DET leads to the addition of the oxygen from the bottom whereas when (-)-DET is employed, the oxygen is added from the top.[28]

To rationalize these observations, X-ray studies and kinetic investigations of Ti_2(dibenzyltartramide)$_2$(OR)$_4$ were carried out. The results suggested a transition state model[28, 29] (Figure 1.9) in which an axial and an equatorial ligand -OR″, originally in the catalyst, undergo exchange with a bidentate peroxide (*t*-BuOOH). Due to the larger steric demand of *t*-butyl, coordination of the peroxide to the

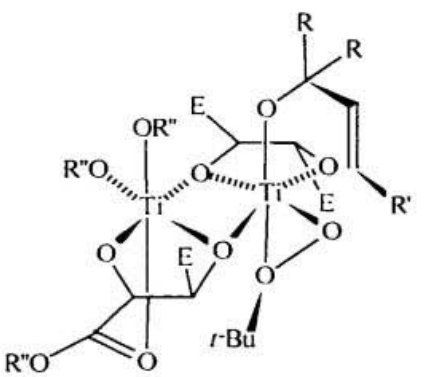

Figure 1.9 The proposed transition state structure in Sharpless epoxidation

axial and equatorial sites occurs on the lower face of the roughly octahedral titanium complex. Another axially coordinated carbonyl is released from the titanium centre and substituted by the allylic alcohol (Figure 1.9). A linear alignment of allylic alkoxide and peroxide oxygen atoms results. The transferred oxygen is thus temporally located directly below (producing one enantiomer) or above (giving the other enantiomer) the double bond in the transition state.

depending on which enantiomer of DET is used.

$$A + B \xrightarrow[k_1]{\text{cat.}} \text{product*} \xleftarrow[k_2]{\text{cat./ligand*}} A + B$$

Scheme 1.5 Ligand acceleration catalysis

Based on the results of epoxidation and subsequent exploration of dihydroxylation of alkenes with osmium tetroxide in the presence of a chiral auxiliary, Sharpless concluded that an important reason for such high enantioselectivity in the processes was the substantial rate acceleration ($k_2 > k_1$), resulting from coordination of the chiral ligand (DET) to the metal ion (Ligand Acceleration Catalysis-LAC).[30] Thus, if the metal-chiral ligand complex rapidly exchanges its ligands in solution, high enantioselectivity would only be observed when catalyst and chiral ligand system is much more active than catalyst (Scheme 1.5).

In the Sharpless system, the chiral ligand is retained in the coordination sphere of titanium. More importantly, temporary coordination of both substrate (allylic alcohol) and oxidant (*t*-butylhydroperoxide) to the titanium atom promotes stereocontrol by

enforcing conformational rigidity through auxiliary interactions. This is not an isolated case since other catalytic systems such as the Ru-BINAP complex developed by Noyori *et al.*[31] for enantioselective hydrogenation of ketones also requires directing groups (-NH_2, -COOH, *etc.*) for temporary binding the substrate to the metal centre. It appears that a good chiral catalyst should be inert in terms of the chiral ligand for maintaining the chiral environment but mobile in terms of the achiral ligand for exchanging with the substrate and/or reagent so that passive bonding[32] (secondary chelation) between substrate and the active centre can occur in the reaction.

1.2.4.2 Epoxidation involving chiral porphyrin-based catalysts

The highly enantioselective Sharpless epoxidation requires a functionalised allylic alcohol with an auxiliary anchoring group (-OH) to favour high ee's and fast rates via chelation. For asymmetric epoxidation of unfunctionalized alkenes, a crucial difficulty arises because conformationally restricting chelate complexes are reluctant to form and only low-energy, non-covalent interactions are available. The development of a catalyst that can differentiate between the two enantiomeric faces of an unfunctionalized alkene is therefore a more challenging task.

Porphyrin-based transition metal complexes based on Fe(III) and Mn(III) show excellent oxidation properties, resembling the activity of natural enzymes such as cytochrome P-450.[33,34] Studies showed that the catalytic properties of metalloporphyrins were related

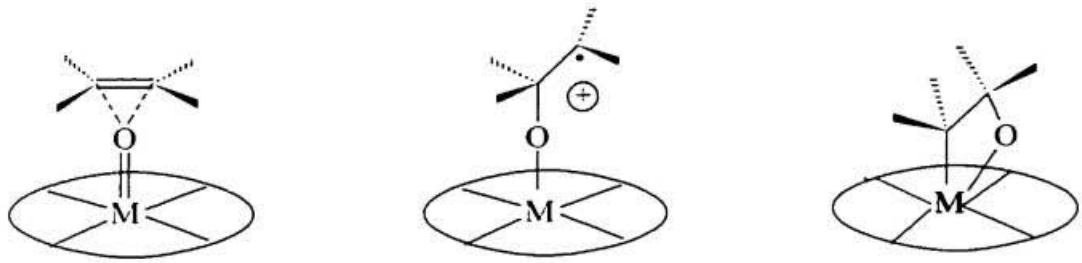

(a) **(b)** **(c)**

Figure 1.10 Possible intermediates in porphyrin-catalysed epoxidation

to the formation of a high-valent transition metal porphyrin intermediate in the presence of an oxidant (H_2O_2, PhIO, C_6F_5IO, RCO_3H, $NaIO_4$, etc.). The electronic properties of the high-valence oxometal porphyrin species, M=O, have been extensively examined by both experimental and theoretical studies[35] and will not be reviewed here since they may not directly relate to asymmetric induction and chirality multiplication.

However, oxygen transfer from M=O to alkene, which precedes epoxidation, is essential. Based on the approach of an alkene parallel to the porphyrin plane and vertical to the M=O bond, three intermediates (Figure 1.10) are proposed:[36] (a) **a concerted [1+2] path** giving an intermediate which maintains the stereochemistry of the alkene; (b) **a non-concerted [1+2] path** generating a C-C-O-M radical, which can explain the loss of stereochemistry of the alkene if the life time of the intermediate is long enough to allow rotation around the C-C bond; and (c) **a [2+2] oxidative cycloaddition** leading to a metalloxetane intermediate, which forms the epoxide by reductive elimination.

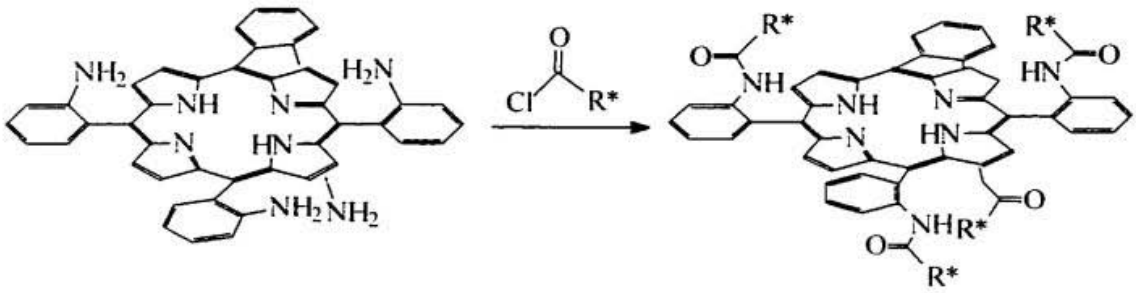

Scheme 1.6 Preparation of the chiral porphyrins

Theoretical investigations[36] suggested that any one of the three intermediates may be favoured in the epoxidation of an alkene. Fe(III) tends to form an open intermediate. Ru(II) catalyses epoxidation via a non-concerted [1+2] route, whereas Mn(III) possibly proceeds via a concerted [1+2] pathway.

Taking the strategy of modifying the porphyrin frame by introduction of chiral groups on the *meso* and β-pyrrolic positions, Groves *et al.* [37] had prepared chiral "picket fence" porphyrins (Scheme 1.6) starting from 5α,10β,15α,20α-tetrakis(*o*-aminophenyl)porphyrin by amide formation with (*R*)-2-phenylpropanoyl chloride. Using the same approach, porphyrin **b** (Scheme 1.7), containing two rigid, axially-chiral binaphthyl bridges, was obtained by Groves.[38] Catalytic

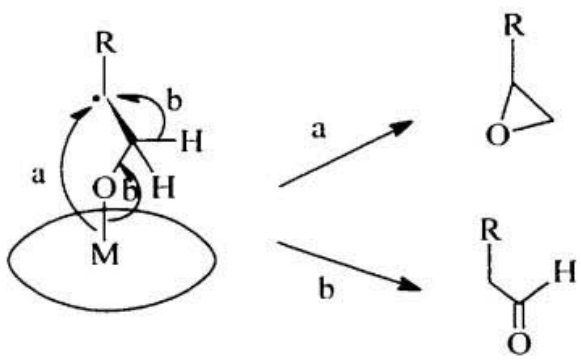

Figure 1.11 Formation of an aldehyde in epoxidation

epoxidation of styrene with PhIO in the presence of these porphyrins and Fe(III) or Mn(III) chloride, gave optical yields of 31% and 48% ee, respectively (Scheme 1.7).

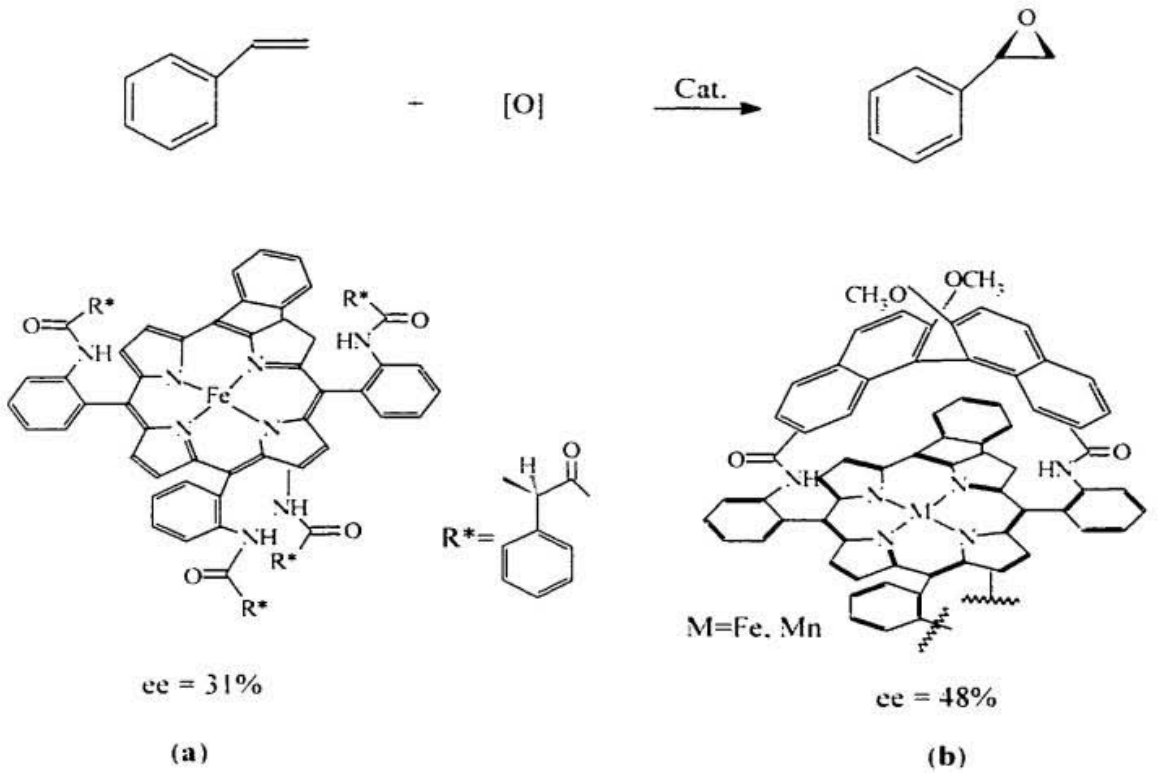

Scheme 1.7 Asymmetric epoxidation of styrene with chiral porphyrin-based catalysts

The relatively low optical yields were ascribed to several shortcomings in the systems:[39] i) similar to chiral peroxy acids, the gap between the chiral centres and the active site may be too large; ii) "leakage reactions" on the achiral face of the porphyrin plane can occur even in the presence of excess axial blocking ligand; iii) radical side-reactions such as those in Figure 1.11 might occur, as indicated by the formation of an aldehyde; and iv)

possible auto-degradation of the porphyrin molecular architecture through dimerizationand/or oxidation may occur.

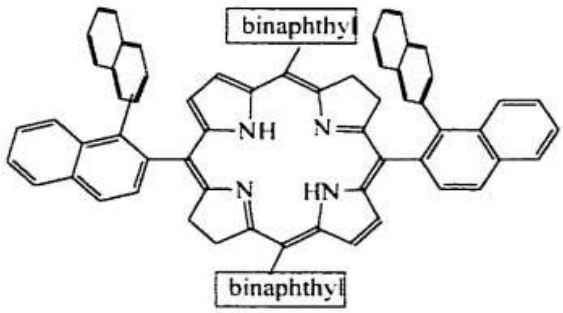

Figure 1.12 Chiral porphyrin wall

To overcome these problems, the Mn(III) complex of 5α,10β,15α,20β-tetrakis[(*R*)-1,1'-binaphthyl-2-yl]porphyrin (Figure 1.12) with a built-in "chiral wall," which should prevent "leakage reactions"and intermolecular dimerization, was prepared and proved to be robust under oxidative conditions. However, the optical yield of 20% ee for the epoxidation of styrene was somewhat discouraging.[40]

1.2.4.3 Epoxidation involving chiral salen-based catalysts

Chiral porphyrin-based catalysts offer an alternative for asymmetric epoxidation of unfunctionalized olefins that is not available with the Sharpless catalyst. However, there are still considerable limitations as stated above for their use in organic synthesis. Other synthetically useful chiral catalysts are therefore highly desirable. Salens, with the general structure shown in Figure 1.13, are similar to

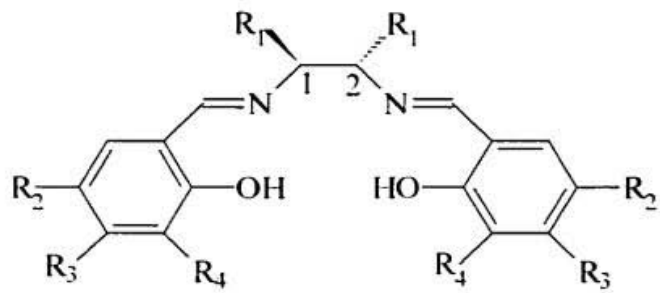

Figure 1.13 A chiral salen

porphyrins with respect to electronic properties. The peripheral carbons in porphyrin are all sp^2, whereas two sp^3, potentially stereogenic, carbons occupy positions 1 and 2 in the salen above. The stereogenic centres, located just two bonds away from the metal, are closer to the active site compared to the situation in the chiral porphyrin system. Furthermore, the salen is a tetradentate ligand and the resulting complexes should be quite stable as a result of the chelation effect. Therefore, the dissociation constant of the salen complexes should be small, and it is expected that the chirality will be maintained within the framework of the chiral complex during epoxidation. If the chiral salen catalysts have higher activity than the corresponding achiral free transition metal ion, higher enantioselectivity should be expected (LAC, Sharpless principle). Additionally, there are at least three positions, R_2 R_3, and R_4 on the phenol ring available both for steric tailoring and electronic adjustment, through the conjugated benzylic ring, to the metal. Manipulation of the R groups will possibly orient the incoming olefin, modify electronic properties of the catalyst, and improve both the enantioselectivity and the catalytic activity.

Despite the advantages of salens and the acknowledged catalytic activity of the corresponding Mn(III) complexes in epoxidation of olefins dating back to 1985,[41] introduction of chirality into a salen framework at positions 1 and 2 to prepare chiral catalysts (Figure 1.14) was not reported until Jacobsen's work in 1990.[42] It was found that the size of the substituent R_4 controlled the enantioselectivity. For R_4 = H or CH_3, the

optical yields were low for epoxidation of *cis*-β-methylstyrene. When the size of R_4 was

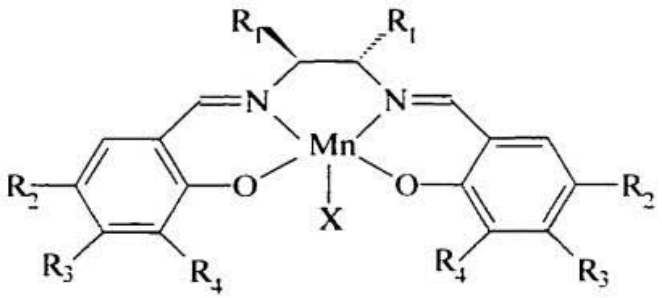

Figure 1.14 Chiral salen-based catalysts

increased to *t*-Bu, a high optical yield of 98% ee was obtained at low temperature.

Jacobsen catalysts (**J**)

J1 R_1 = Ph, R_2 = H, R_3 = H, R_4 = *t*-Bu

J2 R_1, R_1 = -(C_4H_8)-, R_2 = *t*-Bu, R_3 = H, R_4 = *t*-Bu

J3 R_1, R_1 = -(C_4H_8)-, R_2 = R_3 = H, R_4 = *t*-Bu

J4 R_1 = Ph, R_2 = CH_3, R_3 = H, R_4 = *t*-Bu

J5 R_1 = Ph, R_2 = Br, R_3 = H, R_4 = *t*-Bu

X=Cl^- or PF_6^-

Katsuki catalysts (**K**):

K1 R_1 = Ph, R_2 = H, R_3 = H, R_4 = -C(H)(Et)(Ph)

K2 R_1 = Ph, R_2 = H, R_3 = Me, R_4 = -C(H)(Et)(Ph)

K3 R_1 = Ph, R_2 = H, R_3 = Me,
R_4 = -C(H)(4-*t*-Bu-Ph)

K4 R_1, R_1 = -(C_4H_8)-, R_2 = H, R_3 = Me
R_4 = (*R*)-C(H)(Et)(4-*t*-Bu-Ph)
X=PF_6^- or AcO^-

Since the initial discovery, more than 120 chiral Mn(III) salen derivatives have been synthesized and studied as catalysts for the epoxidation of a variety of unfunctionalized

olefins with PhIO, NaOCl, and even O_2 as the oxidant.[44, 45] Some representative catalysts are shown in Figure 1.14.[26, 39, 43, 46-52] The results for the epoxidation of *cis*-β-methylstyrene, styrene, *trans*-β-methylstyrene, and 1,2-dihydronaphthalene are summarized in Table 1.1.

Table 1.1 Epoxidation of various alkenes with Jacobsen and Katsuki catalysts

olefin	catalyst	chemical yield (%)	ee (%)
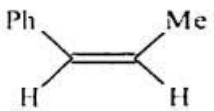	**J1**	73	81
	J2	81	92
	K4	36	86
	K1		50
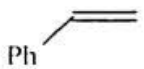	**J1**	75	57
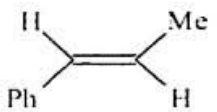	**J2**	34	47
	K4	61	98
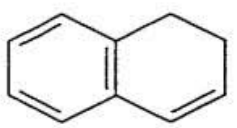	**K1**	25	43
	K2	65	72
	J1	72	78
	J2	67	86

Inspection of Table 1.1 showed that high asymmetric induction was achieved for epoxidation of *cis*-alkenes with Jacobsen catalyst **J2**. Introduction of more stereogenic centres at R_4, as in Katsuki catalysts **K1** and **K2** had only a minor influence on enantioselectivity. The groups likely served as steric bulk similar to the *t*-butyl groups in Jacobsen catalysts. Table 1.1 also showed that the enantioselectivities for epoxidation of

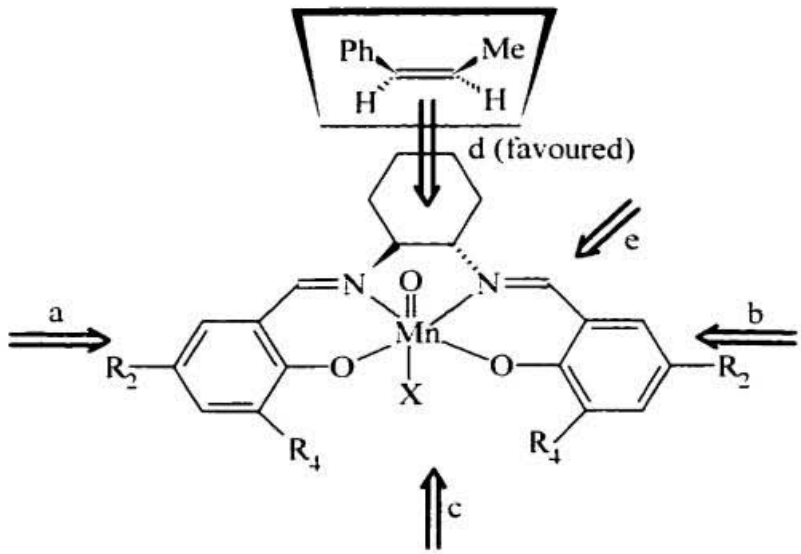

Figure 1.15 The side-on approach of an alkene to a Mn=O centre

trans and terminal alkenes were lower than that for epoxidation of *cis*-alkenes with both Jacobsen and Katsuki catalysts.

To account for the experimental results, a side-on approach of the alkene to the Mn(V)=O centre located in a nearly planar salen framework (Figure 1.15), similar to the one suggested for Grove's porphyrin system, was proposed by Jacobsen.[39] He believed that the bulky *t*-butyl groups in positions R_2 and R_4 shielded the aryl rings and prevented alkene approach via pathways a, b, and c (Figure 1.15). The alkene was forced into approach via pathway d, which was sterically favoured due to the smaller substituent (Me) on the same side as the axial hydrogen atom of the cyclohexyl ring and larger

substituent (Ph) on the other side of the equatorial hydrogen atom of the stereogenic centre.

This side-on approach model was challenged by Katsuki[48] who proposed that a prochiral alkene molecule would approach the Mn=O centre along the direction e (Figure 1.15). He reasoned that, in addition to the steric effect from R_2, π-electron repulsions between the salen benzene ring and the olefin also contributed to asymmetric induction.[54] More interestingly, Jacobsen proposed a radical intermediate (Figure 1.10, **b**) to explain the formation of *trans*-epoxide from epoxidation of a *cis*-alkene. On the other hand, Katsuki favoured a metallaoxetane intermediate (Figure 1.10, **c**) in order to support his experimental results which found that enantiomeric excesses for epoxidation of conjugated dienes were higher than that of alkyl substituted alkenes.[54] Since direct experimental evidence regarding the intermediates has not emerged, the mechanism of asymmetric induction remains an ongoing, intensive debate.[55]

Nevertheless, comparison of the salen-based catalyst results shown in Table 1.1 with the porphyrin-based catalyst results shown in Scheme 1.8 indicates that the enantioselectivities with the former are generally higher for epoxidation of unfunctionalized alkenes. Moreover, a straightforward synthesis based on a readily available chiral source ((*1R,2R*)- or (*1S,2S*)-cyclohexane-1,2-diamine) made chiral salen catalysts more attractive and synthetically useful, at least currently, than porphyrin-based

chiral catalysts. However, problems remain to be solved. Firstly, salen catalysts were not applicable to the epoxidation of *trans*-phenyl and aliphatic alkenes. Secondly, as a consequence of dimerization of the monosalen complexes,[56, 57] the lifetime of salen-based catalysts was short, and turnover numbers were normally lower than 40.

1.3 Enantioselective epoxidation involving heterogeneous chiral catalysts

As stated above, homogeneous chiral catalysts are often unstable. Anchoring or supporting efficient homogeneous chiral catalysts on solids like polymers,[58] silica gel[59] or Molecular Sieves was anticipated to suppress catalyst decomposition caused by intermolecular dimerization and/or oligmerization.

1.3.1 Supported Sharpless catalysts

The first report, which dealt with an anchored Sharpless catalyst on Na^+-montmorillonite with zeolite-like cages, was reported in 1990.[60] Optical yields (> 90% ee) for catalytic epoxidation of allylic alcohols were demonstrated, but no further work with clays has been reported. Very recently, copolymerization of L-(+)-tartaric acid and bis(chloromethyl)benzene afforded several polytartrate esters (Scheme 1.8), which showed relatively low asymmetric induction under Sharpless reaction conditions.

1.3.2 Supported Jacobsen catalysts

Early attempts to immobilize Jacobsen catalysts led to polymeric species, which offered

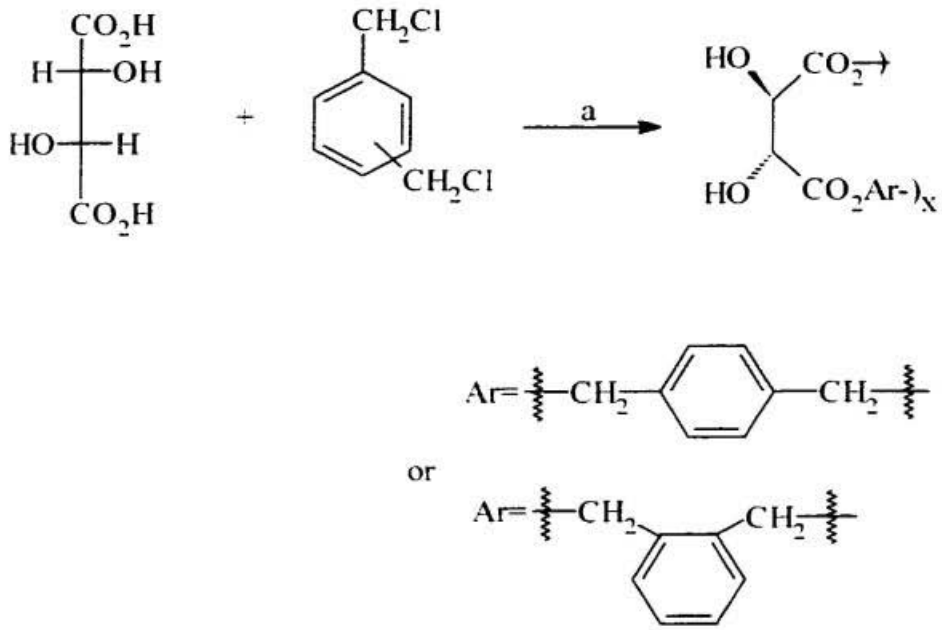

a: t-Bu_4NBr. H_2O. $CHCl_3$. reflux. 7 days

Scheme 1.8 Polymerization of chiral tartaric acid with bis(chloromethyl) benzene

lower ee's in epoxidation.[61] A new "ship-in-the-bottle" approach encapsulates chiral Mn(III) salen complexes in a zeolite cage, so that shape-selective catalysis can occur in the cavity.[62, 63] With cholesterol, a relatively large substrate, no conversion was observed whereas with smaller substrates like styrene more than 15% was converted to epoxide with 34% ee.

1.3.3 Poly(amino acid) catalysts

Poly(amino acids) or peptides have been widely tested as catalysts for Michael additions, carbonylation, hydrogenation and epoxidation. Julia *et al.*[64] used poly-alanine as both a

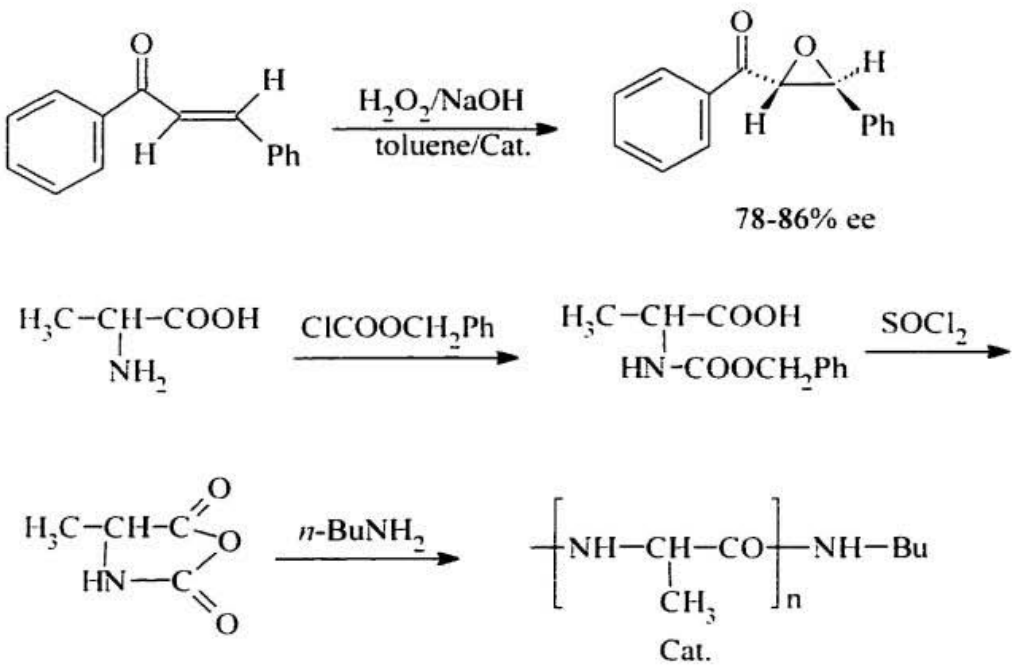

Scheme 1.9 Epoxidation of chalcone with H_2O_2 in the presence of poly(aminoacid)

chiral auxiliary and a catalyst for the epoxidation of electron-deficient α,β-unsaturated carbonyl compounds. High optical yields were achieved (Scheme 1.9). Itsuno *et al.*[65] found that supported poly(amino acid) also can act as an efficient chiral catalyst in the epoxidation of substituted chalcone (Scheme 1.9) with high enantioselectivity (>90% ee). More interestingly, the polymeric catalyst can be recovered without any loss of activity and can be used for further asymmetric epoxidation.

1.4 Research design summary

Review of the progress made during the past 20 years reveals that asymmetric

epoxidation of prochiral alkenes remains a challenge since the synthetically useful chiral catalysts examined so far have limited scope with regard to the alkene substrates. New, efficient chiral catalysts are therefore in high demand, especially for the epoxidation of unfunctionalized alkenes.

Regardless of the details of asymmetric induction in either the Sharpless or Jacobsen systems, three points are crucial for high enantioselectivity: i) passive bonding of substrate and/or reagent to the active centre to generate rigid conformers and thus force oxo transfer to occur within the "coordination sphere"; ii) orientation of alkenes by virtue of steric factors allowing selective approach to the active site on one of the two enantiotopic faces; and iii) introduction of C_2 or higher symmetry to the catalysts to reduce the formation of diasteroisomeric transition states.[26, 66]

In nature, the selectivity of an enzyme is determined by the geometry of the active site embedded in a concave-shaped region of the protein, and non-bonding secondary interactions with the substrate. These concepts have been strategically used in organic synthesis, supramolecular chemistry, and very recently in asymmetric catalysis.[24, 67-70] There is no work to date which takes advantage of macrocyclic architectures with a built-in cavity to impose non-covalent interactions such as π-π stacking, H-bonding, *etc.* for asymmetric induction in enantioselective epoxidation of unfunctionalized alkenes.

This project explores a host/guest approach by the design and syntheses of a series of chiral macrocyclic bimetallic complexes. The catalytic properties of the complexes in epoxidation of unfunctionalized alkenes are evaluated on the basis of understanding the conformation of the complexes both in solution and in the solid state.

1.5 References

1. Eliel, E. L.; Wilen, S. H.; Mander, L. N. *Stereochemistry of Organic Compounds*; Chapter 1 - 4; John Wiley & Sons, Inc.; New York, **1994**.

2. Chambron, J. -C.; Dietrich-Buchecker, Ch.; Sauvage, J. -P. *From Classical Chirality to Topologically Chiral Catenands and Knots*; In *Topics in Current Chemistry*, Weber, E., Ed.; Springer-Verlag; NewYork, **1994**; Vol. 165.

3. Shriver, D. F.; Atkins, P. W.; Langford, C. H. *Inorganic Chemistry*, Chapter 2 and Chapter 7; W. H. Freeman and Company; New York, **1990**.

4. a) Jacqueline S. -P. *Chiral Auxiliaries and Ligands in Asymmetric Synthesis*, John Wiley & Sons, Inc.; New York, **1995**. b) The absolute configuration of (+)- or (-)-Carbovir was unknown. For the biological activity of (±)-Carbovir see: Vince, R.; Brownell, J. *Biochem. Biophys. Res. Commun.* **1990**, *168*, 912. For the synthesis of (±)-Carbovir see: Jung, M. E.; Rhee, H. *Tetrahedron lett.* **1993**, *34*, 4449.

5. Noyori, R. J. *Synth. Org. Chem. Jpn.* **1992**, *50*, 1131.

6. Nugent, W. A.; Rajanbabu, T. V.; Burk, M. J. *Science* **1993**, *259*, 479.

7. Bartok, M.; Lang, K. L. *The Chemistry of Functional Groups*; Wiley; New York, **1980**.

8. Rossiter, B. E. In *Asymmetric Synthesis; Vol. 5, Chiral Catalysis*; Morrison, J. D., Ed.; Academic Press; Orlando, **1985**; p.193.

9. Hanson, R. M. *Chem. Rev.* **1991**, *91*, 437.

10. Jacobsen, E. N. In *Comprehensive Organometallic Chemistry II*; Wilkinson, G. Stone, F. G. A.; Abel, E. W.; Hegedus, L. S., Eds.; Pergamon; New York, **1995**; Vol. 12, Chapter 11.1.

11. Höft, E. *Enantioselective Epoxidation with Peroxidic Oxygen* In *Topics in Current Chemistry*, Herrmann, W. A. Ed.; Springer-Verlag; Berlin, **1993**; Vol. 164.

12. a) Montanari, F. *J. Chem. Soc., Chem. Commun.* **1969**, 135, and references

therein. b) Bowman. R. M.: Collins. J. F.: Grundon. M. F. *J. Chem. Soc., Perkin Trans. 1* **1973**. 626. c) Pirkle. W. H.: Rinaldi. P. L. *J. Org. Chem.* **1977**. *42*. 2080.

13. Curci. R.: Fiorentino. M.: Serio. M. R. *J. Chem. Soc., Chem. Commun.* **1984**. 155.

14. Yang. D.: Yip. Y. C.: Tan. M. W.: Wong. M. K.: Zheng. J. H.: Cheung. K. K. *J. Am. Chem. Soc.* **1996**. *118*. 491.

15. Wang. Z. X.: Shi. Y. A. *J. Org. Chem.* **1997**. *62*. 8622.

16. Davis. F. A.: Harakal. M. E.: Awad. S. B. *J. Am. Chem. Soc.* **1983**. *105*. 3123.

17. Sawaki. Y. In *Organic Peroxides*. Chapter 9. Ando. W. Ed.: John Wiley & Sons: New York. **1992**.

18. Faller. J. W.: Sams. D. W. I.: Liu. X. *J. Am. Chem. Soc.* **1996**. *118*. 1217.

19. Faller. J. W.: Tokunaga. M. *Tetrahedron Lett.* **1993**. *34*. 7359.

20. Larrow. J. F.: Schaus. S. E.: Jacobsen. E. N. *J. Am. Chem. Soc.* **1996**. *118*. 7420.

21. Jorgensen. K. A. *Chem. Rev.* **1989**. *89*. 431.

22. Bolm. C. *Angew. Chem., Int. Ed. Engl.* **1991**. *30*. 403.

23. Schurig. V.: Betschinger. F. *Chem. Rev.* **1992**. *92*. 873.

24. Collman. J. P.: Zhang. X.: Lee. V. L.: Uffelman. E. S.: Brauman. J. I. *Science* **1993**. *261*. 1404.

25. Boschi. T. *Asymmetric Syntheses* In *Metalloporphyrin Catalyzed Oxidations*. Kluwer: Norwell. **1994**.

26. Katsuki. T. *Coord. Chem. Rev.* **1995**. *140*. 189.

27. Katsuki. T.: Sharpless. K. B. *J. Am. Chem. Soc.* **1980**. *102*. 5974.

28. Johnson. R. A.: Sharpless. K. B. In *Catalytic Asymmetric Synthesis*: Ojima. I.. Ed.: VCH: New York. **1993**.

29. Finn, M. G.; Sharpless, K. B. In *Asymmetric Synthesis;* Vol. 5, *Chiral Catalysis*; Morrison, J. D., Ed.; Academic Press: Orlando, **1985**.

30. Berrisford, D. J.; Bolm, C.; Sharpless, K. B. *Angew. Chem., Int. Ed. Engl.* **1995**, *34*, 1059.

31. Takaya, H.; Ohta, T.; Noyori, R. In *Catalytic Asymmetric Synthesis*, Ojima, I., Ed.; V C H : New York, **1993**, p. 1.

32 Kirby, A. J. *Angew. Chem., Int. Ed. Engl.* **1996**, *35*,707.

33. Casella, L. Colonna, S. *Biological Oxidations: Stereochemical Aspects* In *Metalloporphrins Catalyzed Oxidations*, Montanari, F. Casella, L., Eds.; Kluwer: Dordrecht, **1994**.

34. Chorghade, M. S.; Hill, D. R.; Lee, E. C.; Pariza, R. J. *Pure Appl. Chem.* **1996**, *68*, 753.

35. Jorgensen, K. A. In *Metalloporphyrins in Catalytic Oxidations*; Sheldon, R. A., Ed.; Marcel Dekker: New York, **1994**, p. 69.

36. Jorgensen, K. A. *On the Electronic Structure of Oxo-Metalloporphyrins and Mechanistic Aspects of Oxygen-Transfer Reactions* In *Metalloporphyrin Catalyzed Oxidations*, Montanari, F. ; Casella, L., Eds.; Kluwer: Dordrecht, **1994**.

37. Groves, J. T.; Myers, R. S. *J. Am. Chem. Soc.* **1983**, *105*, 5791.

38. Groves, J. T.; Viski, P. *J. Org. Chem.* **1990**, *55*, 3628.

39. Jacobsen, E. N. In *Catalytic Asymmetric Synthesis*; Ojima, I., Ed.; VCH : New York, **1993**; p. 159.

40. O'Malley, S.; Kodadek, T. *J. Am. Chem. Soc.* **1989**, *111*, 9176.

41. Srinivasan, K.; Michaud, P.; Kochi, J. K. *J. Am. Chem. Soc.* **1985**, *108*, 2309.

42. Zhang, W.; Leibach, J. L.; Wilson, S. R.; Jacobsen, E. N. *J. Am. Chem. Soc.* **1990**, *112*, 2801.

43. Zhang, W.; Jacobsen, E. N. *J. Org. Chem.* **1991**, *56*, 2296.

44. Brunner. H.: Zettlmeier. W. *Handbook of Enantioselective Catalysis*. VCH: Weinheim. **1994**: Vol. 1.

45. Brunner. H.: Zettlmeier. W. *Handbook of Enantioselective Catalysis*. VCH: Weinheim. **1994**: Vol. 2.

46. Irie. R.: Noda. K.: Ito. Y.: Matsumoto. N.: Katsuki. T. *Tetrahedron Lett.* **1990**. *31*. 7345.

47. Sasaki. H.: Irie. R.: Hamada. T.: Suzuki. K.: Katsuki. T. *Tetrahedron* **1994**. *50*. 11827.

48. a) Hamada. T.: Fukuda. T.: Imanishi. H.: Katsuki. T. *Tetrahedron* **1996**. *52*. 515. b) Fukuda. T.: Katsuki. T. *Tetrahedron Lett.* **1996**. *37*. 4389.

49. Kuroki. T.: Hamada. T.: Katsuki. T. *Chemistry Lett.* **1995**. 339.

50. Hamachi. K.: Irie. R.: Katsuki. T. *Tetrahedron Lett.* **1996**. *37*. 4979.

51. Jacobsen. E. N.: Zhang. W.: Muci. A. R.: Ecker. J. R.: Deng. L. *J. Am. Chem. Soc.* **1991**. *113*. 7063.

52. Lee. N. H.: Muci. A. R.: Jacobsen. E. N. *Tetrahedron Lett.* **1991**. *32*. 5055.

53. Pospisil. P. J.: Carsten. D. H.: Jacobsen. E. N. *Chem. Eur. J.* **1996**. *2*. 974.

54. Mikame. D.: Hamada. T. Irie. R.: Katsuki. T. *Synlett*. **1995**. 827.

55. a) Linker. T. *Angew. Chem., Int. Ed. Engl.* **1997**. *36*. 2060. b) Linde. C.: Arnold. M.: Norrby. P. -O.: Akermark. B. *Angew. Chem., Int. Ed. Engl.* **1997**. *36*. 1713. c) Finney. N. S.: Pospisil. P. J.: Chang. S.: Palucki. M.: Konsler. R. G.: Hansen. K. B.: Jacobsen. E. N. *Angew. Chem., Int. Ed. Engl.* **1997**. *36*. 1720. d) Norrby. P. -O.: Linde. C.: Akermark. B.: *J. Am. Chem. Soc.* **1995**. *117*. 11305.

56. Ciringh. Y.: GordonWylie. S. W.: Norman. R. E.: Clark. G. R.: Weintraub. S. T.: Horwitz. C. P. *Inorg. Chem.* **1997**. *36*. 4968.

57. Bermejo. M. R.: Fondo. M.: GarciaDeibe. A.: Rey. M.: Sanmartin. J.: Sousa. A.: Watkinson. M.: McAuliffe. C. A.: Pritchard. R. G. *Polyhedron* **1996**. *15*. 4185.

58. Du. X. D.: Yu. X. D. *J. Polym. Sci. A - Polym. Chem.* **1997**. *35*. 3249.

59. Butterworth, A. J.; Clark, J. H.; Walton, P. H.; Barlow, S. J. *J. Chem. Soc., Chem. Commun.* **1996**, 1859.

60. Choudary, B. M.; Valli, V. L. K.; Prasad, A. D. *J. Chem. Soc., Chem. Commun.* **1990**, 1186.

61. De, B. B.; Lohray, B. B.; Sivaram, S.; Dhal, P. K. *J. Polym. Sci. A - Polym. Chem.* **1997**, *35*, 1809.

62. Ogunwumi, S. B.; Bein, T. *J. Chem. Soc., Chem. Commun.* **1997**, 901.

63. Sabater, M. J.; Corma, A.; Domenech, A.; Fornes, V.; Garcia, H. *J. Chem. Soc., Chem. Commun.* **1997**, 1285.

64. Julia, S.; Guixer, J.; Masana, J.; Rocas, J.; Colonna, S.; Annuziata, R.; Molinari, H. *J. Chem. Soc., Perkin Trans. I* **1982**, 1317.

65. Itsuno, S.; Sakakura, M.; Koichi, I. *J. Chem. Soc., Chem. Commun.* **1990**, 6047.

66. Whitesell, J. K. *Chem. Rev.* **1989**, *89*, 1581.

67. Cram, D. J. *Angew. Chem., Int. Ed. Engl.* **1988**, *27*, 1009.

68. Lehn, J. M. *Angew. Chem., Int. Ed. Engl.* **1988**, *27*, 89.

69. Lüning, U. *Concave Acids and Bases* In *Topics in Current Chemistry*, Weber, E. Ed.; Springer: Berlin, **1996**; Vol. 175.

70. Scrimin, P.; Tecilla, P.; Tonellato, U.; Veronese, A. *Transition Metal Ion-Based Supramolecular Catalysts* In *Molecular Design and Bioorganic Catalysis*. Wilcox, C. S. ; Hamilton, A. D. Eds.; Kluwer: Dordrecht **1996**; and references therein.

Chapter 2

Synthesis and Characterization of Chiral Macrocyclic Salens

2.1 Introduction

As demonstrated for asymmetric epoxidation in Chapter 1 and reference to other asymmetric catalytic systems.[1-6] the activity and particularly the enantioselectivity of a chiral catalyst is ligand-mediated. Accordingly, design and synthesis of chiral ligands lies at the heart of asymmetric catalysis.[7] To this end, several chiral ligands for asymmetric epoxidation have been reviewed in Chapter 1. Among these ligands, porphyrin-based macrocycles with chirality located in the bridge(s) spanning one or two faces of the porphyrin plane(s) showed relatively low chiral induction.[8, 9] However, the idea of construction of a chiral macrocycle surrounding the active site seems promising because it is generally recognized that macrocycles such as cyclodextrins,[10, 11] crown ethers.[12, 13] and calixarenes[14-16] with well-defined cavities have enhanced binding abilities by virtue of non-covalent interactions. Consequently, a macrocyclic host can incorporate conformational constraints of the guest and thus possibly reduce the number of diastereoisomers during the course of a reaction.[17-19]

From a structural point of view, macrocycles possessing binuclear coordination sites

without a bridging anion create a pocket for an incoming guest and therefore are of particular interest[20] because they resemble certain metalloproteins.[21, 22] A great deal of effort has been made to mimic the function of these types of enzymes.[23] Lehn[24] indicated that macrocycles, capable of binding two metal ions in a geometry such that they could cooperatively direct a substrate within the cavity between themselves and thereby trigger a reaction on a functional group of the guest, could mimic metalloenzymes. Several such macrocycles have been reported.[25-30] For instance, recent work on the cleavage of phosphate diesters has shown that two metal centres provide enhanced electrophilic assistance. On the other hand, it is quite surprising that chiral macrocycles, especially those with a distinct cavity after coordination of metal(s), are rare. The chiral macrocycles developed so far mainly focus on stereoisomer discrimination.[31] A brief summary of their complexation behaviour toward enantiomers is presented below.

2.2 Chiral macrocycles

Chiral macrocycles can be classified, according to the components of the ring, into functionalized and unfunctionalized macrocycles. In the former case, some heteroatoms such as O, S, N, Si, or even metals are incorporated in the macrocyclic frame whereas in the latter case the ring is carbocyclic. Herein, only functionalized macrocycles are examined due to their inherent complexing ability toward transition metals.

Crown ethers[32] (Figure 2.1, **a**) are generally considered as the first generation of functionalized chiral macrocycles and have a moderate host/guest preorganization

andcomplementarity. Host/guest recognition is mainly based on H-bond formation between acidic guest protons RNH_3^+ and the Lewis base sites. i.e., oxygens of the host.

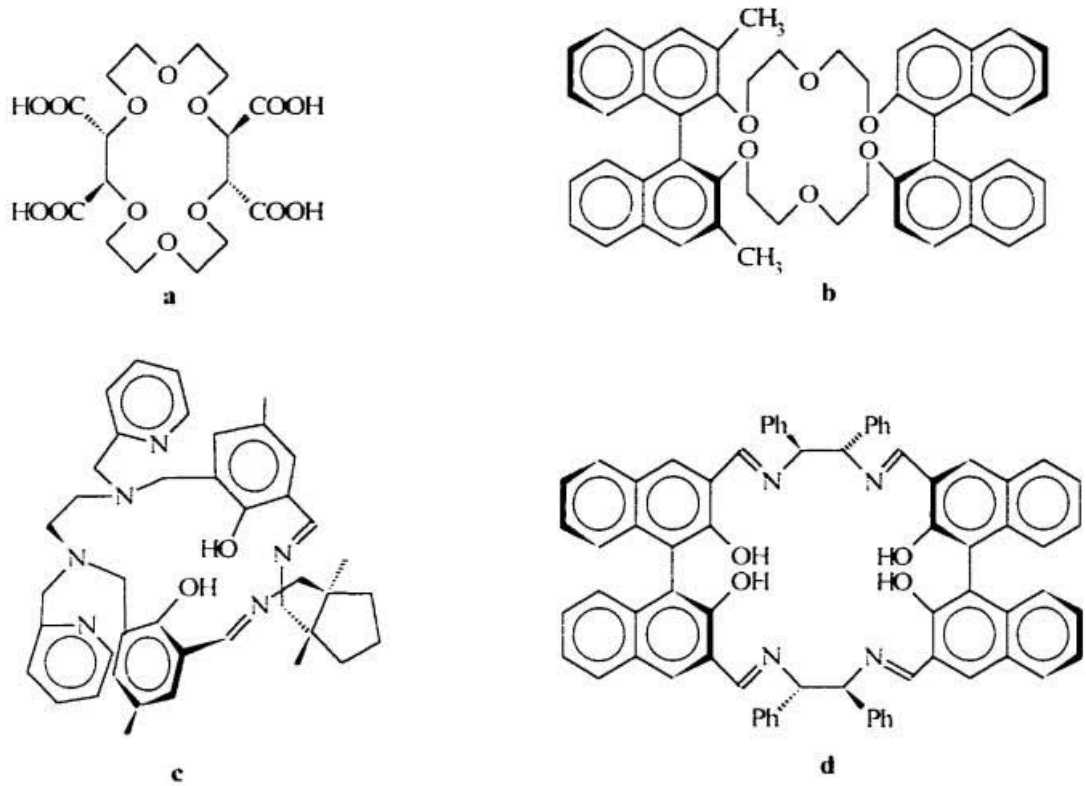

Figure 2.1 Representative functionalized chiral macrocycles

Wudl [33] first reported several chiral crown ethers synthesized from L-proline or D-ephedrine. Subsequently, Cram[31, 34] investigated the enantioselective complexation of enantiomerically pure crown ethers with optically active ammonium salts and achieved good resolution of racemates. Varying "multiplying-point-interaction," that is the difference of H-bond numbers between the host and the guest, was used to explain the observations. The phenomenon of host/guest chiroselective recognition was also

demonstrated by Stoddart[35] who concluded that stereoisomer discrimination could be improved by including several host residues of different sizes for a better steric match. Chiral crown ethers also have been used as catalysts for C-C coupling in Michael additions. An enantiomeric excess of almost 100% was achieved at very low temperature. It was believed that steric effects played a major role in the asymmetric induction.[32]

Second generation functionalized chiral macrocycles have more complicated structures. In addition to steric effects and H-bonding, $\pi-\pi$ stacking plays an important role in host/guest preorganization (Figure 2.1, **b**).[34, 36, 37] Introducing coordination site(s) for transition metals onto the macrocyclic platform forms third generation functionalized chiral macrocycles. Once complexed with a transition metal, the Lewis acids not only further enhance host/guest interactions but also create potential catalytic active sites. Fraser and Bosnich[19] prepared a series of chiral macrocyclic transition metal complexes from the binucleating ligand **c** (Figure 2.1) bearing four-(open) and six-(closed) coordination sites in which the two metals were bridged via two phenolate groups similar to the reported synthetic achiral analogies with no cavity.[38] It was found that the chiral diamine (1*S*,2*S*)-1,2-bis(aminomethyl)cyclopentane induces one topological diastereomer of the macrocyclic framework but no catalytic and stereoisomer discrimination work was reported.

Brunner and Schiessling[39] prepared a 24-membered ring chiral tetradentate salen ligand (Figure 2.1, **d**) by reaction of (*S*)-2,2'-dihydroxy-1,1'-binaphthyl-3,3'-dialdehyde and (*R,R*)-1,2-diphenylethane-1,2-diamine. Inhibited rotation of binaphthyl probably resulted in bidentate coordination-complexation of four metals rather than two. No structural information of the free ligand and complexes has been published.

Prior to this work no chiral macrocycles capable of forming an inherent cavity after complexation of two metals had been reported. Comparatively, achiral salen-crown-ether-based trinuclear complexes[40] are very interesting in that a hard alkaline earth cation is incorporated within the crown ether cavity[21, 42] and forces the two salen moieties into a *syn* conformation. Consequently, a cavity in which two metals were nearly face-to-face was formed. However, based on CPK models, it was suggested that the possibility of introducing chirality appeared unlikely.[41]

Monomeric and dimeric linear chiral salens,[39, 43] which are structurally and electronically similar to porphyrins, have been extensively explored by several groups and showed very positive results in asymmetric epoxidation (Chapter 1). Chiral macrocyclic salen dimer **e** (Figure 2.2), which is structurally analogous with diporphyrin **f**, would be expected to show promise in the same regard. In this Chapter, the synthesis and characterization of this new type of chiral salen-based macrocycles, namely chiral macrocyclic salen dimers, will be described.

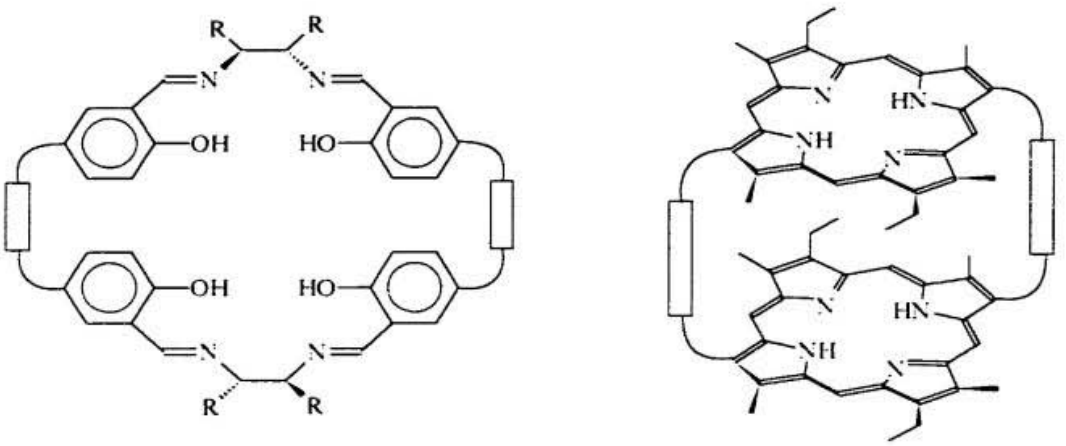

e f

Figure 2.2 Chiral macrocyclic salen (**e**) and analogous diporphyrin (**f**)

2.3 Results and discussion

2.3.1 Basic synthetic strategies

Salen and salophene moieties are known to form very stable complexes with most transition metal ions. These complexes have been widely used as catalysts and reagents in various asymmetric reactions such as epoxidation, epoxide ring-opening,[44-46] oxidation of sulfides,[47-49] cyclopropanation,[50, 51] and Diels-Alder reactions.[52] Macrocyclic salen dimers that contain two salen units are excellent targets. Since they have more free positions to be modified simply by changing the bridges or the substituents on the phenol rings; the salen dimers are electronically more adjustable. Furthermore, complexes derived from these salen dimers would be more stable than the corresponding monomeric salens because of the macrocycle effect. Tailoring of complexes to achieve high activity,

stability, and selectivity might therefore be possible. In this study, the desired macrocyclic salen dimers with different shapes and sizes were constructed through template-directed synthesis using three types of dialdehydes and enantiomerically enriched (*1R,2R*)-(-)- or (*1S,2S*)-(+)-cyclohexane-1,2-diamine as the molecular building blocks (Figure 2.3). For the purpose of comparison, a linear dimeric salen was also synthesized through controlled condensation (Figure 2.3). The outcome of self-assembly

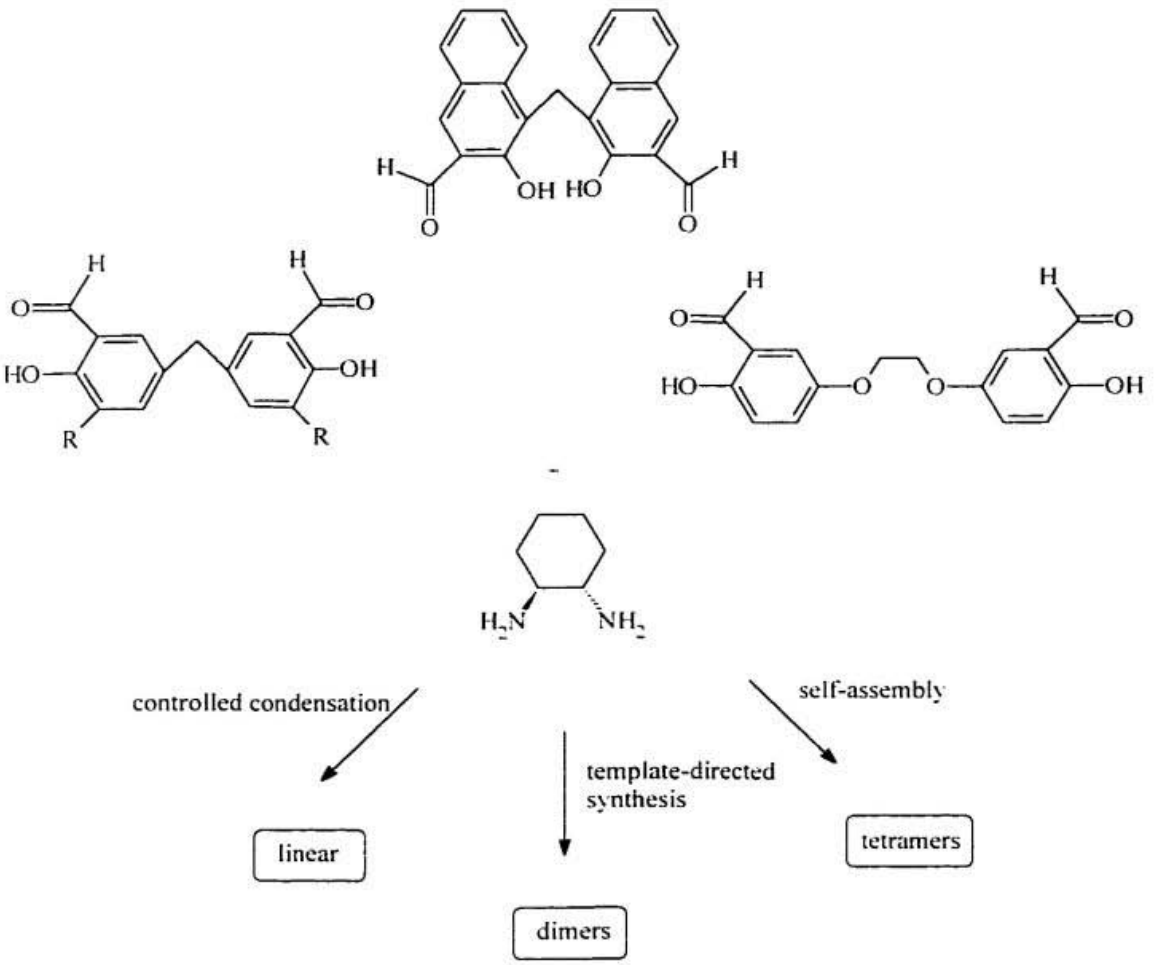

Figure 2.3 Synthetic strategies for chiral macrocyclic salens and linear salen

of dialdehydes and the diamine was also examined (Figure 2.3).

2.3.2 Syntheses of dialdehydes

As shown in Figure 2.3, the crucial starting materials for syntheses of the macrocyclic salen dimers or linear salen are the dialdehydes. Since they were not commercially available, syntheses of these three types of dialdehydes were carried out and illustrated below.

2.3.2.1 Synthesis of 5,5'-methylene-bis-salicylaldehydes 3a-3d

Initial attempts to synthesize salicylaldehydes **2b-2d** through selective *ortho*-formylation of phenols (**1b-1d**) with formaldehyde in the presence of hexamethylphosphoramide (HMPA) in benzene were unsuccessful.[53] An alternative route,[54] treatment of phenols (**1b-1d**) with 2 equivalents of paraformaldehyde in the aprotic and poorly electron-donating solvent toluene in the presence of $SnCl_4$ and tri-*n*-butylamine, was used to obtain the aldehydes **2b-2d** (Scheme 2.1). Chromatography on silica gel (hexane/ethyl acetate), gave **2b-2d** as pale yellow liquids. Subsequent reactions of **2a-2d** with 1,3,5-trioxane in AcOH using H_2SO_4 as a catalyst[55] afforded the dialdehydes **3a-3d** as pale yellow to yellow crystalline solids in yields of 60-70% after chromatography on silica gel (hexane/ethyl acetate) or crystallization from hexane.

Mass spectral data were consistent with the proposed composition as evidenced by

molecular ions that appeared at *m/z* = 256 for **3a**, 284 for **3b**, 340 for **3c**, and 368 for **3d**. The ^{1}H and ^{13}C NMR spectra suggested symmetrical structures for **3a-3d**. Six signals, assigned to the six aromatic carbons of the two phenol groups, were observed for **3a**, **3b**,

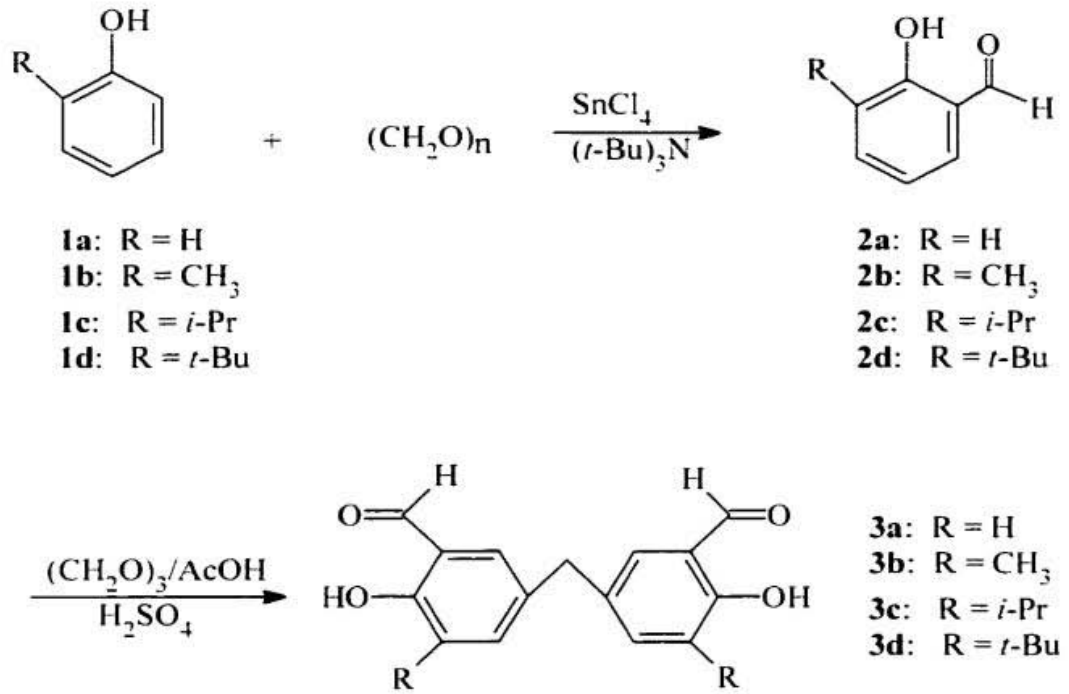

Scheme 2.1 Syntheses of the dialdehydes **3a-3d**

3c, or **3d** at low field. ^{13}C resonances at 196.6 ppm for **3a**, 196.8 ppm for **3b**, 196.9 ppm for **3c**, and 197.2 ppm for **3d** were assigned to the aldehyde groups. A high field peak at 39.5 ppm was assigned to the methylene bridge for **3a**; two peaks at 39.7 ppm and 15.3 ppm were ascribed to methylene bridge and -CH_3 for **3b**; three peaks at 40.0, 26.5, 22.4 ppm corresponded to methylene bridge, and *i*-Pr for **3c**; three peaks at 40.2, 35.0, 29.4

ppm were assigned to the methylene bridge and *t*-Bu group for **3d**.

2.3.2.2 Synthesis of 5-[2-(3-formyl-4-hydroxyphenoxy)ethoxy]-2-hydroxybenzaldehyde 6

Regio-controlled partial *O*-alkylation of polyphenolic compound **4** with **5** to prepare dialdehyde **6** was performed under an inert atmosphere. 2,5-Dihydroxybenzaldehyde, **4**, was treated with 2 eq. of NaH in dry DMSO to give the dianion. Subsequent reaction with ethylene glycol ditosylate **5** in DMSO generated the desired dialdehyde **6** in 60% yield after acidic workup and chromatography (Scheme 2.2).[22]

A molecular ion at *m/z* =302 in the mass spectrum confirmed the formula of the isolated

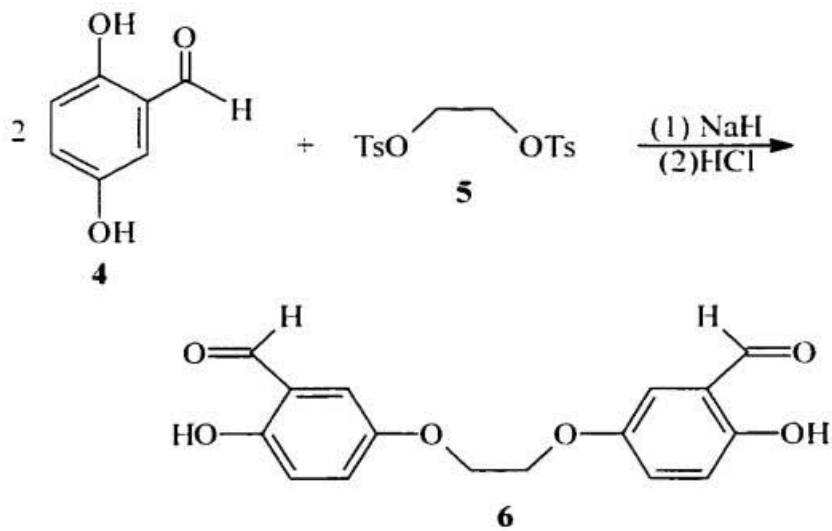

Scheme 2.2 Synthesis of the dialdehyde **6**

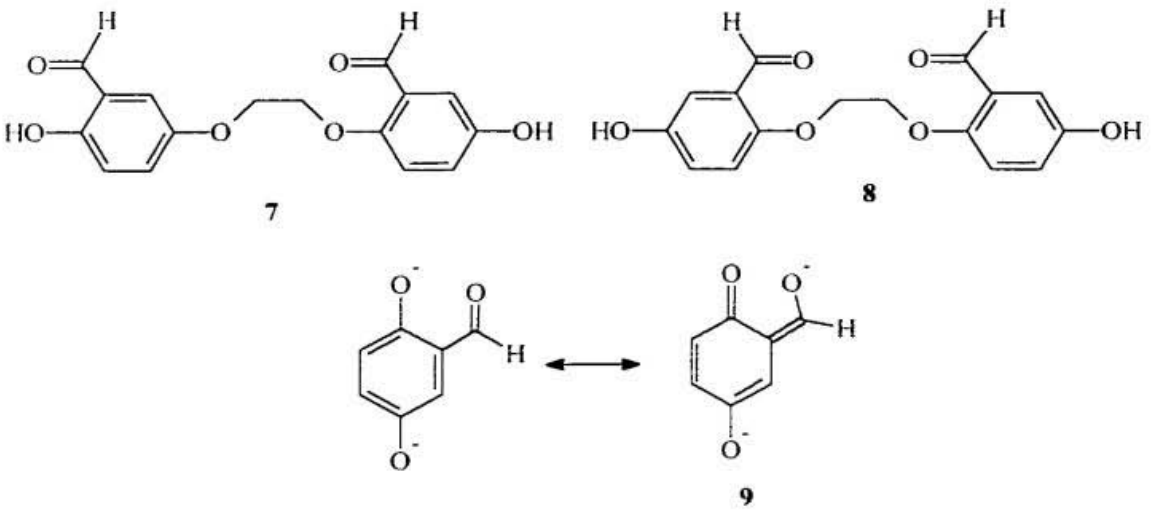

Figure 2.4 Possible products in the *O*-alkylation reaction

product as $C_{16}H_{14}O_6$. The ^1H NMR spectrum was consistent with the dialdehyde structure **6**. The ^{13}C NMR spectrum showed a signal at 196.2 ppm which was assigned to the aldehyde carbon. Only were three aromatic carbon signals observed. The bridge ethylene glycol (-OCH_2CH_2O-) carbons appeared as one signal at 67.8 ppm.

These spectroscopic results excluded structure **7** but could not rule out the possibility of **8** (Figure 2.4). Dialdehyde **8** was, however, less likely because of resonance **9**, which is conjugated and leaves the phenolic site open for *O*-alkylation. See Chapter 4 for the ligand structure.

2.3.2.3 Synthesis of 3-[(3-formyl-2-hydroxy-1-naphthyl)methyl]-2-hydroxy-1-naphthaldehyde 12

Starting from 2-hydroxy-1-naphthoic acid **10**, the dialdehyde **11** was obtained as a yellow

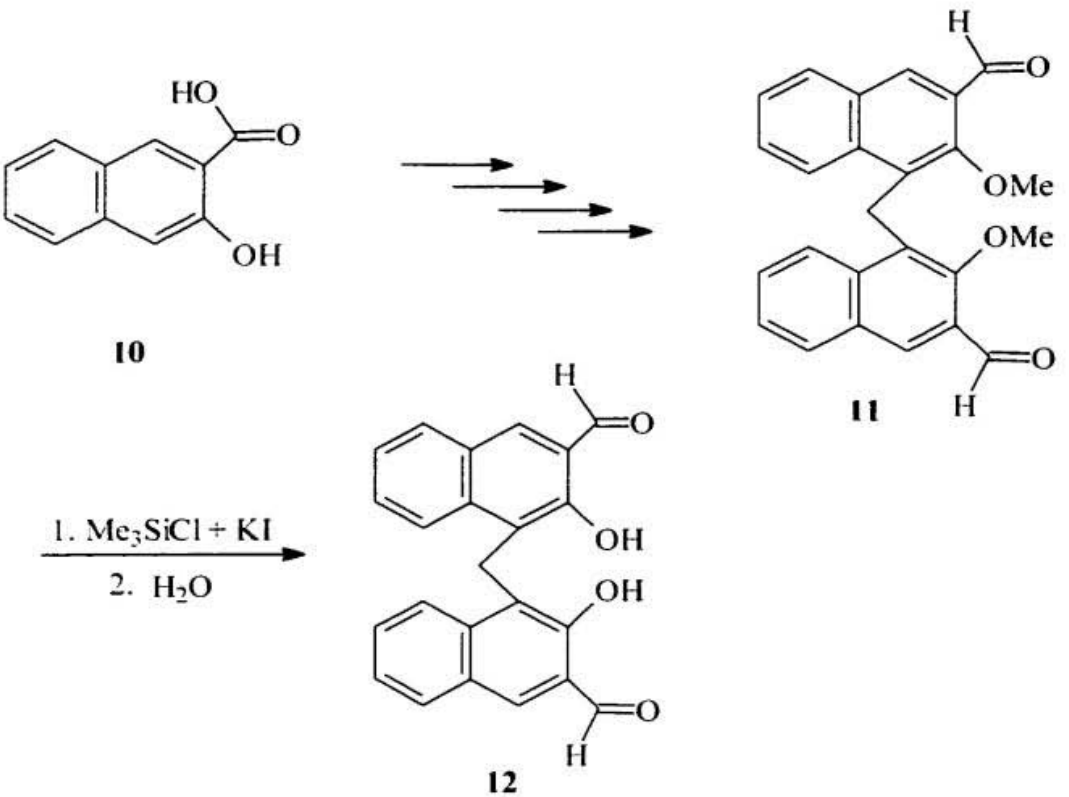

Scheme 2.3 Syntheses of the dialdehydes **11** and **12**

solid according to the route as shown in Scheme 2.3.[56] Attempts to demethylate the protected OH groups by refluxing of dialdehyde **11** with BCl_3 in CH_2Cl_2 overnight did not give **12**.[56] Thin-layer chromatography (TLC) showed only the starting material. Demethylation with Me_3SiCl/KI did produce the desired dialdehyde, but the yield was poor (15%). No further attempts were made.

2.3.3 Preparation of (*1R,2R*)-and (*1S,2S*)-cyclohexane-1,2-diamine 13

Preparation of enantiomerically enriched cyclohexanediamine **13** from the corresponding salt of (*1R.2R*)- or (*1S.2S*)-cyclohexane-1.2-diamine-L-tartrate was carried out according to a modified procedure initially developed by Galsbøl *et al.*[57] After release from the salt by treatment with aqueous KOH, the diamine was extracted with ether and dried over sodium metal. Crystallization at room temperature from ether afforded **13** as clear colourless crystals in good yield (75%). The ^{1}H NMR was consistent with that of an authentic sample from Aldrich.

2.3.4 Template-directed syntheses for 2+2 dimers 14a-14d

Synthesis of macrocycles using template-directed reactions in the presence of a metal ion and high dilution conditions has been shown to be an effective technique.[58] It is generally believed that coordination to the cationic template serves to promote appropriate folding of the growing chain and favours cyclization.

Initial attempts to cyclize the dialdehydes **3** and (*1R.2R*)- or (*1S.2S*)-cyclohexane-1.2-diamine **13** with transition metal ions such as Ni(II) or Cu(II) resulted in the formation of a red or pale blue solid, which did not dissolve in any organic solvents. Barium salts proved to be beneficial in the cyclization of the dialdehyde **3** with the diamine **13**. The reaction was carried out under high dilution by simultaneous slow addition of a solution

of **3** in THF and a solution of **13** in methanol to a solution of $Ba(SCN)_2$ or $Ba(ClO_4)_2$ in THF/MeOH (1:1) at room temperature (Scheme 2.4). The condensation reaction was facile and reliable. Mixing the dialdehyde and the diamine immediately gave a bright yellow solution.

Cyclization of the dialdehyde **3d** and the (*1R,2R*)-diamine **13** with $Ba(SCN)_2$ resulted in three major products with different R_f values on TLC. After the reaction was complete (4 h), slow addition of MeOH to the reaction mixture produced a yellow precipitate identical with the lowest R_f value product, in about 15% yield. Further purification of the precipitate was accomplished by filtration followed by washing with acetone until the washings were colourless. Chromatographic purification (hexane/ethyl acetate, TLC) of the filtrate (yellow solution) afforded the other two products in yields of 7% and 11%. The three products were all air stable and had good solubility in common organic solvents.

The two products isolated from the filtrate, which were confirmed to be the dimer **14d** and trimer **15d** (see below), showed similar ^1H NMR (Figure 2.5, p. 52) and IR spectral patterns and had the same number of ^{13}C NMR peaks. The third product **16d** obtained from the precipitate also showed a spectroscopic pattern similar to that of the dimer **14d** except a peak at around 2.15 ppm, which was ascribed to inclusion-water-molecules.

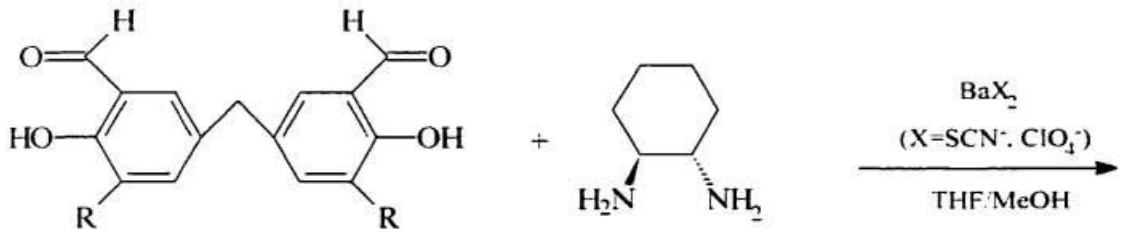

3a: R = H
3b: R = CH_3
3c: R = *i*-Pr
3d: R = *t*-Bu

13

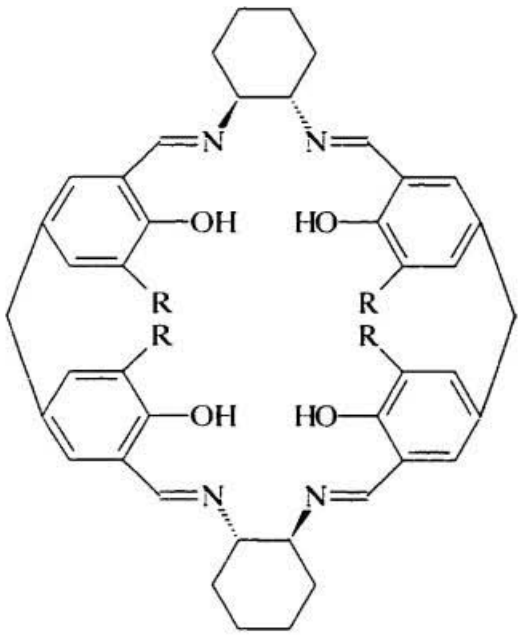

14

+ trimer + tetramer

15 **16**

a: R = H
b: R = CH_3
c: R = *i*-Pr
d: R = *t*-Bu

Scheme 2.4 Template-directed syntheses of chiral macrocyclic salens **14**, **15**, and **16**

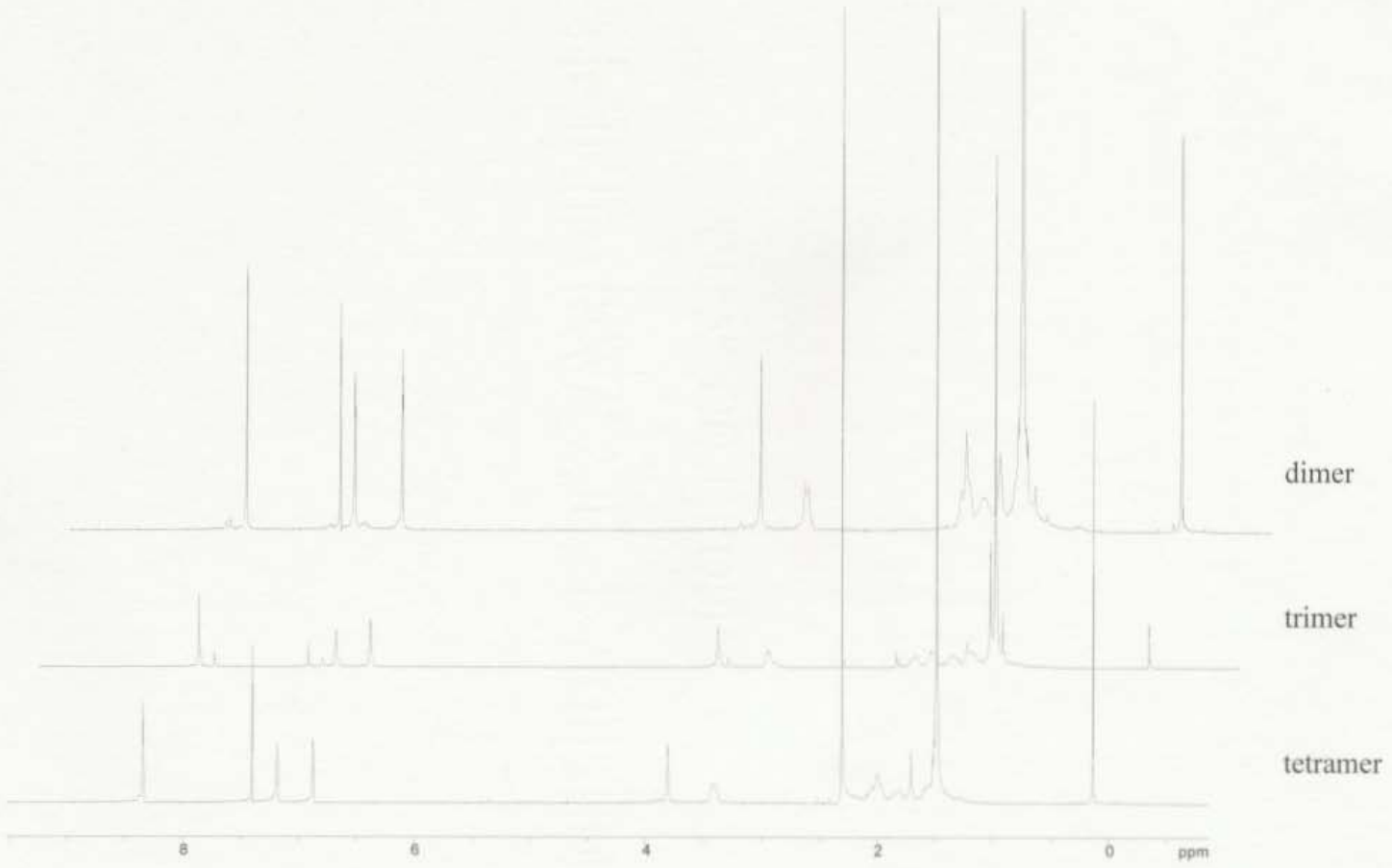

Figure 2.5 ^{1}H NMR spectra of the dimer **14d**, trimer **15d** and tetramer **16d** in $CDCl_3$

Identification of the three cyclic products was made on the basis of mass spectral evidence. Figure 2.6 shows mass spectra of two of the cyclization products formed from **3d** and the diamine **13**. The most mobile product on TLC had peaks at *m/z* 893 (100%), 894 (74%), and 895 (30%), which were consistent with those calculated for the **2+2** metal-free [dimer **14d** + H]$^+$ isotope. The peak at *m/z* = 911 (27%) was the **14d** plus a H_3O^+ ion. The second product showed peaks at *m/z* 1339 (100%) and 1340 (95%), consistent with the isotope of **3+3** [trimer **15d** + H]$^+$. The peaks at *m/z* = 1358 (72%) and 1359 (42%) were the **15d** isotope plus a H_3O^+ ion. The last product did not give a molecular ion in the mass spectrum, but it was believed to be a **4+4** tetramer **16d**.

The ^{1}H NMR chemical shift assignments for the dimer **14d**, trimer **15d**, and putative tetramer **16d** were based on HETCOR analysis (A representative HETCOR for the dimer **14d** is shown in Figure 2.7, p. 55). The phenolic protons were observed at low field: 13.77 ppm for dimer **14d**, 13.80 ppm for trimer **15d**, and 13.77 ppm for tetramer **16d**, indicating that the hydroxy groups in the dimer, trimer, and tetramer were all very acidic. The four imine protons in the dimer **14d** gave one signal at 8.07 ppm. The imine protons of trimer **15d** and tetramer **16d** were identical and appeared as one signal at 8.21 ppm. The bridge methylene protons also appeared as a singlet (3.63 ppm in **14d**, 3.72 ppm in **15d**, and 3.67 ppm in **16d**).

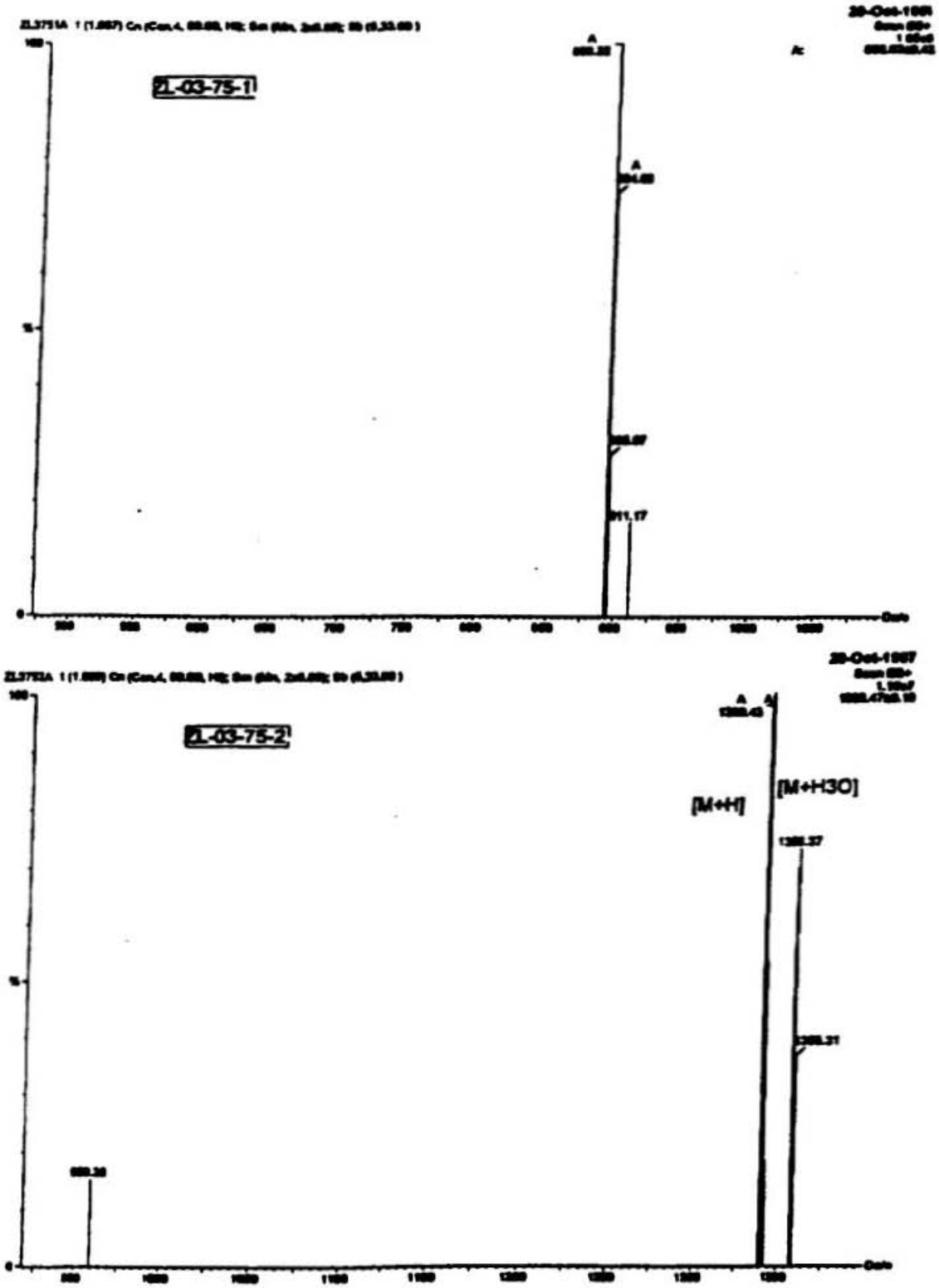

Figure 2.6 ES-MS spestra of the macrocyclic salen dimer **14a** (top) and trimer **15d** (bottom)

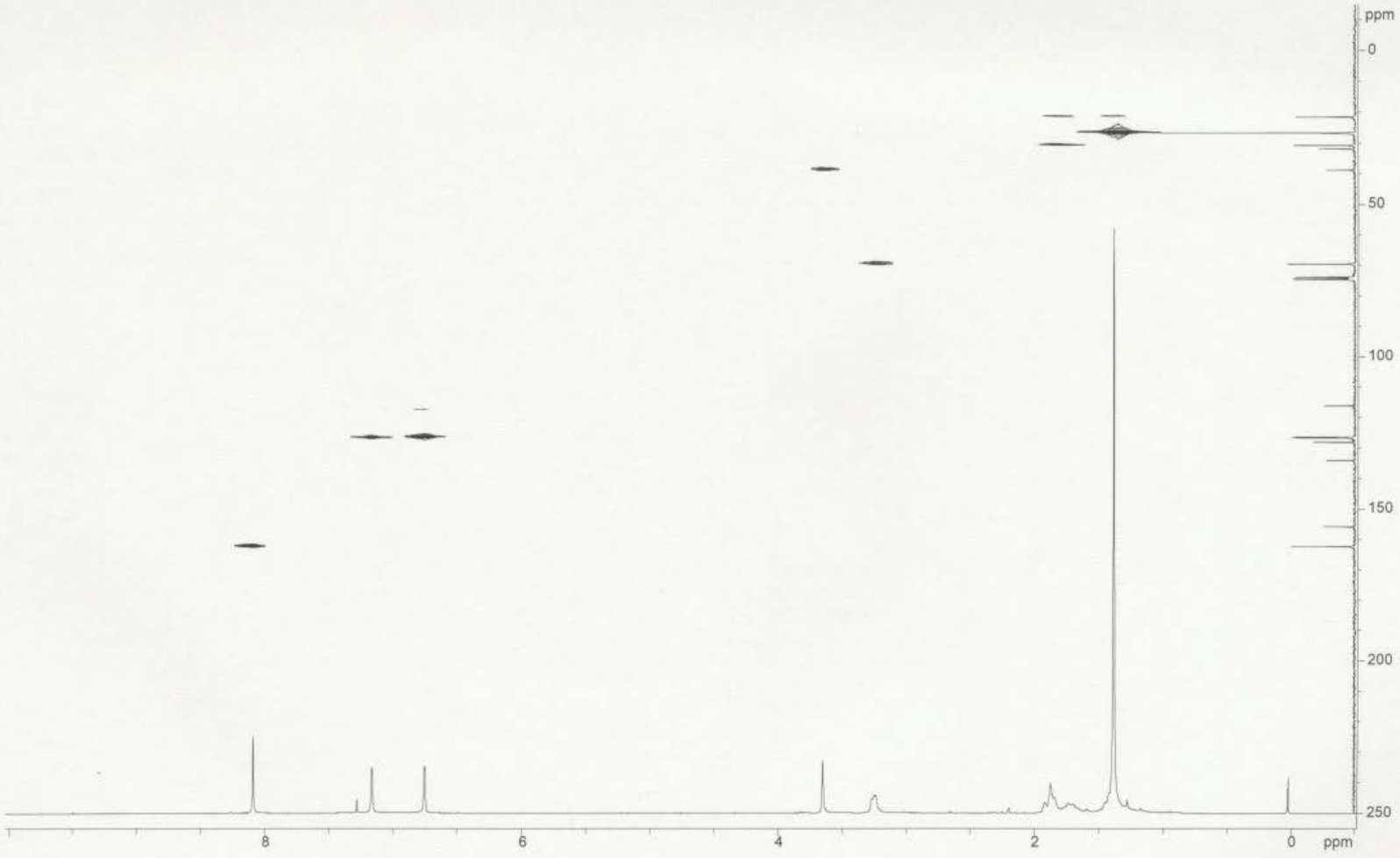

Figure 2.7 HETCOR of the macrocyclic salen dimer **14d** in $CDCl_3$

As the volume of the R group increased along the series of H, CH_3, *i*-Pr, to *t*-Bu, the yield of tetramer increased whereas those of dimer and trimer decreased. When R = H, CH_3, or *i*-Pr, **2+2** and **4+4** products were obtained in yields of 30-20% and 7-10%, respectively. When R = *t*-Bu, **2+2**, **3+3**, and **4+4** products were all separated in yields of 10%, 7%, and 15%, respectively. These results showed that dialdehydes with bulky R groups disfavoured the formation of the dimers. ^{1}H NMR and ^{13}C NMR spectroscopic assignments for each dimer **14a-14c** were based on HETCOR spectra.

The simplicity of the ^{1}H NMR spectra of all dimers **14a-14d** ruled out the possibility of catenanes and suggested that the dimers were symmetric. The ^{13}C NMR spectra provided the clearest evidence regarding the macrocycle structure. There were seven resonances at low field, corresponding to one of the four equivalent imine C=N carbons and six of the twenty four aromatic carbons for each macrocycle **14a-14d**. Consistent with overall D_2 symmetry, four (**14a**), five (**14b**) and six (**14c**, **14d**) high field signals were observed for the remaining carbons. Furthermore, the sharp ^{1}H NMR peaks implied that the molecules were either conformationally rigid or completely mobile on the NMR time scale.

A well formed single crystal of dimer **14a** was obtained by slow evaporation of a DMF

---

[a]Crystal data for **14a** ($C_{42}H_{40}O_4N_4$·DMF): fw = 737.90; yellow, crystal dimensions 0.400 x 0.200 x 0.400 mm; monoclinic, space group $P2_1/c$ (#14), a = 14.640(3), b = 25.679(4), b = 81.97 (2), c = 11.045(6) Å, β = 81.97(2)°, V = 4112(4) Å^3, Z = 4, 5858 unique

solution. Its molecular structure[a] was determined by X-ray crystallography. An ORTEP view of the structure of **14a** is shown in Figure 2.8.

The molecular structure of **14a** showed that the four benzene units adopted an 1.3-alternate conformation (Figure 2.8) with overall D_2 molecular symmetry. Consequently, the hydroxyl groups also deviated from planarity with respect to the imine groups. The *trans*-array of the two closest CH=N bonds and the constrained angles of the sp^3 hybridized methylene bridge might force this arrangement. For example, the intramolecular bond angles of 109.2° for [C(10)-C(14)-C(15)] and 112.8° for [C(31)-C(35)-C(36)] showed a modest 3° increase in comparison to the angles in a tetrahedral sp^3. No hydrogen-bonding between adjacent OH groups was evident in the 1.3-alternate conformation. The two opposing benzene rings were almost face-to-face with a distance of 7.6 Å. As shown in Figure 2.8 the four benzene rings define a calixarene-like structure which we have named a "calixsalen".[62]

When $Ba(ClO_4)_2$ was used as the template, the **3+3** products were not found for R =H, CH_3 and *i*-Pr. The major products were found to be the **2+2** dimers **14a-14c** and small

---

reflections. $R = 0.077$, $R_w = 0.045$, $D_{calcd} = 1.192$ g/cm^3; average CH=N bond length 1.25 Å. Details of the structure determination, crystal data, data collection parameters, atomic coordinates, bond distances, bond angles, and torsional angles can be found in Appendix 1.

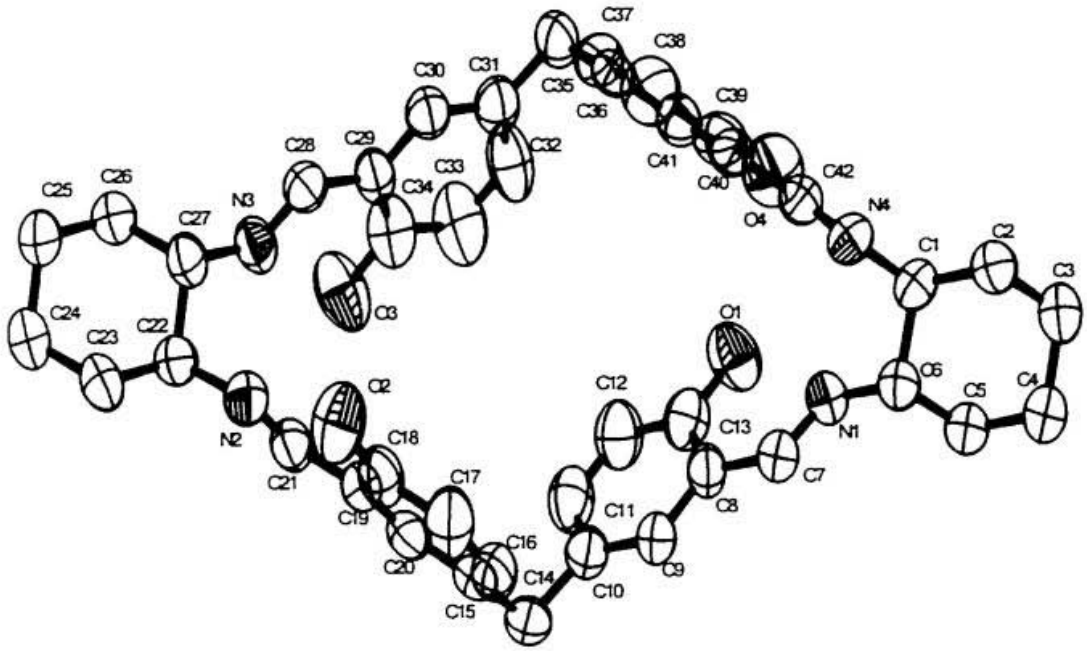

Figure 2.8 ORTEP representation of the calixsalen **14a** (Solvent DMF and hydrogen atoms were removed for clarity.)

amounts of the **4+4** tetramers **16a-16c**. $Ba(ClO_4)_2$ was therefore used in all further preparations of the more rigid **2+2** dimers **14a-14d**. Similar results were obtained from the condensation reactions of (*1S,2S*)-cyclohexane-1,2-diamine and dialdehydes **3a-3d**.

2.3.5 Effects of reaction conditions on the cyclization

2.3.5.1 Template effects

To avoid potentially explosive perchlorates, other metal salts were used to test the cyclization reaction between **3a** and (*1R,2R*)-cyclohexane-1,2-diamine (Table 2.1). With

Mn^{3+} as the template, dark brown, presumably Mn^{3+} salen complexes were found. Tests for cyclization with alkali metal salts gave dimeric product. A larger ion appeared to increase the yield of the dimer ($K^+ > Na^+$), but the yield was still lower than that obtained with Ba^{2+} salts. Based on those observations, $MoO_2(AcAc)_2$ was examined in the template cyclization reaction. The resulting yellow reaction mixture was not soluble in common organic solvents except DMF. Therefore, transition metals tested were not suitable templates for the cyclization reactions.

Table 2.1 The template effect on dimerization of dialdehyde **3a** and the diamine **13**

template	$Ba(ClO_4)_2$	NaCl	KCl	$Mn(OAc)_3$	$MoO_2(AcAc)_2$
dimer yield	45%	5%	8%	not observed	not observed

2.3.5.2 Reaction temperature and time

Using $Ba(ClO_4)_2$ as a template, the effects of reaction temperature and time on the cyclization are summarized in Table 2.2. When the reactions were performed at 25°C, increasing the reaction time decreased the dimer yield and favoured the formation of tetramer. The appropriate reaction time was found to be *ca.* 4 h. A reaction temperature of 50°C was optimal for preparation of the monomeric salen;[63,64] however, the dimer yield was very low and less soluble yellow precipitates, presumably of oligomeric mixtures, dominated.

Table 2.2 The effect of temperature and time on dimerization for **14a**

Temperature	time (hr)	results
	1	no dimer
25°C	4	45% dimer
	overnight	10% dimer
50°C	4	no dimer

2.3.5.3 Solvent effects

Since barium salts have very poor solubility in less polar organic solvents, methanol was used as a co-solvent in all reactions. As shown in Table 2.3 the best solvent system found was THF:MeOH=1:1.

Table 2.3 Solvent effects on the formation of the dimer **14a**

Solvents (1:1)	THF/MeOH	CH_2Cl_2/MeOH	$CHCl_3$/MeOH
dimer yield (%)	40~45	30	20

2.3.6 Template-directed synthesis of macrocyclic salen dimer 17

In order to alter the cavity size, the methylene bridges in **14a** were replaced with longer ethylene glycol links to form a 32-membered macrocyclic ring (Scheme 2.5). With $Ba(ClO_4)_2$ as the template, the **2+2** cyclization of dialdehyde **6** and the chiral diamine **13**

afforded **17** as a pale yellow solid in 45% yield after chromatography.

Ion spray mass spectra gave strong peaks at *m/z* =760 and 778. corresponding to the mass of the salt-free dimer **17** and the dimer plus one water molecule. The ^{1}H NMR spectrum of **17** displayed a series of signals. Four imine signals at 8.05. 8.07. 8.08. and 8.09 ppm with an intensity ratio of 1:2:4:15 were observed by 500 MHZ NMR at room temperature. Two sets of aromatic proton signals were apparent and they showed very similar ^{1}H NMR patterns. These observations suggested the presence of possible four conformers with two in dominant for the dimer **17** in solution (See next section for conformational

analysis). HETCOR and COSY experiments of **17** supported this interpretation.

The ^{13}C NMR spectrum of the dimer **17** showed double the number of carbon peaks which would be expected for D_2 symmetry. Two imine carbon resonances in a ratio of 1:3 appeared at 164.9 ppm and 164.5 ppm. Twelve aromatic carbon signals were observed. The signals of the stereogenic carbons were present at 72.7 ppm and 72.6 ppm.

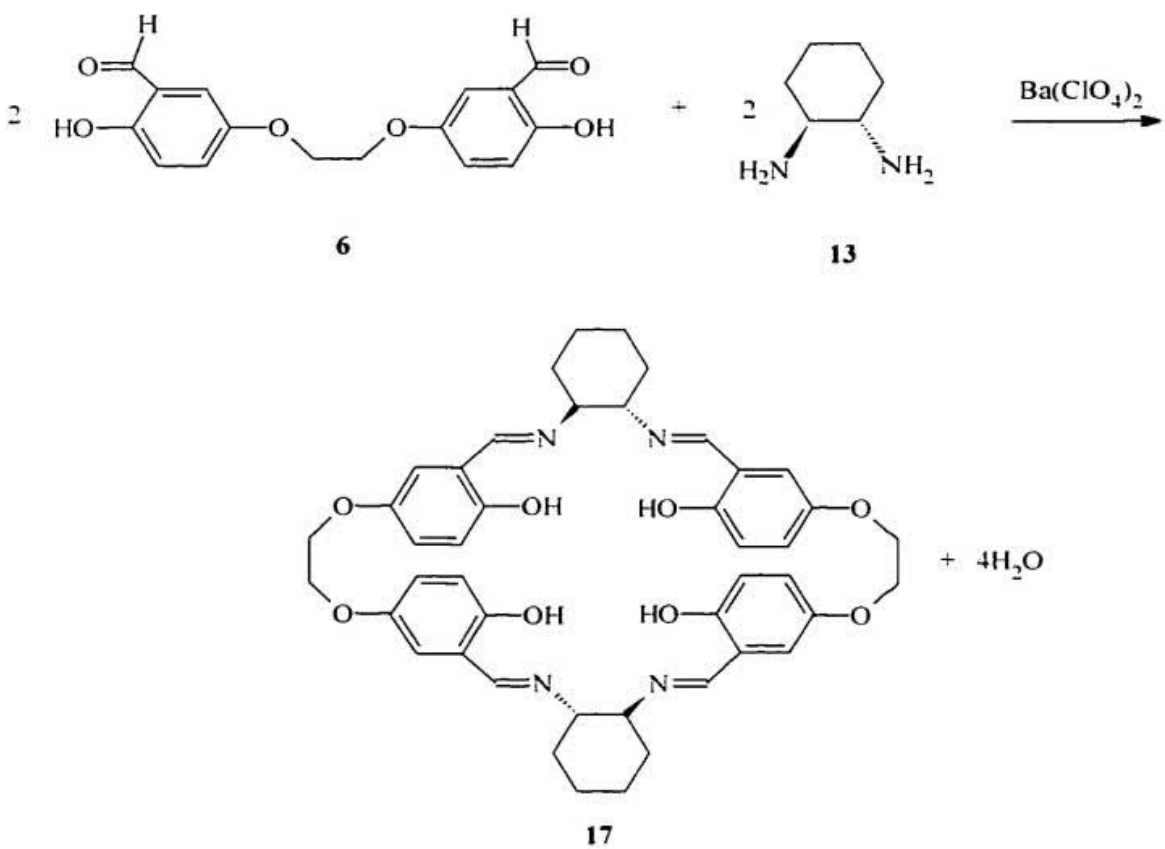

Scheme 2.5 Synthesis of the chiral macrocyclic salen dimer **17**

There were also two ethylene signals at 66.8 ppm and 67.5 ppm and two methylene

carbon signals at 32.9 ppm and 32.8 ppm assigned to the cyclohexyl ring. Another two methylene carbon signals were found at 24.2 ppm as indicated by a almost doubled intensity. The remaining ^{13}C NMR signals of the minor conformations were not observed.

Considering the product distribution pattern observed in the cyclization of dialdehyde **3d** and the diamine **13**, it is likely that the cyclization of dialdehyde **6** and the diamine also would generate a trimer, and a tetramer. Therefore, the remaining solid after initial chromatographic separation, was further separated by preparative TLC using the same eluent. However, instead of trimer or tetramer, another portion of the dimer was obtained in about 10% yield.

2.3.7 Conformational studies of the macrocyclic dimer 17

As discussed in the previous section, the dimer **17** was conformationally mobile at room temperature. Rotation of the phenol rings and the flexible ethylene glycol bridges might made the non-rigidity possible. Comparison of the calixsalen structure **14a** with calix[4]arenes suggested that the four conformers observed by ^{1}H NMR were the 1,3-alternate, 1,2-alternate, cone and partial cone (Figures 2.9 and 2.10). MMX molecular modelling analysis via PC Model V6.0 (Serena software) revealed that the conformation energy (kJ/mole) followed the order: $E_{1,3\text{-alt}}(318) < E_{1,2\text{-alt}}(355) < E_{\text{partial cone}}(422) < E_{\text{cone}}$ (439). Hence, the major species was assigned to the 1,3-alternate and the second most

abundant species was assigned to the 1,2-alternate conformer. Since the difference in the chemical shifts between the imine protons of the conformers was measurable (*ca.* 0.02 ppm): it was possible to calculate a minimum rotational barrier of about 16 kJ/mole.

Variable Temperature (VT) NMR studies at 300 MHZ confirmed the above conclusions. Upon warming the sample to 55°C. the two imine carbon signals observed at RT. coalesced into one and the ten aromatic signals reduced to nine. However. the bridge carbon signals remained unchanged. Therefore. the two major conformers most likely stemmed from phenol ring rotation.

^{1}H NMR experiments at -30°C and - 50°C on the calixsalens **14a** and **14d** with the short methylene link showed no signal coalescence. indicating that the 26-membered macrocyclic dimers. unlike the 32-membered relatives. were conformationally stable. on the above results. it appeared that the shorter methylene link between the two a salen moieties might lock the macrocycle conformation and thereby would benefit Based symmetric induction.

2.3.8 Template-directed synthesis of chiral macrocyclic salen dimer 18

In addition to modifying the cavity shape by changing the substituents on the phenyl rings such as in **14a-14d** and replacing the bridge to adjust the cavity size such as in **17**. it is

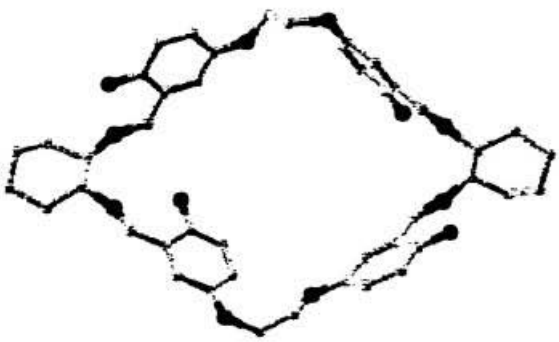

1,3-alternate

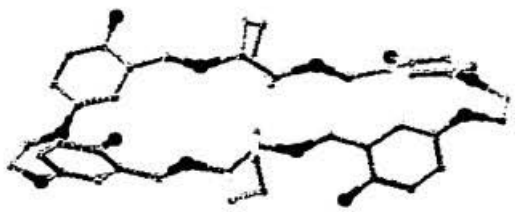

1,2-alternate

Figure 2.9 Possible conformers of the calixsalen **17**

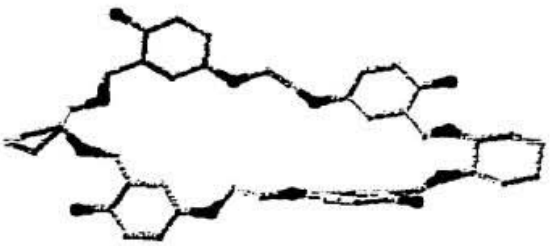

partial cone

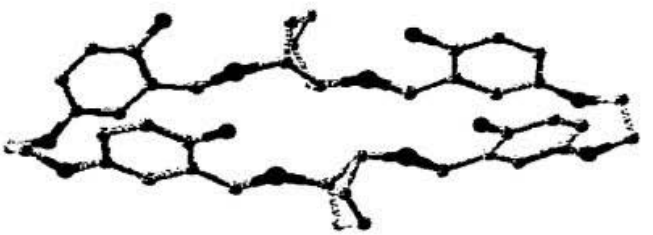

cone

Figure 2.10 Possible conformers of the calixsalen **17**

also possible to tune the depth of the cavity by replacing the four benzene rings (each has a width of *ca.* 6.8 Å) by naphthalene rings (each has a width of *ca.* 8.4 Å[56]). Based on this consideration, the macrocyclic salen dimer **18** was prepared according to the route shown in Scheme 2.6. Condensation of dialdehyde **11** and the chiral diamine **13** was performed in THF/MeOH (1:1) with $Ba(ClO_4)_2$ as template at gentle reflux (There was no

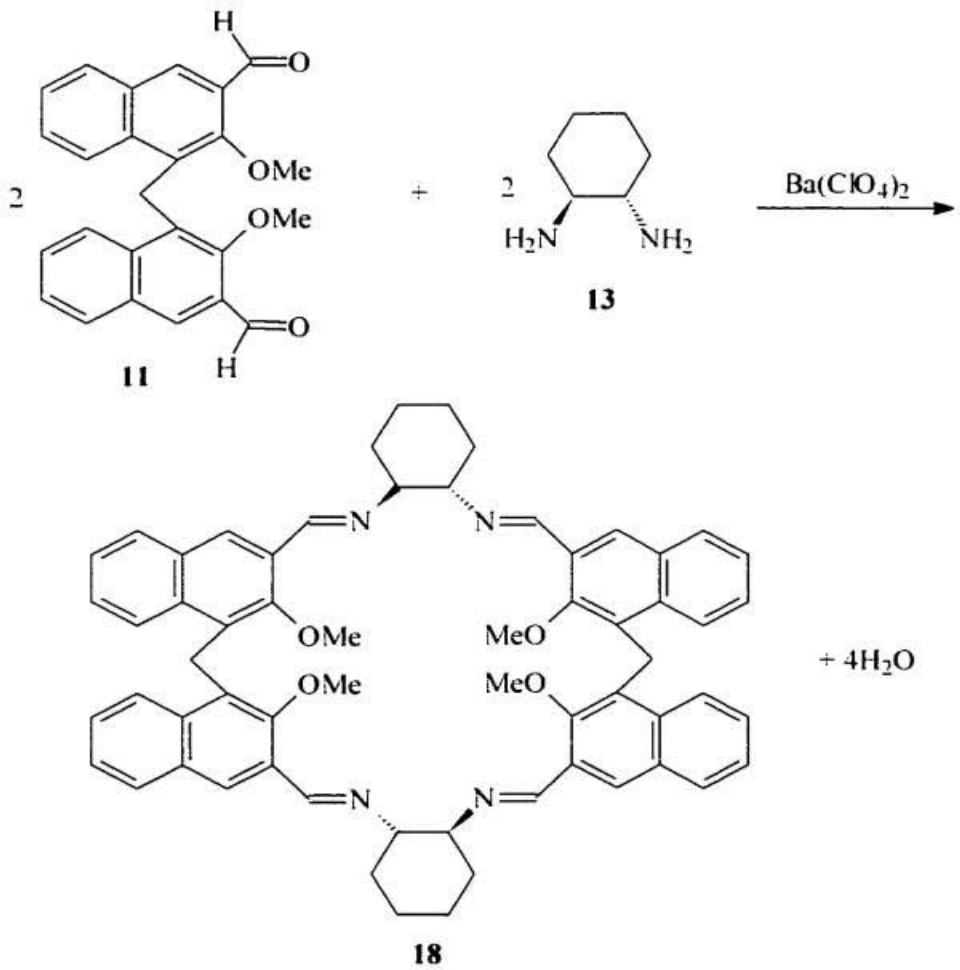

11 **13** **18**

Scheme 2.6 Synthesis of the macrocyclic dimer **18**

reaction at room temperature). The reaction was followed by TLC. After 6 h, a resultant white precipitate was collected by filtration and washed with MeOH. Crystallization from toluene afforded an off-white solid.

The mass spectral peak at m/z = 925 was consistent with the molecular ion [**dimer 18**+ H]$^+$. In the ^{1}H NMR spectrum, an imine signal at 8.42 ppm was overlapped with a naphthalene proton signal (J=7.5 Hz). Unlike the conformationally flexible calix[4]naphthalene[56] in which an AB system was normal for the methylene bridge, the two methylene protons were equivalent (4.61 ppm) in the dimer **18**.

As pointed out previously, the methylene bridge carbon appeared around 41 ppm in macrocycle **14a-14d**; however, in the naphthalene system it was strongly shielded (22.8 ppm). This comparison demonstrated that replacement of benzene with naphthalene changed the dimer properties not only geometrically but also electronically. A difference also can be seen for the imine groups. The imine carbon signals, which appeared at about 165 ppm for dimers **14a-14d**, occurred at 157 ppm for dimer **18**, indicating that the C=N bonds were relatively electron rich in the naphthalene salen dimer.

2.3.9 Directed synthesis of chiral linear salen dimer 20

In order to compare with macrocyclic salens, a linear salen dimer was synthesized

according to the route shown in Scheme 2.7.[65,66] The half-unit **19**, generated by reaction of (*1R,2R*)-(-)-cyclohexane-1,2-diamine and phenol aldehyde **2d** in highly dilute $CHCl_3$

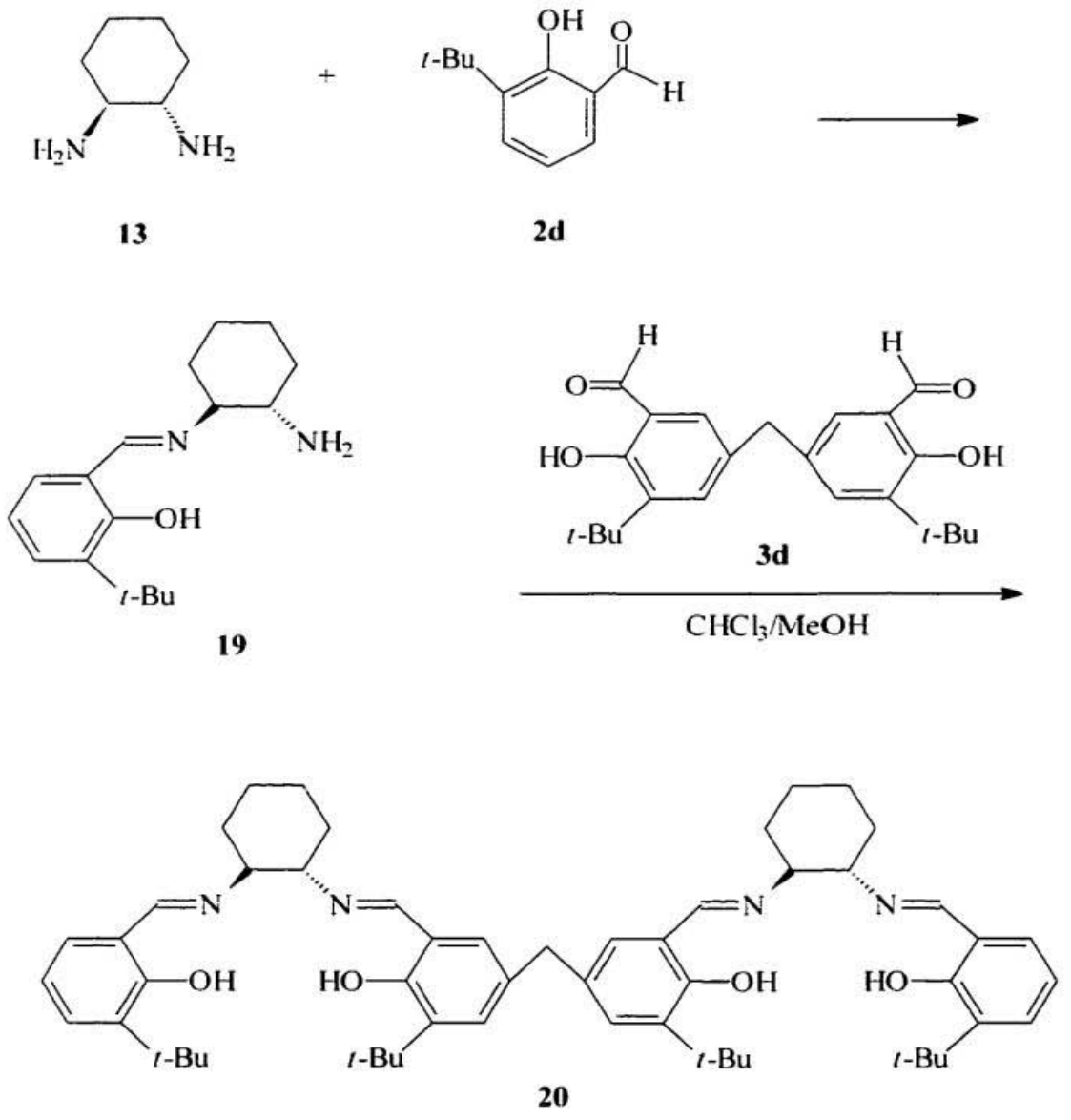

Scheme 2.7 Synthesis of the chiral linear dimeric salen **20**

solution, was very unstable and easily converted to monomeric salen. Attempts to isolate the half-unit failed. The next step was therefore performed *in situ*. A small amount of MeOH was first added to the solution to break the intramolecular hydrogen bonding between -OH and NH_2, the dialdehyde **3d** was then directly introduced to the solution containing the half-salen unit over a period of 24 h. After stirring for an additional 6 h, solvents were evaporated at oil-pump vacuum, leaving a yellow solid, which was purified by preparative TLC (hexane/ethyl acetate) to give a 25% yield of the linear dimeric salen **20**. In the course of this work, Janssen and coworkers reported a similar dimeric salen manganese complex,[43] but no data were available for the free ligand.

The linear salen structure was confirmed by ^1H and ^{13}C NMR. Assignments were based on HETCOR experiments. The ^1H NMR spectrum showed two well separated chemically nonequivalent imine protons at 8.28 ppm and 8.19 ppm. Correspondingly, two C=N stretches were observed at 1654 cm^{-1} and 1635 cm^{-1}. Two different *t*-Bu group signals at 1.38 ppm and 1.35 ppm were also found. Interestingly, the two protons of the methylene bridge in **20** were nonequivalent and a doublet at 3.67 ppm with J=3.6 Hz was observed. This implied that the two salen units on either side of the bridge were twisted. The ^{13}C NMR spectrum showed two imine carbon resonances at 165.7 ppm and 165.6 ppm. As expected, there were twelve aromatic carbon signals, in which two quaternary aromatic carbon signals were overlapped at 137.2 ppm. Overall, twenty three carbon signals, which matched the proposed structure **20**, were found.

2.3.10 Self-assembly for tetramers 21a-21d

Directed reactions and template-directed reactions between the chiral diamine and dialdehydes afforded linear salen and macrocyclic salen dimers, respectively. It was interesting to speculate on the possible outcome of a reaction without template control since polymer or macrocycles could result (Figure 2.11). The reactions were conducted by

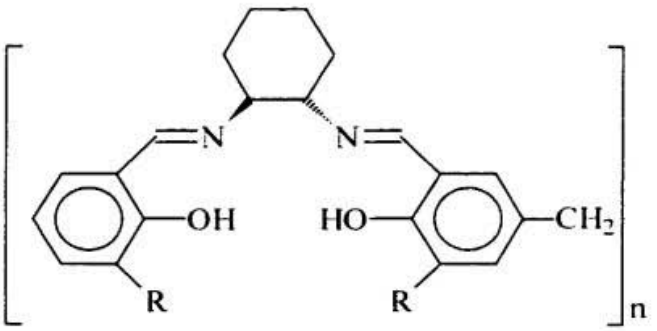

macrocyclic salen **21**

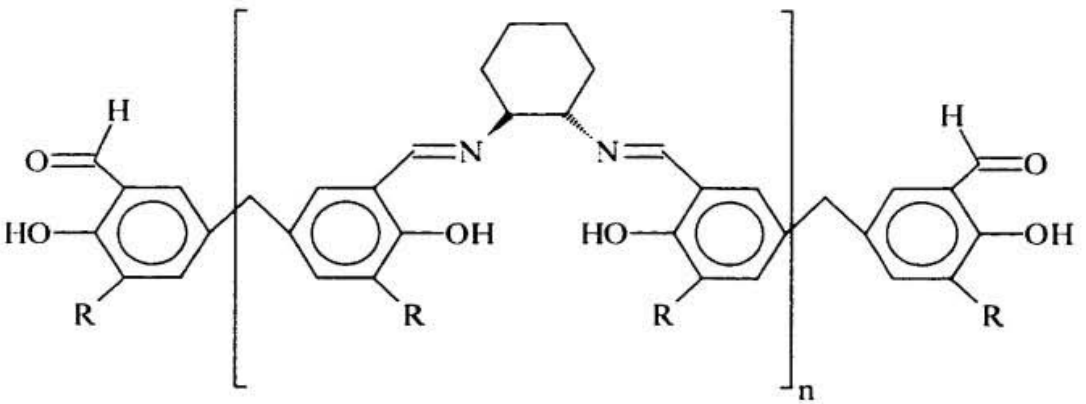

polymer **22**

Figure 2.11 Possible products of the reaction without template

directly mixing 2 eq. of (*1R,2R*)-(-)-cyclohexane-1,2-diamine in methanol with 2 eq. of dialdehyde (**3a**, **3b**, **3c**, or **3d**) in THF at room temperature. During an 8 h reaction period, a yellow precipitate was gradually generated. Workup similar to that used for tetramer **16d** afforded a yellow solid.

^{1}H NMR spectra showed that the products were clean and that there were no aldehyde or amine signals present. A large signal at 2.15 ppm, tentatively assigned to water molecules, was observed in all four products. In the ^{13}C NMR spectra, one imine and six aromatic carbon signals were found for each of the products (**21a**, **21b**, **21c**, **21d**). In addition, six carbon signals for **21d**, six for **21c**, five for **21b**, and four for **21a** were observed at higher field. If the products were polymer **22**, broad proton NMR signals would be expected. The ^{13}C and ^{1}H NMR were therefore more consistent with a macrocyclic structure.

Comparison of the ^{1}H NMR and ^{13}C NMR of **21d** with that of dimer **14d**, trimer **15d**, and tetramer **16d** indicated that it was identical with the spectrum of **16d**. Therefore, it was concluded that the major product in the absence of a metal template was a macrocyclic salen tetramer.

2.4 Summary

New types of chiral macrocyclic and linear salens were synthesized. In the presence of a Ba^{2+} template ion, the condensation reaction between (*1R,2R*)-(-)- or (*1S,2S*)-(+)-cyclohexane-1,2-diamine and dialdehydes **3a-3d**, **6**, or **7** gave macrocyclic salen dimers containing cavities with different shapes, sizes, and depths. Reaction in the absence of a template ion afforded macrocyclic salen tetramers as the major product.

X-ray and NMR studies suggested that the four benzene units in all macrocyclic dimers preferred a 1,3-alternate conformation both in solution and in the solid state. The dimer with longer $-OCH_2CH_2O-$ bridges was flexible and several interconvertible conformers coexisted in solution. The dimers with shorter $-CH_2-$ bridges, on the other hand, were conformationally stable, which was considered to be an advantage in preparation of chiral catalysts.

2.5 Experimental Section

2.5.1 Methods. Unless otherwise specified, all reactions were performed under a nitrogen atmosphere. Nitrogen gas was purified by passing through a series of columns containing DEOX (Aipha) catalyst heated to 120°C, granular P_4O_{10}, and activated 3 Å Molecular Sieves. Organic solutions were concentrated using a rotary evaporator at aspirator pressure. Flash column chromatography was performed with silica gel (230-400) mesh. Preparative thin layer chromatography plates (4 mm) were made from Aldrich silica gel (TLC standard grade 7749, catalogue No. 34644-6). Thin layer chromatography was performed on precoated silica gel plastic sheets with a fluorescent indicator UV_{254} (Macherey-Nagel GmbH & Co. KG, Germany).

2.5.2 Reagents. Chemical reagents and solvents were purchased from Aldrich and used as received with the following exceptions. (*1R,2R*)- or (*1S,2S*)-cyclohexane-1,2-diamine-L-tartrate salts were a gift from SepraChem Company. Dry DMSO was obtained from ACS grade DMSO by drying over activated 4 Å Molecular Sieves. Anhydrous toluene was obtained by distillation of stock toluene from a dark blue solution containing sodium and benzophenone. Anhydrous dichloromethane was obtained by distillation of stock CH_2Cl_2 from CaH_2. *Extreme care should taken when handling $Ba(ClO_4)_2$ which is shock sensitive.*

2.5.3 Instrumentation. Melting points (mp) were determined on a Fisher-Johns apparatus and were uncorrected. Elemental analyses were performed at the Analytical Service Laboratory, Department of Chemistry of the University of Alberta. Electron spray mass spectral (ESMS) analyses were conducted in the Biochemical Mass Spec Laboratory at the Department of Chemistry, University of Waterloo (see Chapter 5. for detailed experiments). Mass spectral (MS) data were from a V. G. Micromass 7070HS instrument. ^{1}H NMR spectra were recorded in $CDCl_3$, CD_2Cl_2, CD_3COCD_3, or toluene-d_8 on a GE 300-NB spectrometer operating at frequency of 300.12 MHZ with Me_4Si as an internal standard. ^{13}C NMR spectra were recorded at 75 MHZ. High field NMR data were recorded in $CDCl_3$ on a Bruker 500 MHZ spectrometer at the Department of Chemistry of the McMaster University with Me_4Si as an internal standard. NMR spectra for each compound synthesized in this study are attached in Appendix 6. Data are reported as follows: chemical shift (ppm), multiplicity (s = singlet, d = doublet, dd = double doublet, t = triplet, br = broad, m = multiplet), coupling constant (J, Hz), integration, and assignment (mH-x, m for the H numbers in the position x of a molecule). ^{1}H NMR and ^{13}C NMR spectra were all processed using Nuts (available from Acorn NMR). Chemical shifts for ^{13}C NMR spectra are relative to the solvents δ = 77.2 ppm for $CDCl_3$, δ =137.9 ppm for $C_6D_5CD_3$, and δ = 54.0 ppm for CD_2Cl_2. Infrared spectra were recorded with a Mattson Polaris Fourier transform spectrometer. Crystal data were collected at ambient temperature on a Rigaku AFC6S diffractometer with graphite monochromated Mo-Kα radiation and a 2 kW sealed tube generator. Details of the X-ray experiments are given in

Appendix 1.

2.5.4 Syntheses of the aldehydes and dialdehydes

2.5.4.1 Syntheses of the 3-alkyl-2-hydroxy-benzaldehydes 2b-2d

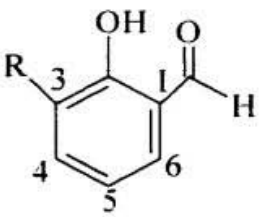

2b: R = CH_3
2c: R = *i*-Pr
2d: R = *t*-Bu

To a three-necked round-bottomed flask (500 mL) equipped with a reflux condenser, stirring bar, and a nitrogen source was added anhydrous toluene (100 mL), the appropriate phenol (0.50 mol), tin(IV) chloride (6.0 mL, 0.050 mol), and tri-*n*-butylamine (34.7 mL, 0.20 mol). The pale yellow mixture was stirred for 20 minutes at room temperature, then paraformaldehyde (33 g, 1.1 mol) was added in one portion. The resulting yellowish solution was heated at 100°C overnight. After cooling, the resultant black mixture was poured into water (2 L), acidified to pH 2 with 6 mol/L hydrochloric acid, and extracted with Et_2O (3 x 100 mL). The combined red ether solutions were evaporated and purified on silica gel (hexane/CH_2Cl_2). Products were obtained as pale yellow liquids in 77-82% yield.

2b[53c] Yield: 56 g (82%). **^{1}H NMR** ($CDCl_3$): δ 11.27 (s, 1H, OH), 9.88 (s, 1H, CHO), 7.40 (d, J=7.5, 2H, H-4, H-6), 6.93 (t, J=7.5, 1H, H-5), 2.27 (s, 3H, CH_3).

2c Yield: 63 g (80%). **^{1}H NMR** ($CDCl_3$): δ 11.37 (s, 1H, OH), 9.88 (s, 1H, CHO), 7.47 (dd, 1H, $J_{6,5}$=7.1, $J_{6,4}$=1.5, H-6), 7.40 (dd, 1H, $J_{4,5}$=7.2, $J_{4,6}$=1.5, H-4), 6.98 (t, 1H, J=7.2, H-5), 3.37 (septet, J=6.9, 1H, *i*-Pr), 1.23 (d, 6H, J=6.9, *i*-Pr).

2d[53b] Yield: 69 g (77%). **^{1}H NMR** ($CDCl_3$): δ 11.81 (s, 1H, OH), 9.83 (s, 1H, CHO), 7.51 (dd, 1H, $J_{6,5}$=7.4, $J_{6,4}$=1.1, H-6), 7.36 (dd, 1H, $J_{4,5}$=7.2, $J_{4,6}$=1.2, H-4), 6.92 (dd, 1H, $J_{5,4}$=7.2, $J_{5,6}$=7.4, H-5), 1.41 (s, 9H, *t*-Bu).

2.5.4.2 Syntheses of the 5,5'-methylene-bis-salicylaldehydes 3a-3d

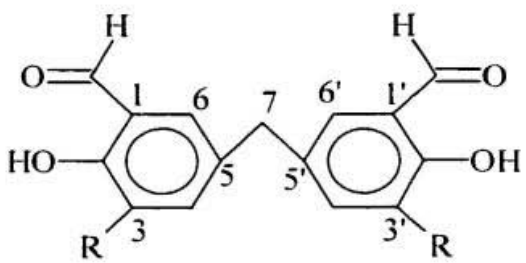

3a: R = H, **3b**: R = CH_3, **3c**: R = *i*-Pr, **3d**: R= *t*-Bu

To a solution of 3-alkyl-2-hydroxy-benzaldehyde (**2a**, **2b**, **2c**, or **2d**) (0.060 mol) in 20 mL of acetic acid was added 1,3,5-trioxane (0.90 g, 0.020 mol) at room temperature. A mixture of 0.25 mL H_2SO_4 in 10 mL acetic acid was then dropped into the solution at 70°C over a one hour period. The resultant solution was stirred for 12 h at 70°C and then poured into ice water. The mixture was allowed to stand overnight, and then hexane or

chloroform (2 x 100 mL) was added to extract the product. The concentrated extract was purified on silica gel (hexane/ethyl acetate) and a pale yellow crystalline product was obtained.

3a Yield: 4.7 g (61%). mp: 136 -138: **MS** (*m/z*) 256 (M^+): **IR** (Nujol): 1661 cm^{-1} (CHO). 1589 cm^{-1} (Ph): ^{1}**H NMR** ($CDCl_3$): δ 10.92 (s, 2H, OH), 9.85 (s, 2H, CHO), 7.37-7.32 (m, 4H, H-4, H-4', H-6, H-6'), 6.97 (d, 2H, J= 7.4, H-3, H-3'), 3.96 (s, 2H, H-7): ^{13}**C NMR** ($CDCl_3$): δ 196.6 (CHO), 160.4 (C-2, C-2'), 137.7 (C-6, C-6'), 133.4 (C-3, C-3'), 132.2 (C-1, C-1'), 120.6 (C-5, C-5'), 118.1 (C-4, C-4'), 39.5 (C-7): Analysis: Calcd. for $C_{15}H_{12}O_4$: C, 70.12; H, 4.56. Found: C, 70.31; H, 4.72.

3b Yield: 6.1 g (72%). mp: 148-149 °C: **MS** *m/z* 284 (M^+): **IR** (Nujol): 1649 cm^{-1} (CHO). 1622 cm^{-1} (Ph): ^{1}**H NMR** ($CDCl_3$): δ 11.16 (s, 2H, OH), 9.83 (s, 2H, CHO), 7.21 (br, 2H, H-6, H-6'), 7.16 (br, 2H, H-4, H-4'), 3.88 (s, 2H, H-7), 2.24 (s, 6H, CH_3): ^{13}**C NMR** ($CDCl_3$): δ 196.8 (CHO), 158.8 (C-2, C-2'), 138.7 (C-6, C-6'), 131.8 (C-1, C-1'), 130.9 (C-4, C-4'), 127.5 (C-5, C-5'), 120.0 (C-3, C-3'), 39.7 (C-7), 15.2 (CH_3): Analysis: Calcd. for $C_{17}H_{16}O_4$: C, 71.80; H, 5.68. Found: C, 71.58; H, 5.65.

3c Yield: 6.3 g (65%). mp 71 -73 °C: **MS** (*m/z*) 340 (M^+): **IR** (Nujol): 1654 cm^{-1} (CHO). 1622 cm^{-1} (Ph): ^{1}**H NMR** ($CDCl_3$): δ 11.28 (s, 2H, OH), 9.83 (s, 2H, CHO), 7.29 (d, 2H, J=2.0, H-6, H-6'), 7.13 (d, 2H, J=2.1, H-4, H-4'), 3.95 (s, 2H, H-7), 3.36 (septet, 1H,

J=6.8, *i*-Pr), 1.23 (d, 6H, J=6.9, *i*-Pr); **^{13}C NMR** ($CDCl_3$): δ 196.9 (CHO), 158.1 (C-2, C-2'), 137.6 (C-1, C-1'), 134.5 (C-6, C-6'), 131.9 (C-5, C-5'), 130.9 (C-4, C-4'), 120.2 (C-3, C-3'), 40.0 (C-7, C-7'), 26.5 (*i*-Pr), 22.40 (*i*-Pr); Analysis: Calcd. for $C_{21}H_{24}O_4$: C, 74.09; H, 7.11. Found: C, 74.23; H, 7.38.

3d Yield: 7.2 g (68%), mp: 123-124°C, **MS** (*m/z*) 368 (M^+); **IR** (Nujol): 1661cm^{-1} (CHO), 1615 cm^{-1} (Ph); **^{1}H NMR** ($CDCl_3$): δ 11.71 (s, 2H, OH), 9.83 (s, 2H, CHO), 7.38 (d, 2H, J=2.1, H-6, H-6'), 7.15 (d, 2H, J=2.1, H-4, H-4'), 3.95 (s, 2H, H-7), 1.42 (s, 18H, *t*-Bu); **^{13}C NMR** ($CDCl_3$): δ 197.2 (CHO), 160.0 (C-2, C-2'), 138.7 (C-1, C-1'), 135.1 (C-5, C-5'), 131.4 (C-6, C-6'), 131.3 (C-4, C-4'), 120.7 (C-3, C-3'), 40.2 (C-7, C-7'), 35.0 (*t*-Bu), 29.4 (*t*-Bu); Analysis: Calcd. for $C_{23}H_{28}O_4$: C, 74.96; H, 7.66. Found: C, 75.14; H, 7.87.

2.5.4.3 Synthesis of 5-[2-(3-formyl-4-hydroxyphenoxy)ethoxy]-2-hydroxybenzaldehyde 6

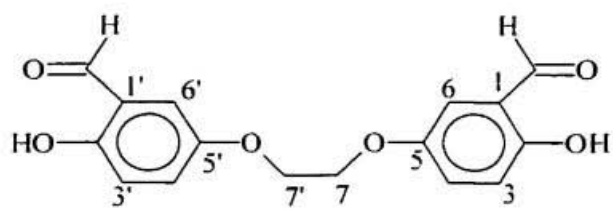

6

To a suspension of NaH (1.32 g, 0.0550 mol) in 12 mL of DMSO was added a solution of 2,5-dihydroxybenzaldehyde (3.47 g, 0.0251 mol) in 12 mL DMSO over a period of 1 h

with vigorous stirring at temperature 0°C. The mixture was allowed to warm to room temperature and ethylene glycol ditosylate (4.36 g, 0.0125 mol) was then added in one portion. The dark brown solution was stirred for 24 h. Subsequently, H_2O (150 mL) was added, and the reaction mixture was extracted with $CHCl_3$ (2 x 50 mL). The organic layers contained only a small amount of unreacted ditosylate and were discarded. The aqueous layer was acidified with 1 mol/L HCl to pH 1, and the mixture was extracted with $CHCl_3$ (2 x 50 mL). The combined organic layers were evaporated, the remaining black mixture was purified by chromatography on silica gel (hexane/chloroform) to give a pale yellow crystalline product 2.1 g (59%).

6 mp: 159-161 °C; **MS** (*m/z*) 302 (M^+); **IR** (Nujol): 1654 cm^{-1} (CHO), 1582 cm^{-1} (Ph); **^{1}H NMR** ($CDCl_3$): δ 10.69 (s, 2H, OH), 9.87 (s, 2H, CHO), 7.22 (dd, 2H, J=2.7, J=9.3, H-4, H-4'), 7.08 (d, 2H, J=2.7, H-6, H-6'), 6.96 (d, 2H, J=9.3, H-3, H-3'), 4.33 (s, 4H, H-7, H-7'); **^{13}C NMR** ($CDCl_3$): δ 196.2 (CHO), 126.2 (C-4, C-4'), 119.1 (C-6, C-6'), 116.9 (C-3, C-3'), 67.8 (C-7, C-7'); **Analysis**: Calcd. for $C_{16}H_{14}O_6$: C, 63.56; H, 4.67. Found: C, 61.12; H, 4.38.

2,5,4.4 Synthesis of 3-[(3-formyl-2-hydroxy-1-naphthyl)methyl]-2-hydroxy-1-naphthaldehyde 12

Dialdehyde **11** 0.300 g (0.756 mmol) was dissolved in 10 mL of anhydrous CH_2Cl_2 at room temperature. To this solution 4 eq. of Me_3SiCl (0.40 mL, 3.1 mmol) and 4 eq. of KI

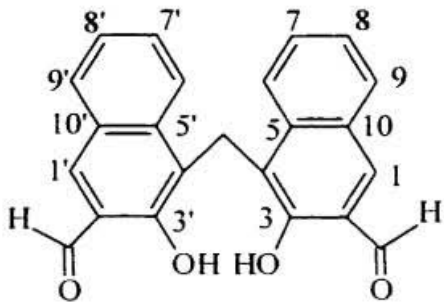

12

(5.80 g. 3.12 mmol) were added under a nitrogen atmosphere. The mixture was then kept at reflux for 24 h. After cooling. 10 mL of water was added and the organic layer was removed. The concentrated organic phase was purified on silica gel (hexane/ethyl acetate = 5:1). A yellow solid product was obtained (0.042 g.15%).

12 ^{1}**H NMR** ($CDCl_3$): δ 11.06 (s. 2H. OH). 10.07 (s. 2H. CHO). 8.23 (d. 2H. J=8.9. H-6. H-6'). 8.02 (s. 2H. H-1. H-1'). 7.75 (d. J=8.1. 2H. H-9. H-9'). 7.41-7.21 (m. 4H. H-8. H-8'. H-7. H-7'). 4.87 (s. 2H. -CH_2-).

2.5.5 Resolution for (*1R,2R*) or (*1S,2S*)-cyclohexane-1,2-diamine 13

An aqueous solution of KOH (4.0 g. 0.10 mol) in 10 mL of water was added to solid (*1R.2R*)-1.2-diaminocyclohexane-L-tartrate (13.2 g. 0.0502 mol) from SepraChem in a separatory funnel. and the mixture was shaken carefully. The amine layer was separated as quickly as possible and ether was added to the solid residue. then the combined ether and amine solutions were dried with excess sodium overnight. After concentration. the

ether solution deposited a clear and colourless crystalline product (4.3 g. 75%) on standing at room temperature. The ^{1}H NMR spectrum was consistent with that of authentic diamine purchased from Aldrich. The diamines are hygroscopic and should be handled appropriately.

2.5.6 Syntheses of the chiral macrocyclic salens

2.5.6.1 Syntheses of the chiral macrocyclic salen dimers 14a-14d and trimer 15d

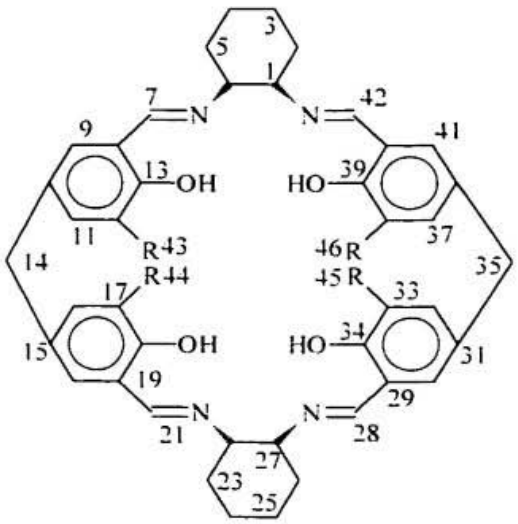

14a R = H. **14b** R = CH_3. **14c** R = *i*-Pr. **14d** R = *t*-Bu

To a solution of $Ba(SCN)_2$ (0.368 g. 1.20 mmol) or $Ba(ClO_4)_2$ (0.469 g. 1.20 mmol) in 20

mL of MeOH and 20 mL of THF was added dropwise (*1R.2R*)-cyclohexane-1.2-diamine (0.137 g. 1.20 mmol) in 15 mL of MeOH and the dialdehyde (1.20 mmol) in 15 mL of THF at room temperature over a 1.5 h period. A yellow solution was generated. After 5 h. 10 mL of MeOH was added to the yellow-orange solution. and the resulting precipitate was collected and washed with MeOH (3 x 5 mL) and acetone until the acetone washings were colourless to yield the tetramer.

The filtrate obtained above was evaporated to dryness to give a yellow-orange solid. which was dissolved in 4.0 mL of CH_2Cl_2 and 2.0 mL of MeOH. The orange solution was purified by preparative TLC developed in hexane/ethyl acetate to give the analytically pure dimer.

14a Yield: 0.16 g (40%). 249 °C dec.: **ESMS** (*m/z*): Calcd. for $C_{42}H_{44}N_4O_4$ 668: Found: 668 (100%). 669 (48%). 670 (12%). 671 (3%): **IR** (Nujol): 1636 cm^{-1} (CH=N). 1589 cm^{-1} (Ph): **^{1}H NMR** ($CDCl_3$): δ 13.14 (s. 4H. -OH). 8.07 (s. 4H. H-7. H-21. H-28. H-42). 7.18 (dd. J_{11-9}=2.4. J_{11-12}=8.3. 4H. H-11. H-16. H-32. H-37). 6.92 (d. J_{9-11}=2.4. 4H. H-9. H-20. H-30. H-41). 6.75 (d. J=7.8. 4H. H-12. H-17. H-33. H-38). 3.64 (s. 4H. H-14. H-35). 3.22-3.18 (m. 4H. H-1. H-6. H-22. H-27). 1.85-1.42 (m. 16H. cyclohexyl rings): **^{13}C NMR** ($CDCl_3$): δ 164.5 (C-7. C-21. C-28. C-42). 159.5 (C-13. C-18. C-34. C-39). 132.2 (C-12. C-17. C-33. C-38). 131.5 (C-8. C-19. C-29. C-40). 131.2 (C-9. C-20. C-30. C-41). 119.2 (C-10. C-15. C-31. C-36). 116.9 (C-11. C-16. C-32. C-37). 73.1 (C-1. C-6. C-22. C-27).

41.1 (C-14, C-35), 33.5 (C-2, C-5, C-23, C-26), 24.4 (C-3, C-4, C-24, C-25).

14b Yield: 0.14 g (32%), 209 °C dec.: **ESMS** (*m/z*): Calcd. for $C_{46}H_{52}N_4O_4$ 724; Found: 724 (M^+,100%), 725 (19%), 726 (15%), 742 ($M^+ + H_2O$): **IR** (Nujol): 1628 cm^{-1} (CH=N), 1603 cm^{-1} (Ph): **^{1}H NMR** ($CDCl_3$): δ 13.49 (s, 4H, -OH), 8.08 (s, 4H, H-7, H-21, H-28, H-42), 7.05 (s, 4H, H-9, H-20, H-30, H-41), 6.80 (s, 4H, H-11, H-16, H-32, H-37), 3.59 (s, 4H, H-14, H-35), 3.21-3.18 (m, 4H, H-1, H-6, H-22, H-27), 2.17 (s, 12H, H-43, H-44, H-45, H-46), 1.85-1.26 (m, 16H, cyclohexyl rings): **^{13}C NMR** ($CDCl_3$): δ 164.6 (C-7, C-21, C-28, C-42), 157.7 (C-13, C-18, C-34, C-39), 133.3 (C-8, C-19, C-29, C-40), 131.9 (C-10, C-15, C-31, C-36), 128.7 (C-9, C-20, C-30, C-41), 125.7 (C-12, C-17, C-33, C-38), 118.4 (C-11, C-16, C-32, C-37), 73.2 (C-1, C-6, C-22, C-27), 41.2 (C-14, C-35), 33.6 (C-2, C-5, C-23, C-26), 24.4 (C-3, C-4, C-24, C-25), 15.7 (C-43, C-44, C-45, C-46): **Analysis**: Calcd. for $C_{46}H_{52}N_4O_4$: C, 76.20; H, 7.23; N, 7.73. Found: C, 75.67; H, 7.25; N, 7.36.

14C Yield: 0.10g (20%), 178 °C dec.: **ESMS** (*m/z*): Calcd. for $C_{54}H_{68}N_4O_4$ 836; Found: 837 ($M + H^+$, 100%): **IR** (Nujol): 1636 cm^{-1} (CH=N), 1603 cm^{-1} (Ph) : **^{1}H NMR** ($CDCl_3$): δ 13.50 (s, 4H, -OH), 8.07 (s, 4H, H-7, H-21, H-28, H-42), 7.09 (s, 4H, H-9, H-20, H-30, H-41), 6.75 (s, 4H, H-11, H-16, H-32, H-37), 3.65 (s, 4H, H-14, H-35), 3.28-3.19 [m, 8H, H-1, H-6, H-22, H-27, H-43 (-C<u>H</u>Me_2), H-44 (-C<u>H</u>Me_2), H-45 (-C<u>H</u>Me_2), H-46 (-C<u>H</u>Me_2)], 1.67-1.23 (m,16H, cyclohexyl ring), 1.19 [d, J= 18.0, 24H, H-43 (-CH<u>Me</u>$_2$), H-44 (-CH<u>Me</u>$_2$), H-45 (-CH<u>Me</u>$_2$), H-46 (-CH<u>Me</u>$_2$)]: **^{13}C NMR** ($CDCl_3$): δ 164.8 (C-7, C-

21. C-28. C-42). 156.9 (C-13. C-18. C-34. C-39). 136.0 (C-8. C-19. C-29. C-40). 131.8 (C-12. C-17. C-33. C-38). 128.8 (C-9. C-20. C-30. C-41). 128.7 (C-11. C-16. C-32. C-37). 118.6 (C-10. C-15. C-31. C-36). 73.0 (C-1. C-6. C-22. C-27). 41.7 (C-14. C-35). 33.7 (C-2. C-5. C-23. C-26). 26.6 [C-43 (-$\underline{C}HMe_2$). C-44 (-$\underline{C}HMe_2$). C-45 (-$\underline{C}HMe_2$). C-46 (-$\underline{C}HMe_2$)]. 24.4 (C-3. C-4. C-24. C-25). 22.7 [C-43 (-$CH\underline{Me_2}$). C-44 (-$CH\underline{Me_2}$). C-45 (-$CH\underline{Me_2}$). C-46 (-$CH\underline{Me_2}$)]. 22.5 [C-43 (-$CH\underline{Me_2}$). C-44 (-$CH\underline{Me_2}$). C-45 (-$CH\underline{Me_2}$). C-46 (-$CH\underline{Me_2}$)]: **Analysis**: Calcd. for $C_{54}H_{68}N_4O_4$: C. 77.46: H. 8.19: N. 6.70. Found: C. 76.56: H. 8.31: N. 6.48.

14d Yield: 0.062 g (11%). 210 °C dec.: **ESMS** (*m/z*): Calcd. for $C_{58}H_{76}N_4O_4$: 892: Found: 893 (M^++H. 100%). 894 (75%). 895 (29%). 911 (19%): **IR** (Nujol): 1636 cm^{-1} (CH=N). 1603 cm^{-1} (Ph): **^{1}H NMR** ($CDCl_3$): δ 13.77 (s. 4H. -OH). 8.07 (s. 4H. H-7. H-21. H-28. H-42). 7.14 (s. 4H. H-9. H-20. H-30. H-41). 6.73 (s. 4H. H-11. H-16. H-32. H-37). 3.63 (s. 4H. H-14. H-35). 3.24-3.22 (br. 4H. H-1. H-6. H-22. H-27). 1.84-1.26 (m. 16H. cyclohexyl rings). 1.36 (s. 36H. H-43. H-44. H-45. H-46): **^{13}C NMR** ($CDCl_3$): δ 165.4 (C-7. C-21. C-28. C-42). 158.8 (C-13. C-18. C-34. C-39). 137.0 (C-8. C-19. C-29. C-40). 131.0 (C-12. C-17. C-33. C-38). 129.6 (C-9. C-20. C-30. C-41). 129.4 (C-11. C-16. C-32. C-37). 119.1 (C-10. C-15. C-31. C-36). 72.5 (C-1. C-6. C-22. C-27). 41.7 (C-14. C-35). 34.9 [C-43 (-$\underline{C}Me_3$). C-44 (-$\underline{C}Me_3$). C-45 (-$\underline{C}Me_3$). C-46 (-$\underline{C}Me_3$)]. 33.8 (C-2. C-5. C-23. C-26). 29.67 [C-43 (-$C\underline{Me_3}$). C-44 (-$C\underline{Me_3}$). C-45 (-$C\underline{Me_3}$). C-46 (-$C\underline{Me_3}$)]. 24.5 (C-3. C-4. C-24. C-25).

Macrocyclic salen trimer 15d

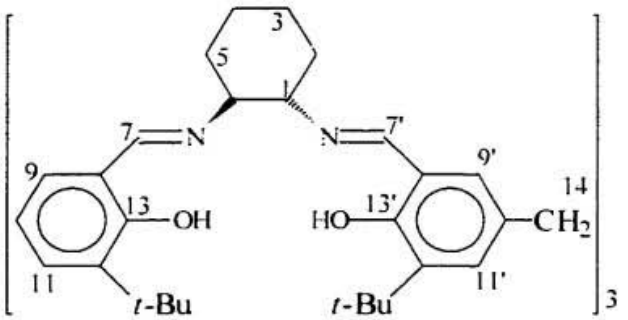

15d Yield: 0.044 g (7.0%).

ESMS (*m/z*): Calcd for $C_{87}H_{114}N_6O_6$ 1338: Found: 1339 (M^+ + H, 100%), 1358 ($M+H_3O^+$); **^{1}H NMR** ($CDCl_3$): δ 13.80 (s, 6H, 6-OH), 8.21 (s, 6H, H-7), 7.02 (s, 6H, H-9), 6.72 (s, 6H, H-11), 3.72 (s, 6H, -CH_2- bridges), 3.30-3.28 (m, 6H, 3H-1, H-6), 1.88-1.26 (m, 24H, cyclohexyl rings), 1.33 (s, 54H, 6 *t*-Bu).

Using $Ba(ClO_4)_2$ as a template, the dimer yields 0.26 g (58%) for **14b** and 0.29 g (53%) for **14d** were higher than those obtained by using $Ba(SCN)_2$ as a template. The cyclizations and workup of (*1S,2S*)-(+)-cyclohexane-1,2-diamine and the dialdehydes were carried out under the same conditions as (*1R,2R*)-(-)-cyclohexane-1,2-diamine. Similar results were obtained.

2.5.6.2 Synthesis of the macrocyclic salen dimer 17

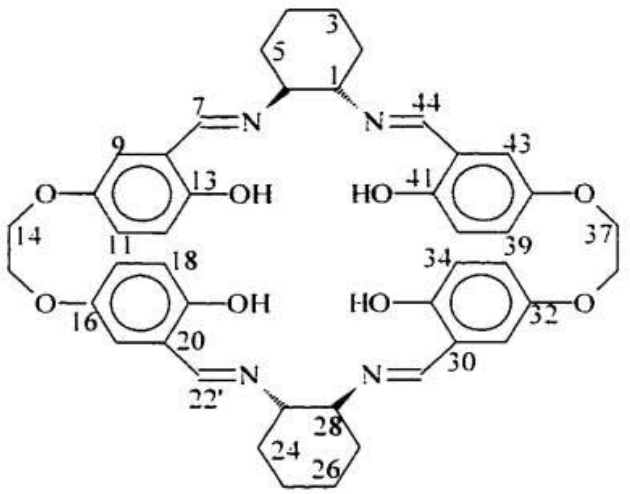

To a solution of $Ba(ClO_4)_2$ (0.390 g, 1.00 mmol) in 20 mL of THF and 20 mL of MeOH was added (*1R,2R*)-cyclohexane-1,2-diamine (0.114 g, 1.00 mmol) in 20 mL MeOH and a solution of the dialdehyde **6** (0.302 g, 1.00 mmol) in 20 mL of THF with stirring at room temperature over a 1.5 h period. The solvents were pumped off and the yellow organic solid was then purified by preparative TLC (hexane/ethyl acetate).

17 Yield: 0.17 g (45%). **ESMS** (*m/z*): Calcd. for $C_{44}H_{48}N_4O_8$: 760: Found: 760 (100%), 778 ($M^+ + H_2O$); **IR** (Nujol): 1636 cm^{-1} (CH=N), 1596 cm^{-1} (Ph); **^{1}H NMR** ($CDCl_3$) of the most stable conformer at RT: δ 12.79 (b, 4H, -OH), 8.04 (s, 4H, H-7, H-22, H-29, H-44), 6.82 (dd, J_{11-9}=3.0, J_{11-12}=9.0, 4H, H-11, H-17, H-33, H-39), 6.77 (d, J_{11-12}=8.9, 4H, H-11, H-18, H-34, H-40), 6.57 (d, J_{9-11}=3.0, 4H, H-9, H-21, H-31, H-43), 4.11 (dd,

$J_{14a\text{-}15b}$=1.1, $J_{14a\text{-}14b}$= 3.2, H-14, H-15, H-36, H-37), 3.22-3.20 (m, 4H, H-1, H-6, H-23, H-28), 1.95-1.45 (m, 16H, cyclohexyl rings): **^{13}C NMR** ($CDCl_3$) at RT: δ 164.5 (C-7, C-22, C-29, C-44), 155.4 (C-13, C-19, C-35, C-41), 150.5 (C-10, C-16, C-32, C-38), 119.8 (C-11, C-17, C-33, C-39), 118.3 (C-8, C-20, C-30, C-42), 117.5 (C-12, C-18, C-34, C-40), 116.8 (C-9, C-21, C-31, C-43), 72.7 (C-1, C-6, C-23, C-28), 66.8 (C-14, C-15, C-36, C-37), 32.9 (C-2, C-5, C-24, C-27), 24.2 (C-3, C-4, C-25, C-26), 24.3 (cyclohexyl rings).

Dimer **17** **^{1}H NMR** ($CDCl_3$) of the second stable conformer at RT: δ 12.79 (br, 4H, -OH), 8.07 (s, 4H, H-7', H-22', H-29', H-44'), 6.83 (dd, $J_{11'\text{-}9'}$=2.9, $J_{11'\text{-}12'}$=9.0, 4H, H-11', H-17', H-33', H-39'), 6.79 (d, $J_{11'\text{-}12'}$=9.0, 4H, H-12', H-18', H-34', H-40'), 6.54 (d, $J_{9'\text{-}11'}$ =2.9, 4H, H-9', H-21', H-31', H-43'), 4.11 (dd, $J_{14a'\text{-}15b'}$=2.0, $J_{14a\text{-}14b}$= 21.4, H-14', H-15', H-36', H-37'), 3.27-3.18 (m, 4H, H-1', H-6', H-23', H-28'), 2.00-1.40 (m, 16H, cyclohexyl rings): **^{13}C NMR** ($CDCl_3$) of the second stable conformer at RT: δ 164.7(C-7', C-22', C-29', C-44'), 155.6 (C-13', C-19', C-35', C-41'), 151.0 (C-10', C-16', C-32', C-38'), 120.6 (C-11', C-17', C-33', C-39'), 118.2 (C-8', C-20', C-30', C-42'), 117.5 (C-12', C-18', C-34', C-40'), 116.3 (C-9', C-21', C-31', C-43'), 72.6 (C-1', C-6', C-23', C-28'), 67.5 (C-14', C-15', C-36', C-37'), 32.8 (C-2', C-5', C-24', C-27'), 24.2 (C-3', C-4', C-25', C-26').

For the two remaining less stable conformers, imine signals appeared at 8.08 and 8.09 ppm. Other signals were very weak and could not be interpreted.

Dimer **17** **^{13}C NMR** ($CDCl_3$) at 55°C: δ 165.1 (C-7, C-22, C-29, C-44), 155.9 (C-13, C-

19, C-35, C-41), 151.4 (C-10, C-16, C-32, C-38), 151.0 (C-10', C-16', C-32', C-38'), 121.1 (C-11, C-17, C-33, C-39), 120.4 (C-11', C-17', C-33', C-39'), 118.7 (C-8, C-20, C-30, C-42), 117.8 (C-12, C-18, C-34, C-40), 117.3 (C-12', C-18', C-34', C-40'), 116.9 (C-9, C-21, C-31, C-43), 72.9 (C-1, C-6, C-23, C-28), 68.2 (C-14, C-15, C-36, C-37), 67.5 (C-14', C-15', C-36', C-37'), 33.2 (C-2, C-5, C-24, C-27), 24.5 (C-3, C-4, C-25, C-26).

2.5.6.3 Synthesis of the macrocyclic salen dimer 18

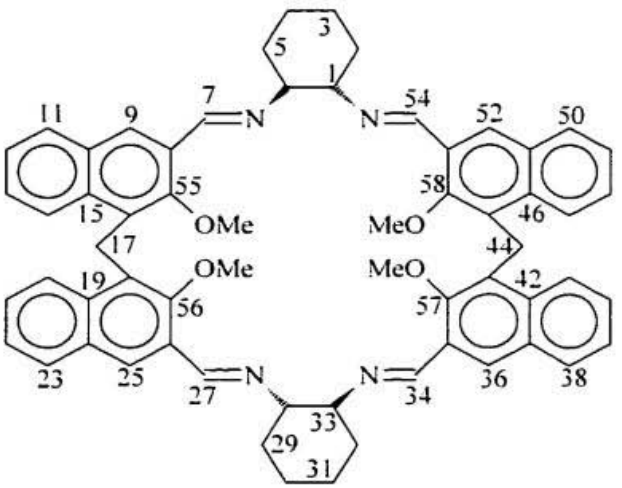

To $Ba(ClO_4)_2$ 0.390 g (1.00 mmol) in 20 mL of THF and 20 mL of MeOH was added 4-[(4-formyl-3-methoxy-1-naphthyl)methyl]-2-methoxy-1-naphthaldehyde **11** 0.397 g (1.00 mmol) in 15 mL of THF and (*1R.2R*)-(-)-cyclohexane-1,2-diamine 0.114 g (1.00 mmol) simultaneously under gentle reflux. The clear colourless solution was kept at reflux for an additional 4 h. A white precipitate formed, which was filtered and washed with MeOH (3

x 5 mL). After crystallization from toluene, an off-white solid was obtained.

Dimer 18 Yield: 0.32 g (64%). **ESMS** (*m/z*): Calcd. for $C_{62}H_{60}N_4O_4$ 924: Found: 925 ($M+H^+$). **IR** (Nujol): 1649 (CH=N) cm^{-1}, 1622 cm^{-1}, 1596 cm^{-1}, 1503 cm^{-1}: **^{1}H NMR** ($CDCl_3$): δ 8.42 (s, 4H, H-7, H-27, H-34, H-54), 8.42 (d, J_{14-13}=7.5, 4H, H-14, H-20, H-41, H-47), 8.06 (s, 4H, H-9, H-25, H-36, H-52), 7.65 (d, 4H, J_{11-12}=8.1, H-11, H-23, H-38, H-50), 7.56 (dd, J_{13-14}=7.5, J_{13-12}=7.5, 4H, H-13, H-21, H-40, H-47), 7.39 (dd, J=8.1, J_{12-13}=7.5, 4H, H-12, H-22, H-39, H-49), 4.61 (s, 4H, H-17, H-44), 3.42 (s, 4H, H-1, H-6, H-28, H-33), 2.16 (s, 12H, 4Me), 1.84-1.44 (m, 16H, cyclohexyl rings): **^{13}C NMR** ($CDCl_3$): δ 157.4 (C-7, C-27, C-34, C-54), 156.1 (C-55, C-56, C-57, C-58), 134.2 (C-15, C-19, C-42, C-46), 130.6 (C-10, C-24, C-37, C-51), 129.3 (C-8, C-26, C-35, C-53), 128.9 (C-16, C-18, C-43, C-45), 128.0 (C-9, C-25, C-36, C-52), 127.1 (C-14, C-20, C-41, C-47), 126.8 (C-11, C-23, C-38, C-50), 124.9 (C-12, C-13, C-21, C-22, C-39, C-40, C-48, C-49), 74.5 (C-1, C-6, C-28, C-33), 61.96 (OMe), 33.3 (C-2, C-5, C-29, C-32), 24.7 (C-3, C-4, C-30, C-31), 22.8 (C-17, C-44).

2.5.7 Synthesis of the chiral linear dimeric salen 20

Salicylaldehyde **2d** (0.446 g, 2.53 mmol) in 50 mL of $CHCl_3$ was added dropwise to a solution of (*1R,2R*)-(-)-cyclohexane-1,2-diamine (0.286 g, 2.50 mmol) in 50 mL of $CHCl_3$ over a 24 h period at room temperature with stirring. Dialdehyde **3d** 0.461 g (1.25 mmol) in 5 mL of $CHCl_3$ and 10 mL of MeOH was then added in one portion. After 6 h, the yellow solution was concentrated and purified by preparative TLC (hexane/ethyl acetate).

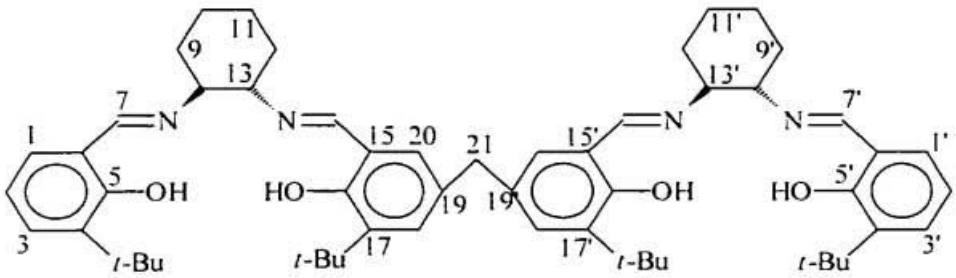

affording analytically pure yellow solid.

Dimeric salen **20** Yield: 0.28 g, 25 %. mp: 83 - 84 °C: **ESMS** (*m/z*): Calcd. for $C_{57}H_{76}N_4O_4$ 880: No molecular ion was found: **IR** (Nujol): 1654 cm^{-1} (CH=N), 1635 cm^{-1} (CH=N): **^{1}H NMR** ($CDCl_3$): δ 13.78 (br, 4H, 4OH), 8.28 (s, 2H, H-7, H-7'), 8.19 (d, J=2.1, 2H, H-14, H-14'), 7.24-7.20 (m, 2H, H-2, H-2'), 7.04-6.98 (m, 4H, H-20, H-20', H-18, H-18'), 6.73-6.68 (m, 4H, H-1, H-1', H-3, H-3'), 3.67 (d, J=3.6, 2H, H-21), 3.36-3.24 (m, 4H, H-8, H-13, H-8', H-13'), 1.98-1.27 (m,16H, cyclohexyl rings), 1.38 (s, 18H, *t*-Bu), 1.35 (s, 18H, *t*-Bu): **^{13}C NMR** ($CDCl_3$): δ 165.7 (C-7, C-7'), 165.6 (C-14, C-14'), 160.5 (C-5, C-5'), 158.7 (C-16, C-16'), 137.2 (C-4, C-4', C-17, C-17'), 130.4 (C-19, C-19'), 130.2 (C-20, C-20'), 130.0 (C-18, C-18'), 129.6 (C-1, C-1'), 129.4 (C-3, C-3'), 118.8 (C-6, C-6'), 118.6 (C-15, C-15'), 117.9 (C-2, C-2'), 72.6 (C-8, C-8'), 72.4 (C-13, C-13'), 40.6 (C-21), 34.9 ($\underline{C}Me_3$), 33.4 (C-12, C-12'), 33.3 (C-9, C-9'), 29.6 ($C\underline{Me}_3$), 24.5 (C-10, C-10', C-11, C-11').

2.5.8 Syntheses of the macrocyclic salen tetramers 21a -21d

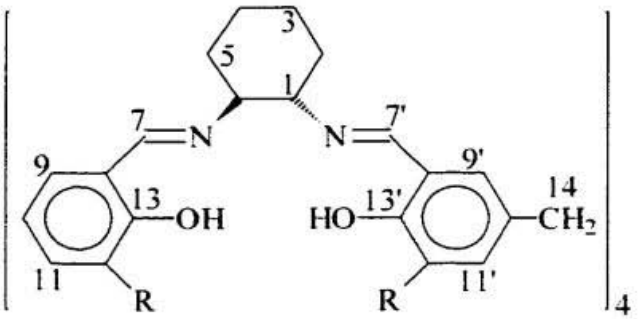

21a: R = H. **21b**: R = CH_3. **21c**: R = *i*-Pr. **21d**: R = *t*-Bu

(*1R.2R*)-(-)-Cyclohexane-1.2-diamine (0.138 g. 1.21 mmol) in 10 mL of MeOH was added dropwise to a one equivalent dialdehyde **3a. 3b. 3c**. or **3d** solution in 10 mL of THF at room temperature over a 30 minute period. Stirring yellow solution for an additional 8 h resulted in formation of a yellow solid. which was collected and washed with acetone (5 x 10 mL) and MeOH (5 x 10 mL).

21a Yield: 0.34 g (85%). 303°C dec.: **IR** (Nujol): 1635 cm^{-1} (CH=N). 1615 cm^{-1} (Ph): **^{1}H NMR** ($CDCl_3$): δ 13.14 (s. 8H. 8OH). 8.19 (s. 8H. 8H-7). 6.99 (dd. J=2.4. J= 6.6. 8H. 8H-11). 6.91 (d. J=6.6. 8H. 8H-12). 6.77 (d. J=2.4. 8H. 8H-9). 3.72 (s. 8H. 8H-14). 3.26 (br. 8H. 4H-1. 4H-6). 1.85-1.44 (br. 32H. 8H-2. 8H-3. 8H-4. 8H-5).

21b Yield: 0.31 g (71%). 235 °C dec.: **IR** (Nujol): 1628 cm^{-1} (CH=N). 1596 cm^{-1} (Ph): **^{1}H NMR** ($CDCl_3$): δ 13.42 (s. 8H. 8OH). 8.20 (s. 8H. 8H-7). 6.89 (s. 8H. 8H-9). 6.78 (s. 8H. 8H-11). 3.66 (s. 8H. 8H-14). 3.28-3.25 (br. 8H. 4H-1. 4H-6). 2.23 (s. $8CH_3$). 1.83-1.42 (br. 32H. 8H-2. 8H-3. 8H-4. 8H-5): **^{13}C NMR** ($CDCl_3$): δ 164.9 (C-7). 157.8 (C-13). 134.0 (C-9). 131.05 (C-8). 129.1 (C-11). 125.9 (C-12). 117.9 (C-10). 72.8 (C-1. C-6). 40.1 (C-14). 33.4 (C-2. C-5). 24.3 (C-3. C-4). 15.7 (CH_3).

21c Yield: 0.42 g (83%). 217 °C dec.: **IR** (Nujol):1628 cm^{-1} (CH=N). 1596 cm^{-1} (Ph): **^{1}H NMR** ($CDCl_3$): δ 13.48 (s. 8H. 8OH). 8.21 (s. 8H. 8H-7). 6.99 (s. 8H. 8H-9). 6.76 (s. 8H. 8H-11). 3.72 (s. 8H. 8H-14). 3.31-3.25 (br. 16H. 4H-1. 4H-6. 8$\underline{CH}Me_2$). 1.84-1.42 (br. 32H. 8H-2. 8H-3. 8H-4. 8H-5). 1.17 (d. 48H. J=3.0. 8CH$\underline{Me_2}$): **^{13}C NMR** ($CDCl_3$): δ 165.2 (C-7). 156.9 (C-13). 136.2 (C-8). 131.1 (C-10). 129.1 (C-11). 118.1 (C-12). 72.7 (C-1. C-6). 40.5 (C-14). 33.5 (C-2. C-5). 26.6 ($\underline{C}HMe_2$). 24.4 (C-3. C-4). 22.7 (CH$\underline{Me_2}$).

21d Yield: 0.44 g (80%). 221°C dec.: **IR** (Nujol):1628 cm^{-1} (CH=N). 1596 cm^{-1}: **^{1}H NMR** ($CDCl_3$): δ 13.69 (s. 8H. 8OH). 8.21 (s. 8H. 8H-7). 7.05 (s. 8H. 8H-9). 6.74 (s. 8H. 8H-

11). 3.67 (s. 8H. 8H-14). 3.28-2.16 (br. 8H. 4H-1. 4H-6). 1.86-1.39 (m. 32H. 8H-2. 8H-3. 8H-4. 8H-5). 1.35 (s. 72H. 8CMe_3); **^{13}C NMR** ($CDCl_3$): δ 165.6 (C-7). 158.7 (C-13). 137.2 (C-12). 130.5 (C-10). 130.2 (C-9). 129.67 (C-11). 118.6 (C-8). 72.54 (C-1. C-6). 40.6 (C-14). 35.0 ($\underline{C}Me_3$). 33.4 (C-2. C-5). 29.6 ($C\underline{Me}_3$). 24.5 (C-3. C-4).

2.6 References

1. Corey, E. J.; Noe, M. C. *J. Am. Chem. Soc.* **1996**, *118*, 8470.

2. Norrby, P. O.; Kolb, H. C.; Sharpless, K. B. *J. Am. Chem. Soc.* **1994**, *116*, 8470.

3. Lucero, M. J.; Houk, K. N. *J. Am. Chem. Soc.* **1997**, *119*, 826.

4. Amendola, M. C.; Stockman, K. E.; Hoic, D. A.; Davis, W. M.; Fu, G. C. *Angew. Chem., Int. Ed. Engl.* **1997**, *36*, .

5. *Catalytic Asymmetric Synthesis*; Ed: Ojima, I. Ed.; VCH: New York, **1993**.

6. Seyden-Penne, J. *Chiral Auxiliaries and Ligands in Asymmetric Synthesis*; John and Wiley & Sons, Inc.; New York, **1995**.

7. Noyori, R.; Takaya, H. *Chem. Scr.* **1985**, *25*, 83.

8. Collman, J. P.; Zhang, X.; Lee, V. L.; Uffelman, E. S.; Brauman, J. I. *Science* **1993**, *261*, 1404.

9. Bolm, C. *Angew. Chem., Int. Ed. Engl.* **1991**, *30*, 403.

10. Takahashi, K.; Furushoh, R. *Polym. Sci. A - Polym. Chem.* **1996**, *28*, 458.

11. Breslow, R. *Rec. Trav. Chim. Pays-Bas- J. Royal Netherlands Chem. Soc.* **1994**, *113*, 493.

12. Seel, C.; Vögtle, F. *Angew. Chem., Int. Ed. Engl.* **1992**, *31*, 528.

13. Vögtle, F.; Knops, P. *Angew. Chem., Int. Ed. Engl.* **1991**, *30*, 958.

14. Shinkai, S. In *Inclusion Phenomena and Molecular Recognition*; Atwood, J. L., Ed.; Plenum Press: New York, **1990**; p.125.

15. Izatt, R. M.; Pawlak, K.; Bradshaw, J. S. *Chem. Rev.* **1991**, *91*, 1721.

16. Wieser, C.; Dieleman, C. B.; Matt, D. *Coord. Chem. Rev.* **1997**, *165*, 93.

17. Luning, U. In *Topics in Current Chemistry*; Springer-Verlag: Berlin, **1995**; Vol. 175.

18. Fraser, C.; Ostrander, R.; Rheingold, A. L.; White, C.; Bosnich, B. *Inorg. Chem.* **1994**, *33*, 324.

19. Fraser, C.; Bosnich, B. *Inorg. Chem.* **1994**, *33*, 338.

20. Lehn, J. M. *Angew. Chem., Int. Ed. Engl.* **1988**, *27*, 89.

21. Van Staveren, C. J.; van Eerden, J.; van Veggel, F. C. J. M.; Harkema, S.; Reinhoudt, D. N. *J. Am. Chem. Soc.* **1988**, *110*, 4994.

22. van Doorn, A. R.; Sshaafstra, R.; Bos, M.; Harkema, S.; Eerden, J.-V.; Verboom, W.; Reinhoudt, D. N. *J. Org. Chem.* **1991**, *56*, 6083.

23. Scrimin, P.; Tecilla, P.; Tonellato, U.; Veronese, A. In *Molecular Design and Bioorganic Catalysis*. Wilcox, C. S.; Hamilton, A. D., Eds.; Kluwer: Dordrecht, **1996**.

24. Lehn, J. M. *Science* **1985**, *227*, 849.

25. Drew, M. G. B. *J. Chem. Soc., Chem. Commun.* **1980**, 1122.

26. Motekaitis, R. J.; Martell, A. E.; Lehn, J. M.; Watanabe, E. I. *Inorg. Chem.* **1982**, *21*, 4253.

27. Agnus, Y.; Louis, R.; Gisselbrecht, J. P.; Weis, R. *J. Am. Chem. Soc.* **1984**, *106*, 93.

28. Motekaitis, J. R.; Martell, A. E.; Dietrich, B.; Lehn, J. M. *Inorg. Chem.* **1984**, *23*, 1588.

29. Vigato, P. A.; Tamburini, S; Fenton, D. E. *Coord. Chem. Rev.* **1990**, *106*, 25.

30. van Veggel, F. C. J. M.; Verboom, W.; Reinhoudt, D. N. *Chem. Rev.* **1994**, *94*, 279.

31. Yoon, J. Y.; Cram, D. J. *J. Am. Chem. Soc.* **1997**, *119*, 11796.

32. a) Weber, D. E.; Vögtle, F. In *Host Guest Complex/Macrocycles*; Springer-Verlag: Berlin, **1985**. b) Vögtle, F. *Supramolecular Chemistry: An Introduction*; John Wiley & Sons: New York, **1995**.

33. Wüdel, F.; Gaeta, F. *J. Chem. Soc., Chem. Commun.* **1972**, 107.

34. Cram, D. J. *Angew. Chem., Int. Ed. Engl.* **1988**, *27*, 1009.

35. Stoddart, J. F. *Chem. Soc. Rev.* **1979**, *8*, 85.

36. Peacock, S. C.; Walba, D. M.; Gaeta, F. C. A.; Helgeson, R. C.; Cram, D. J. *J. Am.*

Chem. Soc. **1978**, *100*, 8190.

37. Peacock, S. C.; Walba, D. M.; Gaeta, F. C. A.; Helgeson, R. C.; Cram, D. J. *J. Am. Chem. Soc.* **1980**, *102*, 2043.

38. Sorrell, T. N. *Tetrahedron* **1989**, *45*, 3.

39. Brunner, H.; Schiessling, H. *Angew. Chem., Int. Ed. Engl.* **1994**, *33*, 125.

40. van Veggel, C. J. M.; Reinhoudt, D. N. *Frontiers in Supramolecular Organic Chemistry and Photochemistry*; Schneider, H. J.; Duerr, H., Eds.; VCH: Weinheim, **1991**; p.83.

41. van Veggel, F. C. J. M.; Bos, M.; Harkema, S.; van de Bovenkamp, H.; Verboom, W.; Reedijk, J.; Reinhoudt, D. N. *J. Org. Chem.* **1991**, *56*, 225.

42. Frack, C. J.; Van Veggel, K. M.; Bos, M. *Angew. Chem., Int. Ed. Engl.* **1989**, *28*, 746.

43. Janssen, K. B. M.; Laquiere, I.; Dehaen, W.; Parton, R. F.; Vankelecom, I. F. J.; Jacobs, P. A. *Tetrahedron: Asymm.* **1997**, *8*, 3481.

44. Martinez, L. E.; Leighton, J. L.; Carsten, D. H.; Jacobsen, E. N. *J. Am. Chem. Soc.* **1995**, *117*, 5897.

45. Larrow, J. F.; Schaus, S. E.; Jacobsen, E. N. *J. Am. Chem. Soc.* **1996**, *118*, 7420.

46. Hansen, K. B.; Leighton, J. L.; Jacobsen, E. N. *J. Am. Chem. Soc.* **1996**, *118*, 10924.

47. Kokubo, C.; Katsuki, T. *Tetrahedron* **1996**, *52*, 13895.

48. Nagata, T.; Imagawa, K.; Yamada, T.; Mukaiyama, T. *Bull. Chem. Soc. Jpn.* **1995**, *68*, 3241.

49. Palucki, M.; Hanson, P.; Jacobsen, E. N. *Tetrahedron Lett.* **1992**, *33*, 7111.

50. Fukuda, T.; Katsuki, T. *Synlett* **1995**, 825.

51. Fukuda, T.; Katsuki, T. *Tetrahedron* **1997**, *53*, 7201.

52. Yamashita, Y.; Katsuki, T. *Synlett* **1995**, 829.

53. a) Casiraghi, G.; Casnati, G.; Cornia, M.; Pochini, A.; Puglia, G.; Sartori, G.; Ungaro, R. *J. Chem. Soc., Perkin Trans. II* **1978**, 318. b) Zwanenburg, D. J.;

Reynen, W. A. P. *Synthesis* **1976**, 624. c) Christensen, H. *Synth. Commun.* **1975**, *5*, 65.

54. Casiraghi, G.; Casnati, G.; Puglia, G.; Sartori, G.; Terenghi, G. *J. Chem. Soc., Perkin Trans. I* **1980**, 1862.

55. Marvel, C. S.; Tarkoy, N. *J. Am. Chem. Soc.* **1957**, *79*, 6000.

56. Li, Zhaopeng, Ph.D. Dissertation, Memorial University, St. John's, NF, **1996**.

57. Galsbol, F.; Steenbol, P.; Sorensen, B. S. *Acta Chem. Scand.* **1972**, *26*, 3605.

58. Lindoy, L. F. In *The Chemistry of Macrocyclic Ligand Complexes*; Cambridge University Press: New York, **1989**.

59. Gullotti, M.; Pasini, A.; Zanderighi, G. M.; Ciani, G.; Sironi, A. *J. Chem. Soc., Dalton Trans.* **1981**, 902.

60. Gullotti, M.; Casella, L.; Pasini, A.; Ugo, R. *J. Chem. Soc., Dalton Trans.* **1977**, 339.

61. Passini, A.; Gullotti, M.; Ugo, R. *J. Chem. Soc., Dalton Trans.* **1977**, 346.

62. Gutsche, C. D.; Vicens, J.; Bohmer, V. *Calixarenes, a Versatile Class of Macrocyclic Compounds*; Kluwer: Dordecht, **1990**.

63. Bermejo, M. R.; Fondo, M.; GarciaDeibe, A.; Rey, M.; Sanmartin, J.; Sousa, A.; Watkinson, M.; McAuliffe, C. A.; Pritchard, R. G. *Polyhedron* **1996**, *15*, 4185.

64. Zhang, W.; Jacobsen, E. N. *J. Org. Chem.* **1991**, *56*, 2296.

65. Elder, R. C. *Aust. J. Chem.* **1978**, *31*, 35.

66. Zaegel, F.; Gallucci, J. C.; Meunier, P.; Gautheron, B.; Bzowej, E. I.; Paquette, L. A. *Organometallics* **1995**, *14*, 4576.

Chapter 3

Studies of Mono- and Binuclear Nickel Chiral Calixsalen Complexes

3.1 Introduction

Almost every transition metal can catalyse epoxidation of alkenes with terminal oxidants such as peroxy acids, hydroperoxides, amine oxides, iodosylbenzene, and hypochlorite.[1,2] It is generally believed[1,2] that a metal-peroxo species (MO_2) for early transition metals or a metal-oxo species (MO) for the middle and late transition metals is involved as an intermediate in the reaction. The metal serves as an oxygen relay, possibly via an oxidative-addition/reductive-elimination sequence, to accomplish catalytic oxidation. Those transition metals that can readily change oxidation states and coordination numbers are good epoxidation catalysts. Fe(III), Mn(III), and Re(IV) are particularly effective.[3-5]

On the other hand, transition-metal-based chiral catalysts effective in asymmetric catalytic epoxidation are scarce and, moreover, chiral binuclear macrocyclic catalysts have not been reported even though they are expected to show better catalytic properties, such as higher activity and selectivity, than their mononuclear analogs.[6] Examples of mononuclear chiral catalysts are the chiral diethyl tartrate- mediated titanium,[7] chiral

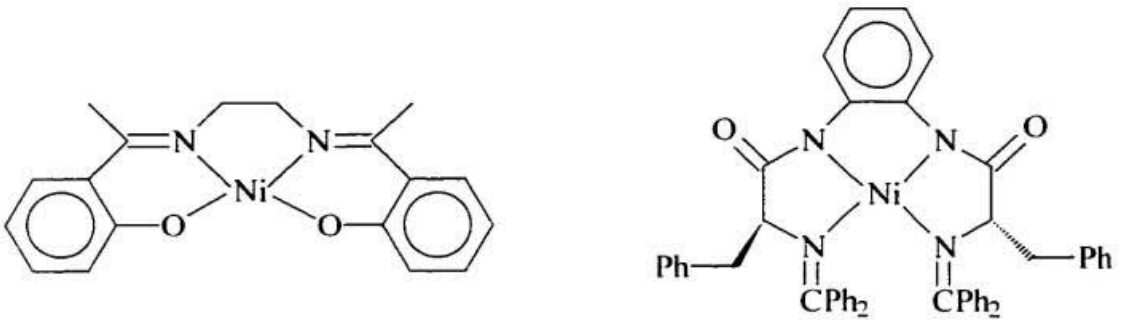

a **b**

Figure 3.1 Representative nickel complexes exploited in epoxidation

BINOL-ligated lanthanoid (La or Yb) complexes,[8] and chiral salen-mediated manganese catalysts[9] (Chapter 1). Other platinum(VI),[10] nickel(II),[11] and iron(III)[12] chiral complexes only gave 30% ee or less.

Since high oxidation state nickel was found in various nickel complexes[13, 14] and particularly macrocycle-based nickel complexes which were synthesized to mimic nickel-containing redox enzymes and co-enzymes, showed catalytic activities in epoxidation reactions,[11, 15-17] preparation of chiral macrocyclic mono- and binuclear nickel "calixsalen" complexes were therefore initially attempted in this study. There were also several other considerations. Firstly, achiral salen-based nickel complex, shown in Figure 3.1 **a**, had the highest activities among the previously developed nickel complexes.[15, 18] However, chiral versions of these catalysts have not been reported. Secondly, salen Ni(II) complexes are normally square planar and diamagnetic. Therefore, conformation and structure studies of this class of complexes became possible using NMR. In this regard,

Dangel *et al.*[19] recently reported a chiral salen-like nickel complex (Figure 3.1 **b**) derived from amino acids, but only 4% ee was reported in epoxidation of *trans*-β-methylstyrene.

This chapter describes the preparation and characterization of the chiral calixsalen mono- as well as binuclear nickel complexes and the results of their host/guest and catalytic properties.

3.2 Results and Discussion

3.2.1 Preparation of chiral mono- and binuclear nickel(II) calixsalen complexes

With regard to complexation of calixsalens, the challenge was how to introduce sequentially transition metals into the two identical coordination sites to obtain mononuclear complexes.[20, 21] If this were possible, both mononuclear complexes and the corresponding homobinuclear and heterobinuclear complexes might be accessible and would provide a new window in the exploration of chiral metallamacrocycles,[22] which are generally synthesized by transition-metal-directed self-assembly of simple racemic or chiral precursors.[22-24] The synthesis of mononuclear macrocyclic complexes was therefore attempted, and it was found that solvent was extremely important in determining the outcome of complexation. With MeOH and CH_2Cl_2, MeOH and $CHCl_3$, or MeOH and THF as solvents, the anticipated mononuclear Ni(II) complexes **3.1-3.4** were formed as the major products at room temperature (Scheme 3.1). Complexation at

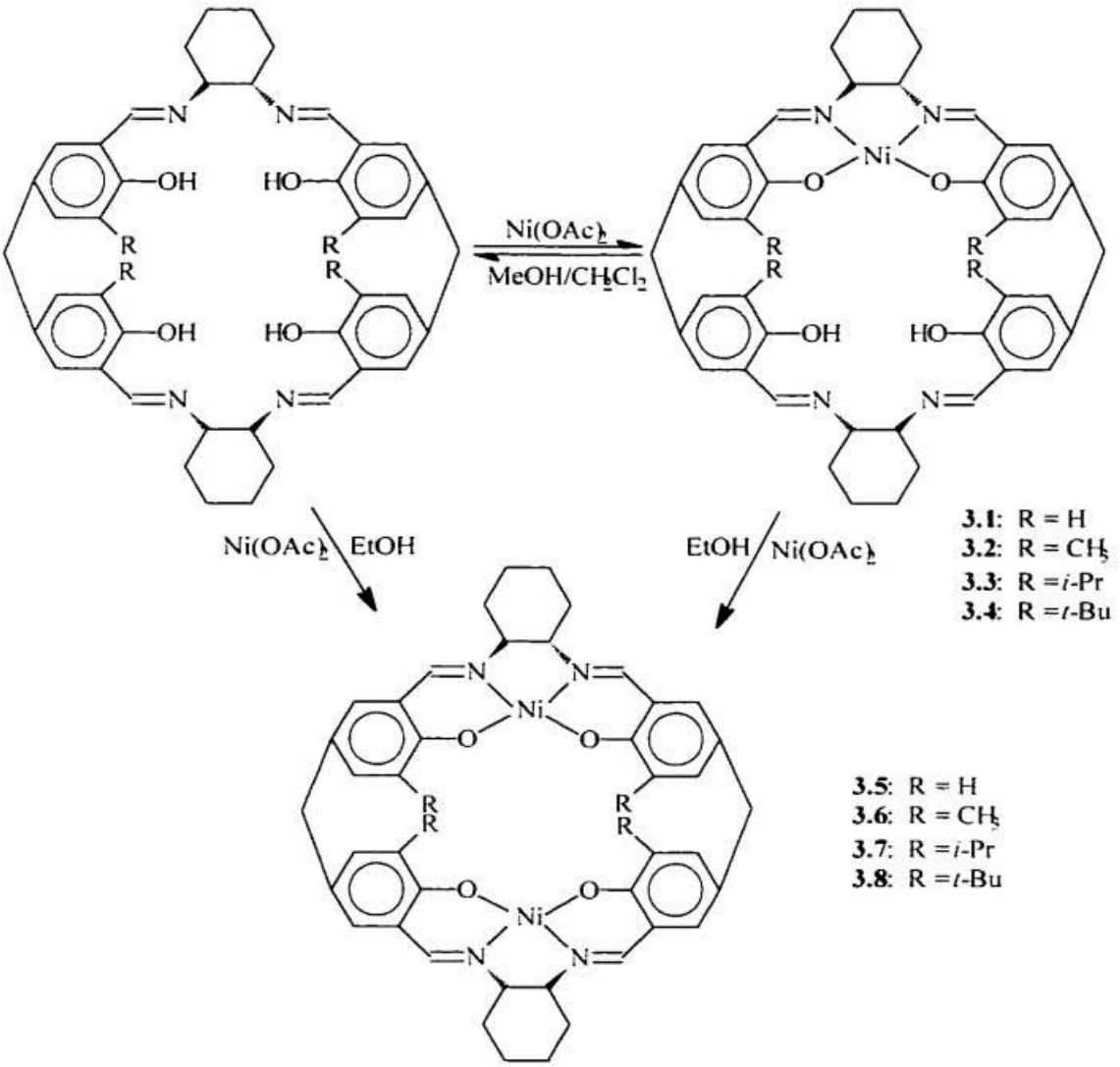

Scheme 3.1 Preparation of the mono- and binuclear calixsalen nickel(II) complexes

higher temperature (50°C) also gave mononuclear Ni(II) complexes in these solvent systems. Increasing the reaction time from 4 h to 24 h at 50°C with an excess of the Ni(II) salt gave ring-opened Ni(II) complexes, which were confirmed by ^{1}H NMR

observation of free OH (11.67 ppm) and CHO (9.80 ppm). Of note was that free ligand was always present during the reaction as observed by TLC, suggesting the presence of an equilibrium between a mononuclear complex and free ligand in solution. This assumption was also supported by the observation that the characteristic imine signal of the free ligands was observed in the ^{1}H NMR spectrum after storing the mononuclear Ni(II) complex in $CDCl_3$ over a period of one week. In contrast, the solid complexes were stable in air at room temperature. Interestingly, the complexes were even more soluble than the corresponding free ligands in almost all organic solvents tested. The nickel complex **3.4** even dissolved in benzene and paraffin oil! Elemental analysis, NMR spectroscopy, infrared spectroscopy and, in the case of **3.4**, X-ray diffraction confirmed that only one of the two tetradentate salen sites was coordinated (sections 3.2.2 and 3.2.4).

Unexpectedly, the binuclear Ni(II) complexes **3.5-3.8** were obtained almost quantitatively by complexation of either the chiral calixsalens or the mononuclear complexes with $Ni(OAc)_2$ when the reactions were carried out in EtOH at room temperature (Scheme 3.1). Structures of the complexes were established from elemental analysis, infrared spectroscopy, NMR and, in the case of **3.8**, X-ray diffraction. The reactions were facile and clean at room temperature. With time, a dark-red, highly crystalline solid gradually appeared and no free ligand was observed by TLC analysis. In the case of **3.8**, ^{1}H NMR (Figure 3.2) of the crude products showed that only mononuclear and binuclear

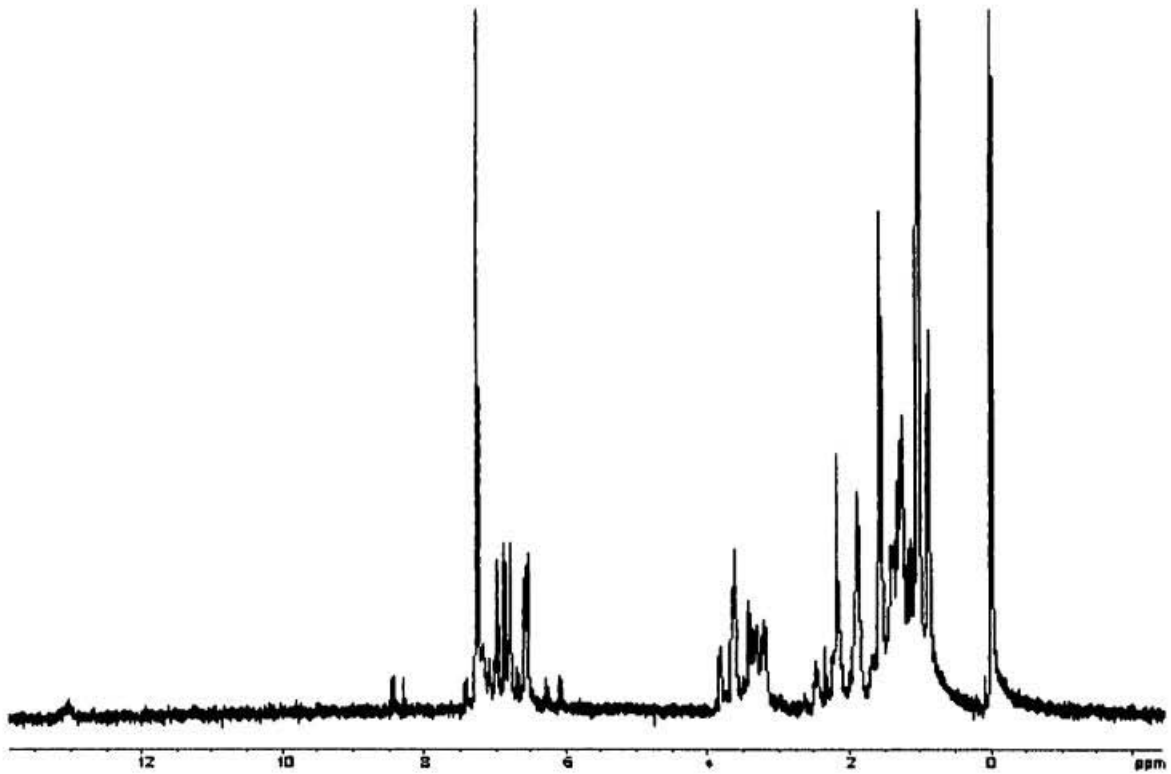

Figure 3.2 1H NMR spectrum of the crude products of 3.8 ($CDCl_3$)

complexes, with the latter dominant, formed.

As indicated above, solvent could change the product distribution. The driving force for formation of the binuclear complexes was a result of the poor solubility of the binuclear products in EtOH.

3.2.2 Spectroscopic analysis of the mononuclear nickel(II) calixsalen complexes in solution

All complexes were diamagnetic and gave sharp, well resolved ^{1}H NMR signals, implying that the d^{8} Ni(II) must adopt a planar geometry in solution. The ^{1}H and ^{13}C NMR chemical shifts observed in the complexes **3.1-3.4** were consistent with a mononuclear nickel calixsalen structure, and the assignments were based on HETCOR spectra (One of the spectra is shown in Figure 3.3). Two ^{1}H NMR signals at low field, corresponding to two free OH groups in the free salen site, were observed in all complexes. The shifts around 8 ppm were assigned to the two free imine protons whereas the complexed CH=N protons were shifted upfield. Eight aromatic resonances corresponding to the eight aromatic protons were observed in all mononuclear complexes and therefore no topological isomers were apparent. For instance, the two free imine protons in the complex **3.8** gave two well-separated signals at 8.42 and 8.20 ppm, which required that they were no longer chemically equivalent as in the free ligand **14d** (Chapter 2). It was further noted that the two free imine protons resonated at significantly

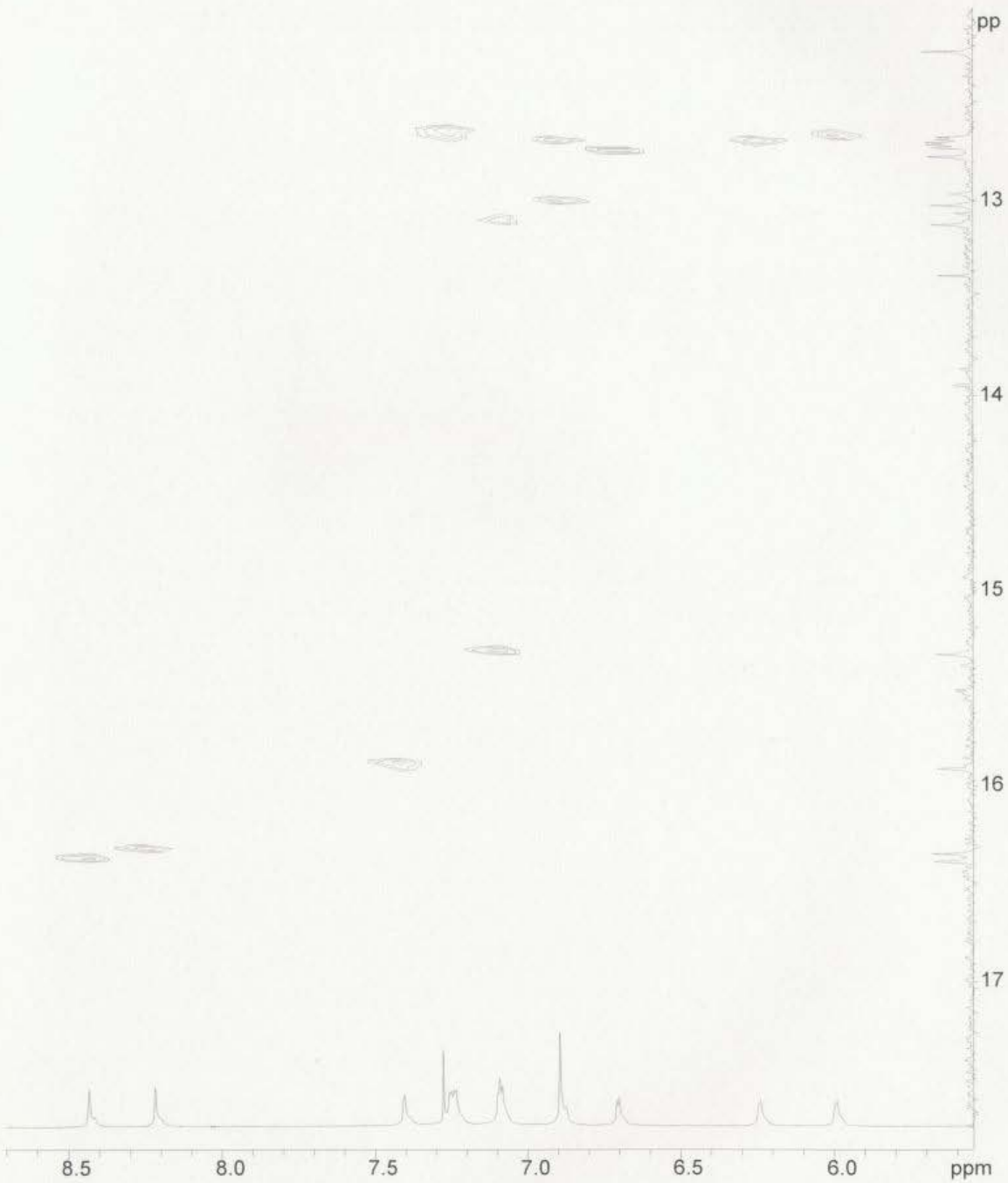

Figure 3.3 Expanded HETCOR spectrum of the mononuclear nickel(II) complex **3.4** ($CDCl_3$)

different downfield shifts ($\Delta\delta\delta_1$ = +0.35 ppm, $\Delta\delta\delta_2$ = +0.13 ppm) in comparison with the imine signal ($\Delta\delta$ = 8.07 ppm) of the corresponding free ligand.

Since conjugation between the two bridged-benzene rings was impossible, the observed chemical shift changes in the free salen moiety were probably due to enhanced ring constraint after embedding one nickel(II) in the remaining salen moiety. The molecular structure (Figure 3.5, p. 111) revealed that one of the free imine signals was forced into the deshielding zone of the other benzene ring in the complexed salen site.

The two complexed imine protons were also non-equivalent but underwent upfield shifts ($\Delta\Delta\delta_1$ = -1.00 ppm, $\Delta\delta\delta_2$ = -0.68 ppm). This was a direct result of complexation which reduced the electron density of the CH=N bonds. The chemical shift difference of the complexed imine protons was likely due to a steric effect since one site might be more crowded than another.

Among the eight aromatic proton signals, four from the complexed salen moiety appeared at higher field because of the positive charge imposed by Ni(II). The other four protons on the free salen moiety were chemically non-equivalent and appeared at lower field (6.68 ppm, 7.24 ppm, 7.07 ppm, and 7.22 ppm).

Analysis of the ^{1}H NMR spectrum revealed that the mononuclear complex had C_1

symmetry in solution. Therefore, fifty carbon signals for complex **3.4** were expected and found. Four imine carbon signals were observed at 167.8 and 167.3 ppm for the free imines and 164.0 and 157.8 ppm for the complexed imines. In the latter case, one of the CH=N carbons shifts significantly upfield ($\Delta\delta\delta$ = -6.3 ppm) compared to the other. This change can be explained on the basis of a steric environment difference around the two imine bonds. One CH=N bond was more twisted than the other and appeared at higher field. This argument was supported by the observation that larger R groups gave greater chemical shift differences. Changing R in the series CH_3, *i*-Pr, *t*-Bu resulted in ^{13}C NMR chemical shift differences between the two complexed imine carbons in each complex of 5.5 ppm, 5.6 ppm, and 6.3 ppm. The same order (0.0 ppm, 0.3 ppm, and 0.4 ppm) was followed for the two free imine carbons. Twenty four aromatic carbon signals were observed. Two aromatic methine carbons were overlapped at 131.0 ppm. The expected four chiral carbons were observed at 73.2, 72.5, 71.2, and 68.7 ppm. The two methylene bridge carbons were found at 40.2 and 39.6 ppm. The quaternary carbons of the *t*-butyl groups appeared at 35.9 ppm on the complexed site and 35.4 ppm on the free site. All remaining carbon signals were buried under acetone solvent signal.

In order to ascertain the remaining resonances mentioned above, ^1H and ^{13}C NMR were measured in $CDCl_3$. Surprisingly, not only did the chemical shifts of the complexes change but also the splitting pattern of the aromatic protons was substantially altered. It was likely that these effects resulted from host/guest complexation between the

mononuclear complex and the solvents (see section 3.2.5).

3.2.3 Spectroscopic studies of the binuclear Ni(II) calixsalen complexes in solution

Figure 3.4 shows the low field expansion of the HETCOR spectrum of the diamagnetic binuclear Ni(II) complex **3.8**. The number of peaks was half of that observed in the mononuclear analogues. For example, two signals for the four imine protons, and four resonances for the eight aromatic protons were observed for the complex **3.8**. These results indicated the presence of a C_2 symmetry element in the binuclear complexes. It was then possible that the complex would have a *syn* or *anti* conformation with respect to the two cyclohexyl rings. Analysis of the bridging methylene proton NMR signals could provide a clear answer. If the conformation of the complex is *anti*, then the two methylene protons would be equivalent and a singlet should be observed in the ^{1}H NMR spectrum. If the conformation is *syn*, then the two protons would be diastereotopic and an AB pattern would be expected. Examination of the ^{1}H NMR spectra (see Figures A3.11 and A3.12 in appendix 6) of the complexes revealed an AB pattern. Therefore, the binuclear complexes were *syn* and the C_2 axis was perpendicular to the cavity. Consistent with the ^{1}H NMR data, the ^{13}C NMR spectrum showed two imine, twelve aromatic, two chiral, one bridge methylene, and six cyclohexyl ring carbon resonances, as expected for the binuclear complex **3.8**.

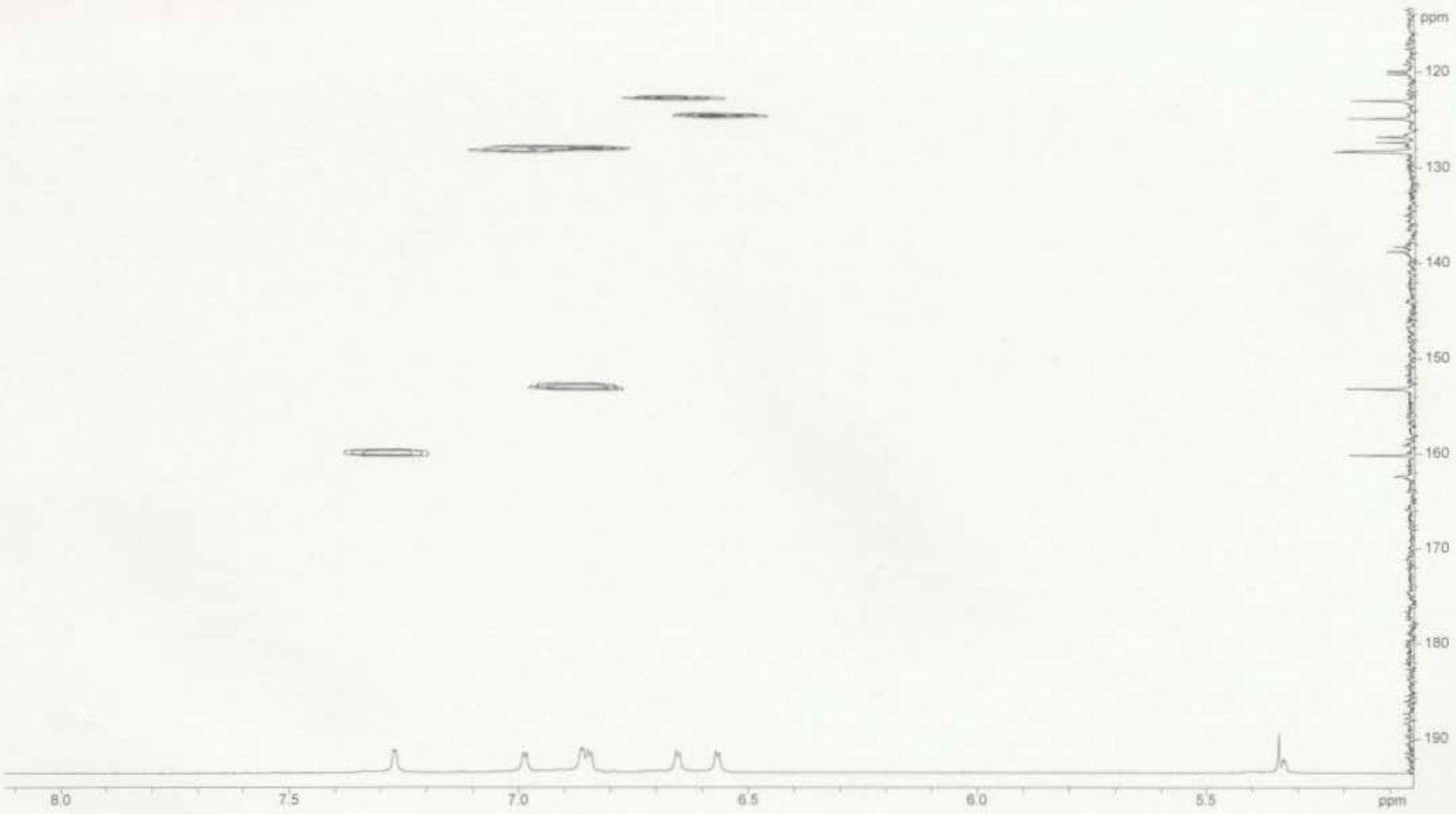

Figure 3.4 Expanded HETCOR spectrum of the binuclear nickel(II) complex **3.8** (CD_2Cl_2)

3.2.4 Characterization of the mono- and binuclear nickel(II) macrocyclic salen complexes by X-ray diffraction

In order to clarify the structure elucidated by solution studies and to investigate the cavity shape, size, and especially the Ni(II)-Ni(II) distance,[25] crystallographic studies were carried out on complexes **3.4** and **3.8**. A dark red crystal of **3.4** was grown by slow evaporation of a solution of **3.4** in CH_2Cl_2/CH_3CN (1:1) at room temperature over a period of about one month. Dark red crystals of **3.8** were obtained through slow evaporation of a $CH_3CN/CH_2Cl_2/EtOH$ solution. The molecular structures[a, b] obtained from X-ray diffraction studies are shown in Figures 3.5-3.7.

Figure 3.5 shows that only one salen site was coordinated to nickel(II) in **3b**. The four donor atoms and the central metal Ni(II) were essentially coplanar, as evidenced by the bond angles O1-Ni-N3 174.0°, O4-Ni-N4 179.1°, O1-Ni-O4 89.0°, and N3-Ni-N4 85.4°.

---

[a]Crystal data for the mononuclear complex **3.4** ($C_{58}H_{74.50}O_{4.25}N_4Ni$): fw = 954.45; dark red, crystal dimension = 0.32 x 0.20 x 0.13 mm, trigonal, $P3_1$ (#144), a = 18.2566(2) Å, c = 15.9244(2) Å, V = 4596.57(8) Å^3, Z = 3, D_{calcd} = 1.04 g/cm^3, R = 0.054, R_w = 0.049.

[b]Crystal data for **3.8** ($C_{60.70}H_{83.40}O_4N_5Ni_2Cl_{1.40}$): fw = 1114.19, red, crystal dimension = 0.25 x 0.10 x 0.40 mm, orthorhombic, $P2_12_12_1$ (#19), a = 19.531(2) Å, b = 22.819(3) Å, c =13.373(1) Å, V = 5960(1) Å^3, Z = 4, D_{calcd} = 1.242 g/cm^3, R = 0.067, R_w = 0.065.

Crystal data, atomic coordinates, selected bond distances, angles, and torsional angles are listed in Appendix 2.

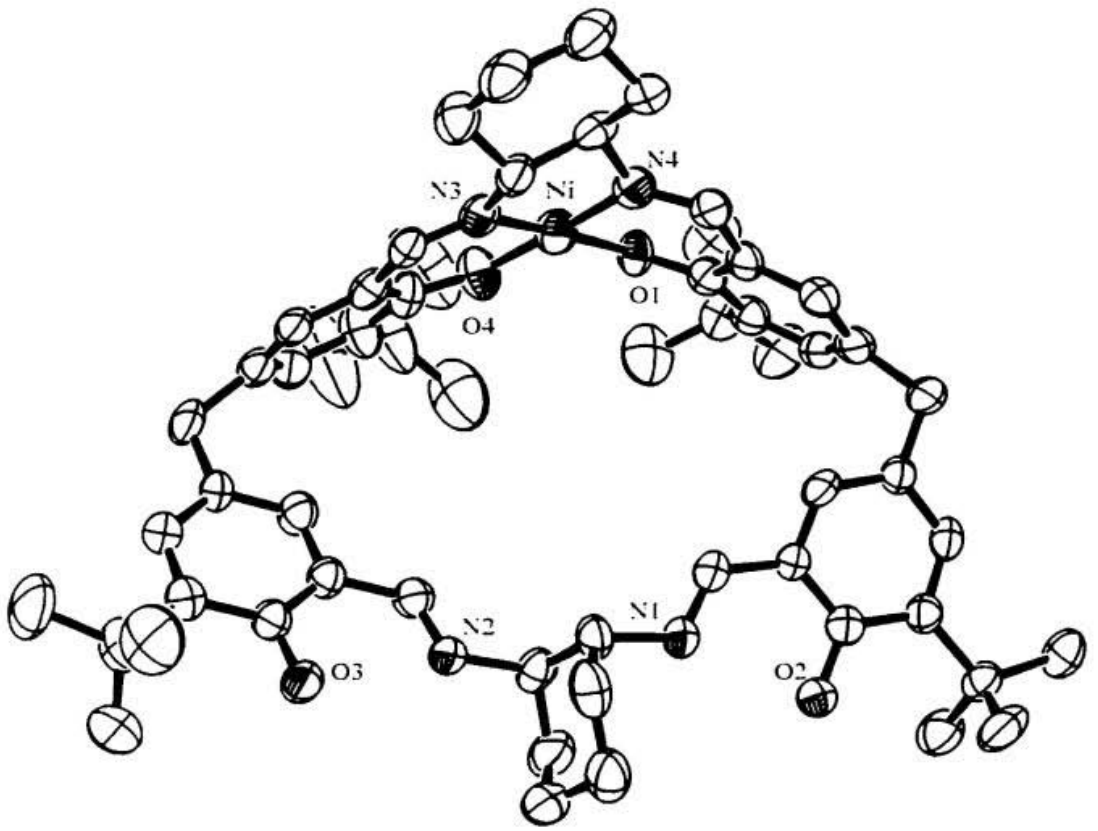

Figure 3.5 ORTEP representation of the chiral mononuclear nickel(II) complex **3.4** (Hydrogen atoms and solvent were removed for clarity.)

The average O-Ni 1.86 Å and N-Ni 1.85 Å bond distances were on the order of 2 Å.[26] which compared favourably with a reported crown-ether-salen-based mononickel macrocyclic complex.[26] As a result of this array, the two benzene rings in the complexed salen site had a roof-like geometry. On the other hand, the two free benzene rings were twisted away from each other, presumably due to the *trans* nature of the two single C-N bonds and steric crowding of the *t*-butyl groups. This in turn resulted in an *anti* disposition of the two imine bonds on both sides of the chair-shaped cyclohexyl ring. Clearly, based on this structure, coordination of the second Ni(II) would require substantial conformation adjustment. Additionally, with a cavity size *ca.* 12.1 x 7.7 Å defined by the four benzene rings and heteroatoms, it would be expected that the mononuclear complex would have host/guest properties.

The X-ray diffraction study of the complex **3.8** (Figures 3.6 and 3.7) confirmed the structural features of the binuclear nickel complexes derived from solution NMR experiments. Both Ni(II) atoms had planar coordination geometry with bond angles about the same as those of its mononuclear analogue **3.4**. Metal-ligand distances were typical for Ni(II).[27] As shown in Figure 3.7, the two nickel atoms were almost face-to-face with a separation of 7.2 Å. The *syn* conformation, derived from the solution study (section 3.2.4) of the molecule which had effective C_s symmetry with a pseudo-C_2 axis passing through the cavity centre, was retained in the solid state. Four phenyl rings established a well

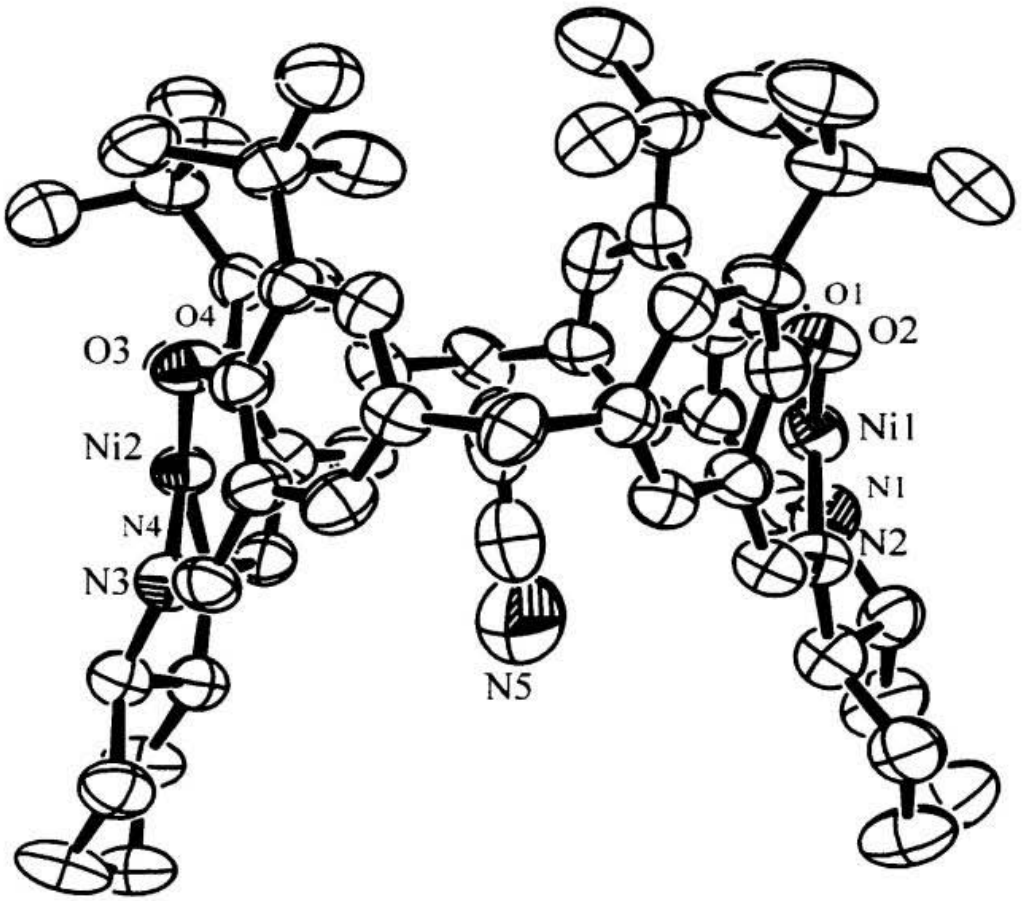

Figure 3.6 ORTEP representation (side view) of the chiral binuclear nickel(II) complex **3.8** (Hydrogen atoms and solvent CH_2Cl_2 outside of the cavity were removed for clarity.)

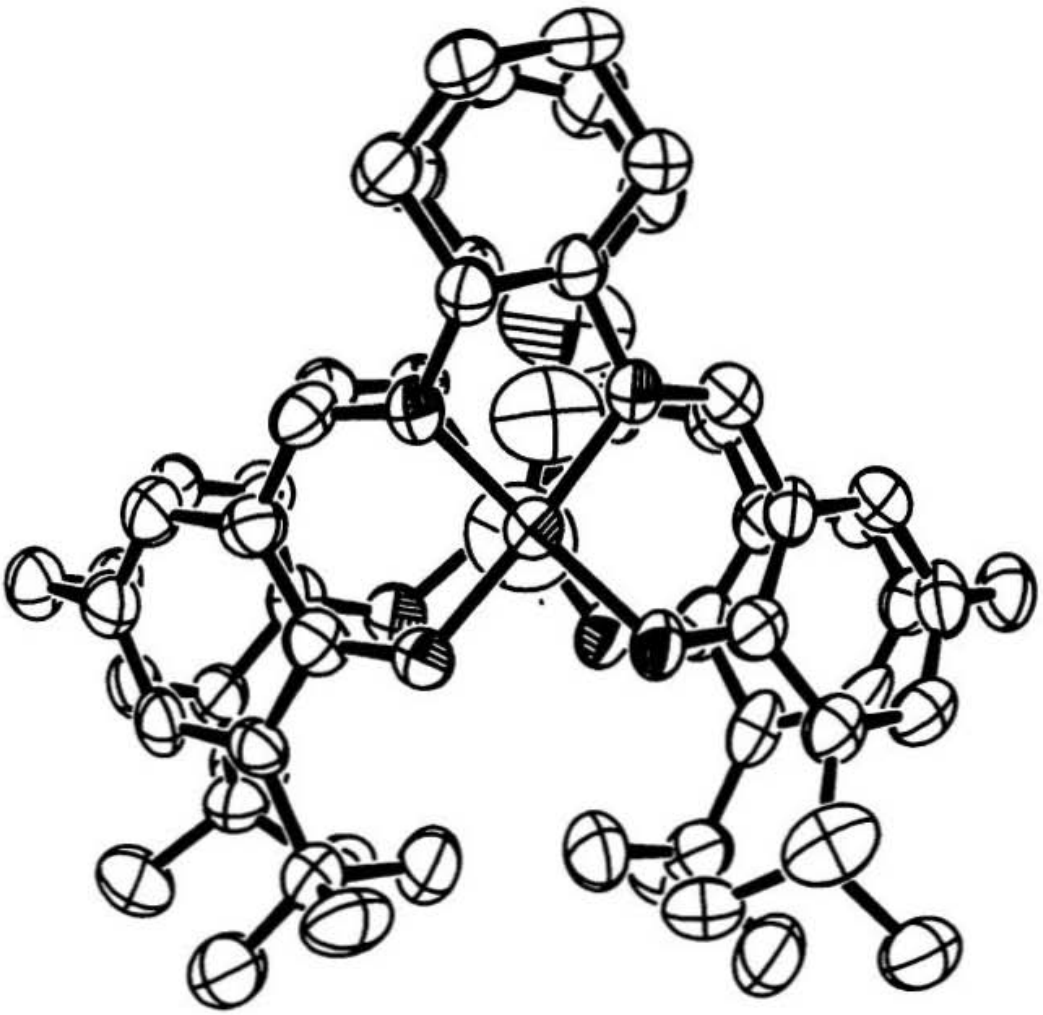

Figure 3.7 ORTEP representation (top view) of the chiral binuclear nickel(II) complex **3.8** (Hydrogen atoms and solvent CH_2Cl_2 outside of the cavity were removed for clarity.)

formed cavity of approximate dimensions 7.2 x 7.2 Å. Two cyclohexyl rings stood on one side of the cavity defining a minimum aperture of 5.4 Å. On the other side, the four *t*-butyl groups formed a *gate* with a maximum width of 2.7 Å. Therefore, it was expected that a guest molecule would prefer to enter the cavity through the cyclohexyl side. This entrance, which is closer to the chiral centres, should result in a more effective chiral communication which would benefit chiral induction in asymmetric catalysis.[28] Figures 3.6 and 3.7 show that a guest acetonitrile molecule resides in the cavity along the twofold axis with the methyl group preferentially lying within the intramolecular cavity between the two Ni(II) atoms in an average Ni(II)...CH_3 distance of 3.8 Å (Figure 3.7). The C≡N group is directed toward the more open cyclohexyl side, suggesting the expected approach of the guest molecule. Furthermore, the shortest contact between the methyl carbon of CH_3CN and the aromatic carbons was *ca.* 3.8 Å. Therefore, it was most likely that -CH_3 -π interactions within the electron-rich cavity imposed by the four benzene rings rather than coordination of -CN to Ni(II) had driven the guest molecule into the cavity. A structurally characterized inclusion compound between *p-tert*-butylcalix[4]arene tetracarbonate and acetonitrile showed a similar phenomenon.[29]

3.2.5 Host/guest and catalytic properties of mono- and binuclear nickel(II) calixsalen complexes

The cavity associated with the heteroatoms N, O, and Ni(II) suggested the possibility of recognition of neutral guest molecules.[26] In a preliminary search, the mono- and

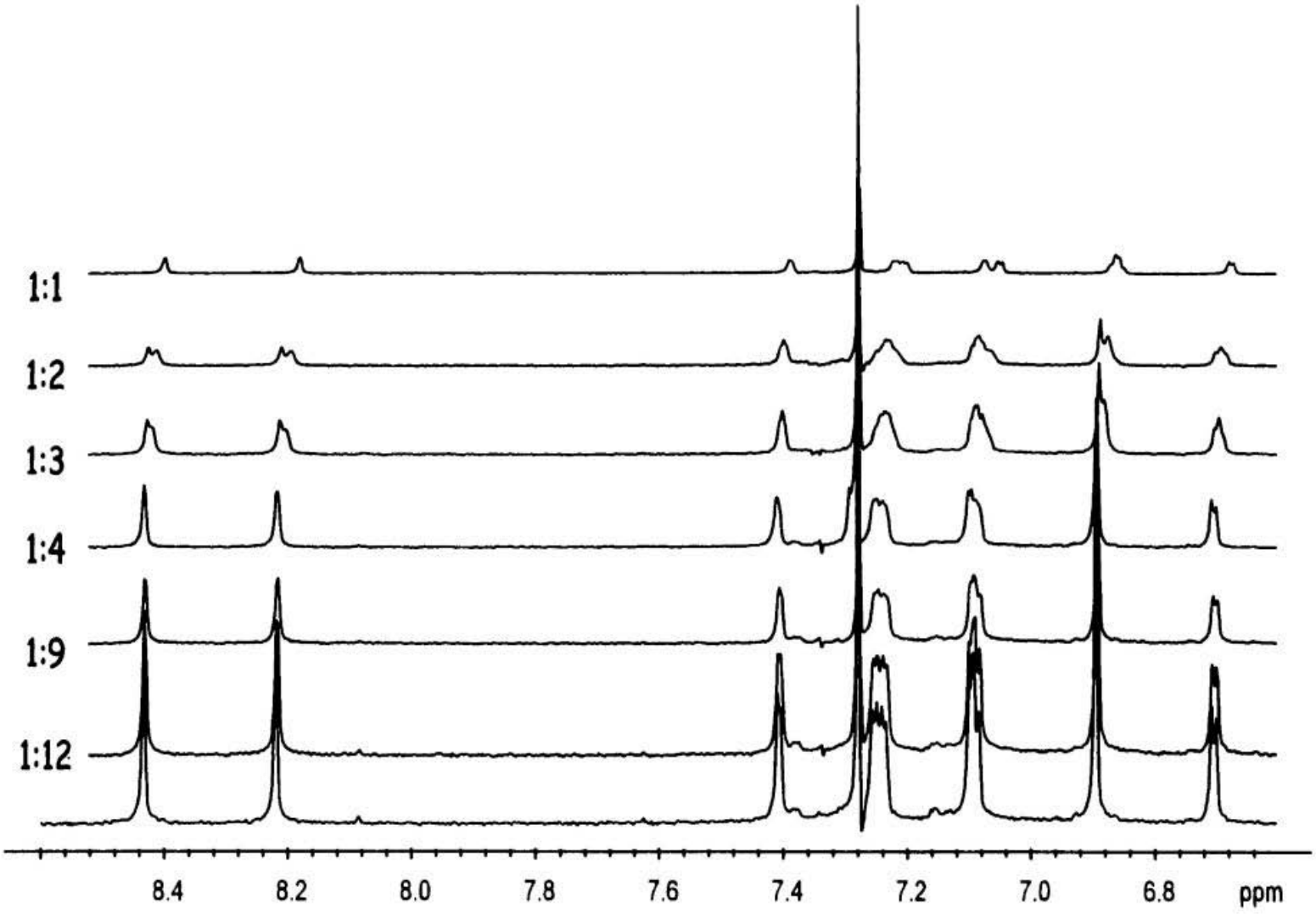

Figure 3.8 ^{1}H NMR spectra for titration of the complex **3.4** with acetone in $CDCl_3$

binuclear nickel complexes **3.4** and **3.8** were examined with acetone, benzene, styrene oxide, acetonitrile, and the chiral molecule 2-bromo-2-chloro-1,1,1-trifluoroethane, using an NMR titration technique.

There were no obvious chemical shift changes observed on gradual addition of acetone to a solution of **3.8** in $CDCl_3$. On the other hand, the chemical shifts of the free imine as well as the aromatic protons of the mononuclear complex **3.4** were moved upfield by 0.05-0.07 ppm. However, the chemical shifts of the complexed imine protons remained unchanged (Figure 3. 8). The observed changes in the proton chemical shifts upon addition of acetone suggested complexation of the host **3.4** and the guest acetone. The calculated association constant was 1.5×10^5 L mol^{-1}. Since only those chemical shifts of the protons around the cavity changed, the acetone guest molecule therefore was likely positioned inside the cavity and not coordinated on Ni(II). In the latter case, broad signals and chemical shift changes of the complexed imines should also be observed. Titration of the other potential guest molecules mentioned above showed no significant chemical shift changes with either mono- or binuclear complexes **3.4** and **3.8.**

The catalytic activity of the mono- and binuclear nickel complexes **3.4** and **3.8** was examined at room temperature, using styrene as the substrate and sodium hypochlorite as the oxidant. Based on TLC analysis, no reactions were evident after 4 h, indicating that these complexes were catalytically inactive for epoxidation.

3.3 Summary

Sequentially, controlled complexation of the macrocyclic salen dimers containing methylene bridges with nickel acetate gave mono- and binuclear calixsalen complexes. NMR and X-ray studies revealed that the mononickel complexes were C_1 symmetric. The relatively large cavity defined by the four benzene rings and five heteroatoms for the mononuclear complex resulted in host/guest interactions with acetone, which were demonstrated by ^{1}H NMR titration experiments. The binuclear complexes were C_2 symmetric with an overall *syn* conformation both in solution and in the solid state. An acetonitrile molecule lies on the twofold axis within the intramolecular cavity between the two almost face-to-face nickel atoms. No catalytic activity was evident for the epoxidation of styrene with NaOCl in the presence of the mono- or the binuclear nickel complexes.

3.4 Experimental Section

3.4.1 Chemicals and instrumentation. All solvents were ACS grade and used as received. Nickel(II) acetate tetrahydrate was purchased from Aldrich and used as received. Ethanol refers to absolute ethanol. All instrumentation was the same as described in Chapter 2 unless otherwise specified.

3.4.2 Preparation of the mononuclear Ni(II) complexes

General procedure. To the yellow, free ligand (0.056 mmol) solution in CH_2Cl_2 (4.0 mL) was added $Ni(OAc)_2 \cdot 4H_2O$ (0.028 g, 0.012 mmol) dissolved in a minimal amount of MeOH. The solution instantly changed to red. After stirring for 4 h at room temperature (if there was any precipitate, more CH_2Cl_2 was added until the solution became clear), solvents were removed under vacuum, and the crude product was extracted with two 4 mL-portions of CH_2Cl_2. The red CH_2Cl_2 solution was then applied to a small silica gel column with CH_2Cl_2 as the initial eluent to remove the unreacted free ligand and then with MeOH to elute the product. Removal of the solvent gave an orange-yellow solid.

***(R,R)*-3.1 Yield:** 0.032 g (78%). **IR** (Nujol): 1628 (CH=N), 1533 (Ph), 1490, 1469,1364, 1318, 1270, 1209, 1225, 1163, 1047, 1016, 954, 933, 901, 821, 792, 731 cm^{-1}; **^{1}H NMR** ($CDCl_3$): δ 8.43 (s, 1H, H-14), 8.37 (s, 1H, H-21), 7.39 (d, J=1.8, 1H, H-42), 7.22 (m, 2H, H-13, H-25), 7.10 (d, J=0.9, 2H, H-9, H-27), 7.05 (d, J=1.8, 1H, H-35), 6.92-6.83 (m, 6H,

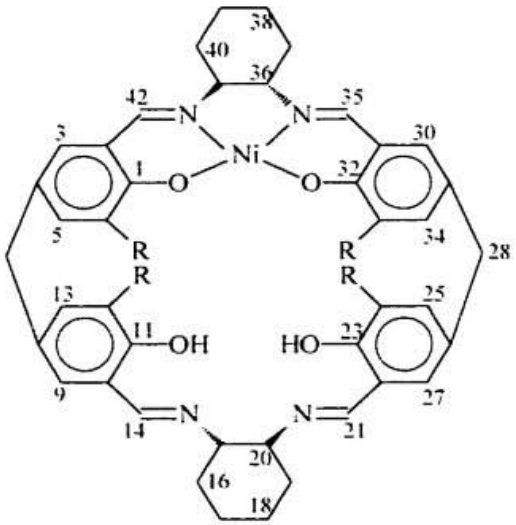

Numbering scheme for **3.1 - 3.4**

H-5. H-6. H-12. H-24. H-33. H-34). 6.29 (d. J=1.8. 1H. H-3). 6.23 (d. J=3.0.1H. H-30). 3.80 (m. 4H. H-7. H-28). 3.61 (br.1H. H-41). 3.29 (s. 1H. H-15). 3.10(s. 1H. H-20). 2.58 (m. 1H. H-36). 2.28-1.23 (br. m.16H. cyclohexyl rings): **^{13}C NMR** was not measured due to poor solubility of the compound.

(*R,R*)-3.2 Yield: 0.041 g (81%). **IR** (Nujol): 1635 (CH=N). 1549 (Ph). 1325. 1272. 1054. 1021. 902. 822. 730 cm^{-1}: **^{1}H NMR** ($CDCl_3$): δ 13.10 (s. 1H .OH). 12.99 (s. 1H. OH). 8.63 (s. 1H. H-14). 8.40 (s. 1H. H-21). 7.35 (s. 1H. H-42). 7.11 (s. 3H. H-35. H-9. H-27). 7.00 (s. 1H. H-13). 6.89 (s. 1H. H-25). 6.82 (s. 1H. H-3). 6.64 (s. 1H. H-30). 6.27 (s. 1H. H-5). 6.23 (s. 1H. H-34). 3.76 (m. 4H. H-7. H-28). 3.35 (s. 2H. H-36. H-41). 3.22 (s. 2H. H-15. H-20). 2.29 (s. 6H. 2Me_f). 2.24 (s. 3H. Me_c). 2.1 6 (s. 3H. Me_c). 2.05-1.2 6 (m. 16H. cyclohexyl rings): **^{13}C NMR** ($CDCl_3$): δ 166.5 (C-24. C-21). 164.5 (C-1). 163.4 (C-

32). 161.7 (C-42). 157.1 (C-11). 157.0 (C-23). 156.3 (C-35). 137.2 (C-13). 136.7 (C-25). 134.4 (C-8). 133.5 (C-9. C-27). 132.8 (C-26). 130.8(C-5). 130.2 (C-34). 129.9 (C-3. C-30). 126.8 (C-12). 125.8 (C-24). 125.2 (C-10). 125.0 (C-22). 121.7 (C-4). 120.9 (C-29. C-6). 118.4 (C-33). 117.6 (C-2. C-31). 72.9 (C-15). 72.0 (C-41). 71.6 (C-20). 67.7 (C-36). 39.0 (C-7). 38.8 (C-28). 30.0 (C-40). 27.9 (C-37. C-16). 27.8 (C-19). 25.1 (C-38). 24.5 (C-39). 21.4 (Me). 17.4 (C-17). 17.1 (C-18). 15.6 (Me): **Anal.** Calcd. for $C_{46}H_{50}N_4O_4Ni \bullet CH_2Cl_2$: C. 64.60 : H. 5.99 : N. 6.40. Found: C. 64.60 : H. 5.98 : N. 6.40.

(*R*,*R*)-3.3 Yield: 0.038 g (76%). **IR** (Nujol): 1628 (CH=N). 1603 (CH=N). 1538 (Ph). 1319. 1288. 1263. 1233. 1170. 1152. 1109. 1049. 1019. 946. 908. 764. 772. 736. 724 cm^{-1}: **^{1}H NMR** ($CDCl_3$): δ 13.09 (s. 1H. OH). 13.04 (s. 1H. OH). 8.45 (s. 1H. H-14). 8.29 (s. 1H. H-21). 7.43 (d. J=2.1. 1H. H-42). 7.21 (d. J=2.1. 1H. H-9). 7.19 (d. J=1.8. 1H. H-27). 7.09 (d. J=2.4. 1H. H-35). 7.02 (d. J=2.4. 1H. H-30). 6.88 (d. J=1.8. 1H. H-25). 6.82 (d. J=2.1. 1H. H-3). 6.69 (d. J=2.1. 1H. H-13). 6.28 (d. J=2.1. 1H. H-5). 6.08 (d. J=1.8. 1H. H-34). 5.31 (s. 1H. H-5). 3.84 (m. 4H. H-7. H-28). 3.65 (br. 1H. H-41). 3.43 (m. 4H. $\underline{CH}Me_2$). 3.25 (s. 1H. H-15). 3.21 (s. 1H. H-20). 2.64 (br. 1H. H-36). 2.31-2.24 (br. 2H. H-40). 1.97-1.92 (br. 6H. H-16. H-19. H-37). 1.72 (br. 4H. H-17. H-18). 1.35-1.28 [m. 12H. ($CH\underline{Me}_2$)$_t$]. 1.17-1.08 [m. 12H. ($CH\underline{Me}_2$)$_c$]: **^{13}C NMR** ($CDCl_3$): δ 166.6 (C-21). 166.4 (C-14). 164.2 (C-1). 163.1 (C-32). 161.8 (C-42). 156.2 (C-11. C-23. C-35). 141.4 (C-2). 140.7 (C-31). 135.7 (C-10. C-22). 134.1 (C-12). 133.2 (C-9. C-24. C-6). 132.2 (C-27). 130.1 (C-3). 129.6 (C-33. C-13. C-30). 129.3 (C-5. C-25). 129.0 (C-34).

125.9 (C-4). 125.8 (C-29). 121.7 (C-8). 118.2 (C-26). 72.4 (C-41). 72.0 (C-20). 71.9 (C-41). 67.7 (C-36). 39.6 (C-7). 39.2 (C-28). 30.0 (C-40). 28.0 (C-37). 27.6 (C-16. C-19). 27.3 ($\underline{CH}Me_2)_c$]. 26.7 [$(\underline{CH}Me_2)_c$]. 26.6 [$(\underline{CH}Me_2)_f$]. 25.1 (C-38). 24.5 (C-39). 23.0 [$(CH\underline{Me}_2)_f$]. 22.8 [$(CH\underline{Me}_2)_c$]. 22.7 [$(CH\underline{Me}_2)_c$]. 22.5 [$(CH\underline{Me}_2)$]. 21.4 (C-17. C-18): **Anal.** Calcd. for $C_{54}H_{70}N_4O_4Ni \bullet 2H_2O$: C. 69.75: H. 7.37 : N. 6.03. Found: C. 70.06: H. 7.27 : N. 5.91.

***(R,R)*-3.4 Yield:** 0.043 g (82%). **IR** (Nujol): 1628 (CH=N). 1536 (Ph). 1318. 1271. 1271. 1239. 1206. 1172. 1021. 946. 908. 789. 736 cm^{-1}: **^{1}H NMR** (CD_3COCD_3): δ 13.32 (s. 1H .OH). 13.21 (s. 1H. OH). 8.42 (s. 1H. H-14). 8.20 (s. 1H. H-21). 7.39 (s. 1H. H-42). 7.24 (d. J=2.1. 1H. H-9). 7.22 (d. J=1.5. 1H. H-27). 7.07 (br. 2H. H-35. H-30). 6.88 (s. 2H. H-3. H-25). 6.68 (d. J=2.7. 1H. H-13). 6.23 (s. 1H. H-5). 5.98 (s. 1H. H-34). 3.81 (s. 4H. H-7. H-28). 3.61 (br. 1H. H-41). 3.26 (s. 1H. H-15). 3.16 (s. 1H. H-20). 2.68 (br. 1H. H-36). 2.30-2.23 (br. 2H. H-40). 2.18-1.85 (br. 4H. H-37. H-16). 1.73-1.62 (br. 2H. H-19). 1.48 [s. 9H. $(C\underline{Me}_3)_f$]. 1.47 [s. 9H. $(C\underline{Me}_3)_f$. 1.37 [s. 9H. $(C\underline{Me}_3)_c$]. 1.27 [s. 9H. $(C\underline{Me}_3)_c$]: **^{13}C NMR** (CD_3COCD_3): δ 167.6 (C-21). 167.3 (C-14). 166.0 (C-1). 165.0 (C-32). 164.0 (C-42). 158.7 (C-11). 158.5 (C-23). 157.8 (C-35). 142.2 (C-2). 141.4 (C-31). 137.2 (C-10). 137.0 (C-22). 135.0 (C-6). 134.4 (C-5). 134.3 (C-33). 133.0 (C-34). 131.8 (C-3). 31.0 (C-13. C-25). 130.9 (C-30). 130.5 (C-9). 130.4 (C-27). 126.0 (C-4). 125.6 (C-29). 123.5 (C-12). 122..9 (C-24). 119.9 (C-8). 119.5 (C-26). 73.2 (C-41). 72.5 (C-36). 71.2 (C-15). 68.7 (C-20). 40.2 (C-7). 39.6 (C-28). 35.9 [two $(\underline{C}Me_3)_c$]. 35.4 [$(\underline{C}Me_3)_f$]. 31.0 [$(C\underline{Me}_3)_f$].

28.5 [(C<u>Me</u>$_3$)$_c$]. 28.4 [(C<u>Me</u>$_3$)$_c$]. 25.8 (C-38). 25.2 (C-39). 22.0 (C-17. C-18): carbon signals of C-37. C-40. C-16. C-19 were buried under the solvent acetone carbon peak and not observed. **Anal.** Calcd. for $C_{58}H_{74}N_4O_4Ni \cdot H_2O$: C. 71.97 : H. 7.91: N. 5.99. Found: C. 71.74: H. 7.97: N. 5.58.

3.4.3 Preparation of the binuclear Ni(II) complexes

General procedure. The free ligand (0.030 mmol) was dissolved in a minimal amount of $CHCl_3$ and then $Ni(OAc)_2 \cdot 4H_2O$ (0.030 g. 0.12 mmol) in hot EtOH solution (2.0 mL) was added. After addition. the solution was concentrated under vacuum and the remaining solution was stirred for an additional 2 h. The resultant red solid was collected by filtration and washed with EtOH (3 x 5 mL). Crystallization from 1:1 EtOH/CH_2Cl_2 solution afforded dark red crystals.

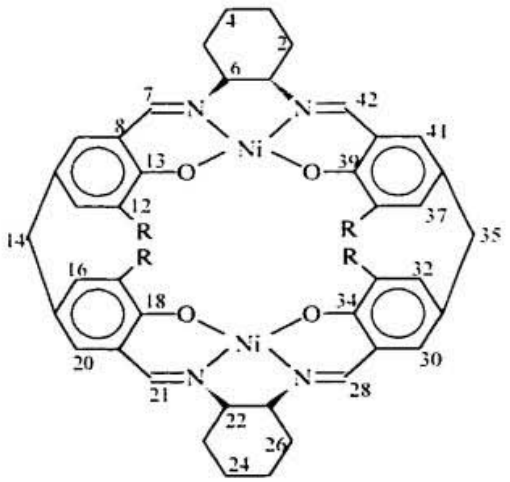

Numbering scheme for **3.5 - 3.8**

***(R,R)*-3.5** This complex did not dissolve in any solvents tested and could not be purified. IR and NMR data were not obtained.

***(R,R)*-3.6 Yield:** 0.025 g (94%). **IR** (Nujol): 1625 (CH=N). 1615 (CH=N). 1549 (Ph). 1320. 1253.1231. 1157. 1096. 1053. 962. 950.894. 857. 770. 727. 691 cm^{-1}.

***(R,R)*-3.7 Yield:** 0.026 g (92%). **IR** (Nujol): 1629 (CH=N). 1613 (CH=CN). 1542 (Ph). 1344. 1285. 1232. 1160. 1107. 1060. 954. 902. 875. 783. 730. 697 cm^{-1}: **^{1}H NMR** (CD_2Cl_2): δ 7.28 (s. 2H. H-7. H-21). 6.95 (d. J=1.8. 2H. H-9. H-20). 6.84 (d. J=2.4. 2H. H-41. H-30). 6.82 (d. J=2.4. 2H. H-42. H-28). 6.67 (d. J=2.1. 2H. H-11. H-16). 6.60 (d. J=2.1. 2H. H-32. H-37). 3.60 (m. 2H. H-6. H-22). 3.57 (d. J=12.6. H-14a. H-35a). 3.46 (d. J=12.6. H-14b. H-35b). 3.20 (m. 4H. C<u>H</u>Me_2). 2.42 (br. 2H. H-1. H-27). 2.23-2.10 (br. 4H. H-5. H-23). 1.86 (br. 4H. H-2. H-26). 1.43-1.36 (m. 8H. H-3. H-4. H-24. H-25). 1.02-0.89 (m. 24H. CH<u>Me</u>$_2$): **^{13}C NMR** (CD_2Cl_2): δ 164.5 (C-13. C-18). 164.4 (C-34. C-39). 163.7 (C-7. C-21). 156.7 (C-28. C-42). 141.4 (C-8. C-19). 141.2 (C-29. C-40). 131.3 (C-12. C-17). 131.1 (C-38. C-33). 130.6 (C-9. C-20). 130.0 (C-30. C-41). 128.0 (C-11. C-16). 126.1 (C-32. C-37). 124.3 (C-10. C-15). 122.7 (C-31. C-36). 72.0 (C-6. C-22). 67.6 (C-1. C-27). 42.3 (C-14. C-35). 30.6 (C-5. C-23). 28.0 (C-2. C-26). 26.5 (C<u>H</u>Me_2). 26.2 (C<u>H</u>Me_2). 25.6 (C-4. C-24). 24.8 (C-3. C-25). 23.5 (CH<u>Me</u>$_2$). 23.3 (CH<u>Me</u>$_2$). 23.1 (CH<u>Me</u>$_2$). 22.9 (CH<u>Me</u>$_2$): **Anal.** Calcd. for $C_{54}H_{68}N_4O_4Ni_2 \cdot CH_2Cl_2$: C. 63.79: H. 6.42: N. 5.41. Found: C. 63.10: H. 6.53: N. 5.36.

***(R,R)*-3.8 Yield:** 0.028 g (94%). **IR** (Nujol): 1632 (CH=N), 1612 (CH=CN), 1535 (Ph), 1318, 1271, 1239, 1206, 1166, 1100, 1060, 1027, 942, 868, 776, 724, 690 cm^{-1}; **^{1}H NMR** (CD_2Cl_2): δ 7.25 (d, J=1.8, 2H, H-7, H-21), 6.96 (d, J=2.4, 2H, H-9, H-20), 6.84 (d, J=1.2, 2H, H-28, H-42), 6.83 (d, J=2.4, 2H, H-30), H-41), 6.63 (d, J=2.4, 2H, H-11, H-16), 6.55 (d, J=2.4, 2H, H-32, H-37), 3.55 (m, 2H, H-1, H-27), 3.54 (d, J=12.3, H-14a, H-35a), 3.44 (d, J=12.3, H-14b, H-35b), 2.54 (br, 2H, H-6, H-22), 2.20-2.11 (br, 4H, H-2, H-26), 1.87-1.44 (br, 4H, H-5, H-23), 1.41-1.10 (m, 8H, H-3, H-4, H-24, H-25), 1.23 (s, 18H, CMe_3), 1.05 (s, CMe_3); **^{13}C NMR** (CD_2Cl_2): δ 165.7 (C-13, C-18), 165.6 (C-34, C-39), 163.5 (C-7, C-21), 156.5 (C-28, C-42), 142.1 (C-8, C-19), 141.6 (C-29, C-40), 131.7 (C-12, C-17), 131.5 (C-9, C-20), 130.7 (C-30, C-41), 130.1 (C-38, C-33), 128.2 (C-11, C-16), 126.3 (C-37, C-32), 123.5 (C-10, C-15), 123.3 (C-31, C-36), 71.6 (C-6, C-22), 67.9 (C-1, C-27), 42.1 (C-14, C-35), 35.5 ($\underline{C}Me_3$), 31.1 ($C\underline{Me}_3$), 30.9 (C-5, C-23), 30.5 ($C\underline{Me}_3$), 28.2 (C-2, C-26), 25.6 (C-4, C-24), 24.9 (C-3, C-25); **Anal.** Calcd. for $C_{58}H_{72}N_4O_4Ni_2 \cdot H_2O$: C, 67.90; H, 7.28; N, 5.47. Found: C, 67.51; H, 6.50; N, 5.19.

3.4.3 ^{1}H NMR titration experiments.[30] A solution of the guest (2.0 mol/L) in $CDCl_3$ was gradually added using a 25 μL syringe to a 0.5 mL $CDCl_3$ host solution (0.025 mmol/L) at room temperature. The ^{1}H NMR spectra of the resultant mixture were then recorded every 10 minutes after each addition. The association constant was determined by integration of the separated signals of the free imine protons of both free host and its complex. On the basis of three measurements, the discrepancy was < ±10%.

3.5 References

1. Jorgensen, K. A. *Chem. Rev.* **1989**, *89*, 431.

2. Sheldon, R. A.; Kochi, J. K. In *Metal-Catalyzed Oxidation of Organic Compounds*; Academic Press: New York, **1981**.

3. Samsel, E. G.; Srinivasan, K.; Kochi, J. K. *J. Am. Chem. Soc.* **1985**, *107*, 7606.

4. Spiro, T. G. In *Metal Ion Activation of Dioxygen*; John Wiley & Sons: New York, **1980**.

5. Nam, W.; Valentine, J. S. *J. Am. Chem. Soc.* **1993**, *115*, 1772.

6. For a review of binuclear complexes see Vigato, P. A.; Tamburini, S.; Fenton, D. E. *Coord. Chem. Rev.*, **1990**, *106*, 25.

7. Johnson, R. A.; Sharpless, K. B. In *Catalytic Asymmetric Synthesis*; Ojima, I., Ed.; VCH: New York, **1993**; p.103.

8. Bougauchi, M.; Watanabe, S.; Arai, T.; Sasai, H.; Shibasaki, M. *J. Am. Chem. Soc.* **1997**, *119*, 2329.

9. Jacobsen, E. N. In *Catalytic Asymmetric Synthesis*; Ojima, I., Ed.; VCH: New York, **1993**; p.159.

10. Baccin, C.; Gusso, A.; Pinna, F.; Strukul, G. *Organometallics* **1995**, *14*, 1087.

11. Kinneary, J. F.; Wagler, T. R.; Burrows, C. J. *Tetrahedron Lett.* **1988**, *29*, 877.

12. Boschi, T. In *Asymmetric Synthesis In Metalloporphyrin Catalyzed Oxidations*. Montanari, F.; Casella, L. Eds., Kluwer: Boston **1994**.

13. Srinivasan, K.; Michaud, P.; Kochi, J. K. *J. Am. Chem. Soc.* **1986**, *108*, 2309.

14. Mahanty, J. G.; Singh, R. P.; Chakravorty, A. *Inorg. Chem.* **1975**, *14*, 2178.

15. Koola, J. D.; Kochi, J. K. *Inorg. Chem.* **1986**, *26*, 908.

16. Kinneary, J. K.; Albert, J. S.; Burrows, C. J. *J. Am. Chem. Soc.* **1988**, *110*, 6124.

17. Burrows. C. J. In *Inclusion Phenomena and Molecular Recognition*: Atwood. J. L.. Ed.: Plenum Press: New York. **1990**. p.199.

18. McCollum. D. G.: Fraser. C.: Ostrander. R.: Theingold. A.: Bosnich. B. *Inorg. Chem.* **1994**. *33*. 2383.

19. Dangel. B.: Clarke. M.: Haley. J.: Sames. D.: Polt. R. *J. Am. Chem. Soc.* **1997**. *119*. 10865.

20. Fraser. C.: Ostrander. R.: Rheingold. A. L.: White. C.: Bosnich. B. *Inorg. Chem.* **1994**. *33*. 324.

21 Belser. P.: Bernhard. S.: Jandrasics. E.: von Zelewsky. A.: DeCola. L.: Balzani. V. *Coord. Chem. Rev.* **1997**. *159*. 1.

22. a) Masood. M. A.: Enemark E. J.: Stack. T. D. P. *Angew. Chem., Int. Ed. Engl.* **1998**. *37*. 928. b) Enemark E. J.: Stack. T. D. P. *Angew. Chem., Int. Ed. Engl.* **1998**. *37*. 932.

23. Duhme. A. K.: Davies. S. D.: Hughes. D. L. *Inorg. Chem.* **1998**. *37*. 5380-5382.

24. a) Müller. C.: Whiteford. P. J.: Stang. P. J. *J. Am. Chem. Soc.* **1998**. *120*. 9827. b) Stang. P. J.: Olenyuk. B. *Angew. Chem., Int. Ed. Engl.* **1996**. *35*. 732.

25 Urease. which catalyzes the hydrolytic reaction of urea. is believed to have two nickel(II) atoms coordinated with O and N residues in its active site. The most striking feature of this enzyme is that the cavity between the two nickel atoms affords space to allow substrate (urea. water) embedding and subsequent transformation. However. the detailed coordination geometry and Ni-Ni separation are unclear. Naturally. elucidation of the structure-activity relationships of the bimetalloenzyme has led to exploration of its synthetic analogues. especially macrocyclic binuclear nickel complexes. For references see: a) Halcrow. M. A.: Christou. G. *Chem. Rev.* **1994**. *94*. 2421. b) Salata. C. A.: Youinou. M. -T.: Burrows. C. J. *Inorg. Chem.* **1991**. *30*. 3454. c) Salata. C. A.: Youinou. M. T.: Burrows. C. J. *J. Am. Chem.* Soc. **1989**. *111*. 9278.

26. van Staveren. C. J.: van Eerden. J.: van Veggel. F. C. J. M.: Harkema. S.: Reinhoudt. D. N. *J. Am. Chem. Soc.* **1988**. *110*. 4994.

27. van Veggel. F. C. J. M.: Bos. S.: Harkema. S.: van de Bovenkamp. H.: Verboom. W.: Reinhoudt. D. N. *J. Org. Chem.* **1991**. *56*. 225.

28. *Catalytic Asymmetric Synthesis.* Ojima, I., Ed., VCH: New York, **1993**.

29. McKervey, M. A.; Seward, E. M.; Ferguson, G.; Ruhl, B. L. *J. Org. Chem.* **1986**, *51*, 3581.

30. Lacy, S. M.; Rudkevich, D. M.; Verboom, W.; Reinhoudt, D. N. *J. Chem. Soc., Perkin Trans. 2* **1995**, 135

Chapter 4

Face-to-Face Bisalen Transition Metal Complexes: A New Class of Potential Enzyme Mimics for Reduction of Dioxygen

4.1 Introduction

As described in the preceding Chapter, the macrocyclic calixsalens containing methylene bridges coordinate two Ni(II) atoms in an almost face-to-face geometry. Their structural congruity with face-to-face diporphyrins, which have been extensively exploited by Collman's group[1] and others,[2] suggests catalytic activity as biomimics of cytochrome *c* oxidase. Referent to this point, it remains a formidable challenge to design artificial models which can catalytically reduce dioxygen to water at neutral pH without formation of the thermodynamically favoured but biologically toxic hydrogen peroxide (Scheme 4.1).

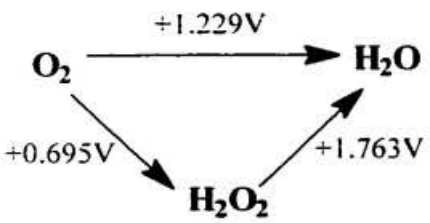

Scheme 4.1 Dioxygen reduction

Amongst the many diporphyrin complexes examined so far, only diporphyrinato anthracene **DPA**, diporphyrinato biphenylene **DPB**, and, particularly, "face-to-face 4" (**FTF4**, where 4 is the number of atoms connecting the two porphyrin rings: Figure 4.1) showed good to excellent four-electron reduction activity under acidic conditions (pH< 3.5) over a limited potential range.[1] Other porphyrin type models varied from exclusive

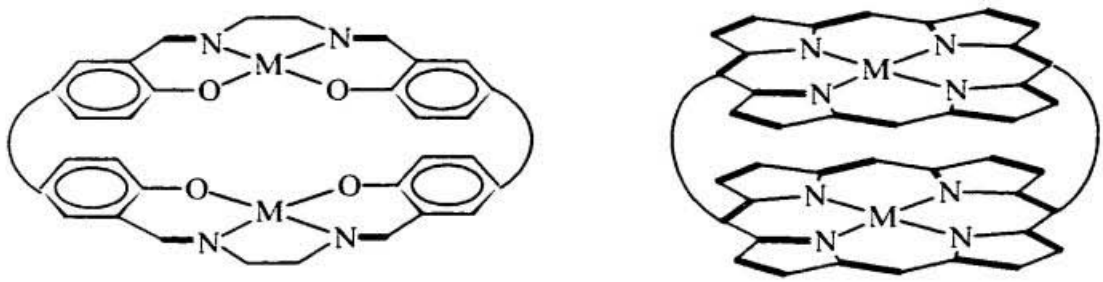

Figure 4.1 Face-to-face salen and porphyrin

two-electron activity to intermediate values.[1] Very recently, a macrocyclic catalyst constructed with a cobalt(II) porphyrin and a copper(I) triazacyclononane cap was reported by Collman and showed high efficiency for four electron reduction at almost biological pH (pH=7.3).[3] Despite this exciting progress, the multistep syntheses, coupled with low yield and purification difficulties, limit its practical application for catalysis.

Bisalen complexes with the general structure shown in Figure 4.1 are similar to diporphyrins in several aspects. Both have parallel planar conformations in salen or porphyrin. We speculated that if two four-atom links between the two porphyrins can establish a critical intermetallic distance (*ca.* 3.5 Å),[1] which appears necessary for achieving efficient catalytic activity in dioxygen reduction, the macrocyclic calixsalen **17** with an ethylene glycol link containing four chain atoms (Chapter 2) might be able to form binuclear complexes with a similar M-M distance. In this regard, van Veggel and coworkers[4, 5] reported trinuclear metallomacrocyclic salen complexes that showed

chemically reversible reduction/oxidation properties. but no reduction of dioxygen was reported.

This Chapter describes application of the binuclear calixsalen complexes for the catalytic reduction of dioxygen.

4.2 Results and Discussion

4.2.1 Preparation of the bisalen Cu(II), Co(II), Ni(II), and Mn(III) complexes

Preparation of the bisalen complexes with an ethylene glycol link (Scheme 4.2) was straightforward and proceeded at room temperature. Unlike the macrocyclic salen dimers with methylene bridges. experiments showed that complexation of the macrocyclic salen

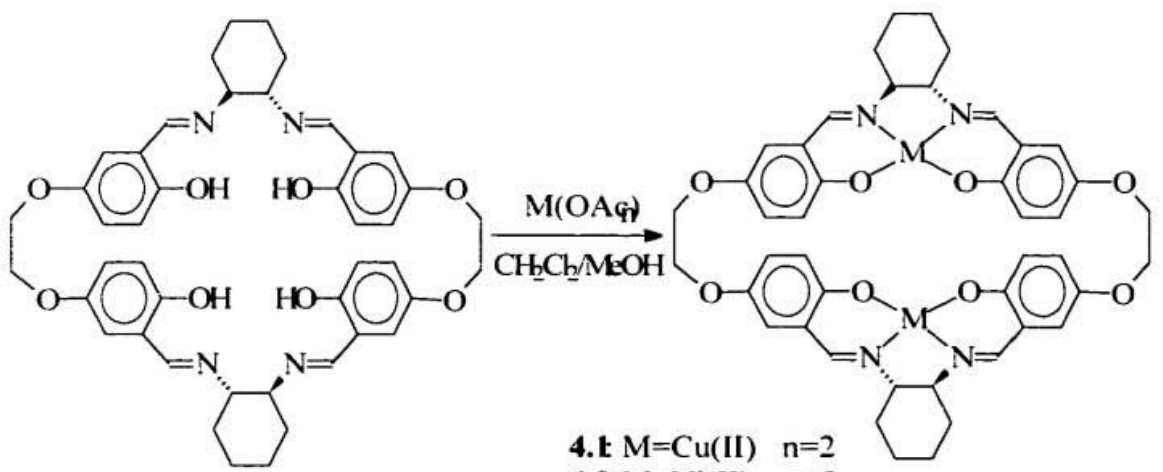

4.1 M=Cu(II) n=2
4.2 M=Ni(II) n=2
4.3 M=Mn(III) n=3
4.4 M=Co(II) n=2

Scheme 4.2 Preparation of the macrocyclic binuclear complexes

dimer having ethylene glycol bridges was not solvent dependent. Treatment of the macrocyclic ligand with metal acetates resulted in the formation of binuclear complexes. Complexes **4.1** and **4.2** were obtained in good yield (≥86%) after crystallization from CH_2Cl_2. Flash chromatography of the complexes **4.3** and **4.4** on silica gel (eluting first with CH_2Cl_2 and then MeOH) afforded dark-brown solid.

The complexes were initially characterized by infrared spectroscopy. The increase of the imine stretching frequency by 10 cm^{-1} reflected nitrogen complexation. ESMS analysis established the formula of complexes **4.1** and **4.2**. Molecular ions, observed at m/z = 882 for complex **4.1** ($C_{44}H_{44}N_4O_8Cu_2$) and 872 for **4.2** ($C_{44}H_{44}N_4O_8Ni_2$), were consistent with the calculated monoisotopic mass of each complex. No molecular ions were found for complexes **4.3** and **4.4**. Satisfactory analytical data were not obtained for the complexes. Interestingly, the Ni(II) and Cu(II) complexes **4.1** and **4.2** were not soluble in CH_3CN, MeOH, EtOH, CH_3COCH_3, THF, or even DMF, but were sightly soluble in CH_2Cl_2, presumably due to inclusion of CH_2Cl_2 in the cavity.

4.2.2 X-ray studies of the binuclear complexes 4.1 and 4.2

Slow evaporation of a CH_2Cl_2 solution of **4.1** afforded yellow irregular crystals. Under similar conditions, red rectangular plates of **4.2** were also obtained. ORTEP representations of the molecular structures resulting from single crystal X-ray diffraction are shown in Figures 4.2 and 4.3 (p.136-137).

Similar to the binuclear nickel(II) complex **3.8** (Chapter 3), the four benzene units formed a well-defined cavity in the macrocyclic binuclear copper complex **4.1**[a] with ethylene glycol bridges. However, the two cyclohexyl rings were located on opposite sides of the cavity and thus defined an overall *anti* conformation with a pseudo C_2 axis parallel to the cavity. In each salen moiety, four ligating atoms and the complexed Cu(II) were almost coplanar and thus established a planar coordination geometry in which the average bond length of Cu-O and Cu-N was about 1.90 and 1.95 Å. The atom (Cu(II), N, O) mean deviation in every salen plane was 0.17 Å, and 0.09 Å, respectively. Furthermore, the two salen planes were almost parallel with a dihedral angle of 6.56° and a distance between the two Cu(II) centres of *ca.* 3.48 Å. However, they were not directly stacked one above another. A lateral shift[1] was observed, which was calculated to be *ca.*1.70 Å based on the offset of the two opposing pair of benzene rings (3.93 Å on the right and 3.74 Å on the left) and the Cu(II) to Cu(II) separation. With regard to the opposing benzene ring arrangements, slightly larger dihedral angles of 26.3° and 21.2° were found.

Comparison of the conformational data of the complex **4.1** with that of the corresponding

---

[a]Crystal data for **4.1** ($C_{44}H_{44}N_4O_8Cu_2 \cdot 2H_2O$), fw = 919.98; yellow, crystal dimensions= 0.15 x 0.05 x 0.35 mm; monoclinic; $P2_1$ (# 4); a = 12.01(3) Å, b = 7.20(2) Å, c = 22.75(1) Å; β = 101.782 (8)°, Z = 2; V = 1925.9 (5) Å^3; D_{calcd} = 1.586 g/cm^3; $2\theta_{max}$ = 121.2°; of 9882 reflections measured, 3178 were unique ($R_{initial}$ = 0.027) and 3174 observed ($I > 0.00\ \sigma(I)$); R = 0.049, R_w = 0.060. See Appendix 3 for X-ray experiments, and crystal data.

free ligand derived from NMR (Chapter 2) demonstrated that metal complexation significantly altered the macrocycle, forcing a planar salen complex with an overall effective 1,2-alternate conformation. A similar conformational change has been observed in complexation of calixarene with transition metals.[9]

The nickel atoms in complex **4.2**[b] also adopted a planar coordination geometry within each salen unit. The resulting cavity was, however, larger than that of **4.1** as evidenced by the longer Ni(II)-Ni(II) distance (3.72 Å) and opposing benzene ring distances 3.99 Å (the left) and 4.07 Å (the right). Consequently, the dihedral angles between the two opposing benzene planes (28.0° for the left and 34.4° for the right) were larger than those of the Cu(II) complex **4.1**.

In diporphyrin systems, the large lateral shift stemmed from strong π-π attractive interactions which resulted in a 3.45 Å inter-ring separation.[1] The similar benzene ring offsets observed in both binuclear nickel and binuclear copper macrocyclic bisalen complexes might also originate in part from π-π interactions between the opposing benzene rings since they lie *ca.* 3.5 Å apart, the basic requirement for two molecules to

---

[b]Crystal data for **4.2** ($C_{46}H_{48}N_4O_8Ni_2Cl_4$): fw = 1044.12; red. crystal dimension = 0.20 x 0.08 x 0.40 mm, triclinic, P1 (# 1), a = 10.37(4) Å, b = 12.17(3) Å, c =10.02(2) Å, V = 1126.3(5) Å^3, α = 106.29(2)°, β=91.69(2)°, γ=68.64(2)°, Z = 1, D_{calcd} =1.539 g/cm^3, R = 0.052, R_w = 0.053.

engage in a π-π stack.[6] Clearly, the flexible ethylene glycol links made the interaction possible. On the other hand, the Ni(II) to Ni(II) distance difference between complex **4.2** and the Cu(II) to Cu(II) in complex **4.1** could not be interpreted on the basis of π-π interactions.

In a square-planar complex, five degenerate d orbitals are split into four levels (Figure 4.4).[7] For the square-planar binuclear copper complex **4.1**, there is a single electron in the HOMO ($d_{x^2-y^2}$) of each Cu(II). Therefore any coupling between the two copper HOMO's will reduce the Cu(II)-Cu(II) distance. The HOMO in the binuclear nickel salen system of complex **4.2** is d_{xy}, which contains a pair of electrons. Therefore, it was likely that d_{xy} - d_{xy} repulsive interactions resulted in relatively larger separation between the two Ni(II).

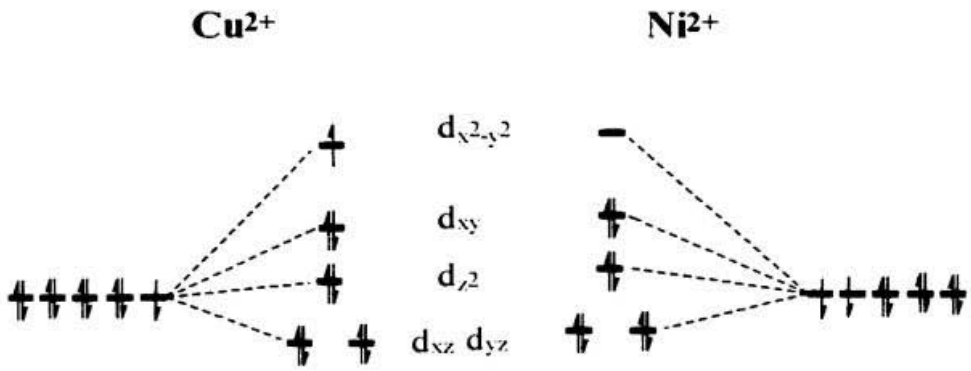

Figure 4.4 The d orbital splitting diagram for square-planar complexes **4.1** and **4.2**

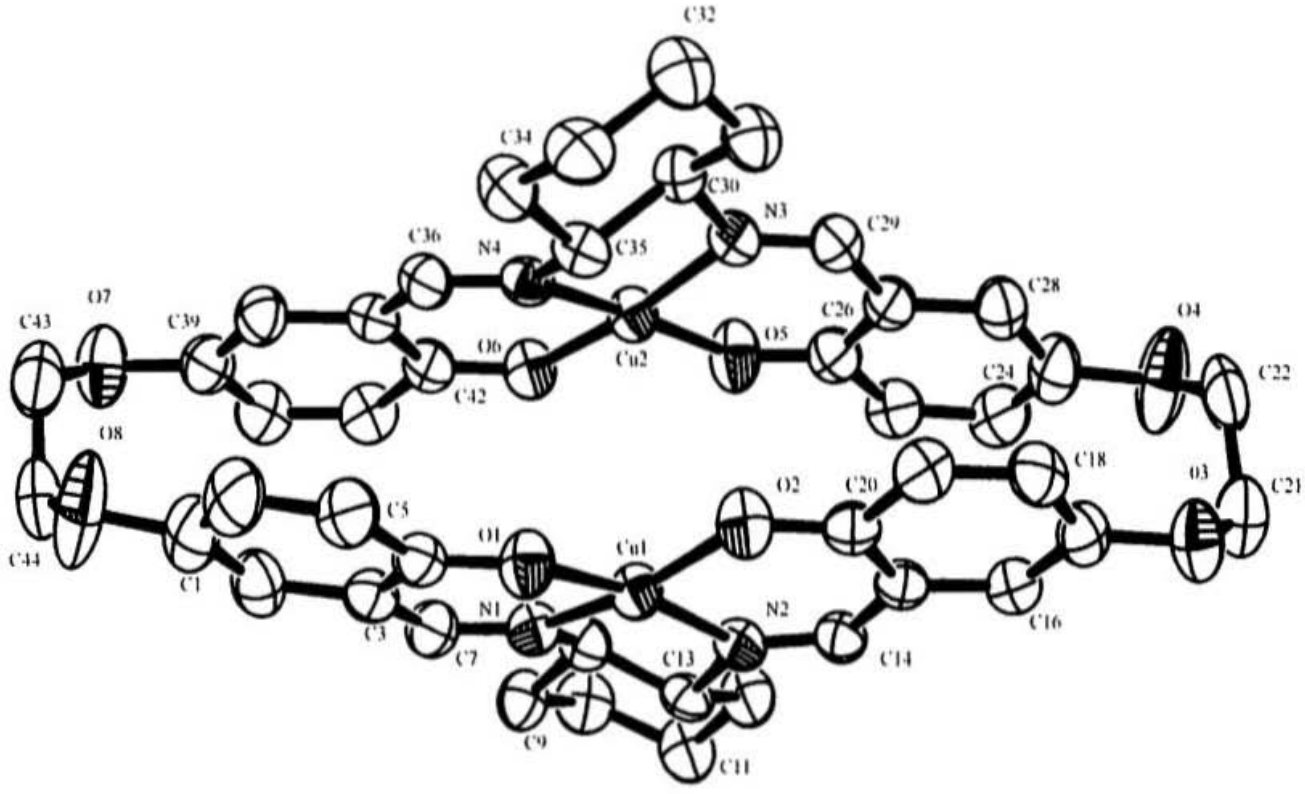

Figure 4.2 ORTEP representation of the binuclear copper(II) complex **4.1** (Hydrogen atoms and solvents were removed for clarity.)

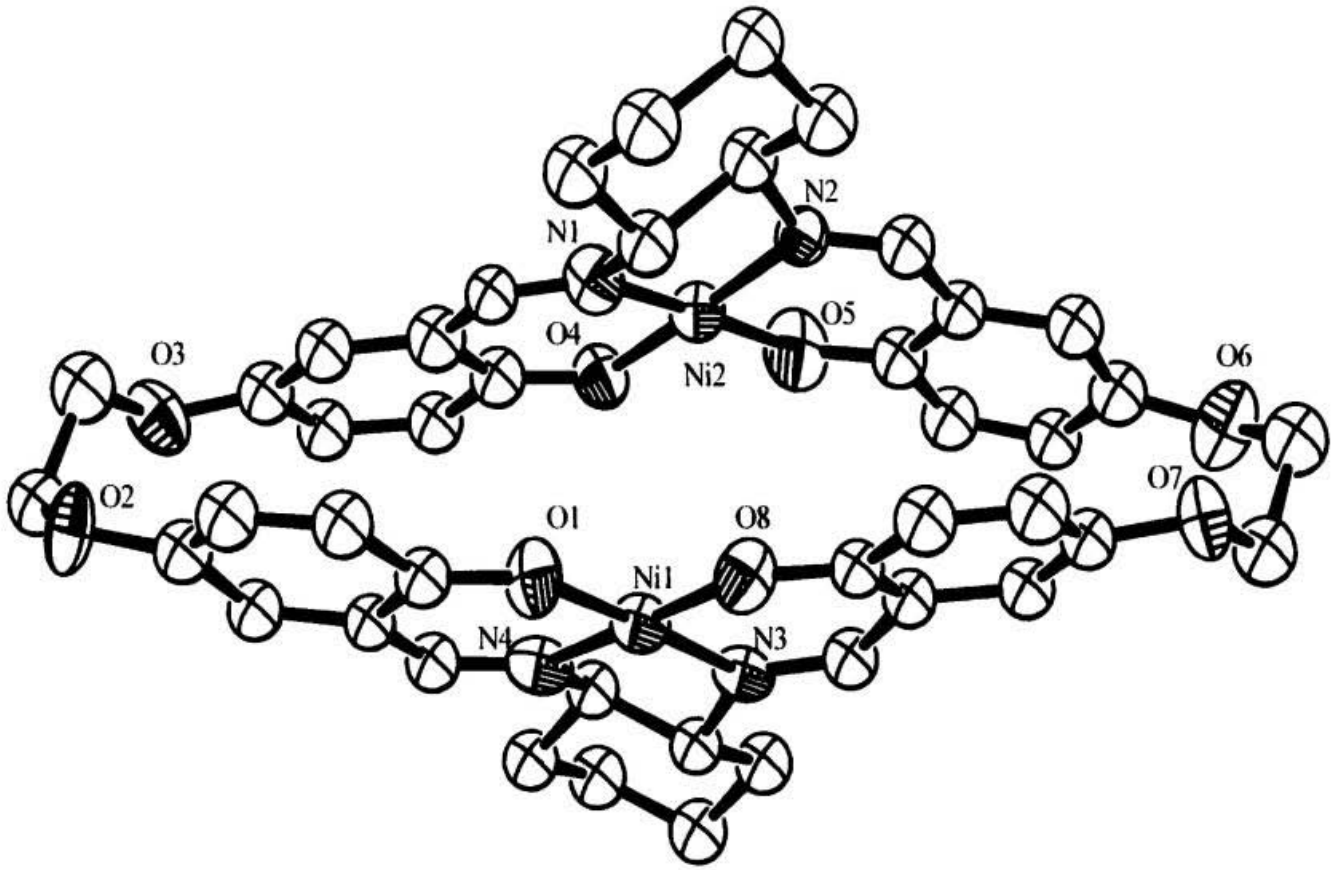

Figure 4.3 ORTEP representation of the binuclear nickel(II) complex **4.2** (Hydrogen atoms and solvents were removed for clarity.)

4.2.3 Rotating ring-disk electrochemical studies

4.2.3.1 Methods. Electrochemical methods are crucial in evaluating the redox catalytic properties of the face-to-face salen complexes. The rotating ring-disk technique[1] is the most effective approach in that it only requires a small amount of catalyst ($<10^{-9}$ mol/cm), which is adsorbed onto an edge-plane graphite electrode (EPGE, the disk). Mass or electron transfer to the electrode-confined species is fast and thus diffusion effects, especially evident in systems involving two phases, are avoided. Additionally, direct observation of intermediates is possible by monitoring the ring current so that more kinetic information is available.

In a typical experiment the EPGE is rotated at ≥100 rpm while the potential of the disk where the oxygen reduction occurs is scanned through the region of interest, usually 0.5 V – -0.5 V versus the normal hydrogen electrode (NHE), for reduction of dioxygen. The cathodic current I_d is an indication of the reduction process. During the scan of the disk potential, the potential of the platinum ring (Figure 4.5) is maintained constant at a value sufficiently high for the oxidation of hydrogen peroxide. Figure 4.5 illustrates the rotating ring disk experiments. The two electrodes are the edge-plane graphite disk (cathode) and a platinum ring (anode), which

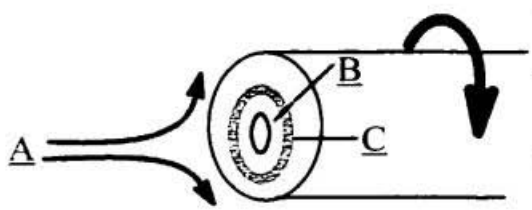

Figure 4.5 Schematic drawing of rotating ring-disk experiments. A) electrolyte and substrate flow, B) disk, C) platinum ring

is separated from the disk by Teflon shrouding. As the ring-disk electrode rotates. thesolution first passes the disk and then the ring. The reduction products from the disk are swept past the ring where oxidation occurs. allowing product detection by further oxidation. For example. if the 4e reduction of dioxygen occurs directly to water then no ring current should be detected at the anode (Figure 4.6).

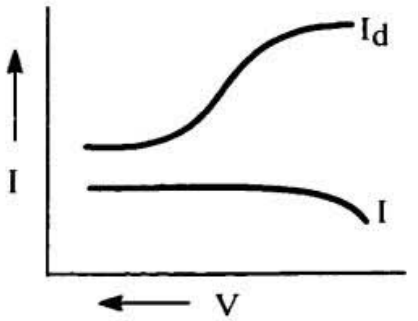

Figure 4.6 The ideal voltammogram of 4e reduction of dioxygen

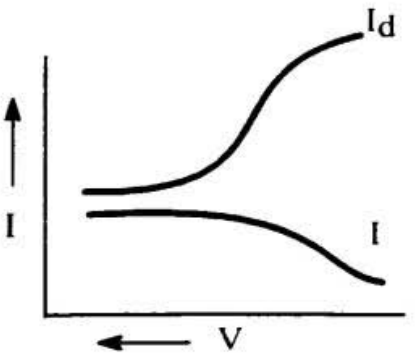

Figure 4.7 The voltammogram of 4e and 2e reduction of dioxygen

However. if the reduction generates hydrogen peroxide then oxidation of H_2O_2 would occur at the anode and ring current will be observed (Figure 4.7). Therefore. the larger the ring current the less effective the catalyst.

4.2.3.2 Reduction of dioxygen. Previous studies using cofacial diporphyrin catalysts showed that a coplanar stacked conformation with a metal-metal distance of

approximately 3.5 Å, which resembles the intermetallic distance in binuclear Cu(I) enzymes such as haemocyanin and tyrosinase which activate and transport O_2 in molluscs,[5-8] is essential in designing a possible reduction catalyst. As described in section 4.2.2, the binuclear calixsalen complexes with a M-M distance of 3.5-3.7 Å and planar conformation meet all the basic requirements and thus are potential enzyme mimics.

The ring-disk cyclic voltammetry experiments of the complexes prepared in this study and of **FTF4** for comparison, are shown in Appendix 5. In neutral conditions (pH=6.86), with a rotation rate of 250 rpm and ring potential held at 1.04 V *vs* NHE, reduction of dioxygen occurred at a half wave potential 0.18V *vs* NHE for complex **4.4** and 0.08 V *vs* NHE for Collman's **FTF4** porphyrin, suggesting that the reduction was catalytic and catalyst **4.4** was more active than **FTF4**. Ring current measurements revealed that H_2O_2 was produced during the reduction with both catalysts. In this aspect, the **FTF4** catalyst generated less H_2O_2 than did catalyst **4.4**, indicating the latter was less efficient. Based on the Koutecky-Levich equation[3] it was estimated, after normalization, that the ratio of 2e : 4e reduction processes was 1:4 with catalyst **4.4** and 1:6 with catalyst **FTF4** (Table 4.1). The activity of the analogous complexes **4.1** and **4.3** was poor and reduction of dioxygen occurred at -0.32 V and -0.26 V *vs* NHE, respectively.

The fact that catalytic properties for dioxygen reduction are normally pH-dependent lead

Collman to suggest that protonation of the binding O_2 between the two metals is involved in the process and that increasing the acidity of the solution should significantly improve activity and favour the four-electron path. In acidic conditions, the activity of both catalyst **4.4** and **FTF4** was increased, but the activity increase was higher for **FTF4**. The intensity of corresponding ring current clearly showed that there was no H_2O_2 produced within 0.30-0.72 V with **FTF4** while a significant amount of H_2O_2 was still evident with catalyst **4.4**. The results showed that **FTF4** was very efficient for reduction of dioxygen at acidic conditions, whereas complex **4.4** was not. Furthermore, the reduction wave did not show a plateau under acidic conditions, suggesting decomposition.

Table 4.1 Catalytic reduction of dioxygen data[a]

catalyst	**4.1**	**4.3**	**4.4**	**FTF4**
$E_{1/2}$ (V)				
pH = 6.86	-0.32	-0.26	0.18	0.08
pH = 3.12	n/a	n/a	0.49	0.62
4e/2e ratio				
pH = 6.86	n/a	n/a	4/1	6/1
pH = 3.12			4/1	only 4e

[a] O_2, 1 atmosphere; ring potential 1.04 V; rotation rate, 250 rpm, potential presented *vs* NHE.

4.3 Summary

Reactions of the macrocyclic salen dimer containing longer ethylene glycol links with Cu(II), Co(II), and Ni(II) salts afforded binuclear complexes. X-ray studies demonstrated that the binuclear complexes were C_2 symmetric and adopted an *anti* conformation. The two salen units stacked one above the other, and the two metals were almost face-to-face within 3.5-3.7 Å, a distance critical for the catalytic reduction of dioxygen. Electrochemical experiments using the rotating ring-disk technique showed that the activity and selectivity of the cobalt complex was comparable with that of Collman's face-to-face porphyrins.

4.4 Experimental Section

4.4.1 Reagents and methods. All manipulations were conducted under the same general conditions as stated in Chapters 2 and 3. Transition metal salts $Ni(OAc)_2$, $Cu(OAc)_2$, $Co(OAc)_2$, $Mn(OAc)_3$ and solvents CH_2Cl_2, MeOH, and $CHCl_3$ were reagent grade and used without further purification.

4.4.2 Preparation of the binuclear complexes. To a solution of ligand (0.050 mmol) in 5.0 mL of $CHCl_3$ and 5.0 mL of MeOH was added the metal acetate (0.11 mmol) as a solid in one portion. The resultant solution was stirred at RT for 2 h. Removal of solvent under vacuum afforded the crude product, which was then washed with MeOH (3 x 5.0 mL). Crystallization of the complexes **4.1** or **4.2** from CH_2Cl_2 afforded crystalline products. Suitable specimens were selected for X-ray analysis.

4.1. Yield: 0.039 g (88%). **ESMS** (*m/z*): Calcd. for $C_{44}H_{44}N_4O_8Cu_2$: 882; Found: 882, 884; **IR** (Nujol):1642 (CH=N), 1536 (Ph), 1325, 1206, 1166, 1054, 981, 875, 836, 730 cm^{-1}.

4.2. Yield: 0.036 g (86%). **ESMS** (*m/z*): Calcd. for $C_{44}H_{44}N_4O_8Ni_2$ 872 (100%); Found: 872, 874, 875, 876; **IR** (neat): 1649 (CH=N), 1568 (Ph), 1556, 1483, 1431, 1285, 1225, 1172, 1407, 882, 822, 697, 618, 565, 472 cm^{-1}.

4.4.3 Electrochemistry experiments. The electrochemical measurements were carried out by Professor Maurice L'Her at Faculté des Sciences. Université de Bretagne Occidentale. France. at room temperature on an edge-plane graphite electrode (EPGE) composed of a graphite disk and a platinum ring. The electrode. repolished before each adsorption with a suspension of 200 Å alumina in water. was impregnated in a CH_2Cl_2 solution of the corresponding complex for 5 minutes and then rinsed. During the scan of the disk potential at a rotation rate of 250 rpm. the potential of the platinum ring was maintained at 0.8 V *vs* NHE; a value sufficiently high for the oxidation of hydrogen peroxide produced by reduction of dioxygen on the disk. The collection number of the electrode is 0.27 (27% hydrogen peroxide could be detected since not all of the hydrogen peroxide generated on the disk could reach the ring).

The dioxygen reduction with the modified electrodes was performed in two different aqueous solutions: a phosphate buffer at pH=6.86 or a 0.2 M $HClO_4$ solution at pH=3.12. The reference electrode was the saturated calomel electrode (potential 0.24 V *vs* NHE).

4.5 References

1. Collman, J. P.; Wagenknecht, P. S.; Hutchison, J. E. *Angew. Chem., Int. Ed. Engl.* **1994**, *33*, 1537.

2. Eaton, S. S.; Eaton, G. R.; Chang, C. K. *J. Am. Chem. Soc.* **1985**, *107*, 3177.

3. Collman, J. P.; Fu, L.; Herrmann, P. C.; Zhang, X. *Science* **1997**, *275*, 949.

4. van Veggel, F. C. J. M.; Bos, M.; Harkema, S.; Verboom, W.; Reinhoudt, D. N. *Angew. Chem., Int. Ed. Engl.* **1989**, *28*, 746.

5. van Veggel, F. C. J. M.; Bos, M.; Harkema, S.; van de Bovenkamp, H.; Verboom, W.; Reedijk, J.; Reinhoudt, D. N. *J. Org. Chem.* **1991**, *56*, 225.

6. Jones, G. B.; Chapman, B. J. *Synthesis* **1995**, 475.

7. Taqui Khan, M. M.; Martell, A. E. In *Homogeneous Catalysis by Metal Complexes*, Academic Press: New York, **1974**; Vol.1.

8. Feringa, B. L.; Gelling, O.-J.; Rispens, M. T.; Lubben, M. In *Transition Metals in Supramolecular Chemistry*; Fabbrizzi, L.; Poggi, A., Eds.; Kluwer: Amsterdam, **1994**; p.171.

9. Wieser, C.; Dieleman, C. B.; Matt, D. *Coord. Chem. Rev.* **1996**, 165, 93.

Chapter 5

Asymmetric Oxidation of Alkenes with Chiral Binuclear Manganese Calixsalen Complexes

5.1 Introduction

As summarized in Chapter 1, manganese(III) salen complexes, resembling the enzyme cytochrome P-450, are very efficient catalysts for the epoxidation of alkenes. Structural analysis of these catalysts revealed that three strategies have been employed to tailor catalytic properties and enantioselectivity: i) tuning the *ortho* and/or *meta* phenol substituents to control the steric environment around the active site in order to fix substrate orientation and force maximum chiral communication; ii) adjusting the electronic properties of the central metal by changing the axial ligand to achieve higher activity for delivery of oxo from the oxotransition-metal O=Mn(V) intermediate; iii) introducing more stereogenic centres on the salen frame to maximize asymmetric induction. This last strategy often failed, probably due to lack of co-operativity with respect to stereoisomer discrimination.

Monomeric salen Mn(III) complexes have notable disadvantages. Mainly, deactivation of the catalysts was often observed due to the formation of μ-oxygen bridged dimer[1-3]

through intermolecular dimerization. Therefore, monomeric salen catalysts sustain the required oxidation state change [Mn(III) ⇌ Mn(V)] in the catalytic cycle with a very short life time. Furthermore, as indicated above, the most successful Jacobsen catalyst was limited to *cis*-alkene, particularly arylalkene, substrates.

As described in Chapters 2, 3 and 4, the methylene-bridged chiral calixsalens **14a-14d** (Chapter 2) and their corresponding binuclear complexes (Chapter 3) were conformationally stable in solution and had a rigid macrocyclic skeleton with a cavity between the two potential metal coordination sites. We therefore anticipated that the binuclear manganese complexes, not unlike natural enzymes,[4] might be suitable chiral host/guest catalysts for epoxidation and stereoisomer discrimination. In addition, the rigid macrocyclic framework might prevent intermolecular destruction. To our knowledge this represents a new approach for the epoxidation of unfunctionalized alkenes.

This Chapter presents the results of catalytic oxidation of prochiral alkenes, particularly styrene, with chiral calixsalen binuclear manganese catalysts as well as a comparative study with a chiral linear, side-by-side dimeric salen manganese catalyst which cannot operate via a host/guest mechanism.

5.2 Results and Discussion

5.2.1 Catalyst preparation

The preparation of the binuclear manganese catalysts is outlined in Scheme 5.1.[5,6] Reaction of a 1:2 molar ratio of the corresponding calixsalen with $Mn(OAc)_3$ at room temperature followed by *in situ* treatment with LiCl or NH_4PF_6 afforded dark brown air stable binuclear manganese complexes in good yield (68%-90%). For the purpose of comparison, a side-by-side linear catalyst **5h** was also prepared in 80% yield by reaction of the chiral linear bisalen ligand **5g** with $Mn(OAc)_3$ and then LiCl at room temperature (Scheme 5.2).

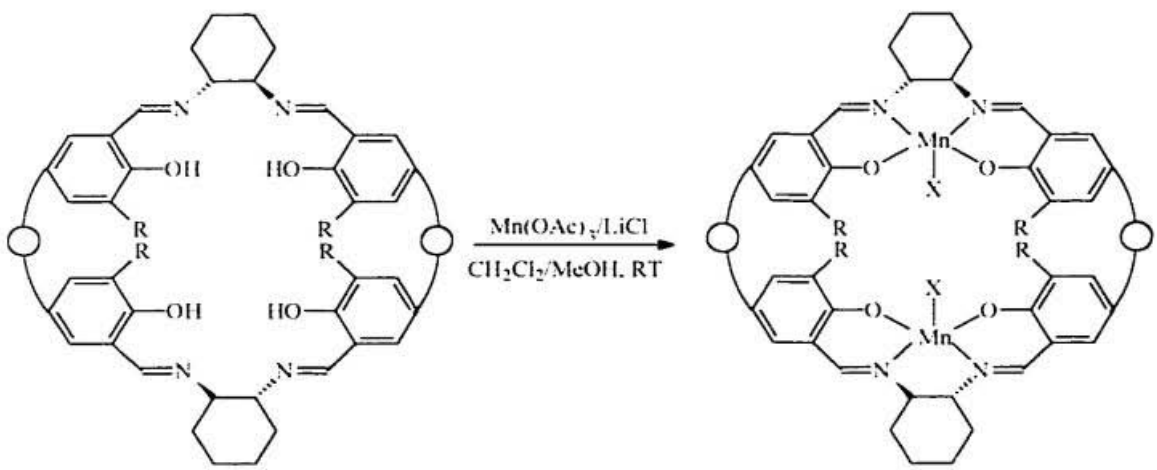

○ = CH_2: **5a**: R = H, X = Cl; **5b**: R = CH_3, X=Cl; **5c**: R = *i*-Pr, X = Cl; **5d**: R = *t*-Bu, X = Cl; **5e**: R = *t*-Bu, X = PF_6

○ = OCH_2CH_2O: **5f**: R = H, X = Cl

Scheme 5.1 Preparation of the chiral binuclear manganese calixsalen complexes

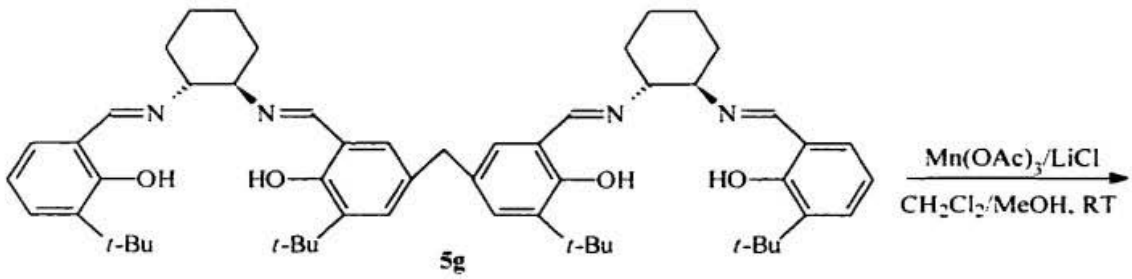

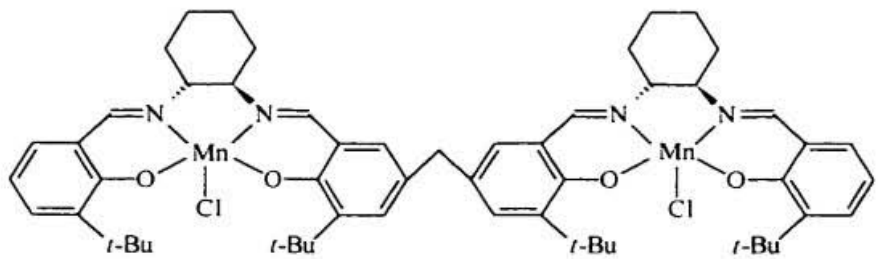

Scheme 5.2 Preparation of the chiral linear binuclear manganese complex

Characterization of the complexes was accomplished by electron spray mass spectra (ESMS) and elemental analysis. ESMS of the dilute solution of complex **5d** in MeOH gave a parent peak at m/z = 1063 corresponding to $[C_{58}H_{72}N_4O_4Mn_2 \cdot 2MeOH + H]^+$ (dechlorinated **5d** plus two MeOH molecules. **5d** - $2Cl^- + H + 2MeOH$). Coordination of solvent, particularly nucleophilic solvents such as MeOH on Mn(III) was also observed in both the monomeric salen system[7] and the binuclear manganese macrocyclic complexes.[8] Lower intensity peaks at m/z = 999, 945, and 892 were assigned to the species of $[C_{58}H_{72}N_4O_4Mn_2]^+$ (**5d**-$2Cl^-$), $[C_{58}H_{74}N_4O_4Mn]^+$ (**5d** -$2Cl^- - Mn^{3+} + 2H^+$), and free ligand $[C_{58}H_{76}N_4O_4]^+$, respectively. These results implied that the two manganese atoms were present in a mixed valence form Mn(III)/Mn(II) in the macrocyclic binuclear complexes.

The reduction of Mn(III)/Mn(III) to Mn(III)/Mn(II) most likely occurred according to the following reactions:[7]

$$2[Mn_2(III)(calixsalen\text{-}4H^{\cdot})]Cl_2 + MeOH \longrightarrow 2[Mn(III)Mn(II)(calixsalen\text{-}4H^{\cdot})]Cl + CH_2O + 2HCl$$

$$2[Mn_2(III)(calixsalen\text{-}4H^{\cdot})]Cl_2 + CH_2O + H_2O \longrightarrow 2[Mn(III)Mn(II)(calixsalen\text{-}4H^{\cdot})]Cl + HCOOH + 2HCl$$

Further evidence for the assignment of the mixed-oxidation state of manganese derived from the species at *m/z* 1045 and 1093 corresponding to $[C_{58}H_{72}N_4O_4Mn_2\cdot(HCOOH) + H]^{\cdot}$ (**5d** $-2Cl^{\cdot} + H + HCOOH$) and $[C_{58}H_{72}N_4O_4Mn_2\cdot(CH_2O)\cdot(2MeOH) + H]^{\cdot}$ (**5d** $-2Cl^{\cdot} + CH_2O + 2MeOH$). Oxidation of MeOH to CH_2O and further to HCOOH with Mn(III)/Mn(III) as an oxidant was not surprising as four mixed valence oxidation states of manganese: Mn(II)/Mn(II), Mn(III)/Mn(II), Mn(III)/Mn(III), and Mn(III)/Mn(IV) are common species in manganese redox enzymes and their synthetic binuclear manganese model complex systems.[7]

The mass spectrometric results for complex **5e** measured in EtOH solution supported the above conclusion. The parent ion at *m/z* = 1043 was consistent with $[C_{58}H_{72}N_4O_4Mn_2\cdot(CH_3CHO) + H]^{\cdot}$ and a group of peaks at 1099, 1100 and 1101 were consistent with the species of $[C_{58}H_{72}N_4O_4Mn_2\cdot(CH_3COOH)\cdot(CH_3CHO)]^{\cdot}$. For the side-by-side linear binuclear manganese complex, a molecular ion appeared at *m/z* =1021, which was in accord with $[C_{57}H_{72}N_4O_4Mn_2Cl]^{\cdot}$. Extensive efforts to obtain single crystals of the binuclear manganese complexes for X-ray structural analysis failed.

5.2.2 Selection of the oxidants

Various oxidants such as organic peroxyacids, alkyl hydroperoxides, dioxirane, oxaziridine reagents, hydrogen peroxide, iodosylbenzene (PhIO), oxone ($NaHSO_5$), hypochlorite, and molecular oxygen coupled with aldehyde are available as the oxygen source for transfer to electron-rich alkenes. Organic peroxyacids can affect epoxidation smoothly without the presence of a catalyst but are not efficient in asymmetric induction and are also a safety problem both in their preparation and storage.[9] Utilization of dioxirane and oxaziridine, especially their chiral derivatives, has attracted attention in recent years[10-12] but product separation is often tedious. Consequently, substitution of organic oxidants with other cheap and easily handled oxidants such as hypochlorite, hydrogen peroxide, and molecular oxygen has been a subject of ongoing investigation. Because of the low reactivity of these species, their utilization in synthetically attractive oxidation reactions requires the presence of an appropriate catalyst.[13] Hydrogen peroxide with V(V), Mo(VI) or Cr(VI) derivatives are excellent oxidizing systems. In the case of manganese porphyrins and salens as epoxidation catalysts, iodosylbenzene (PhIO), oxone ($NaHSO_5$), alkyl hydroperoxides, and hypochlorite have been shown to be a suitable oxygen source. Therefore, tests of the catalysts were initially carried out with *t*-butylhydroperoxide, cumene hydroperoxide, oxone and hypochlorite as the oxygen sources and styrene as the substrate. The results obtained are summarized in Table 5.1, which shows that sodium hypochlorite was an appropriate oxidant.

Table 5.1 Epoxidation of styrene with various oxidants in the presence of catalyst **5d**[a]

oxidant	$PhC(CH_3)_2OOH$	*t*-BuOOH	$NaHSO_5$	NaClO
results	no epoxide	no epoxide	oxygen generated decomposed	epoxide obtained

(a) all reactions were run in the solvent CH_2Cl_2 or CH_2Cl_2/H_2O with a molar ratio of substrate/catalyst = 120:1 and maintaining aqueous pH about 10 at room temperature. There was no epoxidation reaction using oxone in CH_2Cl_2 solvent.

5.2.3 Chemo- and regioselectivity of chiral binuclear Mn(III) calixsalen catalysts

The catalytic properties of the catalysts **5a-5f** were examined in different solvents using styrene as the model substrate. The results obtained are presented in Table 5.2.

Table 5.2 Oxidation of styrene with sodium hypochlorite in the presence of catalyst[a]

entry	cat.	solvents	time (h)	product	yield (%)	ee (%)
1	**5a**	$MeOH/CH_2Cl_2/H_2O$	3.5	chloro ether	80	11
2	**5b**	CH_2Cl_2/H_2O	3	chlorohydrin	43	n/a
3	**5c**	CH_2Cl_2/H_2O	3	epoxide	45	27
4	**5d**	CH_2Cl_2/H_2O	3	epoxide	60	54
5	**5e**	$MeOH/CH_2Cl_2/H_2O$	3	epoxide	70	35
6	**5f**	$MeOH/CH_2Cl_2/H_2O$	2	chloro ether	86	n/a

(a) All reactions were carried out at 25°C with a catalyst loading of 1.2 mol% and the sodium hypochlorite was buffered with Na_2HPO_4 to pH=9. Chemical yields were based on styrene. %ee was determined by HPLC using a ReGIS® (*S,S*)-Whelk-01 column (1% 2-propanol in hexane for styrene epoxide, 0.4% 2-propanol in hexane for chloro ether; flow rate 0.8 mL/min).

The products of the oxidation reaction depended on the catalyst (Scheme 5.3). Catalysts

with larger R groups such as in **5c**, **5d** and **5e** gave the desired epoxide **2** as the major product and only minor amounts of chloro ether **1** were found. The ratio of **2/1** was determined to be about 100/3. Only one product, which was identified as 1-chloro-phenyl-2-methoxy ethane by mass spectrometric analysis and comparison of its NMR data with its regioisomer obtained through direct chlorination of styrene in MeOH, was isolated in the presence of catalyst **5a** or **5f** having a smaller (R=H) group. Interestingly, both epoxide and chlorinated product **3** in the ratio of 10/1 were obtained with catalyst **5b**, and it was tempting to speculate that this resulted from the fact that the steric requirement for methyl lies between *t*-Bu and H. It appeared that chemoselectivity of the oxidation was directly governed by the size of the R group in the binuclear manganese calixsalen catalysts.

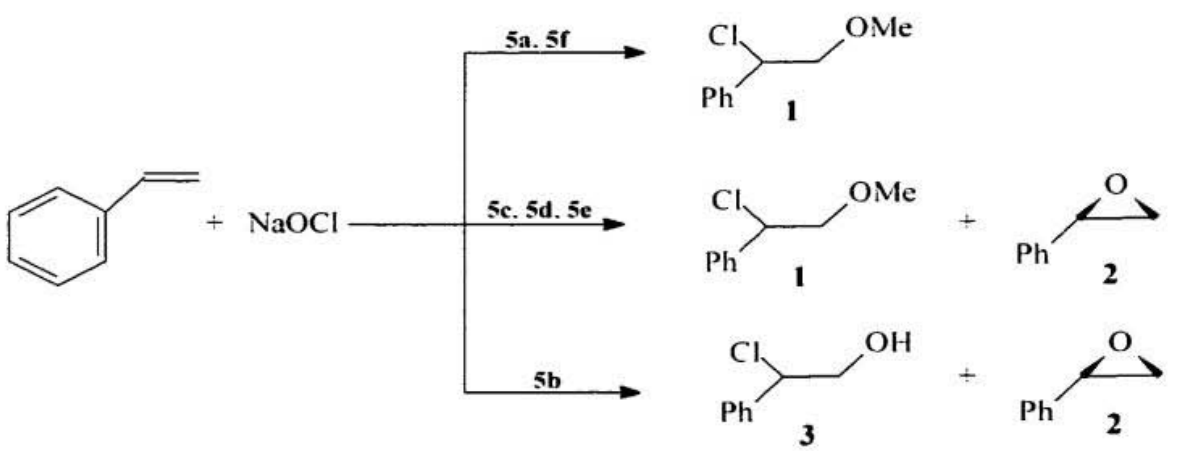

Scheme 5.3 Products in the catalytic epoxidation of styrene

It was noteworthy that the position of the methoxy or hydroxy groups in the product was opposite to that of a conventional electrophilic addition to a double bond, as it might be expected from Cl_2 in H_2O or Cl_2 in MeOH. Reversed regioselective chlorination of alkene was also achieved in alkoxychlorination of allylamines with a bimetallic, Wacker type catalyst composed of $PdCl_4^-$ and $CuCl_2$.[14] However, the major products from any other of the tested alkenes followed the conventional rule in which the nucleophile was incorporated at the more substituted carbon of the double bond. Catalysts **5a** and **5f** were the first known examples which reversed the addition of nucleophiles to an unfunctionalized olefin. This discovery might have some important synthetic applications.

The pH of the solution also affected the products. The major product was the epoxide at pH ≥ 11 with catalysts **5b**, **5c**, **5d** and **5e**, but ring-opened products still remained with catalyst **5a** and **5f** (Table 5.3).

5.2.4 Enantioselectivity of the chiral calixsalen and linear salen manganese catalysts

Enantioselectivity of a chiral catalyst is directly related to both reaction conditions such as solvent,[15-17] reaction temperature,[18-21] pH of the solution, additives to the reaction system[22, 23] and electronic and geometric properties of the substrate itself.[24-26] The effects of these factors were therefore investigated, and the results are presented in Tables 5.3-5.4. It can be seen that addition of donor solvents such as MeOH reduced the

enantioselectivity (entry 4 and 6 in Table 5.3). Whereas, the presence of benzene even further diminished the selectivity (entry 5). Coordination of MeOH to the manganese sites as evidenced by ESMS might have affected the selectivity. The effect from benzene was likely due to its competition with substrate styrene for the cavity.

Table 5.3. Epoxidation of styrene with sodium hypochlorite and the catalysts at 25°C

entry	cat.	solvents	product	yield (%)	ee (%)(config.)[a]	turnover
1	**5a**	$MeOH/CH_2Cl_2/H_2O$	chloro ether	75	38(n/a)	n/a
2	**5b**	$MeOH/CH_2Cl_2/H_2O$	epoxide	32	34(*R*)	24
3	**5c**	CH_2Cl_2/H_2O	epoxide	45	21(*R*)	35
4	**5d**	$MeOH/CH_2Cl_2/H_2O$	epoxide	57	35(*R*)	23
5	**5d**	$PhH/CH_2Cl_2/H_2O$	epoxide	70	22(*R*)	n/a
6	**5d**	CH_2Cl_2/H_2O	epoxide	63	52(*R*)	49
7	**5d**	CH_2Cl_2/H_2O	epoxide	60	28(*R*)[b]	46
8	**5e**	CH_2Cl_2/H_2O	epoxide	35	72(*R*)	23
9	**5f**	$MeOH/CH_2Cl_2/H_2O$	chloro ether	76	n/a	n/a
10	**5d**[c]	$MeOH/CH_2Cl_2/H_2O$	epoxide	57	33(*S*)	43
11	**5h**	CH_2Cl_2/H_2O	epoxide	34	30(*R*)	26

(a) The absolute configuration of the major styrene epoxide enantiomer was determined by comparison of the retention time of the mixture with those of *R*-styrene oxide and *S*-styrene oxide on HPLC. (b) one equiv. pyridine-*N*-oxide added. (c) (*S,S*)-catalyst.

It was noted that the enantioselectivity of the calixsalen catalysts was not directly related to the size of the R groups on the phenol units. Changing the R group from H, CH_3, *i*-Pr, to *t*-Bu did not result in obvious improvement of the enantiomeric excesses (entries 1, 2, 3, 7 in Table 5.3), which contrasted with the observations for the mononuclear salen systems.[20] In the binuclear calixsalen manganese system, stereoisomer discrimination might not rely on controlled approach of the substrate but rather substrate inclusion in the cavity prior to oxidation. The R group therefore was not as important as in the monosalen system since the cavity, determined by the four benzene rings and two methylene bridges, was essentially the same for all catalysts **5a-5d**.

Addition of pyridine *N*-oxide as an external donor to stabilize the high-valence intermediate Mn=O resulted in decreased enantiomeric excess (entry 7). Similar results were also observed for heterogenous polymeric analogs of mononuclear chiral Mn(III)-salen catalysts. Replacement of Cl^- as axial ligand by I^- had a slightly negative effect on the enantioselectivity (entry 11). The optical yield significantly improved on replacement of Cl^- with PF_6^- (entry 8). Another characteristic of the macrocyclic calixsalen system was that the (*R,R*)-catalysts provided *R*-rich (entry 6) while the (*S,S*)-catalysts gave an *S*-rich epoxide mixture (entry 10).

With styrene derivatives as substrates, the electronic effects of the substrate on the enantioselectivity were investigated. The results are shown in Table 5.4. Decreasing

electron density of the double bond decreased the enantioselectivity. This result is different from Naruta's observation[28] that enantioselectivity was improved with electron-deficient styrene derivatives using porphyrin-based catalysts. These results might be explained with the assumption of a radical[29, 30] mechanism. Presumably, electron-withdrawing groups could distribute the electron density of the radical and stabilize the intermediate. Consequently, bond rotation in a radical intermediate would result in decreased enantioselectivity.[24]

Table 5.4 Epoxidation of styrene derivatives[a]

entry	substrate	ee (%)(config.)	Debye (σ)
1	styrene	54 (*S*)	0.0
2	*p*-Cl-styrene	28 (n/a)	1.6
3	*p*-Br-styrene	25 (n/a)	1.5
4	*m*-NO_2-styrene	15 (n/a)	4.0
5	*p*-Me-styrene	16 (n/a)	-0.4
6	pentafluorostyrene	0	

[a] The reaction conditions were the same as indicated in Table 5.3. % ee was determined by ^{1}H NMR using the chiral shift reagent Pr(TFC)$_3$.

Alkene molecules such as *trans*-stilbene and 1,2-dihydronaphthalene did not react with NaOCl in the presence of the macrocyclic calixsalen binuclear manganese catalysts. In contrast, the side-by-side linear binuclear manganese catalyst (*R,R:R,R*) worked well

(Table 5.5), as did the monomeric Mn(III) catalysts (Chapter 1).

Table 5.5 Substrate size effect in epoxidation of various alkenes with sodium hypochlorite and calixsalen catalyst **5d** and side-by-side linear catalyst **5h**[a]

substrate	calixsalen-Mn **5d** yield (%)/ee (%)	side-by-side-Mn **5h** yield (%)/ee (%)
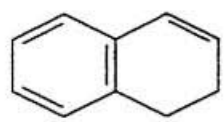		60/71
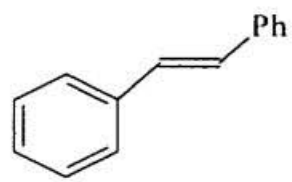		32/10
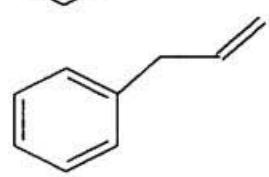	72/34	75/21
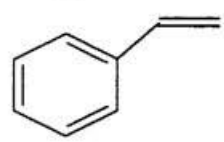	57/54	65/32

(a) The reaction conditions were the same as stated in Table 5.3. % ee were determined by chiral HPLC

Based on the above results, we speculated that the Mn=O group,[27] generated *in situ* in the macrocyclic catalytic system, was inside the cavity created by the macrocyclic framework. Larger alkene molecules could not properly fit into the cavity so delivery of

oxygen to the double bond became impossible.

Efforts to obtain a single crystal of the manganese macrocyclic calixsalen complexes in order to support structurally the above experimental results proved fruitless. Therefore, assignment of a structure to the manganese complexes was based on information provided by the X-ray crystallographic structure of a closely related chiral binuclear Cu(II) calixsalen complex model, which was prepared according to the same route and conditions as the binuclear nickel complex **3.8** (Chapter 3). The structure[a] is shown in Figure 5.1 (p. 162).

The assumption of a structural similarity of the copper and the manganese calixsalen complexes was based on the fact that monosalen manganese complexes often have a square pyramidal geometry with an axial solvent ligand.[27] In the binuclear copper complex, two axial water molecules outside of the cavity coordinated with Cu-O bond distances of *ca.* 2.3 Å and the geometry of each salen unit was square pyramidal and

---

[a]Crystal data of the model binuclear copper complex ($C_{54}H_{64}O_4N_4Cu_2 \cdot CH_2Cl_2 \cdot 5H_2O$): fw=1135.22; crystal dimensions= 0.40 x 0.40 x 0.12 mm; orthorhombic: $P2_1\,2_1\,2_1$ (#19): a =18.410(1) Å, b = 25.200(1) Å, c = 12.738(2) Å, V = 5909.4(7) Å^3, Z = 4; $D_{calcd.}$ = 1.276 g/cm^3; $2\theta_{max}$ = 120.4°; of 4929 reflections measured, 3798 were unique and 3798 observed ($I > 2\,\sigma(I)$); R = 0.062 , R_w = 0.064. Details of the X-ray experiments, bond distances, bond angles, atom coordinates, torsion angles, and crystal data can be found in Appendix 5.

isostructural with the monosalen manganese complexes. Therefore, the binuclear copper complex was a reasonable model to understand the binuclear manganese catalysts. Since one site of the metal centre was blocked by a ligand outside the cavity, the oxo group, required for epoxidation, would most likely position itself within the cavity. Subsequent oxo transfer then occurred only inside the cavity.

A fundamental question arising was how and why a prochiral alkene molecule entered the cavity. As demonstrated in Chapter 3, noncovalent -CH-π interactions forced an acetonitrile molecule into the cavity, and it was also likely that this kind of interaction together with π-π interactions between styrene and the catalyst were responsible. Two different entrances, using the cyclohexyl end ("cyclohexyl gate") or the R substituent (H, CH_3, *i*-Pr, or *t*-Bu) end ("R gate"), were possible for the binuclear Mn(III) catalysts with the *syn* conformation. Reference to the crystal structure showed a substantial difference in the size of the entrance. For example, the *i*-Pr gate with a maximum width of *ca.* 3.1 Å was much more crowded than the cyclohexyl gate with a minimum width of *ca.* 5.1 Å. Therefore, it can be expected that a prochiral alkene molecule would prefer to approach through the cyclohexyl gate to reach the active centres. A further advantage of the entry via the cyclohexyl gate is that the substrate is much closer to the source of chirality and therefore better chiral communication can be anticipated.

MMX modelling studies of the Mn(III) complex **5d** supported this prediction (Figure

5.2). The MMX energy (623 kJ/mol) of host/guest complex **b** where a styrene molecule approached through the cyclohexyl gate was lower than that (644 kJ/mol) of a host/guest complex **a** where a styrene molecule passed through the *t*-Bu gate. The molecular modelling results (Figure 5.2) further indicated that the MMX energy difference mainly stemmed from the torsional energy difference between the two host/guest complexes **a** and **b**. Clearly, increased torsional strain was required to accommodate the styrene guest molecule in the more restricted *t*-Bu entrance. Furthermore, molecular modelling studies (MMX) of Mn(III) complex **5a** also supported the observation that larger alkene molecules did not undergo epoxidation with the macrocyclic manganese catalyst (Table 5.5). It can been seen (Figure 5.3) that the target double bond of terminal alkenes such as styrene and allyl benzene could insert into the cavity (about 8 Å) and reach the active sites (Figure 5.3), whereas the more hindered double bond of 1,2-dihydronaphthalene could not (Figure 5.4).

These results suggested that asymmetric epoxidation of terminal alkenes proceeded through selective inclusion of the substrate within the cavity. To our knowledge this work represented the first direct evidence for host/guest catalysis in homogeneous epoxidation, which mimicked processes in natural enzymes.

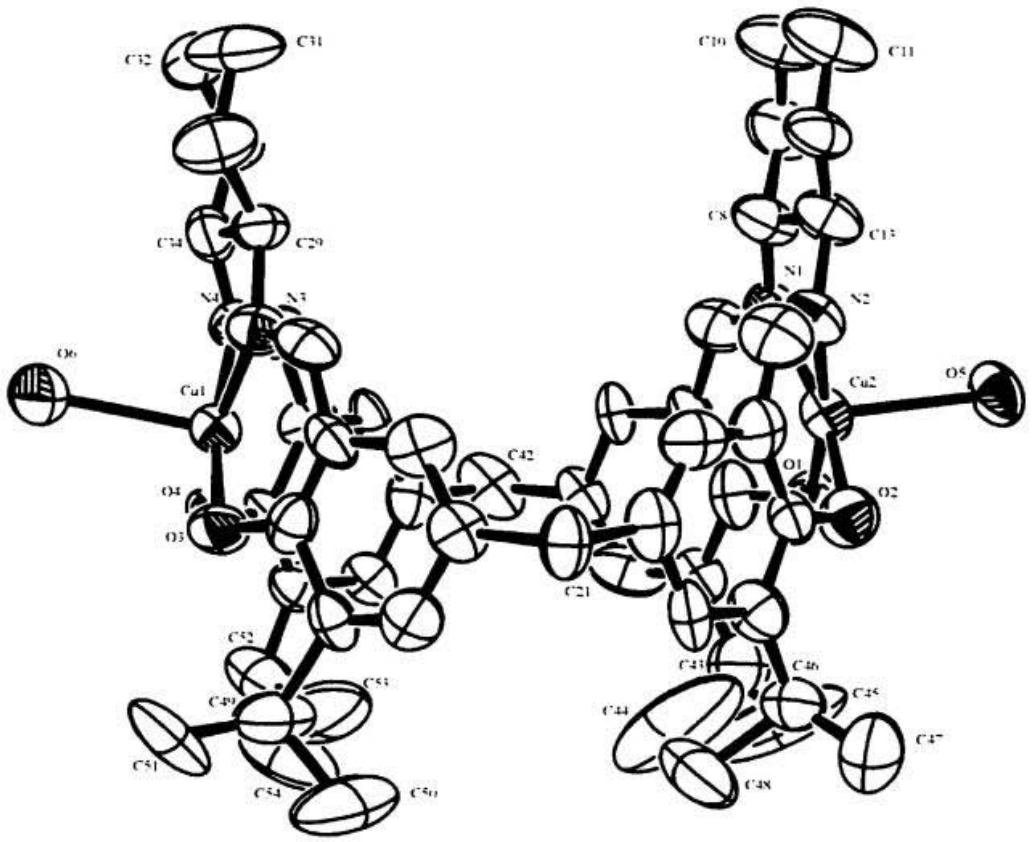

Figure 5.1 ORTEP representation of the chiral binuclear copper calixsalen complex (Hydrogen atoms and solvents were removed for clarity.)

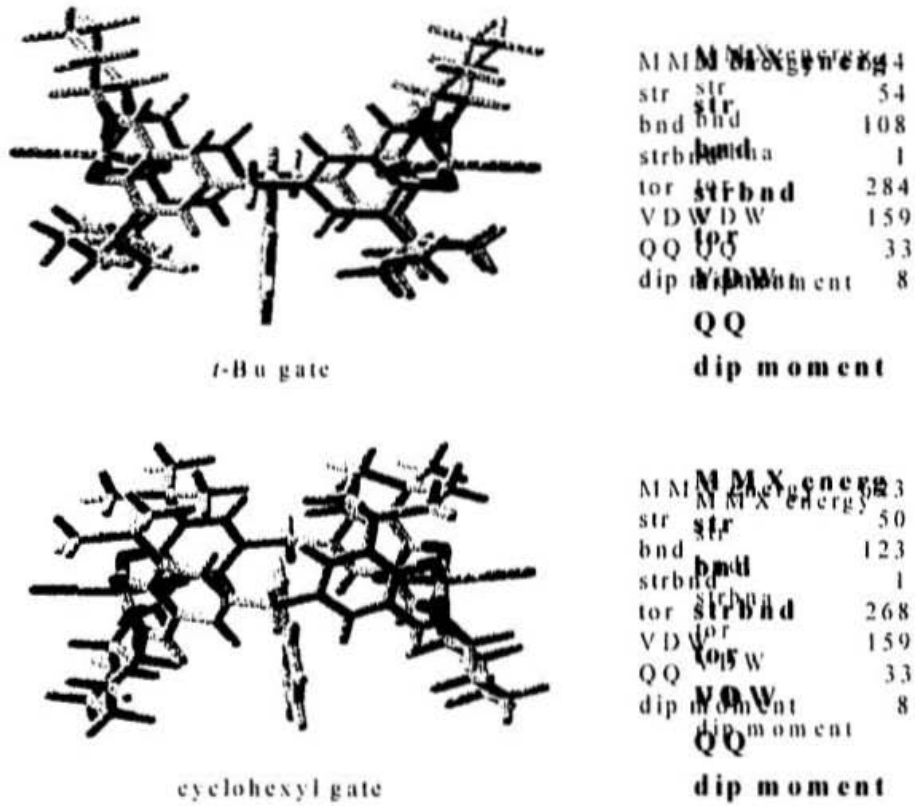

Figure 5.2 MMX results of the calixsalen Mn(III) catalyst host/substrate styrene guest complexes (comparison of *t*-Bu *vs* cyclohexyal entrance). MMX energy (kJ/mol) is broken down to str (stretching), bnd (bending), strbnd (coupled stretch-bend), tor (torsion), VDW (Vander Waals), QQ (electrostatics), and Dip moment (dipole moment) energy.

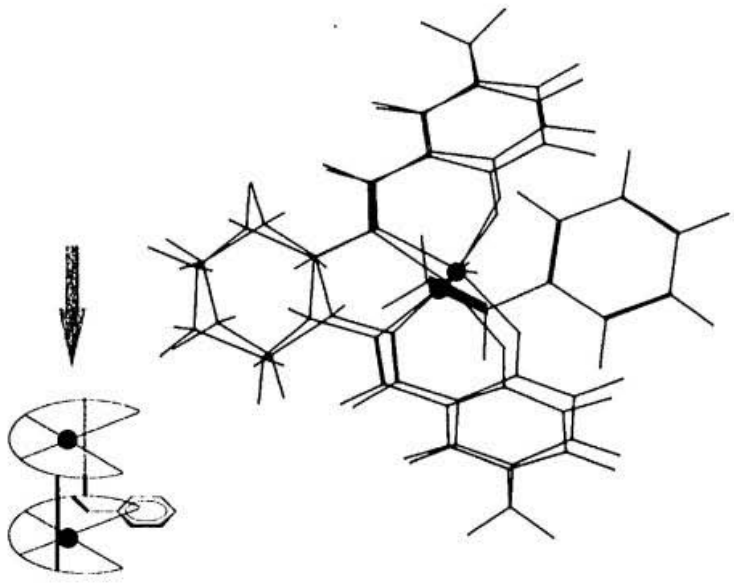

Figure 5.3 MMX picture (top view) of the complex of chiral catalyst **5a** and styrene

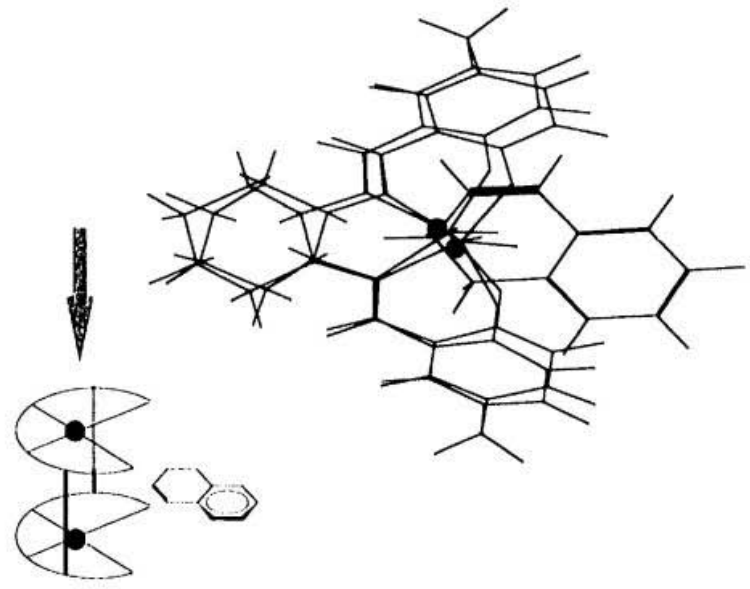

Figure 5.4 MMX picture (top view) of the complex of chiral catalyst **5a** and 1,2-dihydronaphthalene

5.3 Summary

Chiral calixsalen and linear side-by-side binuclear manganese(III) complexes were prepared. Catalytic studies showed that the Mn(III) complexes had good activity and enantioselectivity for epoxidation of unfunctionalized alkenes. It was found that the calixsalen manganese catalysts were size selective and that no epoxidation was observed with alkenes such as 1,2-dihydronaphthalene. An X-ray study of an isostructural calixsalen binuclear copper complex and MMX calculations supported the experimental results and suggested that the epoxidation reaction proceeded through inclusion of a guest alkene molecule within the cavity. Host/guest asymmetric catalytic epoxidation was experimentally demonstrated for the first time.

5.4 Experimental Section

5.4.1 Determination of the enantiomeric excess (% ee) The enantiomeric excess is calculated based on following equation:

$$\% \text{ ee} = \frac{R - S}{R + S} \times 100$$

The relative amount of each enantiomer *R* or *S* was measured by either HPLC, using a chiral column (No: 786101, particle diameter: 5 μm, 100 Å, 250 X 4.6 mm, ReGIS^{x}, Technologies, Inc.) packed with (*S,S*)-Whelk-O1 CSP (Figure 5.5, **a**); and the mobile phase was isopropanol in hexane (1/100), or by ^{1}H NMR using the chiral chemical shift reagent tris[3-(trifluoromethylhydroxymethylene)-(+)-camphorato] praseodymium(III) derivative Pr(TFC)$_3$ (Figure 5.5, **b**).

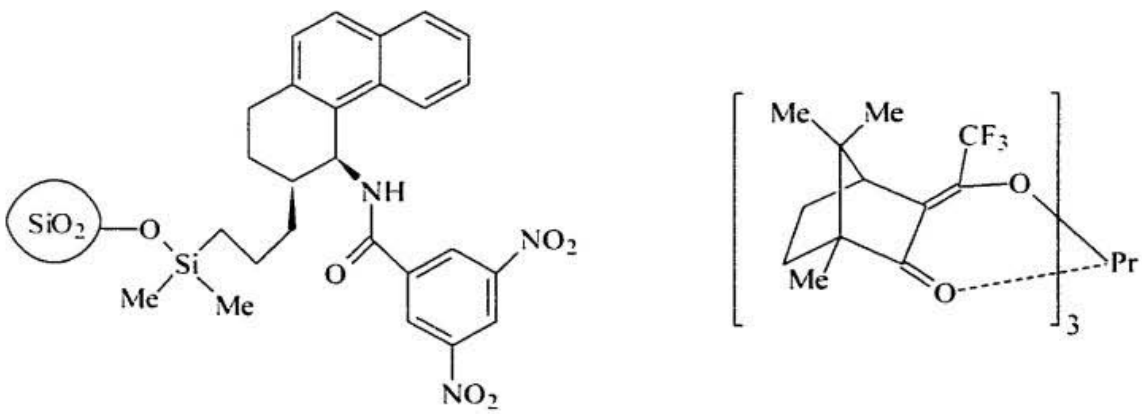

(a) **(b)**

Figure 5.5 Chiral auxiliaries used in HPLC and ^{1}H NMR analysis of chiral oxides.

5.4.2 Reagents 2-Propanol was stored over anhydrous sodium sulfate. Hexane was distilled from sodium and benzophenone. All other solvents were ACS grade and used without further purification. $Pr(TFC)_3$ and manganese(III) acetate dihydrate, lithium chloride, sodium iodide dihydrate, ammonium hexafluorophosphate; styrene, allylbenzene, 4-methylstyrene, 3-nitrostyrene, 4-bromostyrene, 2-vinylnaphthalene, 2,3,4,5,6-pentafluorostyrene, 1,2-dihydronaphthalene, (*R*)-styrene oxide, (*S*)-styrene oxide, oxone, pyridine *N*-oxide, *t*-butylhydroperoxide, *m*-chloroperoxybenzoic acid were purchased from Aldrich. Sodium hypochlorite was prepared by bubbling chlorine gas into aqueous sodium hydroxide solution.

5.4.3 Instrumentation High performance-liquid-chromatography (HPLC) was carried out on an ALTEX (Model 110A) instrument with a UV-visible analytical detector (Model 153). A computer equipped with JCL6000 chromatography software was used for parameter adjustment, data acquisition and spectrum display. GC-MS was done on a Hewlett-Packard (HP) system (model 5890 gas chromatography equipped with a 25 mm x 0.2 mm HP-1 fused silica column coupled to a HP model 5970 mass spectrometer). All other manipulations were performed under conditions similar to those described in Chapter 2.

Electron spray mass spectra (ESMS) were recorded on a Micromass Quattro II triple-stage quadrupole mass spectrometer equipped with an electrospray ionization source at

the Biological Mass Spectrometer Laboratory in the Department of Chemistry, University of Waterloo. All analyses were performed in flow injection mode. A solvent mixture of 50/50 MeOH/H_2O with 0.1% formic acid was used in all determinations. A HP1090LC pump delivered solvent to the electrospray ionization source at a flow rate of 40 μL/minute. 10 μL of the sample was injected through a Rheodyne 7125 valve. A 40 cm long peek tube (0.125 mm i.d.), connected the injection valve to the stainless steel electrospray tube (75μm i.d.), which transported samples to the ionization source. High purity nitrogen served as both nebulization gas and drying gas. The flow rate of nitrogen generated a stable spray at about 20 L/minute, with a flow rate of 300 L/minute for drying gas. The capillary voltage was set at 3.5 kV. The voltages of the HV lens and cone were 0.5 kV and 25 V-40 V depending on the molecular weight. The value of resolution at high and low molecular weight were all adjusted to 15, allowing one Dalton mass resolution. The ES source temperature was maintained at 80°C during the analysis. The mass spectra were recorded under multichannel A(MCA) mode, in which each scan was added together and the total signal intensity was displayed. Normally 10 to 20 scans were accumulated for one spectrum acquisition. A Digital Celebris™ computer was used for system control, parameter adjustment, data acquisition and spectrum display with Masslynx™, version 2.0 (Micromass, UK) under Windows™ 3.11 environment. The raw data were deconvoluted using the Fourier transform or maximum entropy program provided by Micromass as part of the system operation and data acquisition software.

5.4.4 Preparation of the binuclear manganese(III) calixsalen catalysts and side-by-side linear salen catalysts

To a clear, yellow-orange solution of the corresponding ligand (0.050 mmol) in 4.0 mL CH_2Cl_2/MeOH or EtOH (1:1) was added $Mn(OAc)_2 \cdot 2H_2O$ (0.034 g, 0.13 mmol) as a brown solid in one portion. The resultant solution was stirred for about 3 h at room temperature then LiCl (0.017 g, 0.40 mmol) or NH_4PF_6 (0.065 g, 0.041 mmol) was added. After an additional 2 h, solvent was removed, leaving a dark solid, which was dissolved in a minimal amount of CH_2Cl_2 or CH_2Cl_2 /MeOH. Flash chromatography (CH_2Cl_2 and then MeOH) afforded dark brown analytically pure binuclear Mn(III) complex.

5a. Yield: 0.029 g (68%). **IR** (Nujol): 1617 (CH=N), 1540 (Ph), 1462, 1382, 1347, 1310, 1284, 1165, 1132, 1093, 1026, 823 cm^{-1}: **Anal**. Calcd. for $C_{42}H_{40}N_4O_4Cl_2Mn_2 \cdot H_2O$: C, 64.03; H, 6.51; N, 4.94. Found: C, 64.08; H, 5.37; N, 4.86.

5b. Yield: 0.035 g (80%). **IR** (Nujol): 1615 (CH=N), 1550 (Ph), 1392, 1344, 1312, 1232, 1164, 1095, 1039, 830, 795, 760, 733 cm^{-1}: **Anal**. Calcd. for $C_{46}H_{48}N_4O_4Cl_2$ $Mn_2 \cdot H_2O \cdot CH_2Cl_2$: C, 56.19; H, 5.21; N, 5.57. Found: C, 56.66; H, 5.35; N, 4.89.

5c. Yield: 0.038 g (75%). **IR** (Nujol): 1606 (CH=N), 1547 (Ph), 1430, 1383, 1325, 1162, 1110, 1079, 972, 786, 733, 703 cm^{-1}: **Anal**. Calcd. for $C_{54}H_{64}N_4O_4Cl_2Mn_2 \cdot H_2O$: C, 64.03; H, 6.51; N, 4.94. Found: C, 64.08; H, 5.37; N, 4.86.

5d. Yield: 0.048 g (90%). **ESMS** (*m/z*): Calcd. for $C_{58}H_{72}N_4O_4Mn_2 \cdot 2MeOH$ 1062: Found:1063 $[C_{58}H_{72}N_4O_4Mn_2 \cdot 2MeOH + H]^+$, 998, 945, 892, 1045 $[C_{58}H_{72}O_4N_4Mn_2 \cdot HCOOH + H]^+$, 1093 $[C_{58}H_{72}O_4N_4Mn_2 \cdot 2MeOH \cdot CH_2O + H]^+$: **IR** (Nujol):1615 (CH=N),1542 (Ph), 1344, 1311, 1206, 1172, 1100, 1027, 836, 789, 736 cm^{-1}: **Anal**. Calcd. for $C_{58}H_{72}N_4O_4Cl_2Mn_2 \cdot 2CH_2Cl_2$: C, 58.12; H, 6.18; N, 4.52. Found: C, 58.44; H, 6.28; N, 4.58.

5e.Yield: 0.045 g (80%). **ESMS** (*m/z*): Calcd. for $C_{58}H_{72}N_4O_4Mn_2 \cdot CH_3CHO$: 1042: Found: 1101, 1100, 1099, 1043 $[C_{58}H_{72}N_4O_4Mn_2 \cdot CH_3CHO + H]^+$: **IR** (Nujol): 1611(CH=N), 1544 (Ph), 1393, 1342, 1297, 1270, 1243, 1211, 1173, 1046, 1036, 850 (PF_6), 777, 742, 721, 691 cm^{-1}.

Linear 5h.Yield: 0.042 g (80%). **ESMS** (*m/z*): Calcd. for $C_{57}H_{72}N_4O_4ClMn_2$: 1021: Found: 1021: **IR** (Nujol): 1615 (CH=N), 1549 (Ph), 1470, 1424, 1311, 1245, 1206, 1027, 875, 842, 757 cm^{-1}: **Anal**. Calcd. for $C_{57}H_{72}N_4O_4Cl_2Mn_2 \cdot H_2O$: C, 64.03; H, 6.51; N, 4.94. Found: C, 64.08; H, 5.37; N, 4.86.

5.4.5 Preparation of the model binuclear copper complex. This complex was prepared according to the procedure described in Chapter 4 for the binuclear copper complex **4.2**. Yield: 0.047 g (93%). **IR** (Nujol): 3511, 1642, 1615, 1542, 1384, 1344, 1278, 1232, 1160, 946, 862, 822, 789, 750, 690 cm^{-1}: **Anal**. Calcd. for $C_{54}H_{64}N_4O_4Cu_2 \cdot 2H_2O \cdot$

$2CH_2Cl_2$: C, 57.72; H, 6.18; N, 4.81. Found: C, 57.69; H, 6.09; N, 4.72.

5.4.6 Epoxidation Catalytic oxidations were carried out at room temperature. The macrocyclic calixsalen manganese catalyst (0.012 mmol) was dissolved in CH_2Cl_2 (10.0 mL; 1 mL MeOH may be added, depending on the solubility of a catalyst). Then alkene (1.0 mmol) followed by addition of $NaOCl_{(aq)}$ (4-5%, 10.0 mL) was added. The dark biphasic solution was vigorously stirred and the reaction progress was monitored by TLC (hexane/2-propanol). After 3 h, the organic phase was separated and the aqueous layer was extracted with CH_2Cl_2 (2 x 2 mL). The solvent was removed, and the residue was extracted with hexane (2 x 1 mL). The combined hexane extracts were applied to a small silica column to afford the epoxide. Chemical yields were determined from the isolated products and presented in Tables 5.2-5.5. Enantiomeric excesses were measured by chiral HPLC or ^1H NMR titration of the products with the chiral chemical shift reagent in $CDCl_3$. Reported enantiomeric excesses were the average of at least three measurements.

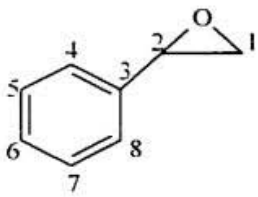

Styrene oxide. Its proton NMR data were consistent with that of a standard sample from Aldrich. **^1H NMR** ($CDCl_3$): δ 7.41-7.28 (m, 5H, Ph), 3.87 (dd, $J_{2\text{-}1a}$=3.9, $J_{2\text{-}1b}$= 2.5, 1H, H-2), 3.16 (d, $J_{1a\text{-}2}$ = 3.9, $J_{1a\text{-}1b}$ = 5.4, 1H, H-1A), 2.82 (dd, $J_{1b\text{-}2}$ = 2.7, $J_{1b\text{-}1a}$ = 5.6, 1H, H-1B).

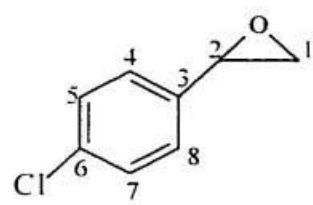

***p*-Chlorostyrene oxide.**[31] **^{1}H NMR** ($CDCl_3$): δ 7.35-7.18 (m. 4H. Ph). 3.84 (dd. $J_{2\text{-}1a}$= 3.8. $J_{2\text{-}1b}$= 2.4. 1H. H-2). 3.15 (dd. $J_{1a\text{-}2}$ = 3.8. $J_{1a\text{-}1b}$= 5.4. 1H. H-1A). 2.75 (dd. $J_{1b\text{-}2}$= 2.4. $J_{1b\text{-}1a}$= 5.4. 1H. H-1B).

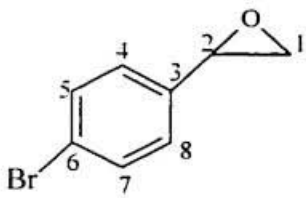

***p*-Bromostyrene oxide.**[31] **^{1}H NMR** ($CDCl_3$): δ 7.75-7.15 (m. 4H. Ph). 3.83 (dd. $J_{2\text{-}1a}$= 3.8. $J_{2\text{-}1b}$= 2.4. 1H. H-2). 3.14 (dd. $J_{1a\text{-}1b}$ =5.4. $J_{1a\text{-}2}$ =4.0. 1H. H-1A). 2.76 (dd. $J_{1b\text{-}1a}$= 5.3. $J_{1b\text{-}2}$ = 2.6. 1H. H-1B).

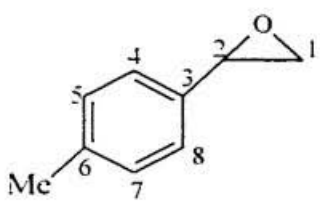

***p*-Methylstyrene epoxide.**[31] **^{1}H NMR** ($CDCl_3$): δ 7.81-7.17 (m. 4H. Ph). 3.84 (dd. $J_{2\text{-}1a}$= 4.4. $J_{2\text{-}1b}$= 2.7. 1H. H-2). 3.14 (dd. $J_{1a\text{-}1b}$ =5.4. $J_{1a\text{-}2}$ = 4.2. 1H. H-1A). 2.80 (dd. $J_{1b\text{-}1a}$= 5.4. $J_{1b\text{-}2}$ = 2.71H. H-1B). 2.36 (s. 3H. Me).

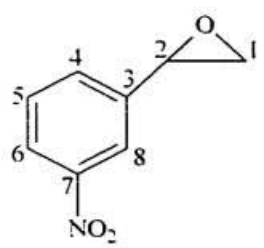

***m*-Nitrostyrene epoxide.**[31] **^{1}H NMR** ($CDCl_3$): δ 8.19 (s. 1H. H-8). 7.64-7.54 (m. 3H. H-4. H-5. H-6). 3.99 (dd. $J_{2\text{-}1a}$= 3.5. $J_{2\text{-}1b}$=2.4. 1H. H-2). 3.24 (dd. $J_{1a\text{-}1b}$= 5.4. $J_{1a\text{-}2}$= 3.5. 1H. H-1A). 2.82 (dd. $J_{1b\text{-}1a}$= 5.4. $J_{1b\text{-}2}$= 2.4. 1H. H-1B).

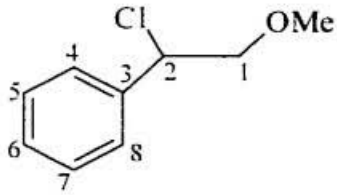

^{1}H NMR ($CDCl_3$): δ 7.44-7.34 (m. 5H. Ph). 5.02 (m. 1H. H-2). 3.80 (m. 2H. H-1). 3.42 (s. 3H. Me): **^{13}C NMR** ($CDCl_3$): δ 138.8 (1C. C-3). 128.9 (3C. C-5. C-6. C-7). 127.6 (2C. C-4. C-8). 77.45 (1C. C-1). 61.0 (1C. OMe). 59.3 (1C. C-2): **GC-MS** (*m/z*): Calcd. for $C_9H_{11}ClO$: 170: Found 170 (M^+).

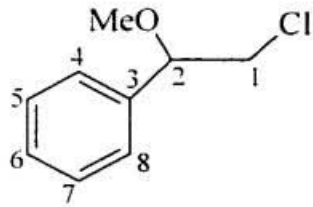

^{1}H NMR ($CDCl_3$): δ 7.42-7.32 (m. 5H. Ph). 4.36 (dd. $J_{2\text{-}1a}$ = 8.0. $J_{2\text{-}1b}$= 3.9. 1H. H-2). 3.42 (m. 2H. H-1). 3.32 (s. 3H. Me).

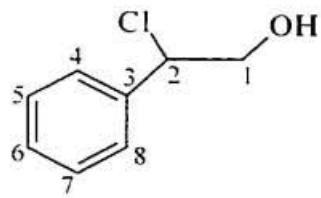

^{1}H NMR ($CDCl_3$): δ 7.43-7.37 (m. 5H. Ph). 5.01 (dd. $J_{2\text{-}1a}$=8.3. $J_{2\text{-}1b}$=6.3. 1H. H-2). 4.89 (m. 2H. H-1): **^{13}C NMR** ($CDCl_3$): δ (1C. C-3) not observed. 129.4 (1C. C-6.). 129.1 (2C. C-4. C-8). 127.7 (2C. C-5. C-7). 62.0 (1C. C-1). 48.6 (1C. C-2).

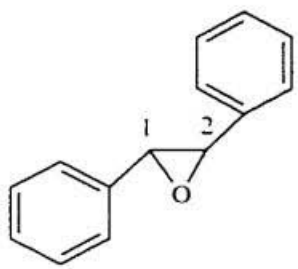

^{1}H NMR ($CDCl_3$):[32a] δ 7.38-7.33 (m. 10H. Ph). 3.87 (s. 2H. H-1. H-2).

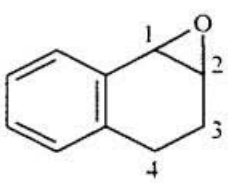

^{1}H NMR ($CDCl_3$):[32b] δ 7.41- 7.08 (m. 4H. Ph). 3.85 (d. J= 4.2. 1H. H-1). 3.73 (dd. J= 4.4. J=3.4. 1H. H-2). 2.75 (ddd. J_1=14.2. J_2 = 6.4. J_3 = 14.9. 1H). 2.53 (dd. J_1= 5.6. J_2 = 13.8. 1H). 2.47 (ddd. J_1= 5.6. J_2 = 13.8. J_3 = 15.5. 1H). 1.77 (ddd.J_1= 5.6. J_2= 13.8. J_3 = 15.2. 1H).

5.5 References

1. Feichtinger, D.; Plattner, D. A. *Angew. Chem., Int. Ed. Engl.* **1997**, *36*, 1718.

2. Sheldon, R. A.; Kochi, J. K. In *Metal-Catalyzed Oxidation of Organic Compounds*. Academic Press, London: New York, **1981**.

3. Srinivasan, K.; Michaud, P.; Kochi, J. K. *J. Am. Chem. Soc.* **1986**, *108*, 2309.

4. Collman, J. P.; Zhang, X.; Lee, V. L.; Uffelman, E. S.; Brauman, J. I. *Science* **1993**, *261*, 1404.

5. Boucher, L. J. *J. Inorg. Nucl. Chem.* **1974**, *36*, 531.

6. Srinivasan, K.; Michaud, P.; Kochi, J. K. *J. Am. Chem. Soc.* **1985**, *108*, 2309.

7. Pecoraro, V. L.; Gelasco, A.; Baldwin, M. J. In *Mechanistic Bioinorganic Chemistry*, Chapter 10; American chemical society, **1995**.

8. Fenton, D. In *Transition Metals in Supermolecular Chemistry*, Fabbrizzi, F. and Poggi, A., Eds., Kluwer: Boston, **1994**.

9. Sawaki, Y. In *Organic Peroxides*, Chapter 9, Ando, W. Ed., John Wiley & Sons: New York, **1992**.

10. Yang, D.; Wong, M., -K.; Yip, Y.-C.; Wang, X. C.; Tang, M. W.; Zheng, J. H.; Cheung, K. K. *J. Am. Chem. Soc.* **1998**, *120*, 5943.

11. Wang, Z. X.; Shi, Y. A. *J. Org. Chem.* **1997**, *62*, 8622.

12. Yang, D.; Yip, Y. C.; Tan, M. W.; Wong, M. K.; Zheng, J. H.; Cheung, K. K. *J. Am. Chem. Soc.* **1996**, *118*, 491.

13. Conte, V.; Furia, F. D.; Modena, G. In *Organic Peroxides*; John Wiley & Sons Ltd.; New York, **1992**.

14. Lai, J. Y.; Shi, X. X.; Dai, L. X. *J. Org. Chem.* **1992**, *57*, 3485.

15. Imanishi, H.; Katsuki, T. *Tetrahedron Lett.* **1997**, *38*, 251.

16. Hamachi, K.; Irie, R.; Katsuki, T. *Tetrahedron Lett.* **1996**, *37*, 4979.

17. Fukuda, T.; Katsuki, T. *Tetrahedron Lett.* **1996**, *37*, 4389.

18. Hamada, T.; Fukuda, T.; Imanishi, H.; Katsuki, T. *Tetrahedron* **1996**, *52*, 515.

19. Mikame, D.; Hamada, T.; Irie, R.; Katsuki, T. *Synlett* 1995, 827.

20. Palucki, M.; Pospisil, P. J.; Zhang, W.; Jacobsen, E. N. *J. Am. Chem. Soc.* **1994**, *116*, 9333.

21. Palucki, M.; McCormick, G. J.; Jacobsen, E. N. *Tetrahedron Lett.* **1995**, *36*, 5457.

22. Hashihayata, T.; Ito, Y.; Katsuki, T. *Synlett* **1996**, 1079.

23. Senanayake, C. H.; Smith, G. B.; Ryan, K. M.; Fredenburgh, L. E.; Liu, J.; Roberts, F. E.; Hughes, D. L.; Larsen, R. D.; Verhoeven, T. R.; Reider, P. J. *Tetrahedron Lett.* **1996**, *37*, 3271.

24. Jacobsen, E. N. In *Catalytic Asymmetric Synthesis*; Ojima, I., Ed.; VCH: New York, **1993**; p.159.

25. Katsuki, T. *Coord. Chem. Rev.* **1995**, *140*, 189.

26. Katsuki, T. *J. Synth. Org. Chem. Jpn.* **1995**, *53*, 940.

27. Pospisil, P. J.; Carsten, D. H.; Jacobsen, E. N. *Chem. Eur. J.* **1996**, *2*, 974.

28. Naruta, Y.; Tani, F.; Ishihars, N.; Maruyama, K. *J. Am. Chem. Soc.* **1991**, *113*, 6865.

29. Finney, N. S.; Pospisil, P. J.; Chang, S.; Palucki, M.; Konsler, R. G.; Hansen, K. B.; Jacobsen, E. N. *Angew. Chem., Int. Ed. Engl.* **1997**, *36*, 1720.

30. Linde, C.; Arnold, M.; Norrby, P. O.; Akermark, B. *Angew. Chem., Int. Ed. Engl.* **1997**, *36*, 1723.

31 Pedragosa-Moreau, S.; Morisseau, C.; Zylber, J.; Archelas, A.; Baratti, J.; Furstoss, R. *J. Org. Chem.* **1996**, *61*, 7402.

32 a) Colonna, S.; Molinari, H.; Banfi, S. *Tetrahedron* **1983**, *39*, 1635. b) Nagata, T.; Imagawa, K.; Yamada, T.; Mukaiyama, T. *Bull. Chem. Soc. Jpn.* **1995**, *68*, 1455.

Appendicies

Appendix 1- Appendix 3 contain X-ray results of the macrocyclic chiral salen dimer **14a.** chiral mono- and binuclear nickel and copper complexes **3.4. 3.8. 4.1. 4.2**. Appendix 4 contains the voltammograms provided by Professor M. L'Her (Université de Bretagne Occidentale. France). Appendix 5 contains the X-ray data of a chiral binuclear copper complex. Appendix 6 contains the selected ^{1}H NMR. ^{13}C NMR. and ESMS spectra of the compounds prepared in this study. The X-ray reports for the complexes **3.4. 3.8. 4.1. 4.2** were provided by Mr. D. Miller in the Department of Chemistry. The X-ray report for the binuclear copper complex was provided by Dr. J. Bridson in the Department of Chemistry.

Appendix 1

Crystal structure determinations of the calixsalen dimer 14a

A yellow irregular crystal of $C_{45}H_{47}O_5N_5$ having approximate dimensions of 0.400 x 0.200 x 0.400 mm was mounted on a glass fibre. All measurements were made on a Rigaku AFC6S diffractometer with graphite monochromated Mo-Kα radiation and a 2 kW sealed tube generator. Cell constants and an orientation matrix for data collection, obtained from a least-squares refinement using the setting angles of 23 carefully centered reflections in the range $20.28 < 2\theta < 24.88^0$ corresponded to a monoclinic cell with dimensions:

$a = 14.640\ (3)$ Å

$b = 25.679\ (4)$ Å $\qquad b = 81.97(2)^0$

$c = 11.045\ (6)$ Å

$V = 4112\ (4)$ Å^3

For $Z = 4$ and $F.W. = 737.90$, the calculated density was 1.192 g/cm^3. Based on the systematic absences of:

h0l: l = 2n

0k0: k = 2n

and the successful solution and refinement of the structure, the space group was determined to be $P2_1/c$ (#14).

The data were collected at a temperature of 26 ± 1^{0}C using the ω-2θ scan technique to a maximum 2θ value of 50.1^{0}. Omega scans of several intense reflections, made prior to data collection, had an average width at half-height of 0.34^{0} with a take-off angle of 6.0^{0}. Scans of $(0.84 + 0.35 \tan\theta)^{0}$ were made at a speed of 4.0^{0}/minute (in omega). The weak reflections ($I < 10.0\ \sigma(I)$) were rescanned (maximum of 2 rescans) and the counts were accumulated to assure good counting statistics. Stationary background counts were recorded on each side of the reflection. The ratio of peak counting time to background counting time was 2:1. The diameter of the incident beam collimator was 1.0 mm and the crystal to detector distance was 400.0 mm.

The structure was solved by direct methods[1] and expanded using Fourier techniques.[3] The non-hydrogen atoms were refined anisotropically. The final cycle of full-matrix least-squares refinement was based on 3003 observed reflections ($I > 1.20\ (I)$) and 497 variable parameters and converged (largest parameter shift was 0.00 times its esd) with unweighted and weighted agreement factors of:

$$R = \Sigma||Fo| - |Fc|| \ / \ \Sigma\ |Fo| = 0.077$$

$$R_{w} = [(\Sigma w\ (|Fo| - |Fc|)^{2}\ \ / \Sigma w\ Fo^{2}\ \ )]^{1/2} = 0.045$$

The standard deviation of an observation of unit weight was 1.80.[3] The weighting scheme was based on counting statistics and included a factor ($p = 0.01$) to downweight

the intense reflections. Plots of $w(|Fo| - |Fc|)^2$ versus |Fo|, reflection order in data collection, $\sin\theta/\lambda$, and various classes of indices showed no unusual trends. The maximum and minimum peaks on the final difference Fourier map corresponded to 0.27 and -0.21 $e^-/Å^3$, respectively.

Neutral atom scattering factors were taken from Cromer and Waber.[3] Anomalous dispersion effects were included in Fcalc:[4] the values for Df' and Df" were those of Cromer.[5a] All calculations were performed using the TEXSAN[6] crystallographic software package(**1997**) of Molecular Structure Corporation.

Table 2.1 Crystal data of the calixsalen **14a**

Empirical Formula	$C_{45}H_{47}O_5N_5$
Formula Weight	737.90
Crystal Colour, Habit	yellow, irregular
Crystal Dimensions (mm)	0.400 x 0.200 x 0.400
Crystal System	monoclinic
No. Reflections Used for	
Unit Cell Determination (2 range)	23 (20.3 - 24.9^0)
Omega Scan Peak Width	
at Half-height	0.34
Lattice Parameters:	
	a = 14.640 (3) Å
	b = 25.679 (4) Å b = 81.97 (2)^0
	c = 11.045 (6) Å
	V = 4112 (4) Å^3
Space Group	$P2_1/c$ (#14)
Z value	4
D_{calcd}	1.192 g/cm^3
F_{000}	1568
μ (Mo-Kα)	0.73 cm^{-1}

Table 2.2 Crystal data collection and structure solution refinement parameters **14a**

Diffractometer	Rigaku AFC6S
Radiation	Mo-Kα (λ= 0.71069 Å)
Temperature	26^{0}C
Take-off Angle	6.0^0
Detector Aperture	4.5 mm horizontal 3.0 mm vertical
Crystal to Detector Distance	40 cm
Scan Type	-2θ
Scan Rate	4.0^0/minute (in omega) (2 rescans)
Scan Width	(0.84 + 0.35 tanθ)^0
$2\theta_{max}$	50.1^0
No. of Reflections Measured	Total: 15181 Unique: 5858 (R_{int} = .064)
Corrections	Lorentz-polarization Absorption (trans. factors: 0.97 - 1.00) Secondary Extinction (coefficient: 0.86987E-07)
Structure Solution	Direct methods
Refinement	Full-matrix least-squares
Function Minimized	$\Sigma w (\|Fo\| - \|Fc\|)^2$
Least-squares Weights	$4Fo^2 / \sigma^2 (Fo^2)$
p-Factor	0.01
Anomalous Dispersion	All non-hydrogen atoms
No. Observations (I>1.20σ(I))	3003
No. Variables	497
Reflection/Parameter Ratio	6.04
Residuals: R^a: $R_w{}^b$	0.077: 0.045
Goodness of Fit Indicator	1.80
Max Shift/Error in Final Cycle	0.00
Maximum Peak in Final Diff. Map	0.27 e$^-$/Å^3
Minimum Peak in Final Diff. Map	-0.21 e$^-$/Å^3

[a] $R=\Sigma||Fo| - |Fc|| / \Sigma|Fo|$. [b] $R_w = [(\Sigma w (|Fo| - |Fc|)^2/\Sigma w Fo^2)]^{1/2}$

Table 2.3. Atom coordinates and B(eq) of the calixsalen **14a**

atom	x	y	z	B(eq)
O(1)	1.0686(3)	0.0014(1)	0.8215(3)	7.8(3)
O(2)	1.5091(3)	0.2283(2)	0.8729(4)	7.8(3)
O(3)	1.4400(3)	0.0378(2)	1.1664(4)	9.3(3)
O(4)	0.9585(3)	0.2315(2)	0.8982(3)	7.9(3)
N(1)	1.0069(3)	0.0638(2)	0.6705(3)	5.4(3)
N(2)	1.5918(3)	0.1667(2)	1.0050(4)	5.4(3)
N(3)	1.5010(3)	0.1244(2)	1.2279(4)	5.5(3)
N(4)	0.9062(3)	0.1431(2)	0.8152(4)	5.7(3)
C(1)	0.8619(3)	0.1096(2)	0.7324(4)	5.6(4)
C(2)	0.7834(4)	0.1387(2)	0.6869(4)	6.9(4)
C(3)	0.7364(4)	0.1046(3)	0.6022(5)	7.8(4)
C(4)	0.8058(4)	0.0862(2)	0.4934(5)	7.2(4)
C(5)	0.8861(3)	0.0586(2)	0.5395(4)	6.3(4)
C(6)	0.9328(3)	0.0929(2)	0.6249(4)	5.1(3)
C(7)	1.0903(4)	0.0737(2)	0.6242(4)	5.4(3)
C(8)	1.1677(3)	0.0469(2)	0.6671(5)	5.2(4)
C(9)	1.2574(4)	0.0580(2)	0.6086(4)	5.7(4)
C(10)	1.3343(4)	0.0356(3)	0.6484(5)	6.0(4)
C(11)	1.3190(5)	0.0013(3)	0.7456(6)	6.9(5)
C(12)	1.2322(5)	-0.0105(2)	0.8044(5)	7.4(4)
C(13)	1.1549(4)	0.0124(2)	0.7652(5)	5.9(4)
C(14)	1.4312(4)	0.0513(3)	0.5933(5)	7.0(4)
C(15)	1.4605(3)	0.0990(3)	0.6607(5)	5.7(4)
C(16)	1.4365(4)	0.1491(3)	0.6294(5)	6.7(4)
C(17)	1.4539(4)	0.1914(3)	0.6975(6)	7.3(4)
C(18)	1.4971(4)	0.1866(3)	0.8030(5)	5.7(4)
C(19)	1.5249(3)	0.1366(3)	0.8333(5)	4.8(3)
C(20)	1.5055(3)	0.0941(2)	0.7630(5)	5.4(3)

Table 2.3 (cont.) Atom coordinates and B(eq) of the calixsalen **14a**

atom	x	y	z	B(eq)
C(21)	1.5741(3)	0.1288(2)	0.9386(5)	5.1(3)
C(22)	1.6417(3)	0.1564(2)	1.1086(4)	5.0(3)
C(23)	1.7215(3)	0.1944(2)	1.1037(4)	6.4(4)
C(24)	1.7715(3)	0.1883(2)	1.2140(5)	6.8(4)
C(25)	1.7068(4)	0.1948(2)	1.3319(5)	6.4(4)
C(26)	1.6265(3)	0.1567(2)	1.3372(4)	5.8(3)
C(27)	1.5762(3)	0.1628(2)	1.2270(5)	5.1(3)
C(28)	1.4187(4)	0.1399(2)	1.2580(4)	5.2(3)
C(29)	1.3399(4)	0.1061(3)	1.2485(5)	5.2(4)
C(30)	1.2504(4)	0.1252(2)	1.2805(4)	5.9(4)
C(31)	1.1726(4)	0.0969(3)	1.2620(5)	6.1(4)
C(32)	1.1884(5)	0.0489(3)	1.2107(7)	8.5(5)
C(33)	1.2765(5)	0.0275(2)	1.1790(7)	9.1(5)
C(34)	1.3534(5)	0.0574(3)	1.1983(6)	7.0(5)
C(35)	1.0762(4)	0.1177(3)	1.2915(4)	7.3(4)
C(36)	1.0447(3)	0.1472(3)	1.1859(5)	5.4(4)
C(37)	1.0575(4)	0.2007(3)	1.1733(6)	6.9(4)
C(38)	1.0296(4)	0.2291(2)	1.0788(7)	7.3(4)
C(39)	0.9867(4)	0.2040(3)	0.9900(5)	5.6(4)
C(40)	0.9736(3)	0.1501(2)	1.0002(4)	4.6(3)
C(41)	1.0027(3)	0.1227(2)	1.0972(5)	5.2(3)
C(42)	0.9284(3)	0.1217(2)	0.9110(5)	5.1(3)

Table 2.4. Selected bond distances for the calixsalen ligand **14a**

atom	atom	distance	atom	atom	distance
O(2)	C(18)	1.346(6)	C(15)	C(16)	1.391(8)
O(3)	C(34)	1.364(7)	C(15)	C(20)	1.390(6)
O(4)	C(39)	1.347(6)	C(16)	C(17)	1.364(8)
N(1)	C(6)	1.464(6)	C(17)	C(18)	1.407(7)
N(1)	C(7)	1.283(5)	C(18)	C(19)	1.402(7)
N(2)	C(21)	1.267(6)	C(19)	C(20)	1.391(7)
N(2)	C(22)	1.465(5)	C(19)	C(21)	1.464(6)
N(3)	C(27)	1.478(6)	C(22)	C(23)	1.516(6)
N(3)	C(28)	1.269(5)	C(22)	C(27)	1.519(6)
N(4)	C(1)	1.470(6)	C(23)	C(24)	1.515(6)
N(4)	C(42)	1.275(5)	C(24)	C(25)	1.508(6)
C(1)	C(2)	1.514(6)	C(25)	C(26)	1.523(7)
C(1)	C(6)	1.526(6)	C(26)	C(27)	1.516(6)
C(2)	C(3)	1.516(7)	C(28)	C(29)	1.459(7)
C(3)	C(4)	1.536(7)	C(29)	C(30)	1.397(6)
C(4)	C(5)	1.520(7)	C(29)	C(34)	1.372(7)
C(5)	C(6)	1.522(6)	C(30)	C(31)	1.391(7)
C(7)	C(8)	1.460(6)	C(31)	C(32)	1.363(8)
C(8)	C(9)	1.409(6)	C(31)	C(35)	1.500(7)
C(8)	C(13)	1.392(6)	C(32)	C(33)	1.399(8)
C(9)	C(10)	1.389(6)	C(33)	C(34)	1.403(8)
C(10)	C(11)	1.382(7)	C(35)	C(36)	1.516(7)
C(10)	C(14)	1.519(7)	C(36)	C(37)	1.390(8)
C(11)	C(12)	1.378(7)	C(36)	C(41)	1.380(6)
C(12)	C(13)	1.398(7)	C(37)	C(38)	1.380(7)
C(38)	C(39)	1.395(7)	C(39)	C(40)	1.399(7)
C(40)	C(41)	1.397(6)	C(40)	C(42)	1.458(6)

Table 2.5. Selected bond angles in the calixsalen **14a**

atom	atom	atom	angle	atom	atom	atom	angle
C(6)	N(1)	C(7)	118.1(5)	C(8)	C(13)	C(12)	118.8(6)
C(21)	N(2)	C(22)	118.6(5)	C(10)	C(14)	C(15)	109.2(4)
C(27)	N(3)	C(28)	118.1(5)	C(14)	C(15)	C(16)	121.6(6)
C(1)	N(4)	C(42)	116.7(5)	C(14)	C(15)	C(20)	121.5(6)
N(4)	C(1)	C(2)	109.9(5)	C(16)	C(15)	C(20)	116.7(6)
N(4)	C(1)	C(6)	109.7(4)	C(15)	C(16)	C(17)	121.8(6)
C(2)	C(1)	C(6)	110.2(4)	C(16)	C(17)	C(18)	121.8(6)
C(1)	C(2)	C(3)	110.6(5)	O(2)	C(18)	C(17)	121.0(6)
C(2)	C(3)	C(4)	110.6(4)	O(2)	C(18)	C(19)	121.7(5)
C(3)	C(4)	C(5)	109.8(4)	C(17)	C(18)	C(19)	117.2(6)
C(4)	C(5)	C(6)	111.9(5)	C(18)	C(19)	C(20)	119.7(5)
N(1)	C(6)	C(1)	109.4(4)	C(18)	C(19)	C(21)	120.4(5)
N(1)	C(6)	C(5)	109.6(5)	C(20)	C(19)	C(21)	120.0(6)
C(1)	C(6)	C(5)	109.2(4)	C(15)	C(20)	C(19)	122.7(5)
N(1)	C(7)	C(8)	121.1(5)	N(2)	C(21)	C(19)	121.3(5)
C(7)	C(8)	C(9)	118.1(5)	N(2)	C(22)	C(23)	108.8(4)
C(7)	C(8)	C(13)	121.7(5)	N(2)	C(22)	C(27)	109.2(4)
C(9)	C(8)	C(13)	120.1(5)	C(23)	C(22)	C(27)	110.6(4)
C(8)	C(9)	C(10)	121.0(5)	C(22)	C(23)	C(24)	111.1(4)
C(9)	C(10)	C(11)	117.4(6)	C(23)	C(24)	C(25)	111.5(4)
C(9)	C(10)	C(14)	121.1(6)	C(24)	C(25)	C(26)	110.5(4)
C(11)	C(10)	C(14)	121.4(6)	C(25)	C(26)	C(27)	111.2(4)
C(10)	C(11)	C(12)	123.0(6)	N(3)	C(27)	C(22)	108.3(4)
C(11)	C(12)	C(13)	119.7(6)	N(3)	C(27)	C(26)	111.8(4)
O(1)	C(13)	C(8)	120.3(5)	C(22)	C(27)	C(26)	111.1(4)
O(1)	C(13)	C(12)	120.8(6)	N(3)	C(28)	C(29)	121.7(5)

Table 2.6 Selected torsional angles for the calixsalen **14a**

(1)	(2)	(3)	(4)	angle	(1)	(2)	(3)	(4)	angle
O(1)	C(13)	C(8)	C(7)	2.3(8)	N(4)	C(1)	C(2)	C(3)	-179.6(4)
O(1)	C(13)	C(8)	C(9)	-179.7(5)	N(4)	C(1)	C(6)	C(5)	-179.7(4)
O(1)	C(13)	C(12)	C(11)	-180.0(5)	N(4)	C(42)	C(40)	C(39)	6.2(8)
O(2)	C(18)	C(17)	C(16)	-176.3(5)	N(4)	C(42)	C(40)	C(41)	-174.6(5)
O(2)	C(18)	C(19)	C(20)	175.7(5)	C(1)	N(4)	C(42)	C(40)	179.4(4)
O(2)	C(18)	C(19)	C(21)	-4.1(8)	C(1)	C(2)	C(3)	C(4)	-57.9(6)
O(3)	C(34)	C(29)	C(28)	5.7(9)	C(1)	C(6)	N(1)	C(7)	-136.6(5)
O(3)	C(34)	C(29)	C(30)	-179.9(5)	C(1)	C(6)	C(5)	C(4)	57.8(6)
O(3)	C(34)	C(33)	C(32)	-178.9(6)	C(2)	C(1)	N(4)	C(42)	138.5(5)
O(4)	C(39)	C(38)	C(37)	179.4(5)	C(2)	C(1)	C(6)	C(5)	-58.6(6)
O(4)	C(39)	C(40)	C(41)	-179.3(4)	C(2)	C(3)	C(4)	C(5)	55.7(7)
O(4)	C(39)	C(40)	C(42)	-0.1(8)	C(3)	C(2)	C(1)	C(6)	59.4(6)
N(1)	C(6)	C(1)	N(4)	60.4(5)	C(3)	C(4)	C(5)	C(6)	-56.3(6)
N(1)	C(6)	C(1)	C(2)	-178.5(5)	C(5)	C(6)	N(1)	C(7)	103.6(5)
N(1)	C(6)	C(5)	C(4)	177.6(4)	C(6)	N(1)	C(7)	C(8)	178.7(4)
N(1)	C(7)	C(8)	C(9)	177.2(5)	C(6)	C(1)	N(4)	C(42)	-100.2(5)
N(1)	C(7)	C(8)	C(13)	-4.7(8)	C(7)	C(8)	C(9)	C(10)	177.1(5)
N(2)	C(21)	C(19)	C(18)	0.6(7)	C(7)	C(8)	C(13)	C(12)	-177.8(5)
N(2)	C(21)	C(19)	C(20)	-179.2(5)	C(8)	C(9)	C(10)	C(11)	1.4(8)
N(2)	C(22)	C(23)	C(24)	175.8(4)	C(8)	C(9)	C(10)	C(14)	-174.2(5)
N(2)	C(22)	C(27)	N(3)	61.3(5)	C(8)	C(13)	C(12)	C(11)	0.1(9)
N(2)	C(22)	C(27)	C(26)	-175.5(4)	C(9)	C(8)	C(13)	C(12)	0.2(8)
N(3)	C(27)	C(22)	C(23)	-179.0(4)	C(9)	C(10)	C(11)	C(12)	-1.0(9)
N(3)	C(27)	C(26)	C(25)	177.2(4)	C(9)	C(10)	C(14)	C(15)	86.4(6)
N(3)	C(28)	C(29)	C(30)	-178.8(5)	C(10)	C(9)	C(8)	C(13)	-1.0(8)
N(3)	C(28)	C(29)	C(34)	-4.4(8)	C(10)	C(11)	C(12)	C(13)	0(1)

Table 2.6 (cont.) Selected torsional angles for the calixsalen **14a**

(1)	(2)	(3)	(4)	angle	(1)	(2)	(3)	(4)	angle
C(10)	C(14)	C(15)	C(16)	-84.3(7)	C(28)	C(29)	C(30)	C(31)	173.3(5)
C(10)	C(14)	C(15)	C(20)	90.1(6)	C(28)	C(29)	C(34)	C(33)	-173.8(5)
C(11)	C(10)	C(14)	C(15)	-89.1(7)	C(29)	C(30)	C(31)	C(32)	0.3(8)
C(12)	C(11)	C(10)	C(14)	174.5(6)	C(29)	C(30)	C(31)	C(35)	-177.6(5)
C(14)	C(15)	C(16)	C(17)	172.9(5)	C(29)	C(34)	C(33)	C(32)	1(1)
C(14)	C(15)	C(20)	C(19)	-173.6(5)	C(30)	C(29)	C(34)	C(33)	0.5(9)
C(15)	C(16)	C(17)	C(18)	0.0(9)	C(30)	C(31)	C(32)	C(33)	1(1)
C(15)	C(20)	C(19)	C(18)	1.3(8)	C(30)	C(31)	C(35)	C(36)	88.7(7)
C(15)	C(20)	C(19)	C(21)	-178.8(4)	C(31)	C(30)	C(29)	C(34)	-1.0(8)
C(16)	C(15)	C(20)	C(19)	1.1(8)	C(31)	C(32)	C(33)	C(34)	-1(1)
C(16)	C(17)	C(18)	C(19)	2.4(8)	C(31)	C(35)	C(36)	C(37)	-91.3(7)
C(17)	C(16)	C(15)	C(20)	-1.7(8)	C(31)	C(35)	C(36)	C(41)	88.3(6)
C(17)	C(18)	C(19)	C(20)	-3.0(7)	C(32)	C(31)	C(35)	C(36)	-89.1(8)
C(19)	C(21)	N(2)	C(22)	-179.6(4)	C(35)	C(36)	C(37)	C(38)	-179.8(5)
C(21)	N(2)	C(22)	C(23)	130.3(5)	C(35)	C(36)	C(41)	C(40)	179.9(5)
C(21)	N(2)	C(22)	C(27)	-108.9(5)	C(36)	C(37)	C(38)	C(39)	0(1)
C(22)	C(23)	C(24)	C(25)	-56.5(6)	C(36)	C(41)	C(40)	C(39)	0.1(8)
C(22)	C(27)	N(3)	C(28)	-133.3(4)	C(36)	C(41)	C(40)	C(42)	-179.1(4)
C(22)	C(27)	C(26)	C(25)	56.0(6)	C(37)	C(36)	C(41)	C(40)	-0.5(8)
C(23)	C(22)	C(27)	C(26)	-55.9(6)	C(37)	C(38)	C(39)	C(40)	-0.2(9)
C(23)	C(24)	C(25)	C(26)	55.9(7)	C(38)	C(37)	C(36)	C(41)	0.6(9)
C(24)	C(23)	C(22)	C(27)	55.9(6)	C(38)	C(39)	C(40)	C(41)	0.3(8)
C(24)	C(25)	C(26)	C(27)	-55.8(6)	C(38)	C(39)	C(40)	C(42)	179.4(5)
C(26)	C(27)	N(3)	C(28)	103.9(5)	C(27)	N(3)	C(28)	C(29)	173.1(4)

The sign is positive if when looking from atom 2 to atom 3 a clock-wise motion of atom 1would superimpose it on atom 4.

Appendix 2

X-ray crystal structure determination of the macrocyclic complexes 3.4 and 3.8.

For complex **3.4**, a dark red, multifaceted crystal of $C_{58}H_{74.50}N_4O_{4.25}Ni$ having approximate dimensions of 0.32 x 0.20 x 0.13 mm was mounted on a glass fibre. All measurements were made on a Siemens P4 diffractometer equipped with a SMART CCD detector (Department of Chemistry, McMaster University), graphite monochromated Mo-Kα radiation and a rotating anode generator.

The data were collected at a temperature of -60 ± 1°C. The hemisphere of data was collected with 30 second, 0.3 degree frames to a maximum 2θ value of 55.15°. Of the 48854 reflections which were collected, 6852 were unique (R_{int} = 0.083). The linear absorption coefficient, μ, for Mo-Kα radiation was 3.6 cm^{-1}. The Siemens area detector absorption correction routine (SADABS) was used to correct the data. This included incident and diffracted beam corrections, decay correction and an absorption correction. Maximum and minimum effective transmissions were 0.934761 and 0.826849. The data were corrected for Lorentz and polarization effects. A correction for secondary extinction was applied (coefficient = 3.77458e-007).

For complex **3.8**, a red irregular crystal of $C_{60.70}H_{83.40}O_4N_5Ni_2Cl_{1.40}$ having approximate

dimensions of 0.25 x 0.10 x 0.40 mm was mounted on a glass fibre. All measurements were made on a Rigaku AFC6S diffractometer with graphite monochromated Cu-Kα radiation. The data were collected at a temperature of 26 ± 1°C using the ω-2θ scan technique to a maximum 2θ value of 120.1°. Omega scans of several intense reflections, made prior to data collection, had an average width at half-height of 0.33° with a take-off angle of 6.0°. Scans of (1.57 + 0.14 tan θ)° were made at a speed of 4.0°/min (in ω). The weak reflections ($I < 10.0\sigma(I)$) were rescanned (maximum of 10 scans) and the counts were accumulated to ensure good counting statistics. Stationary background counts were recorded on each side of the reflection. The ratio of peak counting time to background counting time was 2:1. The diameter of the incident beam collimator was 1.0 mm, the crystal to detector distance was 400 mm, and the detector aperture was 9.0 x 4.5 mm (horizontal x vertical).

The two structures of **3.4** and **3.8** were solved by direct methods[1] and expanded using Fourier techniques.[2] Non-hydrogen atoms were refined anisotropically, with the exception of one water molecule in complex **3.4** which was refined isotropically. Hydrogen atoms were included but not refined. The final cycle of full-matrix least-squares refinement was based on 4162 (complex **3.4**) or 3752 (complex **3.8**) observed reflections ($I > 1.50\sigma(I)$ for complex **3.4** and, $I > 2.00\sigma(I)$ for complex **3.8**) and 609 (complex **3.4**) or 641 (complex **3.8**) variable parameters and converged (largest parameter shift was 0.00 times its esd) with unweighted and weighted agreement factors of:

Complex **3.4**

$$R = \Sigma \, ||Fo| - |Fc|| \, / \, \Sigma \, |Fo| = 0.054$$

$$R_w = [(\Sigma w \, (|Fo| - |Fc|)^2 \, / \, \Sigma w \, Fo^2)]^{1/2} = 0.049$$

Complex **3.8**

$$R = \Sigma \, ||Fo| - |Fc|| \, / \, \Sigma \, |Fo| = 0.067$$

$$R_w = [(\Sigma w \, (|Fo| - |Fc|)^2 \, / \, \Sigma w \, Fo^2)]^{1/2} = 0.065$$

The standard deviation of an observation of unit weight[3] was 1.17 for complex **3.4** and 3.60 for complex **3.8**. The weighting scheme was based on counting statistics and a factor ($p = 0.005$) was included for complex **3.8**. Plots of $\Sigma w \, (|Fo| - |Fc|)^2$ versus $|Fo|$, reflection order in data collection, $\sin\theta/\lambda$ and various classes of indices showed no unusual trends. The maximum and minimum peaks on the final difference Fourier map corresponded to 0.53 and -0.31 $e^-/Å^3$, respectively for complex **3.4** and, 0.89 and -0.61 $e^-/Å^3$ for complex **3.8**.

Neutral atom scattering factors were taken from Cromer and Waber.[4] Anomalous dispersion effects were included in Fcalc:[5] the values for Df' and Df'' were those of Creagh and McAuley.[6] The values for the mass attenuation coefficients are those of Creagh and Hubbell.[7] All calculations were performed using the TEXSAN[8] crystallographic software package (**1997**) of Molecular Structure Corporation.

Table 3.1 Crystal data of the complexes **3.4** and **3.8**

Complex	**3.4**	**3.8**
Empirical Formula	$C_{58}H_{74.50}O_{4.25}N_4Ni$	$C_{60.70}H_{83.40}O_4N_5Ni_2Cl_{1.40}$
Formula Weight	954.45	1114.19
Crystal Colour. Habit	dark red. multifaced	red. irregular
Crystal Dimension	0.32 x 0.20 x 0.13 mm	0.25 x 0.10 x 0.40 mm
Crystal System	trigonal	orthorhombic
Lattice Type	primitive	primitive
Lattice Parameters	a = 18.2566(2) Å	a = 19.531(2) Å
		b = 22.819(3) Å
	c = 15.9244(2) Å	c = 13.373(1) Å
	V = 4596.57(8) Å^3	V = 5960(1) Å^3
Space Group	$P3_1$ (#144)	$P2_12_12_1$ (#19)
Z value	3	4
D_{calcd}	1.034 g/cm^3	1.242 g/cm^3
F_{000}	1537.50	2377.60
μ (Mo-Kα)	3.59 cm^{-1}	μ (Cu-Kα) 17.35 cm^{-1}

Table 3.2. Intensity measurements and structure solution and refinement for the complex **3.4**

Diffractometer	Siemens P4, CCD detector
Radiation	Mo-Kα (l = 0.71069 Å), graphite monochromated
Temperature	-60°C
Scan Rate	30s, 0.3deg frames
$2\theta_{max}$	55.15°
No. of Reflections Measured Total:	48854 unique: 6852 (R_{int} = 0.083)
Corrections Lorentz-polarization	
	Secondary extinction
	(coefficient: 3.77458e-007)
	SADABS correction
	(trans. factors: 0.826849 - 0.934761)
Structure Solution	Direct methods (SHELXS86)
Refinement	Full-matrix least-squares
Function Minimized	$\Sigma w (\|Fo\| - \|Fc\|)^2$
Least Squares Weights	$1/\sigma^2(Fo) = 4Fo^2/\sigma^2(Fo^2)$
p-factor	0.0000
Anomalous Dispersion	All non-hydrogen atoms
No. Observations (I>1.50σ(I))	4162
No. Variables	609
Reflection/Parameter Ratio	6.83
Residuals: R: R_w	0.054 : 0.049
Goodness of Fit Indicator	1.17
Max Shift/Error in Final Cycle	0.00
Maximum peak in Final Diff. Map	0.53 $e^-/Å^3$
Minimum peak in Final Diff. Map	-0.31 $e^-/Å^3$

Table 3.3 Positional parameters and B(eq) for the nickel complex **3.4**

atom	x	y	z	B(eq)
Ni(1)	0.56510(5)	0.01225(5)	0.0590(5)	3.90(2)
O(1)	0.4555(2)	-0.0411(3)	0.1027(6)	4.02(10)
O(2)	0.3898(2)	-0.5384(2)	0.2322(6)	4.48(11)
O(3)	0.9001(2)	-0.1755(3)	0.3071(6)	5.01(12)
O(4)	0.6058(3)	0.0598(3)	0.1636(6)	4.97(12)
O(5)	0.293(2)	0.440(2)	0.868(2)	8.9(6)*
N(1)	0.5354(3)	-0.4033(3)	0.2008(6)	4.06(13)
N(2)	0.7376(3)	-0.2446(3)	0.2996(6)	3.62(12)
N(3)	0.6722(3)	0.0543(3)	0.0122(6)	3.62(13)
N(4)	0.5253(3)	-0.0333(3)	-0.0454(6)	3.89(13)
C(1)	0.3973(4)	-0.1185(4)	0.0813(7)	3.6(2)
C(2)	0.4000(4)	-0.1561(4)	0.0025(6)	3.6(2)
C(3)	0.3434(4)	-0.2427(4)	-0.0113(6)	3.7(2)
C(4)	0.2851(3)	-0.2920(4)	0.0460(7)	3.7(2)
C(5)	0.2760(3)	-0.2515(4)	0.1193(6)	3.7(2)
C(6)	0.3271(4)	-0.1662(4)	0.1362(6)	3.9(2)
C(7)	0.2370(4)	-0.3875(4)	0.0411(6)	3.8(2)
C(8)	0.2775(4)	-0.4295(3)	0.0918(6)	3.3(1)
C(9)	0.3629(4)	-0.3873(3)	0.1054(6)	3.7(2)
C(10)	0.4020(3)	-0.4223(4)	0.1537(7)	3.4(1)
C(11)	0.3527(4)	-0.5044(4)	0.1853(6)	3.7(2)
C(12)	0.2648(4)	-0.5489(4)	0.1732(6)	3.6(2)
C(13)	0.2313(3)	-0.5085(4)	0.1269(7)	3.7(1)
C(14)	0.4938(4)	-0.3754(4)	0.1609(7)	4.1(2)
C(15)	0.6276(4)	-0.3466(4)	0.2056(7)	4.2(2)
C(16)	0.6719(4)	-0.3963(5)	0.1796(7)	5.3(2)
C(17)	0.6554(4)	-0.4665(5)	0.2407(8)	6.5(2)
C(18)	0.6823(4)	-0.4304(4)	0.3279(8)	6.2(2)
C(19)	0.6372(4)	-0.3936(4)	0.3569(7)	5.0(2)
C(20)	0.6507(4)	-0.3149(4)	0.2958(7)	3.9(2)
C(21)	0.7496(4)	-0.1692(4)	0.3011(6)	3.8(2)
C(22)	0.8332(4)	-0.0937(4)	0.3057(6)	3.7(2)
C(23)	0.9063(4)	-0.0999(4)	0.3088(6)	4.0(2)
C(24)	0.9855(4)	-0.0249(4)	0.3128(7)	5.0(2)
C(25)	0.9859(4)	0.0521(4)	0.3122(7)	4.7(2)

a. solvent

Table 3.3 (cont.) Positional parameters and B(eq) for the nickel complex **3.4**

atom	x	y	z	B(eq)
C(26)	0.9136(4)	0.0585(4)	0.3090(7)	3.9(2)
C(27)	0.8380(4)	-0.0148(4)	0.3049(7)	4.0(2)
C(28)	0.9188(4)	0.1452(4)	0.3063(7)	5.0(2)
C(29)	0.8432(4)	0.1404(4)	0.2623(7)	3.8(2)
C(30)	0.8303(4)	0.1243(3)	0.1795(7)	3.7(2)
C(31)	0.7504(4)	0.1014(4)	0.1419(7)	3.7(2)
C(32)	0.6820(4)	0.0940(4)	0.1925(7)	4.3(2)
C(33)	0.7008(4)	0.1215(5)	0.2784(7)	5.5(2)
C(34)	0.7799(5)	0.1426(4)	0.3089(7)	5.5(2)
C(35)	0.7410(4)	0.0830(3)	0.0551(7)	3.4(2)
C(36)	0.6722(4)	0.0342(4)	-0.0792(7)	3.9(2)
C(37)	0.7426(4)	0.1002(4)	-0.1319(7)	5.3(2
C(37)	0.7426(4)	0.1002(4)	-0.1319(7)	5.3(2)
C(38)	0.7304(5)	0.0721(4)	-0.2225(7)	5.6(2)
C(39)	0.6434(5)	0.0527(4)	-0.2556(7)	5.8(2)
C(40)	0.5716(4)	-0.0138(4)	-0.2007(7)	4.6(2)
C(41)	0.5862(4)	0.0182(4)	-0.1129(7)	3.9(2)
C(42)	0.4583(4)	-0.1071(4)	-0.0607(6)	3.7(2)
C(43)	0.3081(4)	-0.1237(4)	0.2094(7)	5.1(2)
C(44)	0.3020(5)	-0.0486(5)	0.1751(8)	7.0(2)
C(45)	0.3799(5)	-0.0901(6)	0.2736(7)	7.9(3)
C(46)	0.2242(5)	-0.1842(5)	0.2540(7)	6.8(2)
C(47)	0.2097(4)	-0.6390(4)	0.2092(6)	4.4(2)
C(48)	0.2390(5)	-0.6987(4)	0.1732(7)	5.9(2)
C(49)	0.1158(4)	-0.6750(4)	0.1859(7)	6.7(2)
C(50)	0.2165(4)	-0.6378(4)	0.3053(7)	5.4(2)
C(51)	1.0693(4)	-0.0280(5)	0.3155(8)	7.3(3)
C(52)	1.0730(5)	-0.0715(7)	0.2340(10)	9.9(3)
C(53)	1.1467(5)	0.0622(6)	0.3180(10)	11.3(3)
C(54)	1.0699(5)	-0.0751(6)	0.3950(9)	9.6(3)
C(55)	0.6340(6)	0.1198(8)	0.3376(8)	9.2(3)
C(56)	0.5256(8)	0.1555(9)	0.2963(9)	12.6(5)
C(57)	0.6739(6)	0.1721(10)	0.4173(9)	15.2(5)
C(58)	0.5704(6)	0.0228(9)	0.3585(8)	11.3(4)

Table 3.4 Intramolecular distances involving the nonhydrogen atoms for the complex **3.4**

atom	atom	distance	atom	atom	distance
Ni(1)	O(1)	1.867(4)	C(8)	C(9)	1.367(8)
Ni(1)	O(4)	1.854(5)	C(8)	C(13)	1.387(8)
Ni(1)	N(3)	1.862(5)	C(9)	C(10)	1.384(8)
Ni(1)	N(4)	1.839(6)	C(10)	C(11)	1.412(8)
O(1)	C(1)	1.319(7)	C(10)	C(14)	1.461(8)
O(2)	C(11)	1.350(7)	C(11)	C(12)	1.402(8)
O(3)	C(23)	1.346(8)	C(12)	C(13)	1.384(9)
O(4)	C(32)	1.292(7)	C(12)	C(47)	1.547(8)
N(1)	C(14)	1.276(8)	C(15)	C(16)	1.544(9)
N(1)	C(15)	1.472(8)	C(15)	C(20)	1.524(9)
N(2)	C(20)	1.461(7)	C(16)	C(17)	1.51(1)
N(2)	C(21)	1.281(7)	C(17)	C(18)	1.51(1)
N(3)	C(35)	1.288(7)	C(18)	C(19)	1.52(1)
N(3)	C(36)	1.501(8)	C(19)	C(20)	1.507(9)
N(4)	C(41)	1.494(8)	C(21)	C(22)	1.460(8)
N(4)	C(42)	1.313(8)	C(22)	C(23)	1.384(9)
C(1)	C(2)	1.442(9)	C(22)	C(27)	1.400(9)
C(1)	C(6)	1.431(9)	C(23)	C(24)	1.403(9)
C(2)	C(3)	1.409(8)	C(24)	C(25)	1.402(9)
C(2)	C(42)	1.412(8)	C(24)	C(51)	1.56(1)
C(3)	C(4)	1.370(8)	C(25)	C(26)	1.383(9)
C(4)	C(5)	1.409(9)	C(26)	C(27)	1.361(8)
C(4)	C(7)	1.513(8)	C(26)	C(28)	1.540(9)
C(5)	C(6)	1.385(9)	C(28)	C(29)	1.511(9)
C(6)	C(43)	1.533(9)	C(29)	C(30)	1.346(9)
C(7)	C(8)	1.521(8)	C(29)	C(34)	1.390(9)
C(30)	C(31)	1.432(9)	C(31)	C(32)	1.436(9)
C(31)	C(35)	1.413(9)	C(32)	C(33)	1.437(9)
C(33)	C(34)	1.38(1)	C(33)	C(55)	1.53(1)
C(36)	C(37)	1.502(9)	C(36)	C(41)	1.542(9)
C(37)	C(38)	1.51(1)	C(38)	C(39)	1.54(1)
C(39)	C(40)	1.538(9)	C(40)	C(41)	1.486(9)
C(43)	C(44)	1.53(1)	C(43)	C(45)	1.53(1)
C(43)	C(46)	1.54(1)	C(47)	C(48)	1.54(1)
C(47)	C(49)	1.54(1)	C(47)	C(50)	1.54(1)
C(51)	C(52)	1.54(1)	C(51)	C(53)	1.54(1)
C(51)	C(54)	1.53(1)	C(55)	C(56)	1.49(1)
C(55)	C(57)	1.53(1)	C(55)	C(58)	1.59(2)

Distances are in angstroms. Estimated standard deviations in the least significant figure are given in parentheses.

Table 3.5 Intramolecular bond angles involving the nonhydrogen atoms in the complex **3.4**

atom	atom	atom	angle	atom	atom	atom	angle
O(1)	Ni(1)	O(4)	89.0(2)	C(4)	C(5)	C(6)	123.9(6)
O(1)	Ni(1)	N(3)	174.0(2)	C(1)	C(6)	C(5)	117.4(6)
O(1)	Ni(1)	N(4)	91.3(2)	C(1)	C(6)	C(43)	121.1(6)
O(4)	Ni(1)	N(3)	94.3(2)	C(5)	C(6)	C(43)	121.4(6)
O(4)	Ni(1)	N(4)	179.1(3)	C(4)	C(7)	C(8)	112.5(5)
N(3)	Ni(1)	N(4)	85.4(2)	C(7)	C(8)	C(9)	120.9(5)
Ni(1)	O(1)	C(1)	122.8(4)	C(7)	C(8)	C(13)	122.9(5)
Ni(1)	O(4)	C(32)	129.0(4)	C(9)	C(8)	C(13)	116.2(6)
C(14)	N(1)	C(15)	116.5(5)	C(8)	C(9)	C(10)	122.5(5)
C(20)	N(2)	C(21)	118.1(5)	C(9)	C(10)	C(11)	119.5(5)
Ni(1)	N(3)	C(35)	124.4(5)	C(9)	C(10)	C(14)	119.2(6)
Ni(1)	N(3)	C(36)	114.6(4)	C(11)	C(10)	C(14)	121.2(6)
C(35)	N(3)	C(36)	119.6(5)	C(2)	C(11)	C(10)	120.0(5)
Ni(1)	N(4)	C(41)	111.4(4)	C(2)	C(11)	C(12)	120.1(6)
Ni(1)	N(4)	C(42)	125.9(5)	C(10)	C(11)	C(12)	119.9(6)
C(41)	N(4)	C(42)	122.1(5)	C(11)	C(12)	C(13)	116.6(6)
O(1)	C(1)	C(2)	122.2(6)	C(11)	C(12)	C(47)	120.8(6)
O(1)	C(1)	C(6)	119.4(6)	C(13)	C(12)	C(47)	122.6(6)
C(2)	C(1)	C(6)	118.4(6)	C(8)	C(13)	C(12)	125.3(6)
C(1)	C(2)	C(3)	119.3(6)	N(1)	C(14)	C(10)	123.9(6)
C(1)	C(2)	C(42)	120.9(6)	N(1)	C(15)	C(16)	108.8(5)
C(3)	C(2)	C(42)	119.8(6)	N(1)	C(15)	C(20)	108.6(5)
C(2)	C(3)	C(4)	121.5(6)	C(16)	C(15)	C(20)	110.5(5)
C(3)	C(4)	C(5)	117.8(6)	C(15)	C(16)	C(17)	112.6(6)
C(3)	C(4)	C(7)	121.3(6)	C(16)	C(17)	C(18)	109.8(6)
C(5)	C(4)	C(7)	120.7(6)	C(17)	C(18)	C(19)	112.0(6)
C(18)	C(19)	C(20)	111.2(6)	C(32)	C(31)	C(35)	122.0(6)
N(2)	C(20)	C(15)	110.2(5)	O(4)	C(32)	C(31)	121.5(6)
N(2)	C(20)	C(19)	110.9(5)	O(4)	C(32)	C(33)	121.3(6)
C(15)	C(20)	C(19)	113.1(5)	C(31)	C(32)	C(33)	117.2(6)
N(2)	C(21)	C(22)	123.4(6)	C(32)	C(33)	C(34)	117.7(6)
C(21)	C(22)	C(23)	121.7(6)	C(32)	C(33)	C(55)	122.1(7)
C(21)	C(22)	C(27)	118.0(6)	C(34)	C(33)	C(55)	119.9(7)
C(23)	C(22)	C(27)	120.3(6)	C(29)	C(34)	C(33)	124.9(7)
O(3)	C(23)	C(22)	119.1(6)	N(3)	C(35)	C(31)	126.4(6)
O(3)	C(23)	C(24)	120.7(6)	N(3)	C(36)	C(37)	116.7(5)

Table 3.5 (cont.) Intramolecular bond angles involving the nonhydrogen atoms in the complex **3.4**

atom	atom	atom	angle	atom	atom	atom	angle
C(22)	C(23)	C(24)	120.1(7)	N(3)	C(36)	C(41)	105.0(5)
C(23)	C(24)	C(25)	116.8(6)	C(37)	C(36)	C(41)	109.8(6)
C(23)	C(24)	C(51)	121.7(7)	C(36)	C(37)	C(39)	109.9(6)
C(25)	C(24)	C(51)	121.6(7)	C(37)	C(38)	C(39)	111.4(6)
C(24)	C(25)	C(26)	123.9(6)	C(38)	C(39)	C(40)	111.2(6)
C(25)	C(26)	C(27)	117.5(6)	C(39)	C(40)	C(41)	109.0(6)
C(25)	C(26)	C(28)	121.2(6)	N(4)	C(41)	C(36)	103.6(5)
C(27)	C(26)	C(28)	121.3(6)	N(4)	C(41)	C(40)	119.9(5)
C(22)	C(27)	C(26)	121.4(6)	C(36)	C(41)	C(40)	111.6(6)
C(26)	C(28)	C(29)	111.6(5)	N(4)	C(42)	O(2)	122.5(6)
C(28)	C(29)	C(30)	121.5(6)	C(6)	C(43)	C(44)	109.6(6)
C(28)	C(29)	C(34)	119.9(7)	C(6)	C(43)	C(45)	110.3(6)
C(30)	C(29)	C(34)	118.1(6)	C(6)	C(43)	C(46)	112.5(6)
C(29)	C(30)	C(31)	121.0(6)	C(44)	C(43)	C(45)	109.1(7)
C(30)	C(31)	C(32)	120.3(6)	C(44)	C(43)	C(46)	108.3(6)
C(30)	C(31)	C(35)	117.6(6)	C(45)	C(43)	C(46)	109.9(7)
C(12)	C(47)	C(48)	110.1(6)	C(12)	C(47)	C(49)	111.0(6)
C(12)	C(47)	C(50)	110.2(5)	C(48)	C(47)	C(49)	108.3(6)
C(48)	C(47)	C(50)	109.2(6)	C(49)	C(47)	C(50)	108.0(6)
C(24)	C(51)	C(52)	107.0(8)	C(24)	C(51)	C(53)	110.7(7)
C(24)	C(51)	C(54)	108.9(8)	C(52)	C(51)	C(53)	108.7(9)
C(52)	C(51)	C(54)	113.1(9)	C(53)	C(51)	C(54)	108.5(9)
C(33)	C(55)	C(56)	111(1)	C(33)	C(55)	C(57)	111.9(8)
C(33)	C(55)	C(58)	106.3(9)	C(56)	C(55)	C(57)	107(1)
C(56)	C(55)	C(58)	108.4(9)	C(57)	C(55)	C(58)	112(1)

Angles are in degrees. Estimated standard deviations in the least significant figure are given in parentheses.

Table 3.6 Selected torsion or conformation angles for the complex **3.4**

(1)	(2)	(3)	(4)	angle	(1)	(2)	(3)	(4)	angle
Ni(1)	O(1)	C(1)	C(2)	-24.4(8)	C(3)	C(23)	C(24)	C(51)	0(1)
Ni(1)	O(1)	C(1)	C(6)	158.0(4)	O(4)	Ni(1)	O(1)	C(1)	-142.0(5)
Ni(1)	O(4)	C(32)	C(31)	1(1)	O(4)	Ni(1)	N(3)	C(35)	16.4(5)
Ni(1)	O(4)	C(32)	C(33)	-174.6(5)	O(4)	Ni(1)	N(3)	C(36)	-177.4(4)
Ni(1)	N(3)	C(35)	C(31)	-11.6(9)	O(4)	Ni(1)	N(4)	C(41)	43(14)
Ni(1)	N(3)	C(36)	C(37)	145.3(5)	O(4)	Ni(1)	N(4)	C(42)	-146(14)
Ni(1)	N(3)	C(36)	C(41)	23.4(5)	O(4)	C(32)	C(31)	C(30)	-168.0(6)
Ni(1)	N(4)	C(41)	C(36)	46.6(5)	O(4)	C(32)	C(31)	C(35)	9(1)
Ni(1)	N(4)	C(41)	C(40)	171.8(5)	O(4)	C(32)	C(33)	C(34)	168.1(7)
Ni(1)	N(4)	C(42)	C(2)	10.1(9)	O(4)	C(32)	C(33)	C(55)	-6(1)
O(1)	Ni(1)	O(4)	C(32)	163.2(6)	N(1)	C(14)	C(10)	C(9)	-179.2(7)
O(1)	Ni(1)	N(3)	C(35)	-107(2)	N(1)	C(14)	C(10)	C(11)	0(1)
O(1)	Ni(1)	N(3)	C(36)	59(2)	N(1)	C(15)	C(16)	C(17)	-65.9(7)
O(1)	Ni(1)	N(4)	C(41)	156.7(4)	N(1)	C(15)	C(20)	N(2)	-167.4(5)
O(1)	Ni(1)	N(4)	C(42)	-32.1(5)	N(1)	C(15)	C(20)	C(19)	67.9(7)
O(1)	C(1)	C(2)	C(3)	170.7(6)	N(2)	C(20)	C(15)	C(16)	73.3(7)
O(1)	C(1)	C(2)	C(42)	-9.6(9)	N(2)	C(20)	C(19)	C(18)	-71.4(7)
O(1)	C(1)	C(6)	C(5)	-168.6(6)	N(2)	C(21)	C(22)	C(23)	0(1)
O(1)	C(1)	C(6)	C(43)	13.0(9)	N(2)	C(21)	C(22)	C(27)	179.5(6)
O(2)	C(11)	C(10)	C(9)	-177.6(6)	N(3)	Ni(1)	O(1)	C(1)	-18(2)
O(2)	C(11)	C(10)	C(14)	3(1)	N(3)	Ni(1)	O(4)	C(32)	-11.8(6)
O(2)	C(11)	C(12)	C(13)	177.8(6)	N(3)	Ni(1)	N(4)	C(41)	-28.4(4)
O(2)	C(11)	C(12)	C(47)	-3.3(9)	N(3)	Ni(1)	N(4)	C(42)	142.8(5)
N(4)	Ni(1)	O(1)	C(1)	38.8(5)	C(5)	C(6)	C(43)	C(44)	-124.9(7)
N(4)	Ni(1)	O(4)	C(32)	-83(14)	C(5)	C(6)	C(43)	C(45)	116.9(7)
N(4)	Ni(1)	N(3)	C(35)	-164.5(5)	C(5)	C(6)	C(43)	C(46)	-5(1)
N(4)	Ni(1)	N(3)	C(36)	1.7(4)	C(6)	C(1)	C(2)	C(42)	168.0(6)

The sign is positive if when looking from atom 2 to atom 3 a clock-wise motion of atom 1 would superimpose it on atom 4.

Table 3.7 Data collection and refinement parameters for the complex **3.8**

Diffractometer	Rigaku AFC6S
Radiation	Cu-Kα (l = 1.54178 Å), graphite monochromated
Take-off Angle	6.0°
Detector Aperture	9.0 mm horizontal, 4.5 mm vertical
Crystal to Detector Distance	400 mm
Voltage, Current	50 kV, 27.5 mA
Temperature	26.0°C
Scan Type	ω-2θ
Scan Rate	4.0°/minute (in ω) (up to 10 scans)
Scan Width	$(1.57 + 0.14 \tan\theta)^{\circ}$
$2\theta_{max}$	120.1°
No. of Reflections Measured:	4946
Corrections	Lorentz-polarization Absorption (trans. factors: 0.8442 - 1.0000)
	Secondary extinction (coefficient: 2.38205e-007)
Structure Solution	Direct Methods (SIR92)
Refinement	Full-matrix least-squares
Function Minimized	$\Sigma w (\|Fo\| - \|Fc\|)^2$
Least Squares Weights	$1/\sigma^2(Fo) = 4Fo^2/\sigma^2(Fo^2)$
p-factor	0.0052
Anomalous Dispersion	all non-hydrogen atoms
No. Observations (I>2.00σ(I))	3752
No. Variables	641
Reflection/Parameter Ratio	5.85
Residuals: R; R_w	0.067 ; 0.065
Goodness of Fit Indicator	3.60
Max Shift/Error in Final Cycle	0.00
Maximum peak in Final Diff. Map	0.89 $e^-/Å^3$
Minimum peak in Final Diff. Map	-0.61 $e^-/Å^3$

Table 3.8 Atom coordinates and B(eq) for the complex **3.8**

atom	x	y	z	B(eq)
Ni(1)	-0.89589(6)	-0.08704(5)	-0.70077(9)	4.26(3)
Ni(2)	-1.14210(5)	-0.25768(4)	-0.43326(8)	3.57(2)
Cl(1)	0.1175	0.1912	0.4213	29.777'
Cl(2)	0.0500	0.2277	0.5400	26.494'
O(1)	-0.9682(2)	-0.0346(2)	-0.7059(4)	4.6(1)
O(2)	-0.8676(2)	-0.0519(2)	-0.5816(4)	4.9(1)
O(3)	-1.1174(2)	-0.2113(2)	-0.3253(3)	4.1(1)
O(4)	-1.2103(2)	-0.2049(2)	-0.4670(3)	4.1(1)
N(1)	-0.9159(3)	-0.1188(3)	-0.8249(4)	4.4(1)
N(2)	-0.8382(3)	-0.1519(2)	-0.6832(4)	4.2(1)
N(3)	-1.0836(3)	-0.3161(2)	-0.3948(4)	3.8(1)
N(4)	-1.1499(3)	-0.2983(2)	-0.5513(4)	3.5(1)
N(5)	0.4960(7)	0.2449(5)	0.824(1)	13.3(5)'
C(1)	-1.0255(4)	-0.0458(3)	-0.7544(6)	4.9(2)
C(2)	-1.0860(4)	-0.0139(3)	-0.7252(6)	4.7(2)
C(3)	-1.1455(4)	-0.0355(3)	-0.7703(6)	5.8(2)
C(4)	-1.1536(4)	-0.0795(3)	-0.8375(5)	4.7(2)
C(5)	-1.0982(4)	-0.1024(3)	-0.8704(5)	4.7(2)
C(6)	-1.0327(4)	-0.0875(3)	-0.8316(5)	4.4(2)
C(7)	-0.9741(4)	-0.1180(3)	-0.8672(5)	4.9(2)
C(8)	-0.8562(4)	-0.1539(3)	-0.8642(5)	4.8(2)
C(9)	-0.8691(4)	-0.1931(4)	-0.9544(5)	6.4(2)
C(10)	-0.8026(5)	-0.2253(4)	-0.9772(6)	7.7(3)
C(11)	-0.7747(4)	-0.2565(4)	-0.8957(6)	6.7(2)
C(12)	-0.7655(4)	-0.2207(3)	-0.7936(6)	5.5(2)
C(13)	-0.8362(4)	-0.1915(3)	-0.7725(5)	4.4(2)
C(14)	-0.8215(4)	-0.1711(3)	-0.5969(5)	4.3(2)
C(15)	-0.8274(4)	-0.1408(3)	-0.5053(5)	4.0(2)
C(16)	-0.8438(3)	-0.0798(3)	-0.5024(5)	4.2(2)
C(17)	-0.8358(3)	-0.0503(3)	-0.4089(6)	4.5(2)
C(18)	-0.8310(3)	-0.0846(3)	-0.3240(5)	4.3(2)
C(19)	-0.8270(3)	-0.1463(3)	-0.3267(5)	4.0(2)
C(20)	-0.8209(3)	-0.1720(3)	-0.4181(5)	3.8(2)
C(21)	-0.8392(3)	-0.1819(3)	-0.2327(5)	4.5(2)
C(22)	-0.9140(3)	-0.1980(3)	-0.2320(5)	4.1(2)
C(23)	-0.9627(3)	-0.1537(3)	-0.2137(5)	3.8(2)
C(24)	-1.0320(3)	-0.1575(3)	-0.2373(4)	3.4(1)
C(25)	-1.0552(3)	-0.2096(3)	-0.2891(5)	3.9(2)

' solvent

Table 3.8 (cont.)

atom	x	y	z	B(eq)
C(26)	-1.0080(3)	-0.2564(3)	-0.2965(5)	4.0(2)
C(27)	-0.9371(3)	-0.2482(3)	-0.2699(5)	4.5(2)
C(28)	-1.0283(3)	-0.3106(3)	-0.3442(5)	4.1(2)
C(29)	-1.1038(3)	-0.3724(3)	-0.4430(5)	3.9(2)
C(30)	-1.0566(3)	-0.4256(3)	-0.4341(6)	4.9(2)
C(31)	-1.0899(5)	-0.4755(3)	-0.4882(6)	6.1(2)
C(32)	-1.1048(4)	-0.4607(3)	-0.5979(6)	5.9(2)
C(33)	-1.1487(4)	-0.4057(3)	-0.6083(5)	5.2(2)
C(34)	-1.1133(3)	-0.3544(3)	-0.5514(5)	3.8(2)
C(35)	-1.1669(3)	-0.2745(3)	-0.6351(5)	3.9(2)
C(36)	-1.2011(3)	-0.2176(3)	-0.6423(5)	3.7(2)
C(37)	-1.2256(3)	-0.1888(3)	-0.5573(5)	3.6(2)
C(38)	-1.2690(3)	-0.1406(3)	-0.5750(6)	4.1(2)
C(39)	-1.2737(3)	-0.1182(3)	-0.6712(6)	4.4(2)
C(40)	-1.2399(4)	-0.1425(3)	-0.7536(5)	4.4(2)
C(41)	-1.2063(4)	-0.1938(3)	-0.7397(5)	4.5(2)
C(42)	-1.2260(4)	-0.2178(3)	-0.8504(6)	5.1(2)
C(43)	-1.0829(4)	-0.0370(3)	-0.6483(6)	5.5(2)
C(44)	-1.0317(4)	-0.0833(3)	-0.6698(6)	6.5(2)
C(45)	-1.0675(4)	-0.0051(4)	-0.5427(6)	6.3(2)
C(46)	-1.1503(4)	-0.0695(4)	-0.6265(7)	7.8(3)
C(47)	-0.8367(4)	-0.0179(3)	-0.4054(6)	5.3(2)
C(48)	-0.7859(5)	-0.0418(3)	-0.4792(7)	6.9(3)
C(49)	-0.9094(5)	-0.0387(4)	-0.4194(8)	6.7(3)
C(50)	-0.8147(5)	-0.0391(4)	-0.2998(7)	7.5(3)
C(51)	-1.0797(4)	-0.1056(3)	-0.2193(5)	4.6(2)
C(52)	-1.1468(4)	-0.1247(3)	-0.1728(6)	6.2(2)
C(53)	-1.0453(4)	-0.0598(3)	-0.1515(6)	6.1(2)
C(54)	-1.0915(4)	-0.0777(3)	-0.3259(6)	6.2(2)
C(55)	-1.3088(4)	-0.1119(3)	-0.4910(6)	4.9(2)
C(56)	-1.3564(4)	-0.0613(3)	-0.5262(6)	6.0(2)
C(57)	-1.2598(4)	-0.0876(3)	-0.4186(6)	6.3(2)
C(58)	-1.3557(4)	-0.1576(3)	-0.4410(7)	7.0(2)
C(59)	0.5079(7)	0.2107(5)	0.874(1)	9.5(5)
C(60)	0.5220(6)	0.1649(5)	0.9393(9)	10.1(4)'
C(61)	0.0458	0.2302	0.4140	13.026'

'solvent

Table 3.9 Selected bond distances for the complex **3.8**

atom	atom	distance	atom	atom	distance
Ni(1)	O(1)	1.853(4)	C(2)	C(3)	1.40(1)
Ni(1)	O(2)	1.869(5)	C(2)	C(43)	1.60(1)
Ni(1)	N(1)	1.853(6)	C(3)	C(4)	1.36(1)
Ni(1)	N(2)	1.874(5)	C(4)	C(5)	1.28(1)
Ni(2)	O(3)	1.855(4)	C(4)	C(42)	1.56(1)
Ni(2)	O(4)	1.852(5)	C(5)	C(6)	1.42(1)
Ni(2)	N(3)	1.829(5)	C(6)	C(7)	1.42(1)
Ni(2)	N(4)	1.837(5)	C(8)	C(9)	1.52(1)
C(8)	C(13)	1.55(1)	C(9)	C(10)	1.54(1)
C(10)	C(11)	1.54(1)	C(1)	O(1)	1.318(9)
C(11)	C(12)	1.51(1)	O(2)	C(16)	1.321(8)
C(12)	C(13)	1.54(1)	O(3)	C(25)	1.307(8)
C(14)	C(15)	1.41(1)	O(4)	C(37)	1.298(8)
C(15)	C(16)	1.43(1)	N(1)	C(7)	1.271(9)
C(15)	C(20)	1.37(1)	N(1)	C(8)	1.509(9)
C(16)	C(17)	1.43(1)	N(2)	C(13)	1.500(9)
C(17)	C(18)	1.38(1)	N(2)	C(14)	1.278(9)
C(17)	C(47)	1.55(1)	N(3)	C(28)	1.282(8)
C(18)	C(19)	1.41(1)	N(3)	C(29)	1.492(8)
C(19)	C(20)	1.36(1)	N(4)	C(34)	1.467(9)
C(19)	C(21)	1.52(1)	N(4)	C(35)	1.289(8)
C(21)	C(22)	1.51(1)	C(22)	C(23)	1.409(9)
C(1)	C(2)	1.44(1)	C(22)	C(27)	1.33(1)
C(1)	C(6)	1.41(1)	C(23)	C(24)	1.393(9)
C(24)	C(25)	1.450(9)	C(51)	C(52)	1.51(1)
C(24)	C(51)	1.53(1)	C(51)	C(53)	1.54(1)
C(25)	C(26)	1.415(9)	C(51)	C(54)	1.56(1)
C(26)	C(27)	1.442(9)	C(55)	C(56)	1.56(1)
C(26)	C(28)	1.448(9)	C(55)	C(57)	1.47(1)
C(29)	C(30)	1.529(9)	C(55)	C(58)	1.54(1)
C(29)	C(34)	1.519(9)	C(30)	C(31)	1.50(1)
C(31)	C(32)	1.53(1)	C(32)	C(33)	1.53(1)
C(33)	C(34)	1.557(9)	C(35)	C(36)	1.464(9)
C(36)	C(37)	1.40(1)	C(36)	C(41)	1.42(1)
C(37)	C(38)	1.409(9)	C(38)	C(39)	1.39(1)
C(38)	C(55)	1.51(1)	C(39)	C(40)	1.40(1)
C(40)	C(41)	1.35(1)	C(40)	C(42)	1.54(1)
C(43)	C(44)	1.50(1)	C(43)	C(45)	1.56(1)
C(43)	C(46)	1.52(1)	C(47)	C(48)	1.50(1)
C(47)	C(49)	1.51(1)	C(47)	C(50)	1.55(1)

Distances are in angstroms. Estimated standard deviations in the least significant figure are given in parentheses.

Table 3.10 Intramolecular bond angles involving nonhydrogen atoms in the complex **3.8**

atom	atom	atom	angle	atom	atom	atom	angle
O(1)	Ni(1)	O(2)	98.8(2)	C(26)	N(3)	C(29)	122.3(5)
O(1)	Ni(1)	N(1)	93.4(2)	Ni(2)	N(4)	C(34)	113.6(4)
O(1)	Ni(1)	N(2)	166.6(2)	Ni(2)	N(4)	C(35)	123.7(4)
O(2)	Ni(1)	N(1)	174.1(2)	C(34)	N(4)	C(35)	119.5(5)
O(2)	Ni(1)	N(2)	93.1(2)	O(1)	C(1)	C(2)	117.5(6)
N(1)	Ni(1)	N(2)	86.0(2)	O(1)	C(1)	C(6)	125.2(7)
O(3)	Ni(2)	O(4)	90.3(2)	C(2)	C(1)	C(6)	117.3(7)
O(3)	Ni(2)	N(3)	92.0(2)	C(1)	C(2)	C(3)	112.5(7)
O(3)	Ni(2)	N(4)	168.2(2)	C(1)	C(2)	C(43)	121.5(6)
O(4)	Ni(2)	N(3)	172.7(2)	C(3)	C(2)	C(43)	125.7(6)
O(4)	Ni(2)	N(4)	93.4(2)	C(2)	C(3)	C(4)	130.1(7)
N(3)	Ni(2)	N(4)	85.7(2)	C(3)	C(4)	C(5)	115.6(7)
C(3)	C(4)	C(42)	118.9(6)	C(5)	C(4)	C(42)	123.9(7)
Ni(1)	O(1)	C(1)	122.6(4)	C(4)	C(5)	C(6)	120.4(7)
Ni(1)	O(2)	C(16)	125.5(4)	C(1)	C(6)	C(5)	121.3(7)
Ni(2)	O(3)	C(25)	123.1(4)	C(1)	C(6)	C(7)	119.7(7)
Ni(2)	O(4)	C(37)	125.2(4)	C(5)	C(6)	C(7)	118.9(6)
Ni(1)	N(1)	C(7)	125.6(5)	N(1)	C(7)	C(6)	125.3(7)
Ni(1)	N(1)	C(8)	110.9(4)	N(1)	C(8)	C(9)	117.4(6)
C(7)	N(1)	C(8)	123.0(6)	N(1)	C(8)	C(13)	110.8(5)
Ni(1)	N(2)	C(13)	113.6(4)	C(9)	C(8)	C(13)	110.2(6)
Ni(1)	N(2)	C(14)	122.6(5)	C(8)	C(9)	C(10)	107.6(7)
C(13)	N(2)	C(14)	120.1(6)	C(9)	C(10)	C(11)	112.3(7)
Ni(2)	N(3)	C(26)	127.2(5)	C(10)	C(11)	C(12)	114.1(7)
Ni(2)	N(3)	C(29)	110.0(4)	C(11)	C(12)	C(13)	106.9(6)
N(2)	C(13)	C(8)	106.5(5)	O(3)	C(25)	C(24)	119.4(6)
N(2)	C(13)	C(12)	116.2(6)	O(3)	C(25)	C(26)	123.9(6)
C(8)	C(13)	C(12)	109.1(6)	C(24)	C(25)	C(26)	116.7(6)
N(2)	C(14)	C(15)	126.4(6)	C(25)	C(26)	C(27)	120.7(6)
C(14)	C(15)	C(16)	121.3(6)	C(25)	C(26)	C(28)	119.8(6)
C(14)	C(15)	C(20)	118.4(6)	C(27)	C(26)	C(28)	118.9(6)
C(16)	C(15)	C(20)	120.2(6)	C(22)	C(27)	C(26)	122.1(6)
O(2)	C(16)	C(15)	121.9(6)	N(3)	C(28)	C(26)	123.1(6)
O(2)	C(16)	C(17)	120.8(6)	N(3)	C(29)	C(30)	119.4(5)

Table 3.10 (cont.)

atom	atom	atom	angle	atom	atom	atom	angle
C(15)	C(16)	C(17)	117.3(6)	N(3)	C(29)	C(34)	102.2(5)
C(16)	C(17)	C(18)	117.3(6)	C(30)	C(29)	C(34)	111.2(5)
C(16)	C(17)	C(47)	119.6(6)	C(29)	C(30)	C(31)	107.7(6)
C(18)	C(17)	C(47)	122.8(7)	C(30)	C(31)	C(32)	112.2(6)
C(17)	C(18)	C(19)	123.2(6)	C(31)	C(32)	C(33)	112.1(6)
C(18)	C(19)	C(20)	117.2(6)	C(32)	C(33)	C(34)	109.0(6)
C(18)	C(19)	C(21)	120.3(6)	N(4)	C(34)	C(29)	107.1(5)
C(20)	C(19)	C(21)	121.9(6)	N(4)	C(34)	C(33)	116.1(5)
C(15)	C(20)	C(19)	122.2(6)	C(29)	C(34)	C(33)	108.4(5)
C(19)	C(21)	C(22)	106.7(5)	N(4)	C(35)	C(36)	123.3(6)
C(21)	C(22)	C(23)	118.7(6)	C(35)	C(36)	C(37)	121.3(6)
C(21)	C(22)	C(27)	122.4(6)	C(35)	C(36)	C(41)	115.7(6)
C(23)	C(22)	C(27)	117.1(6)	C(37)	C(36)	C(41)	123.1(6)
C(22)	C(23)	C(24)	124.9(6)	O(4)	C(37)	C(36)	123.1(6)
C(23)	C(24)	C(25)	117.6(6)	O(4)	C(37)	C(38)	121.0(6)
C(23)	C(24)	C(51)	121.7(6)	C(36)	C(37)	C(38)	115.9(6)
C(25)	C(24)	C(51)	121.4(6)	C(37)	C(38)	C(39)	118.9(6)
C(37)	C(38)	C(55)	121.8(6)	C(38)	C(55)	C(56)	113.8(6)
C(39)	C(38)	C(55)	119.6(6)	C(38)	C(55)	C(57)	108.6(6)
C(38)	C(39)	C(40)	123.6(6)	C(38)	C(55)	C(58)	119.5(6)
C(39)	C(40)	C(41)	117.5(6)	C(56)	C(55)	C(57)	108.0(6)
C(39)	C(40)	C(42)	122.7(6)	C(56)	C(55)	C(58)	106.1(6)
C(41)	C(40)	C(42)	119.3(6)	C(57)	C(55)	C(58)	110.9(7)
C(36)	C(41)	C(40)	119.5(6)	N(5)	C(59)	C(60)	178(2)
C(4)	C(42)	C(40)	106.1(6)	Cl(1)	C(61)	Cl(2)	88.22
C(2)	C(43)	C(44)	112.1(6)	C(2)	C(43)	C(45)	105.3(6)
C(2)	C(43)	C(46)	114.4(6)	C(44)	C(43)	C(45)	113.9(7)
C(44)	C(43)	C(46)	106.3(6)	C(45)	C(43)	C(46)	105.1(7)
C(17)	C(47)	C(48)	109.4(6)	C(17)	C(47)	C(49)	109.8(6)
C(17)	C(47)	C(50)	109.8(6)	C(48)	C(47)	C(49)	115.0(7)
C(48)	C(47)	C(50)	107.5(6)	C(49)	C(47)	C(50)	105.8(7)
C(24)	C(51)	C(52)	111.7(6)	C(24)	C(51)	C(53)	110.7(6)
C(24)	C(51)	C(54)	105.0(5)	C(52)	C(51)	C(53)	109.4(6)
C(52)	C(51)	C(54)	111.1(6)	C(53)	C(51)	C(54)	109.8(6)

Angles are in degrees. Estimated standard deviations in the least significant figure are given in parentheses.

Table 3.11 Selected torsional angles for the complex **3.8**

(1)	(2)	(3)	(4)	angle	(1)	(2)	(3)	(4)	angle
Ni(1)	O(1)	C(1)	C(6)	-21(1)	O(1)	C(1)	C(6)	C(5)	171.3(7)
Ni(1)	O(2)	C(16)	C(15)	9.7(9)	O(1)	C(1)	C(6)	C(7)	-5(1)
Ni(1)	O(2)	C(16)	C(17)	-168.0(5)	O(2)	Ni(1)	O(1)	C(1)	-155.4(5)
Ni(1)	N(1)	C(7)	C(6)	7(1)	O(2)	Ni(1)	N(1)	C(7)	-136(2)
Ni(1)	N(1)	C(8)	C(9)	167.6(5)	O(2)	Ni(1)	N(1)	C(8)	52(2)
Ni(1)	N(1)	C(8)	C(13)	46.6(6)	O(2)	Ni(1)	N(2)	C(13)	-171.6(4)
Ni(1)	N(2)	C(13)	C(9)	23.0(8)	O(2)	Ni(1)	N(2)	C(14)	30.1(6)
Ni(1)	N(2)	C(13)	C(12)	144.8(5)	O(2)	C(16)	C(15)	C(14)	14(1)
Ni(1)	N(2)	C(14)	C(15)	-17(1)	O(2)	C(16)	C(15)	C(20)	-162.4(6)
Ni(2)	O(3)	C(25)	C(24)	153.7(5)	O(2)	C(16)	C(17)	C(18)	161.0(6)
Ni(2)	O(3)	C(25)	C(26)	-26.7(9)	O(2)	C(16)	C(17)	C(47)	-16(1)
Ni(2)	O(4)	C(37)	C(36)	12.4(9)	O(3)	Ni(2)	O(4)	C(37)	139.4(5)
Ni(2)	O(4)	C(37)	C(38)	-167.9(4)	O(3)	Ni(2)	N(3)	C(28)	-27.3(6)
Ni(2)	N(3)	C(28)	C(26)	9(1)	O(3)	Ni(2)	N(3)	C(29)	160.6(4)
Ni(2)	N(3)	C(29)	C(30)	171.3(5)	O(3)	Ni(2)	N(4)	C(34)	84(1)
Ni(2)	N(3)	C(29)	C(34)	46.1(5)	O(3)	Ni(2)	N(4)	C(35)	-76(1)
Ni(2)	N(4)	C(34)	C(29)	22.0(6)	O(3)	C(25)	C(24)	C(23)	-170.2(6)
Ni(2)	N(4)	C(34)	C(33)	143.2(5)	O(3)	C(25)	C(24)	C(51)	3.2(9)
Ni(2)	N(4)	C(35)	C(36)	-18.8(9)	O(3)	C(25)	C(26)	C(27)	169.6(6)
O(1)	Ni(1)	O(2)	C(16)	139.7(5)	O(3)	C(25)	C(26)	C(28)	-2(1)
O(1)	Ni(1)	N(1)	C(7)	-23.7(6)	O(4)	Ni(2)	O(3)	C(25)	-151.5(5)
O(1)	Ni(1)	N(1)	C(8)	164.3(4)	O(4)	Ni(2)	N(3)	C(28)	-135(2)
O(1)	Ni(1)	N(2)	C(13)	90(1)	O(4)	Ni(2)	N(3)	C(29)	53(2)
O(1)	Ni(1)	N(2)	C(14)	-68(1)	O(4)	Ni(2)	N(4)	C(34)	-168.1(4)
O(1)	C(1)	C(2)	C(3)	-170.7(7)	O(4)	Ni(2)	N(4)	C(35)	32.0(5)
O(4)	C(37)	C(36)	C(35)	12(1)	N(3)	C(28)	C(26)	C(27)	-160.0(6)
O(4)	C(37)	C(36)	C(41)	-167.1(6)	N(3)	C(29)	C(30)	C(31)	179.4(6)
O(4)	C(37)	C(38)	C(39)	167.9(6)	N(3)	C(29)	C(34)	N(4)	-42.7(6)
O(4)	C(37)	C(38)	C(55)	-10.2(9)	N(3)	C(29)	C(34)	C(33)	-168.7(5)
N(1)	Ni(1)	O(1)	C(1)	30.0(5)	N(4)	Ni(2)	O(3)	C(25)	-43(1)
N(1)	Ni(1)	O(2)	C(16)	-108(2)	N(4)	Ni(2)	O(4)	C(37)	-29.3(5)
N(1)	Ni(1)	N(2)	C(13)	2.6(4)	N(4)	Ni(2)	N(3)	C(28)	141.1(6)
N(1)	Ni(1)	N(2)	C(14)	-155.7(6)	N(4)	Ni(2)	N(3)	C(29)	-31.0(4)

Table 3.11 Torsion or conformation angles (cont.)

(1)	(2)	(3)	(4)	angle	(1)	(2)	(3)	(4)	angle
N(1)	C(7)	C(6)	C(1)	13(1)	N(4)	C 34	C(29	C(30)	-171.3(5)
N 1	C(8)	C(13)	C(12)	-168.4(5)	C(1)	C(2'	C'3	C(4)	-2(1)
N(1)	C(7)	C(6)	C(5)	-163.4(7)	N(4)	C(34)	C 33	C(32)	-178.1(6)
N 1	C(8)	C(9)	C(10)	-177.9(6)	N(4)	C(35)	C(36	C'37	-9(1)
N(1)	C(8)	C(13)	N(2)	-42.3(7)	N(4)	C(35)	C(36)	C.41	170.5(6)
N(1)	C'8'	C(13)	C'12'	-168.4(5	C 1)	C'2'	C(3)	C'4	-2(1
N 2	Ni(1	O(1)	C(1)	-57 1	C(1)	C 2)	C.43	C'44	55.3(9)
N(2)	Ni(1)	O(2)	C(16)	-27.0(5)	C(1)	C(2)	C 43	C(45)	-68.9(8)
N(2)	Ni(1)	N(1)	C(7)	142.9(6)	C 1)	C.2)	C'43	C 46	176.4(7)
N(2)	Ni(1)	N(1)	C(8)	-29.1(4)	C(1)	C 6	C.5	C 4'	3(1)
N'2	C'13)	C,8)	C(9)	-168.2(6)	C(2)	C(1)	C(6	C(5)	-8(1)
N(2)	C(13)	C(12)	C(11)	179.7(6)	C(2)	C(1)	C.6	C(7)	176.5(7)
N 2)	C(14)	C(15)	C(16)	-10(1)	C(2)	C'3	C.4	C(5)	-5(1)
N 2)	C 14)	C(15)	C(20)	166.4(7)	C'2)	C.3)	C(4)	C(42)	180.9(8)
N.3)	Ni(2)	O(3)	C(25)	35.4 5	C.3)	C'2)	C(1)	C(6)	8 1)
N'3	Ni(2	O(4)	C(37)	-112 2'	C 3)	C'2	C 43	C 44	-129.9(8)
N 3)	Ni(2)	N(4)	C(34)	4.6(4'	C 3)	C(2	C 43	C(45)	105.9(8)
N.3)	Ni(2)	N(4)	C(35)	-155.3(5	C'3)	C'2	C(43	C(46)	-9(1)
N.3)	C(29)	C(26)	C(25)	12 1'	C'3)	C'4	C(5'	C 6	7(1)
C.3)	C(4)	C(42)	C(40)	-69.9(8)	C 16	C(15	C'20	C 19	-2(1)
C.4)	C(3)	C(2	C(43)	-177.5(8)	C 16	C.17)	C.18	C(19	6(1)
C.4)	C(5)	C(6)	C(7)	175.5(7)	C(16	C(17)	C(47	C 48	-52.4(9)
C(4)	C(42)	C(40)	C(39)	91.8(8)	C'16	C(17)	C(47	C 49	74.3(9)
C'4)	C(42)	C(40)	C(41)	-74.3(6)	C'16	C(17	C(47)	C 50	-171.3(6)
C'5)	C(4)	C 42)	C(40)	95.2(8)	C'17	C(16)	C(15	C(20	15(1)
C(6)	C(1)	C 2)	C(43)	-176.2(7)	C(17	C.18)	C(19	C.21	7(1)
C(6)	C(5)	C(4)	C(42)	-168.9(7)	C(17	C(18)	C(19)	C(21	-165.0(6)
C(6)	C(7)	N(1)	C(8)	177.7(7)	C.18)	C'17	C(47	C(48	130.9(7
C(7)	N(1)	C(8)	C(9)	-5(1)	C(19)	C(17)	C(47)	C(49	-102.4(9)
C(7)	N(1)	C(8)	C(13)	-125.6(7	C 18)	C(17)	C(47	C(50	13.0(9)
C(8)	C(9)	C(10)	C(11)	54.4(9)	C(18	C(19)	C(21)	C(22	93.1(7)
C(8)	C(13)	N(2)	C(14)	-178.1(6	C(19)	C(18)	C(17)	C(47	-177.0(6)
C(8)	C(13)	C(12)	C(11)	-59.9(7)	C(19)	C(21)	C(22)	C(23	-71.1(8)

Table 3.11 Torsion or conformation angles (cont.)

(1)	(2)	(3)	(4)	angle	(1)	(2)	(3)	(4)	angle
C(9)	C(8)	C(13)	C(12)	65.7(8)	C(19)	C(21)	C(22)	C(27)	93.1(8)
C(9)	C(10)	C(11)	C(12)	-54(1)	C(20)	C(19)	C(21)	C(22)	-78.2(8)
C(10)	C(9)	C(8)	C(13)	-60.7(8)	C(21)	C(22)	C(23)	C(24)	161.4(6)
C(10)	C(11)	C(12)	C(13)	55.3(8)	C(21)	C(22)	C(27)	C(26)	-161.2(6)
C(12)	C(13)	N(2)	C(14)	-56.3(8)	C(22)	C(23)	C(24)	C(25)	-3(1)
C(13)	N(2)	C(14)	C(15)	-174.1(7)	C(22)	C(23)	C(24)	C(51)	-176.7(6)
C(14)	C(15)	C(16)	C(17)	-168.2(7)	C(22)	C(27)	C(26)	C(25)	4(1)
C(14)	C(15)	C(20)	C(19)	-178.9(7)	C(22)	C(27)	C(26)	C(28)	175.5(7)
C(15)	C(16)	C(17)	C(18)	-16.9(9)	C(23)	C(22)	C(27)	C(26)	3(1)
C(15)	C(16)	C(17)	C(47)	166.3(6)	C(23)	C(24)	C(25)	C(26)	10.2(9)
C(15)	C(20)	C(19)	C(18)	-9(1)	C(23)	C(24)	C(51)	C(52)	-136.3(7)
C(15)	C(20)	C(19)	C(21)	162.9(6)	C(23)	C(24)	C(51)	C(53)	-14.1(9)
C(23)	C(24)	C(51)	C(54)	103.1(7)	C(37)	C(38)	C(41)	C(40)	-4(1)
C(24)	C(23)	C(22)	C(27)	-4(1)	C(37)	C(38)	C(39)	C(40)	3(1)
C(24)	C(25)	C(26)	C(27)	-10.8(9)	C(37)	C(38)	C(55)	C(56)	-177.2(6)
C(24)	C(25)	C(26)	C(28)	177.9(6)	C(37)	C(38)	C(55)	C(57)	62.4(8)
C(25)	C(24)	C(51)	C(52)	50.5(9)	C(37)	C(38)	C(55)	C(58)	-58.8(8)
C(25)	C(24)	C(51)	C(53)	172.7(6)	C(38)	C(37)	C(36)	C(41)	13.3(9)
C(25)	C(24)	C(51)	C(54)	-70.1(7)	C(38)	C(39)	C(40)	C(41)	6(1)
C(26)	C(25)	C(24)	C(51)	-176.4(6)	C(38)	C(39)	C(40)	C(42)	-159.7(7)
C(26)	C(28)	N(3)	C(29)	-179.7(6)	C(39)	C(38)	C(55)	C(56)	4.6(9)
C(28)	N(3)	C(29)	C(30)	-1.3(9)	C(39)	C(38)	C(55)	C(57)	-115.7(7)
C(28)	N(3)	C(29)	C(34)	-179.5(6)	C(39)	C(38)	C(55)	C(58)	123.1(7)
C(29)	C(30)	C(31)	C(32)	57.2(8)	C(40)	C(39)	C(38)	C(55)	-178.7(6)
C(29)	C(34)	N(4)	C(35)	-177.2(5)	C(29)	C(34)	C(33)	C(32)	-57.6(7)
C(30)	C(29)	C(34)	C(33)	62.7(7)	C(30)	C(31)	C(32)	C(33)	-56.1(9)
C(31)	C(30)	C(29)	C(34)	-61.9(7)	C(31)	C(32)	C(33)	C(34)	54.6(8)
C(33)	C(34)	N(4)	C(35)	-56.0(8)	C(34)	N(4)	C(35)	C(36)	-177.6(6)
C(35)	C(36)	C(37)	C(38)	-168.0(6)	C(35)	C(36)	C(41)	C(40)	177.1(6)
C(36)	C(37)	C(38)	C(39)	-12.4(9)	C(36)	C(37)	C(39)	C(55)	169.5(6)
C(36)	C(41)	C(40)	C(39)	-6(1)	C(36)	C(41)	C(40)	C(42)	160.9(6)

The sign is positive if when looking from atom 2 to atom 3 a clock-wise motion of atom 1 would superimpose it on atom 4.

Appendix 3

X-ray crystal structure determination of the macrocyclic complex 4.1 and 4.2

A yellow irregular crystal of $C_{44}H_{48}N_4O_{10}Cu_2$ **4.1** having approximate dimensions of 0.15 x 0.05 x 0.35 mm and a red rectangular plate crystal of $C_{46}H_{48}N_4O_8Ni_2Cl_4$ **4.2** having approximate dimensions of 0.20 x 0.08 x 0.40 mm were mounted on glass fibres. The data were collected at a temperature of 26 ± 1°C using the ω-2θ scan technique to a maximum 2θ value of 121.2° (**4.1**), 50.1° (**4.2**) on a Rigaku AFC6S diffractometer with graphite monochromated Cu-Kα radiation or Mo-Kα radiation. Cell constants and an orientation matrix for data collection, obtained from a least-squares refinement using the setting angles 24 (**4.1**) or 16 (**4.2**) carefully centered reflections in the range $56.20 < 2\theta < 59.68°$ (**4.1**) or $20.47 < 2\theta < 22.84°$ (**4.2**) corresponded to a primitive monoclinic cell (constants are given in Table 4.2 of crystal data). Based on the systematic absences of 0k0: k ± 2n for **4.1**, packing considerations, a statistical analysis of intensity distribution, and the successful solution and refinement of the structure, the space group was determined to be $P2_1$ (#4) **4.1** and P1 (#1) for **4.2**.

Omega scans of several intense reflections, made prior to data collection, had an average width at half-height of 0.31° (**4.1**), 0.33° (**4.2**) with a take-off angle of 6.0°. Scans of $(1.15 + 0.14 \tan\theta)°$ for (**4.1**) or $(1.26 + 0.35\tan\theta)°$ for (**4.2**) were made at a speed of

2.0°/min (**4.2**), 4.0°/minute (**4.2**) (in ω). The weak reflections ($I < 10.0\sigma(I)$) were rescanned (maximum of 10 scans) and the counts were accumulated to ensure good counting statistics. Stationary background counts were recorded on each side of the reflection. The ratio of peak counting time to background counting time was 2:1. The diameter of the incident beam collimator was 1.0 mm, the crystal to detector distance was 400 mm, and the detector aperture was 4.5 x 3.0 mm (**4.1**), 6.0 x 3.0 mm(**4.2**) (horizontal x vertical).

Of the 9882 reflections for complex **4.1** which were collected, 3178 were unique (R_{int} = 0.027). The intensities of three representative reflections were measured after every 150 reflections. No decay correction was applied. During data collection of the complex (**4.2**) the crystal underwent slow decomposition. The resulting data was corrected for decay but was limited to 50.1 degrees in 2θ. Of the 3564 reflections which were collected for crystal **4.2**, 3326 were unique (R_{int} = 0.033); equivalent reflections were removed. The intensities of three representative reflection were measured after every 150 reflections. Over the course of data collection, the standards decreased by 38.8%. A linear correction factor was applied to the data to account for this phenomenon.

The linear absorption coefficient, μ, for Cu-Kα radiation was 19.4 cm^{-1} and 11.3 cm^{-1} for Mo-Kα radiation. An empirical absorption correction based on azimuthal scans of several reflections was applied which resulted in transmission factors ranging from 0.86

to 1.00. The data were corrected for Lorentz and polarization effects. A correction for secondary extinction was applied to crystal (**4.2**) (coefficient = 4.17322e-007).

The structures were solved by direct methods and expanded using Fourier techniques.[2] The non-hydrogen atoms were refined anisotropically for **4.1**. Some non-hydrogen atoms were refined anisotropically, while the rest were refined isotropically for **4.2**. Hydrogen atoms were included but not refined. The final cycle of full-matrix least-squares refinement[2] was based on 3174 (**4.1**) 2385 (**4.2**) observed reflections ($I > 0.00\sigma(I)$ for **4.1**. $I > 2.00\ \sigma(I)$ for **4.2**) and 542 (**4.1**). 357 (**4.2**) variable parameters and converged (largest parameter shift was 0.00 times its esd) with unweighted and weighted agreement factors of:

For complex **4.1:**

$$R(F^2) = \Sigma\,|F(obs)^2 - F(calcd.)^2| \,/\, \Sigma F(obs)^2 = 0.049$$

$$R_w = [\,\Sigma\,|w\,|Yo - Yc|^2|\,/\,\Sigma\,|w\,Yo^2|\,]^{1/2} = 0.060$$

where $Yo = F(obs)^2$, $Yc = F(calcd.)^2$

For complex **4.2:**

$$R = \Sigma\,||Fo| - |Fc||\,/\,\Sigma\,|Fo| = 0.052$$

$$R_w = [(\,\Sigma w\,(|Fo| - |Fc|)^2 \,/\, \Sigma w\,Fo^2)\,]^{1/2} = 0.053$$

The standard deviation of an observation of unit weight[3] was 1.87 (**4.1**), and 1.94 (**4.2**).

The weighting scheme was based on counting statistics and included a factor ($p = 0.007$ for **4.1** and 0.017 for **4.2**) to downweight the intense reflections. Plots of $\Sigma w (|Fo| - |Fc|)^2$ versus |Fo|, reflection order in data collection, $\sin\theta/\lambda$ and various classes of indices showed no unusual trends. The maximum and minimum peaks on the final difference Fourier map corresponded to 0.41 and -0.44 $e^-/Å^3$ **4.1**, 0.55 and -0.43 $e^-/Å^3$ **4.2**, respectively.

Neutral atom scattering factors were taken from Cromer and Waber.[4] Anomalous dispersion effects were included in Fcalc:[5] the values for Df' and Df'' were those of Creagh and McAuley.[6] The values for the mass attenuation coefficients are those of Creagh and Hubbell.[7] All calculations were performed using the TEXSAN[8] crystallographic software package of Molecular Structure Corporation.

Table 4.2 Crystal Data for the complexes **4.1** and **4.2**

	4.1	**4.2**
Empirical Formula	$C_{44}H_{48}N_4O_{10}Cu_2$	$C_{46}H_{48}N_4O_8Ni_2Cl_4$
Formula Weight	919.98	1044.12
Crystal Colour, Habit	yellow, irregular	red, rectangular plate
Crystal Dimensions	0.15 x 0.05 x 0.35 mm	0.20 x 0.08 x 0.40 mm
Crystal System	monoclinic	triclinic
Lattice Type	Primitive	Primitive
No. of Reflections Used for Unit Cell Determination (2θ range)	24 (56.2 - 59.7°)	16 (20.5 - 22.8°)
Omega Scan Peak Width at Half-height	0.31°	0.33°
Lattice Parameters	a = 12.009(3) Å	a = 10.366(4) Å
	b = 7.200(2) Å	b = 12.170(3) Å
	c = 22.751(1) Å	c = 10.021(2) Å
	β = 101.782(8)°	α = 106.29(2)°
	V = 1925.9(5) Å^3	β = 91.69(2)°
		γ = 68.64(2)°
		V = 1126.3(5) Å^3
Space Group	$P2_1$ (#4)	P1 (#1)
Z value	2	1
D_{calcd}	1.586 g/cm^3	1.539 g/cm^3
F_{000}	956.00	540.00
μ (Cu-Kα)	19.39 cm^{-1}	
μ (Mo-Kα)		11.32 cm^{-1}

Table 4.3 Intensity measurements for crystals **4.1** and **4.2**

	4.1	**4.2**
Diffractometer	Rigaku AFC6S	Rigaku AFC6S
Radiation	Cu-Kα (l = 1.54178 Å)	Mo-Kα (l = 0.71069 Å)
	graphite monochromated	graphite monochromated
Take-off Angle	6.0°	6.0°
Detector Aperture	4.5 mm horizontal	6.0 mm horizontal
	3.0 mm vertical	3.0 mm vertical
Crystal to Detector Distance	400 mm	400 mm
Voltage, Current	50 kV, 27.5 mA	50 kV, 27.5 mA
Temperature	26.0°C	26.0°C
Scan Type	ω-2θ	ω-2θ
Scan Rate	2.0°/minute (in ω) (up to 10 scans)	4.0°/minute (in ω) (up to 10 scans)
Scan Width	(1.15 + 0.14 tanθ)°	(1.26 + 0.35 tanθ)°
$2\theta_{max}$	121.2°	50.1°
No. of Reflections Measured	Total: 9882	Total: 3564
Corrections	Unique: 3178 (R_{int} = 0.027) Lorentz-polarization Absorption (trans. factors: 0.8630 - 0.9996) Secondary Extinction (coefficient: 4.17322e-007)	Unique: 3326 (R_{int} = 0.033) Lorentz-polarization Absorption (trans. factors: 0.7992 - 1.0000) Decay(38.80% decline)

Table 4.4 Structure solution and refinement of the crystals **4.1** and **4.2**

	4.1	**4.2**
Structure Solution	Direct Methods	Direct Methods (SHELX86)
Refinement	Full-matrix least-squares	Full-matrix least-squares
Function Minimized	$\Sigma w (\|Yo - Yc\|)^2$	$\Sigma w (\|Fo - Fc\|)^2$
Least Squares Weights	$1/\sigma^2(Yo) = 4Yo^2/\sigma^2(Yo^2)$	$1/\sigma^2(Fo) = 4Fo^2/\sigma^2(Fo^2)$
p-Factor	0.0065	0.071
Anomalous Dispersion	All non-hydrogen atoms	All non-hydrogen atoms
No. Observations ($I>0.00\sigma(I)$)	3174	2385
No. Variables	542	357
Reflection/Parameter Ratio	5.86	6.68
Residuals: R: R_w	0.049 ; 0.060	0.052; 0.053
Goodness of Fit Indicator	1.87	1.94
Max Shift/Error in Final Cycle	0.00	0.00
Maximum peak in Final Diff. Map	0.41 $e^-/Å^3$	0.55 $e^-/Å^3$
Minimum peak in Final Diff. Map	-0.44 $e^-/Å^3$	-0.43 $e^-/Å^3$

Table 4.5 least-squares planes in complex **4.1**

Plane number 1

Atoms Defining Plane		Distance	esd
O(1)	(1)	-.1872	.0148
O(2)	(1)	.2308	.0151
N(1)	(1)	.1138	.0148
N(2)	(1)	-.1554	.0150

Additional Atoms		Distance
Cu(1)	(1)	-.0180

Mean deviation from plane was .1718 angstroms
Chi-squared: 2953.2

Plane number 2

Atoms Defining Plane		Distance	esd
O(1)	(1)	-.1872	.0148
O(2)	(1)	.2308	.0151
N(1)	(1)	.1138	.0148
N(2)	(1)	-.1554	.0150

Additional Atoms		Distance
Cu(2)	(1)	3.4565

Mean deviation from plane was .1718 angstroms
Chi-squared: 2953.2

Plane number 3

Atoms Defining Plane		Distance	esd
O(5)	(1)	-.0858	.0152
O(6)	(1)	.1126	.0153
N(3)	(1)	.0844	.0151
N(4)	(1)	-.0846	.0153

Additional Atoms		Distance
Cu(2)	(1)	-.0043

Mean deviation from plane was .0919 angstroms
Chi-squared: 703.4

Plane number 4

Atoms Defining Plane		Distance	esd
O(5)	(1)	-.0858	.0152
O(6)	(1)	.1126	.0153
N(3)	(1)	.0844	.0151
N(4)	(1)	-.0846	.0153

Additional Atoms		Distance
Cu(1)	(1)	-3.4480

Mean deviation from plane was .0919 angstroms
Chi-squared: 703.4

Dihedral angles between least-squares planes

plane	plane	angle	plane	plane	angle
2	1	.00	4	1	6.56
3	1	6.56	4	2	6.56
3	2	6.56	4	3	.00

Table 4.6 Positional parameters and B(eq) for the binuclear copper complex **4.1**

atom	x	y	z	B(eq)
Cu(1)	-0.25189(5)	-0.524(1)	-0.77314(3)	3.25(2)
Cu(2)	-0.24024(5)	-0.060(1)	-0.72986(3)	3.119(2)
O(1)	-0.3565(3)	-0.490(2)	-0.8477(1)	3.88(9)
O(2)	-0.3759(2)	-0.525(2)	-0.7329(1)	3.18(9)
O(3)	-0.3986(3)	-0.752(2)	-0.5035(2)	4.0(1)
O(4)	-0.2203(4)	-0.388(2)	-0.4444(2)	5.1(1)
O(5)	-0.1368(3)	-0.111(2)	-0.6568(1)	4.0(1)
O(6)	-0.1144(2)	-0.033(2)	-0.7574(1)	3.0(1)
O(7)	-0.0973(3)	0.168(2)	-0.9996(2)	3.8(1)
O(8)	-0.2844(4)	-0.180(2)	-1.0586(2)	4.8(2)
O(9)	-0.0958(4)	-0.569(2)	-0.8328(2)	4.8(2)
O(10)	-0.5926(4)	-0.527(2)	-0.8204(2)	4.8(2)
N(1)	-0.1190(3)	-0.473(2)	-0.8064(2)	3.2(1)
N(2)	-0.1413(3)	-0.599(2)	-0.7016(2)	3.0(1)
N(3)	-0.3734(3)	-0.057(2)	-0.6930(2)	3.0(1)
N(4)	-0.3511(3)	-0.031(2)	-0.8050(2)	3.3(1)
C(1)	-0.2942(6)	-0.269(2)	-1.0052(3)	4.4(2)
C(2)	-0.2028(5)	-0.324(2)	-0.9623(2)	3.6(2)
C(3)	-0.2201(5)	-0.403(2)	-0.9076(2)	3.6(2)
C(4)	-0.3327(4)	-0.426(2)	-0.8978(2)	3.5(2)
C(5)	-0.4228(5)	-0.374(2)	-0.9449(2)	4.1(2)
C(6)	-0.4033(5)	-0.293(2)	-0.9963(3)	4.6(2)
C(7)	-0.1207(4)	-0.430(2)	-0.8615(2)	3.6(2)
C(8)	-0.0143(4)	-0.466(2)	-0.7596(2)	3.4(2)
C(9)	0.0970(4)	-0.481(2)	-0.7607(2)	3.4(2)
C(10)	0.1967(4)	-0.465(2)	-0.7262(2)	3.4(2)
C(11)	0.1882(4)	-0.602(2)	-0.6770(2)	3.4(2)
C(12)	0.0716(4)	-0.588(2)	-0.6854(2)	3.4(2)
C(13)	-0.0247(3)	-0.610(2)	-0.7136(2)	3.1(2)
C(14)	-0.1644(4)	-0.642(2)	-0.6880(2)	3.4(2)
C(15)	-0.2749(4)	-0.636(2)	-0.6958(2)	3.4(2)
C(16)	-0.2831(4)	-0.691(2)	-0.7478(2)	3.4(2)
C(17)	-0.3844(5)	-0.687(2)	-0.7558(2)	4.1(2)
C(18)	-0.4798(4)	-0.624(2)	-0.7119(2)	3.9(2)
C(19)	-0.4751(4)	-0.577(2)	-0.6605(2)	3.7(2)
C(20)	-0.3734(4)	-0.576(2)	-0.6508(2)	3.3(2)
C(21)	-0.3187(6)	-0.693(2)	-0.4458(3)	4.7(2)
C(22)	-0.3184(7)	-0.489(2)	-0.4399(3)	5.2(2)
C(23)	-0.2106(5)	-0.314(2)	-0.4499(2)	4.1(2)
C(24)	-0.1016(5)	-0.309(2)	-0.5092(2)	3.9(2)
C(25)	-0.0785(5)	-0.238(2)	-0.5614(2)	3.8(2)
C(26)	-0.1642(5)	-0.169(2)	-0.6074(2)	3.8(2)
C(27)	-0.2746(5)	-0.179(2)	-0.5954(2)	3.8(2)
C(28)	-0.2961(5)	-0.239(2)	-0.5408(2)	3.8(2)
C(29)	-0.3731(4)	-0.108(2)	-0.6903(2)	3.3(2)
C(30)	-0.4755(3)	-0.004(2)	-0.7355(2)	3.1(2)
C(31)	-0.5898(4)	-0.041(2)	-0.7199(2)	3.6(2)
C(32)	-0.6858(4)	-0.025(2)	-0.7688(2)	3.9(2)
C(33)	-0.6791(4)	-0.059(2)	-0.8293(2)	3.8(2)
C(34)	-0.5649(4)	-0.012(2)	-0.8461(2)	3.6(2)
C(35)	-0.4663(3)	-0.075(2)	-0.7967(2)	3.1(2)
C(36)	-0.3293(4)	0.025(2)	-0.8546(2)	3.4(2)
C(37)	-0.2185(4)	0.056(2)	-0.8666(2)	3.7(2)
C(38)	-0.2115(5)	0.111(2)	-0.9254(2)	4.1(2)
C(39)	-0.1106(5)	0.117(2)	-0.9437(2)	4.1(2)
C(40)	-0.0121(4)	0.072(2)	-0.9028(2)	3.9(2)
C(41)	-0.0142(4)	0.023(2)	-0.8448(2)	3.9(2)
C(42)	-0.1178(4)	0.016(2)	-0.8239(2)	3.2(2)
C(43)	-0.1817(6)	0.117(2)	-1.0488(3)	5.3(2)
C(44)	-0.1851(7)	-0.083(2)	-1.0640(3)	6.2(2)

Table 4.7 Intramolecular distances involving the nohydrogen atoms in the complex **4.1**

atom	atom	distance	atom	atom	distance
Cu(1)	O(1)	1.909(5)	N(4)	C(35)	1.470(7)
Cu(1)	O(2)	1.902(4)	N(4)	C(36)	1.276(8)
Cu(1)	N(1)	1.937(5)	C(1)	C(2)	1.37(1)
Cu(1)	N(2)	1.955(5)	C(1)	C(6)	1.37(1)
Cu(2)	O(5)	1.897(5)	C(2)	C(3)	1.42(1)
Cu(2)	O(6)	1.898(4)	C(3)	C(4)	1.424(9)
Cu(2)	N(3)	1.951(5)	C(3)	C(7)	1.43(1)
Cu(2)	N(4)	1.951(5)	C(4)	C(5)	1.41(1)
O(1)	C(4)	1.314(8)	C(5)	C(6)	1.38(1)
O(2)	C(20)	1.322(8)	C(8)	C(9)	1.514(8)
O(3)	C(17)	1.381(8)	C(8)	C(13)	1.496(8)
O(3)	C(21)	1.41(1)	C(9)	C(10)	1.543(9)
O(4)	C(22)	1.38(1)	C(10)	C(11)	1.51(1)
O(4)	C(23)	1.389(9)	C(11)	C(12)	1.544(8)
O(5)	C(26)	1.305(8)	C(12)	C(13)	1.532(9)
O(6)	C(42)	1.315(8)	C(14)	C(15)	1.436(9)
O(7)	C(39)	1.365(8)	C(15)	C(16)	1.399(9)
O(7)	C(43)	1.40(1)	C(15)	C(20)	1.417(9)
O(8)	C(1)	1.40(1)	C(16)	C(17)	1.374(9)
O(8)	C(44)	1.41(1)	C(17)	C(18)	1.39(1)
N(1)	C(7)	1.287(8)	C(18)	C(19)	1.374(9)
N(1)	C(8)	1.473(8)	C(19)	C(20)	1.405(8)
N(2)	C(13)	1.483(7)	C(21)	C(22)	1.50(2)
N(2)	C(14)	1.283(8)	C(23)	C(24)	1.37(1)
N(3)	C(29)	1.288(8)	C(23)	C(28)	1.36(1)
N(3)	C(30)	1.469(7)	C(24)	C(25)	1.37(1)
C(25)	C(26)	1.40(1)	C(26)	C(27)	1.417(9)
C(27)	C(28)	1.409(9)	C(27)	C(29)	1.45(1)
C(30)	C(31)	1.524(8)	C(30)	C(35)	1.526(7)
C(31)	C(32)	1.51(1)	C(32)	C(33)	1.520(9)
C(33)	C(34)	1.534(9)	C(34)	C(35)	1.526(9)
C(36)	C(37)	1.430(9)	C(37)	C(38)	1.414(9)
C(37)	C(42)	1.419(9)	C(38)	C(39)	1.36(1)
C(39)	C(40)	1.39(1)	C(40)	C(41)	1.37(1)
C(41)	C(42)	1.420(8)	C(43)	C(44)	1.46(2)

Distances are in angstroms. Estimated standard deviations in the least significant figure are given in parentheses.

Table 4.8 Intramolecular bond angles involving the nonhydrogen atoms for the complex **4.1**

atom	atom	atom	angle	atom	atom	atom	angle
O(1)	Cu(1)	O(2)	99.5(2)	Cu(2)	N(3)	C(29)	124.5(5)
O(1)	Cu(1)	N(1)	94.2(2)	Cu(2)	N(3)	C(30)	111.5(3)
O(1)	Cu(1)	N(2)	170.7(3)	C(29)	N(3)	C(30)	123.9(5)
O(2)	Cu(1)	N(1)	168.3(3)	Cu(2)	N(4)	C(35)	110.8(4)
O(2)	Cu(1)	N(2)	93.6(2)	Cu(2)	N(4)	C(36)	125.7(4)
N(1)	Cu(1)	N(2)	84.5(2)	C(35)	N(4)	C(36)	123.5(5)
O(5)	Cu(2)	O(6)	88.8(2)	O(8)	C(1)	C(2)	123.7(8)
O(5)	Cu(2)	N(3)	94.2(2)	O(8)	C(1)	C(6)	115.5(8)
O(5)	Cu(2)	N(4)	174.9(3)	C(2)	C(1)	C(6)	120.7(8)
O(6)	Cu(2)	N(3)	173.3(3)	C(1)	C(2)	C(3)	120.1(7)
O(6)	Cu(2)	N(4)	93.1(2)	C(2)	C(3)	C(4)	119.9(7)
N(3)	Cu(2)	N(4)	84.4(2)	C(3)	C(4)	C(7)	116.6(7)
Cu(1)	O(1)	C(4)	126.5(4)	C(4)	C(7)	O(7)	123.0(7)
Cu(1)	O(2)	C(20)	127.0(4)	O(1)	C(4)	C(3)	124.0(7)
C(17)	O(3)	C(21)	116.6(7)	O(1)	C(4)	C(5)	118.8(6)
C(22)	O(4)	C(23)	120.9(7)	C(3)	C(4)	C(5)	117.1(6)
Cu(2)	O(5)	C(26)	125.6(4)	C(4)	C(5)	C(6)	121.7(7)
Cu(2)	O(6)	C(42)	126.9(4)	C(1)	C(6)	C(5)	120.4(8)
C(39)	O(7)	C(43)	118.2(7)	N(1)	C(7)	C(8)	126.2(6)
C(1)	O(8)	C(44)	121.7(7)	N(1)	C(8)	C(9)	116.8(5)
Cu(1)	N(1)	C(7)	125.2(5)	N(1)	C(8)	C(13)	107.5(5)
Cu(1)	N(1)	C(8)	111.9(4)	C(9)	C(8)	C(13)	112.0(5)
C(7)	N(1)	C(8)	122.5(6)	C(8)	C(9)	C(10)	109.9(5)
Cu(1)	N(2)	C(13)	111.6(4)	C(9)	C(10)	C(11)	112.7(6)
Cu(1)	N(2)	C(14)	125.7(4)	C(10)	C(11)	C(12)	111.4(6)
C(13)	N(2)	C(14)	122.6(5)	C(11)	C(12)	C(13)	110.2(5)
N(2)	C(13)	C(8)	108.0(5)	C(26)	C(27)	C(28)	121.5(7)
N(2)	C(13)	C(12)	115.4(5)	C(26)	C(27)	C(29)	122.9(6)
C(8)	C(13)	C(12)	110.3(6)	C(28)	C(27)	C(29)	115.9(6)
N(2)	C(14)	C(15)	125.9(7)	C(28)	C(28)	C(27)	120.4(7)
C(14)	C(15)	C(16)	117.5(7)	N(3)	C(29)	C(27)	125.7(6)
C(14)	C(15)	C(20)	122.8(6)	N(3)	C(30)	C(31)	116.7(5)
C(16)	C(15)	C(20)	119.7(6)	N(3)	C(30)	C(35)	106.3(5)
C(15)	C(16)	C(17)	122.1(7)	C(31)	C(30)	C(35)	111.8(5)
O(3)	C(17)	C(16)	124.3(7)	C(30)	C(31)	C(32)	110.3(6)
O(3)	C(17)	C(18)	117.5(6)	C(31)	C(32)	C(33)	111.7(6)
C(16)	C(17)	C(18)	118.1(7)	C(32)	C(33)	C(34)	110.8(6)
C(17)	C(18)	C(19)	121.5(6)	C(33)	C(34)	C(35)	110.5(6)
C(18)	C(19)	C(20)	121.7(7)	N(4)	C(35)	C(30)	106.3(5)
O(2)	C(20)	C(15)	124.8(6)	N(4)	C(35)	C(34)	116.7(5)
O(2)	C(20)	C(19)	118.4(6)	C(30)	C(35)	C(34)	111.7(5)
C(15)	C(20)	C(19)	116.7(6)	N(4)	C(36)	C(37)	125.8(6)
O(3)	C(21)	C(22)	118(1)	C(36)	C(37)	C(38)	117.5(7)
O(4)	C(22)	C(21)	118(1)	C(36)	C(37)	C(42)	122.3(6)
O(4)	C(23)	C(24)	116.3(9)	C(38)	C(37)	C(42)	119.9(6)
O(4)	C(23)	C(28)	124.8(8)	C(37)	C(38)	C(39)	121.7(7)
C(24)	C(23)	C(28)	118.8(7)	O(7)	C(39)	C(38)	125.0(7)
C(23)	C(24)	C(25)	121.4(8)	O(7)	C(39)	C(40)	116.2(6)
C(24)	C(25)	C(26)	122.1(7)	C(38)	C(39)	C(40)	118.7(7)
O(5)	C(26)	C(25)	118.8(6)	C(39)	C(40)	C(41)	121.6(6)
O(5)	C(26)	C(27)	125.6(7)	C(40)	C(41)	C(42)	121.5(7)
C(25)	C(26)	C(27)	115.6(7)	O(6)	C(42)	C(37)	124.9(6)
O(6)	C(42)	C(41)	118.7(6)	O(7)	C(43)	C(44)	115.1(9)
C(37)	C(42)	C(41)	116.4(6)	O(8)	C(44)	C(43)	116(1)

Angles are in degrees.

Table 4.9 Positional parameters and B(eq) for the binuclear nickel complex **4.2**

Table 4.10 Intramolecular distances involving the nonhydrogen atoms in the complex **4.2**

atom	atom	distance	atom	atom	distance
Ni(1)	O(1)	1.86(1)	N(2)	C(21)	1.48(2)
Ni(1)	O(8)	1.84(1)	N(2)	C(22)	1.28(2)
Ni(1)	N(3)	1.81(1)	N(3)	C(37)	1.32(2)
Ni(1)	N(4)	1.94(1)	N(3)	C(38)	1.46(2)
Ni(2)	O(4)	1.85(1)	N(4)	C(43)	1.49(2)
Ni(2)	O(5)	1.84(1)	N(4)	C(44)	1.30(2)
Ni(2)	N(1)	1.89(1)	C(1)	C(2)	1.39(2)
Ni(2)	N(2)	1.87(1)	C(1)	C(6)	1.46(2)
Cl(1)	C(45)	1.64(2)	C(2)	C(3)	1.40(2)
Cl(2)	C(45)	1.63(2)	C(2)	C(44)	1.45(2)
Cl(3)	C(46)	1.75(2)	C(3)	C(4)	1.41(2)
Cl(4)	C(46)	1.75(2)	C(4)	C(5)	1.33(2)
O(1)	C(1)	1.31(2)	C(5)	C(6)	1.36(2)
O(2)	C(4)	1.38(2)	C(7)	C(8)	1.50(2)
O(2)	C(7)	1.34(2)	C(9)	C(10)	1.39(2)
O(3)	C(8)	1.44(2)	C(9)	C(14)	1.44(2)
O(3)	C(9)	1.38(2)	C(10)	C(11)	1.39(2)
O(4)	C(12)	1.30(2)	C(11)	C(12)	1.43(2)
O(5)	C(24)	1.31(2)	C(11)	C(15)	1.42(2)
O(6)	C(27)	1.36(2)	C(12)	C(13)	1.46(2)
O(6)	C(29)	1.50(2)	C(13)	C(14)	1.41(2)
O(7)	C(30)	1.42(2)	C(16)	C(17)	1.51(2)
O(7)	C(31)	1.39(2)	C(16)	C(21)	1.55(2)
O(8)	C(34)	1.32(2)	C(17)	C(18)	1.61(2)
N(1)	C(15)	1.24(2)	C(18)	C(19)	1.54(2)
N(1)	C(16)	1.45(2)	C(19)	C(20)	1.50(2)
C(20)	C(21)	1.52(2)	C(22)	C(23)	1.42(2)
C(23)	C(24)	1.41(2)	C(23)	C(28)	1.43(2)
C(24)	C(25)	1.39(2)	C(25)	C(26)	1.35(2)
C(26)	C(27)	1.44(2)	C(27)	C(28)	1.36(2)
C(29)	C(30)	1.52(2)	C(31)	C(32)	1.34(2)
C(31)	C(36)	1.37(2)	C(32)	C(33)	1.43(2)
C(33)	C(34)	1.39(2)	C(33)	C(37)	1.43(2)
C(34)	C(35)	1.38(2)	C(35)	C(36)	1.32(2)
C(38)	C(39)	1.55(2)	C(36)	C(43)	1.47(2)
C(39)	C(40)	1.55(2)	C(40)	C(41)	1.48(2)
C(41)	C(42)	1.54(2)	C(42)	C(43)	1.53(2)

Distances are in angstroms. Estimated standard deviations in the least significant figure are given in parentheses.

Table 4.11 Intramolecular bond angles involving the nonhydrogen atoms in the complex **4.2**

atom	atom	atom	angle	atom	atom	atom	angle
O(1)	Ni(1)	O(6)	94.6(5)	Ni(1)	N(3)	C(37)	128(1)
O(1)	Ni(1)	N(3)	176.0(6)	Ni(1)	N(3)	C(38)	112.2(9)
O(1)	Ni(1)	N(4)	95.3(6)	C(37)	N(3)	C(38)	119(1)
O(6)	Ni(1)	N(3)	93.1(6)	Ni(1)	N(4)	C(43)	112(1)
O(6)	Ni(1)	N(4)	178.8(5)	Ni(1)	N(4)	C(44)	129(1)
N(3)	Ni(1)	N(4)	86.9(6)	C(43)	N(4)	C(44)	119(1)
O(4)	Ni(2)	O(5)	94.5(5)	O(1)	C(1)	C(2)	127(2)
O(4)	Ni(2)	N(1)	96.4(6)	O(1)	C(1)	C(6)	119(2)
O(4)	Ni(2)	N(2)	176.1(5)	C(2)	C(1)	C(6)	114(2)
O(5)	Ni(2)	N(1)	176.6(6)	C(1)	C(2)	C(3)	122(2)
O(5)	Ni(2)	N(2)	93.4(6)	C(1)	C(2)	C(44)	121(2)
N(1)	Ni(2)	N(2)	86.9(6)	C(3)	C(2)	C(44)	116(2)
Ni(1)	O(1)	C(1)	124(1)	C(2)	C(3)	C(4)	122(2)
C(4)	O(2)	C(7)	119(1)	O(2)	C(4)	C(3)	125(1)
C(8)	O(3)	C(9)	119(1)	O(2)	C(4)	C(5)	118(2)
Ni(2)	O(4)	C(12)	124(1)	C(3)	C(4)	C(5)	117(2)
Ni(2)	O(5)	C(24)	127(1)	C(4)	C(5)	C(6)	124(2)
C(27)	O(6)	C(29)	122(1)	C(1)	C(6)	C(5)	122(2)
C(30)	O(7)	C(31)	122(1)	O(2)	C(7)	O(8)	118(1)
Ni(1)	O(8)	C(34)	130(1)	O(3)	C(8)	C(7)	113(1)
Ni(2)	N(1)	C(15)	125(1)	O(3)	C(9)	C(10)	131(2)
Ni(2)	N(1)	C(16)	112(1)	O(3)	C(9)	C(14)	112(1)
C(15)	N(1)	C(16)	123(1)	C(10)	C(9)	C(14)	117(2)
Ni(2)	N(2)	C(21)	111.6(9)	C(9)	C(10)	C(11)	124(2)
Ni(2)	N(2)	C(22)	126(1)	C(10)	C(11)	C(12)	122(2)
C(21)	N(2)	C(22)	123(1)	C(10)	C(11)	C(15)	119(2)
C(12)	C(11)	C(15)	120(2)	O(6)	C(27)	C(26)	113(2)
O(4)	C(12)	C(11)	127(2)	O(6)	C(27)	C(28)	123(2)
O(4)	C(12)	C(13)	117(2)	C(26)	C(27)	C(28)	122(2)
C(11)	C(12)	C(13)	115(2)	C(23)	C(28)	C(27)	117(2)

Table 4.11 (cont.)

C(12)	C(13)	C(14)	122(2)	O(6)	C(29)	C(30)	114(1)
C(9)	C(14)	C(13)	120(2)	O(7)	C(30)	C(29)	114(1)
N(1)	C(15)	C(11)	127(2)	O(7)	C(31)	C(32)	124(2)
N(1)	C(16)	C(17)	118(1)	O(7)	C(31)	C(36)	116(1)
N(1)	C(16)	C(21)	106(1)	C(32)	C(31)	C(36)	120(2)
C(17)	C(16)	C(21)	110(1)	C(31)	C(32)	C(33)	119(2)
C(16)	C(17)	C(18)	112(1)	C(32)	C(33)	C(34)	119(2)
C(17)	C(18)	C(19)	112(1)	C(32)	C(33)	C(37)	118(2)
C(18)	C(19)	C(20)	111(1)	C(34)	C(33)	C(37)	121(1)
C(19)	C(20)	C(21)	109(1)	C(8)	C(34)	C(33)	122(2)
N(2)	C(21)	C(16)	104(1)	O(8)	C(34)	C(35)	120(2)
N(2)	C(21)	C(20)	117(1)	C(33)	C(34)	C(35)	117(2)
C(16)	C(21)	C(20)	112(1)	C(34)	C(35)	C(36)	122(2)
N(2)	C(22)	C(23)	126(2)	C(31)	C(36)	C(35)	121(2)
C(22)	C(23)	C(24)	120(2)	N(3)	C(37)	C(33)	124(1)
C(22)	C(23)	C(28)	119(2)	N(3)	C(38)	C(39)	118(1)
C(24)	C(23)	C(28)	121(2)	N(3)	C(38)	C(43)	106(1)
C(5)	C(24)	C(23)	124(2)	C(39)	C(38)	C(43)	113(1)
C(5)	C(24)	C(25)	116(2)	C(38)	C(39)	C(40)	108(1)
C(23)	C(24)	C(25)	120(2)	C(39)	C(40)	C(41)	114(1)
C(24)	C(25)	C(26)	119(2)	C(40)	C(41)	C(42)	111(1)
C(25)	C(26)	C(27)	121(1)	C(41)	C(42)	C(43)	110(1)
N(4)	C(43)	C(38)	106(1)	N(4)	C(43)	C(42)	118(1)
C(38)	C(43)	C(42)	112(1)	N(4)	C(44)	C(2)	122(2)
Cl(1)	C(45)	Cl(2)	119(2)	Cl(3)	C(46)	Cl(4)	105(1)

Angles are in degrees. Estimated standard deviations in the least significant figure are given in parentheses.

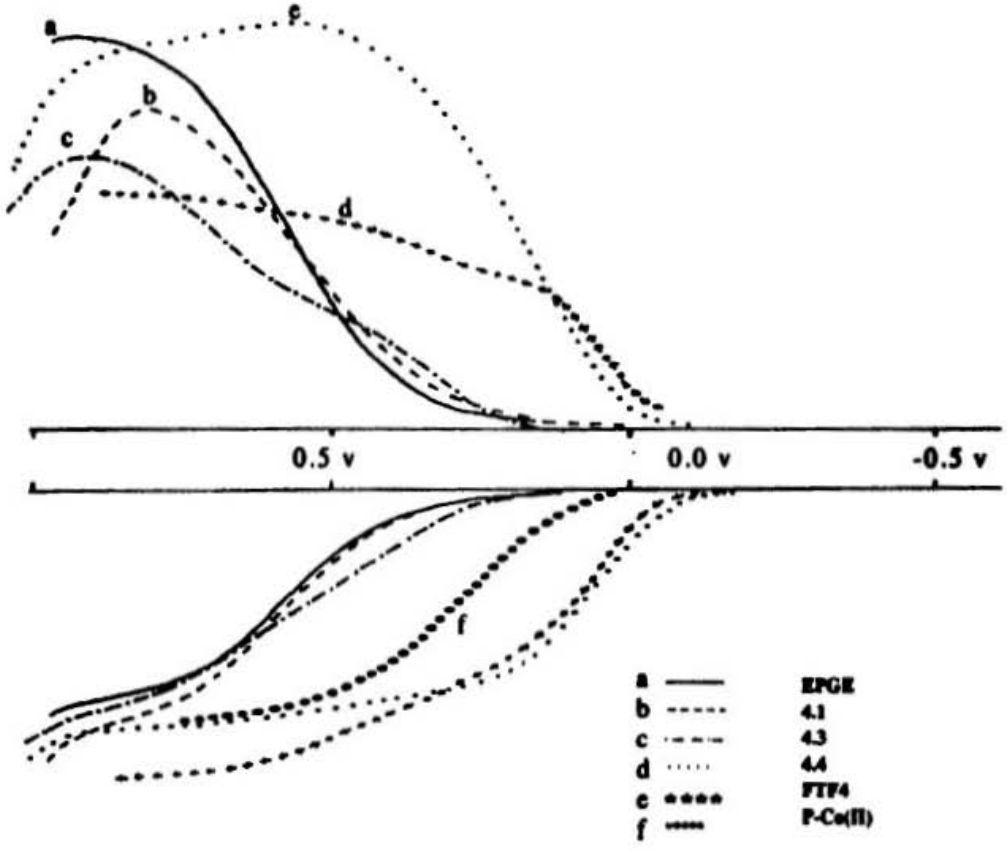

Figure A4.9 Rotating ring-disk voltammogram for reduction of dioxygen with the complexes 4.1, 4.3, 4.4, and FTF4 at pH= 6.86. (EPGE: blank graphite, P-Co(II): a Co(II) porphyrin complex)

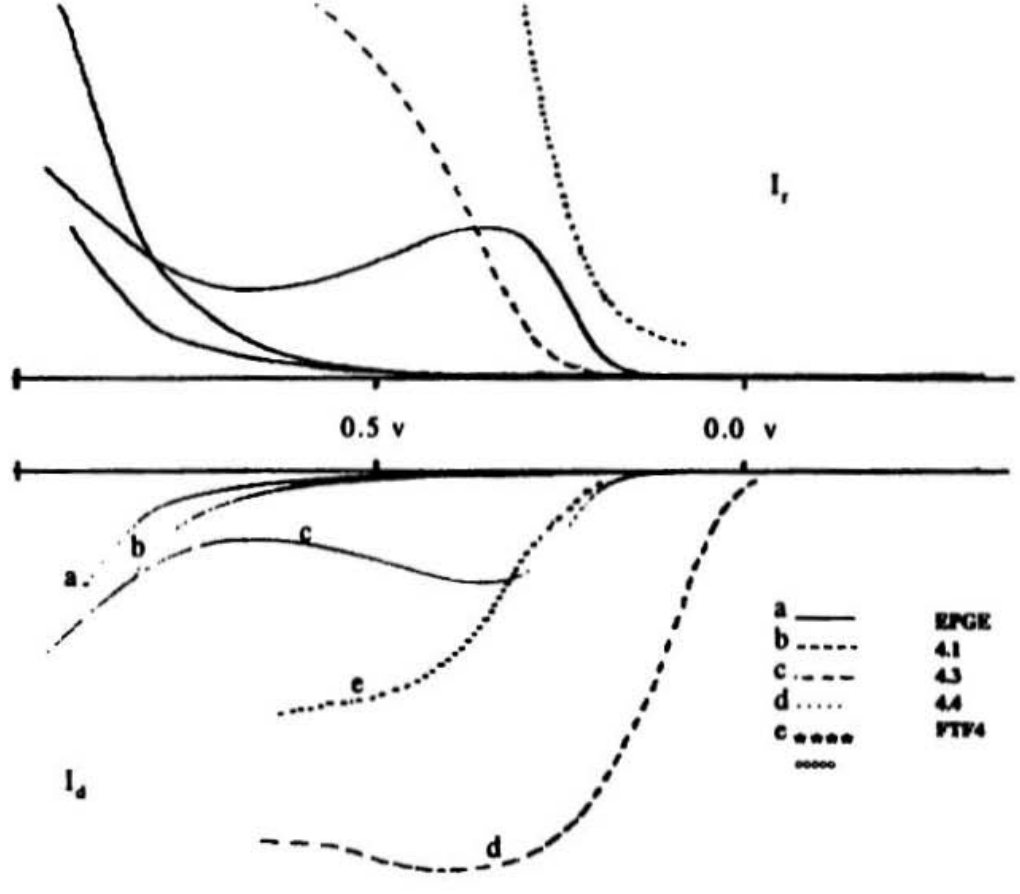

Figure A4.9 Rotating ring-disk voltammogram for reduction of dioxygen with the complexes **4.1**, **4.3**, **4.4**, and **FTF4** at pH= 3.12.

Appendix 5

X-ray crystal structure determinations of the chiral macrocyclic binuclear copper complex

Introduction

The structure solved partially but further development proved troublesome and refinement impossible. until it was realized that significant but diffuse electron density was located in the cavity of this complex. There were also water molecules surrounding the complex and through H-bonds linking it to neighbours in the lattice. Two of these water sites were partially occupied. The isopropyl groups appeared to have a strongly preferred conformation. but the anisotropic thermal parameters and peaks in difference maps close to these units suggested some disorder might exist. It is important to note that the modelling of the internal electron density and the partially occupied water sites has been of necessity somewhat arbitrary. It was impossible to reach convergence while all variables were still set to refine and so the "problem" atoms have been fixed in both position and thermal parameters for the last rounds of least squares. Hydrogen location had also been a problem for some of the water molecules. Furthermore a persistent difference map peak seemed to suggest that O5 has three fairly close hydrogens. Whether this makes chemical sense or not depends very much on the nature of the inclusion. It had been modelled as a highly disordered CH_2Cl_2 molecule in which one chlorine (Cl1) was fairly static but the rest of the molecule was highly mobile. The geometry of the various partially occupied carbon and chlorine sites constituting the rest of the molecule was not convincing.

Alternatives might be partially hydrolysed CH_2ClOH. or water with a localised chlorine ion (Cl1). The latter might allow O5 to be a hydronium ion. Without evidence from other analytical techniques it was impossible to distinguish. (Elemental analysis of the crystals suggested that the molecules within the cavity were most likely to be CH_2Cl_2)

Experimental

Data Collection

A dark-green irregular plate crystal of $C_{55}H_{76}O_9N_4Cu_2Cl_2$ having approximate dimensions of 0.40 x 0.40 x 0.12 mm was mounted on a glass fibre. All measurements were made on a Rigaku AFC6S diffractometer with graphite monochromated Cu-Kα radiation. Cell constants and an orientation matrix for data collection, obtained from a least-squares refinement using the setting angles of 25 carefully centered reflections in the range $58.51 < 2\theta < 59.91°$ corresponded to a primitive orthorhombic cell with dimensions:

a = 18.410(1) Å

b = 25.200(1) Å

c = 12.738(2) Å

V = 5909.4(7) Å^3

For $Z = 4$ and $F.W.$ = 1135.22, the calculated density was 1.28 g/cm^3. The systematic absences of:

h00: h ± 2n

0k0: k ± 2n

00l: l ± 2n

uniquely determine the space group to be:

$P2_12_12_1$ (#19)

The data were collected at a temperature of 26 ± 1°C using the ω-2θ scan technique to a maximum 2θ value of 120.4°. Omega scans of several intense reflections, made prior to data collection, had an average width at half-height of 0.33° with a take-off angle of 6.0°. Scans of $(1.31 + 0.14 \tan\theta)°$ were made at a speed of 8.0°/min (in ω). The weak reflections ($I < 10.0\ (I)$) were rescanned (maximum of 10 scans) and the counts were accumulated to ensure good counting statistics. Stationary background counts were recorded on each side of the reflection. The ratio of peak counting time to background

counting time was 2:1. The diameter of the incident beam collimator was 1.0 mm. the crystal to detector distance was 400 mm. and the detector aperture was 6.0 x 3.0 mm (horizontal x vertical).

Data Reduction

A total of 4929 reflections was collected. The intensities of three representative reflections were measured after every 150 reflections. Over the course of data collection. the standards decreased by 4.5%. A linear correction factor was applied to the data to account for this phenomenon.

The linear absorption coefficient, μ, for Cu-Kα radiation is 21.6 cm^{-1}. An empirical absorption correction based on azimuthal scans of several reflections was applied which resulted in transmission factors ranging from 0.67 to 1.00. The data were corrected for Lorentz and polarization effects.

Structure Solution and Refinement

The structure was solved by direct methods[1] and expanded using Fourier techniques.[2] Some non-hydrogen atoms were refined anisotropically. some isotropically. and some were fixed. Hydrogen atoms were included but not refined. The final cycle of full-matrix least-squares refinement[3] was based on 3798 observed reflections ($I > 2.00\sigma(I)$) and 622 variable parameters and converged (largest parameter shift was 0.00 times its esd) with unweighted and weighted agreement factors of:

$$R = \Sigma \, ||F_o| - |F_c|| \, / \, \Sigma \, |F_o| = 0.062$$

$$R_w = [(\Sigma w \, (|F_o| - |F_c|)^2 \, / \, \Sigma w \, F_o^2)]^{1/2} = 0.064$$

The standard deviation of an observation of unit weight[4] was 2.85. The weighting scheme was based on counting statistics and included a factor ($p = 0.010$) to downweight the intense reflections. Plots of $\Sigma w \, (|F_o| - |F_c|)^2$ versus $|F_o|$, reflection order in data

collection. $\sin\theta/\lambda$ and various classes of indices showed no unusual trends. The maximum and minimum peaks on the final difference Fourier map corresponded to 0.41 and -0.56 $e^-/Å^3$, respectively.

Neutral atom scattering factors were taken from Cromer and Waber.[5] Anomalous dispersion effects were included in Fcalc:[6] the values for Df' and Df" were those of Creagh and McAuley.[7] The values for the mass attenuation coefficients are those of Creagh and Hubbell.[8] calculations were performed using the teXsan[9] crystallographic software package of Molecular Structure Corporation.

Table A5.1 Crystal data of the chiral binuclear Cu(II) complex

Empirical Formula	$C_{55}H_{76}O_9N_4Cu_2Cl_2$
Formula Weight	1135.22
Crystal Collor. Habit	dark-green. irregular plate
Crystal Dimensions	0.40 x 0.40 x 0.12 mm
Crystal System	orthorhombic
Lattice Type	primitive
No. of Reflections Used for Unit	
Cell Determination (2θ range)	25 (58.5 - 59.9°)
Omega Scan Peak Width	
at Half-height	0.33°
Lattice Parameters	a = 18.410(1) Å
	b = 25.200(1) Å
	c = 12.738(2) Å
	V = 5909.4(7) Å^3
Space Group	$P2_12_12_1$ (#19)
Z value	4
Dcalcd	1.276 g/cm^3
F000	2392.00
μ (Cu-Kα)	21.56 cm^{-1}

Table A5.2 Intensity measurements and structure solution and refinement

intensity measurements		structure solution and refinement	
Diffractometer	Rigaku AFC6S	Structure Solution	Direct Methods (SIR92)
Radiation	Cu-Kα (l = 1.54178 Å) graphite monochromated	Refinement	Full-matrix least-squares
		Function Minimized	$\Sigma w (\|F_o\| - \|F_c\|)^2$
		Least Squares Weights	$1/\sigma^2(F_o) = 4F_o^2/\sigma^2(F_o^2)$
Take-off Angle	6.0°	p-factor	0.0100
Detector Aperture	6.0 mm horizontal 3.0 mm vertical	Anomalous Dispersion	all non-hydrogen atoms
		No. Observations (I>2.00σ(I))	3798
Crystal to Detector Distance	400 mm	No. Variables	622
Voltage, Current	50 kV, 27mA	Reflection/Parameter Ratio	6.11
Temperature	26.0°C	Residuals: *R*; R_w	0.062 ; 0.064
Scan Type	ω-2θ	Goodness of Fit Indicator	2.85
Scan Rate	8.0°/min (in w) (10 scans)	Max Shift/Error in Final Cycle	0.00
Scan Width	(1.31 + 0.14 tanθ)°	Maximum peak in Final Diff. Map	0.41 e⁻/Å³
2θ max.	120.4°	Minimum peak in Final Diff. Map	-0.56 e⁻/Å³
No. of Reflections	4929		
Corrections	Lorentz-polarization absorption		
Trans. factors	0.6681 - 1.0000		
Decay	4.52% decline		

Table A5.3 Positional parameters and B(eq) for the chiral binuclear copper complex

atom	x	y	z	B(eq)
Cl(1)	0.4956(4)	0.3794(1)	0.5574(3)	23.4(2)
Cl(2)	0.5437	0.3617	0.7574	14.310
Cl(2)	0.5098	0.3152	0.7996	15.538
Cl(2)	0.4648	0.3331	0.7450	10.146
Cl(2)	0.4829	0.3767	0.7715	11.364
Cl(2)	0.5161	0.3213	0.7147	10.138
O(1)	0.5758(2)	0.5096(2)	0.8173(4)	4.7(1)
O(2)	0.4207(3)	0.5120(2)	0.8263(4)	5.4(1)
O(3)	0.4242(2)	0.1962(2)	0.6380(4)	4.6(1)
O(4)	0.5822(2)	0.1939(2)	0.6368(4)	4.0(1)
O(5)	0.4976(3)	0.6153(1)	0.7563(3)	5.66(9)
O(6)	0.5046(4)	0.1287(2)	0.4483(3)	7.9(1)
O(7)	0.6357(4)	0.0950(2)	0.5560(6)	9.5(2)
O(8)	0.3781(4)	0.0931(3)	0.5540(7)	11.4(3)
O(9)	0.7736	0.0862	0.6446	35.152
O(10)	0.1779	0.0843	0.6149	34.187
N(1)	0.5649(3)	0.5198(2)	0.6015(5)	4.4(1)
N(2)	0.4256(3)	0.5278(2)	0.6102(5)	4.7(1)
N(3)	0.4376(3)	0.2482(2)	0.4472(5)	4.2(1)
N(4)	0.5774(3)	0.2403(2)	0.4417(5)	4.2(1)
C(1)	0.6318(4)	0.4744(3)	0.7969(6)	5.0(2)
C(2)	0.6552(4)	0.4676(3)	0.6963(7)	4.4(2)
C(3)	0.7106(3)	0.4302(3)	0.6763(7)	4.4(2)
C(4)	0.7414(3)	0.3999(3)	0.7603(7)	4.4(2)
C(5)	0.7120(4)	0.4088(4)	0.8569(8)	6.1(3)
C(6)	0.6607(4)	0.4435(3)	0.8797(7)	4.4(2)
C(7)	0.6227(4)	0.4938(3)	0.8061(7)	5.2(2)
C(8)	0.5306(4)	0.5282(3)	0.5013(6)	5.6(2)
C(9)	0.5755(5)	0.5568(4)	0.4124(8)	7.1(3)
C(10)	0.5303(4)	0.5663(4)	0.3193(7)	7.3(2)
C(11)	0.4529(5)	0.5836(4)	0.3302(8)	8.6(3)
C(12)	0.4153(4)	0.5582(4)	0.4207(7)	5.4(2)
C(13)	0.4562(4)	0.5541(3)	0.5139(6)	5.1(2)
C(14)	0.3677(4)	0.4995(4)	0.6105(8)	6.0(2)
C(15)	0.3733(4)	0.4787(3)	0.8006(6)	4.1(2)
C(16)	0.3408(4)	0.4731(3)	0.6956(8)	5.0(2)
C(17)	0.2868(4)	0.4356(3)	0.6792(7)	5.1(2)
C(18)	0.2635(3)	0.4009(3)	0.7481(7)	4.9(2)
C(19)	0.2891(3)	0.4067(2)	0.8532(8)	4.6(2)
C(20)	0.3454(4)	0.4445(3)	0.8804(7)	5.0(2)
C(21)	0.2133(4)	0.3536(3)	0.7316(7)	4.9(2)
C(22)	0.3701(3)	0.2323(3)	0.6491(7)	4.1(2)
C(23)	0.3464(4)	0.2639(3)	0.5755(6)	4.1(2)
C(24)	0.2902(3)	0.3041(3)	0.6023(7)	4.7(2)
C(25)	0.2627(3)	0.3072(3)	0.6948(7)	4.3(2)
C(26)	0.2869(4)	0.2717(3)	0.7711(7)	5.2(2)
C(27)	0.3360(3)	0.2354(3)	0.7556(6)	3.8(2)
C(28)	0.3798(3)	0.2690(3)	0.4746(6)	4.2(2)
C(29)	0.4726(3)	0.2673(2)	0.3456(5)	4.1(1)
C(30)	0.4321(4)	0.2580(4)	0.2445(6)	6.9(2)

Table A5.3 (cont.)

atom	x	y	z	B(eq)
C(31)	0.4728(6)	0.2844(5)	0.1536(7)	9.3(3)
C(32)	0.5488(6)	0.2643(4)	0.1509(7)	8.1(3)
C(33)	0.5925(4)	0.2703(3)	0.2536(5)	5.0(2)
C(34)	0.5487(4)	0.2428(2)	0.3396(6)	4.8(2)
C(35)	0.6388(3)	0.2627(3)	0.4686(6)	4.4(2)
C(36)	0.6356(3)	0.2265(3)	0.6601(6)	3.5(2)
C(37)	0.6648(3)	0.2633(3)	0.5769(6)	4.1(2)
C(38)	0.7183(3)	0.2983(2)	0.6008(7)	4.6(2)
C(39)	0.7445(3)	0.3065(3)	0.7036(7)	4.7(2)
C(40)	0.7206(3)	0.2689(3)	0.7782(7)	4.5(2)
C(41)	0.6675(4)	0.2274(3)	0.7537(6)	4.7(2)
C(42)	0.7896(4)	0.3539(3)	0.7247(8)	6.2(2)
C(43)	0.6278(6)	0.4469(4)	0.9856(9)	7.7(3)
C(44)	0.594(1)	0.4016(7)	1.022(1)	28.3(9)
C(45)	0.6824(6)	0.4606(8)	1.0737(8)	18.1(6)
C(46)	0.3767(4)	0.4498(3)	0.9928(7)	5.6(2)
C(47)	0.3297(8)	0.4770(4)	1.0571(8)	11.7(4)
C(48)	0.3965(7)	0.3924(4)	1.038(1)	10.9(4)
C(49)	0.3611(5)	0.1917(4)	0.8382(8)	6.8(3)
C(50)	0.3410(6)	0.2114(6)	0.9454(7)	10.6(4)
C(51)	0.3111(5)	0.1382(3)	0.8168(8)	8.9(3)
C(52)	0.6462(5)	0.1936(4)	0.8385(9)	7.2(3)
C(53)	0.5582(6)	0.2185(4)	0.8825(7)	11.7(4)
C(54)	0.6818(6)	0.1939(5)	0.9398(9)	11.1(4)
C(55)	0.5177	0.3450	0.6404	5.483
C(56)	0.5136	0.3994	0.6747	4.362
C(57)	0.4722	0.3792	0.6989	5.805
C(58)	0.5408	0.3545	0.6768	5.219

Table A5.4 Intramolecular distances involving the nonhydrogen atoms in the binuclear copper complex

atom	atom	distance	atom	atom	distance
Cu(1)	O(1)	1.904(5)	Cl(2B)	C(55C)	1.6778(1)
Cu(1)	O(2)	1.978(5)	Cl(2B)	C(55B)	1.9029(1)
Cu(1)	N(1)	1.970(6)	Cl(2B)	C(55)	1.3088(1)
Cu(1)	N(2)	1.966(6)	Cl(2B)	C(55A)	1.7322(1)
Cu(2)	O(3)	1.964(5)	Cl(2C)	Cl(2D)	1.6870(1)
Cu(2)	O(4)	1.943(5)	Cl(2C)	C(55C)	1.9584(2)
Cu(2)	N(3)	1.937(6)	Cl(2C)	C(55B)	1.3943(1)
Cu(2)	N(4)	1.979(6)	Cl(2C)	C(55)	0.9473(1)
Cl(1)	C(55C)	1.426(4)	Cl(2C)	C(55A)	1.7039(1)
Cl(1)	C(55B)	1.550(4)	Cl(2D)	C(55C)	1.1196(1)
Cl(1)	C(55)	1.853(4)	Cl(2D)	C(55B)	1.7898(1)
Cl(1)	C(55A)	1.843(5)	Cl(2D)	C(55)	1.6793(1)
Cl(2)	Cl(2A)	1.4324(1)	Cl(2D)	C(55A)	1.067
Cl(2)	Cl(2B)	1.6297(1)	O(1)	C(1)	1.384(9)
Cl(2)	Cl(2C)	1.1964(1)	O(2)	C(15)	1.255(9)
Cl(2)	Cl(2D)	1.2610(1)	O(3)	C(22)	1.356(8)
Cl(2)	C(55C)	1.6199(2)	O(4)	C(36)	1.315(7)
Cl(2)	C(55B)	1.3804(1)	N(1)	C(7)	1.25(1)
Cl(2)	C(55)	1.5759(1)	N(1)	C(8)	1.44(1)
Cl(2)	C(55A)	1.0436(1)	N(2)	C(13)	1.50(1)
Cl(2A)	Cl(2B)	1.1728(1)	N(2)	C(14)	1.28(1)
Cl(2A)	Cl(2C)	1.6671(1)	N(3)	C(28)	1.236(8)
Cl(2A)	Cl(2D)	1.0982(1)	N(3)	C(29)	1.524(8)
Cl(2A)	C(55A)	1.9366(2)	N(4)	C(34)	1.417(9)
Cl(2B)	Cl(2C)	1.1966(1)	N(4)	C(35)	1.310(9)
Cl(2B)	Cl(2D)	1.0624(1)	C(1)	C(2)	1.36(1)

Table A5.4 (cont.)

atom	atom	distance	atom	atom	distance
C(1)	C(6)	1.41(1)	C(23)	C(24)	1.49(1)
C(2)	C(3)	1.41(1)	C(23)	C(28)	1.43(1)
C(2)	C(7)	1.46(1)	C(24)	C(25)	1.28(1)
C(3)	C(4)	1.43(1)	C(25)	C(26)	1.39(1)
C(4)	C(5)	1.36(1)	C(26)	C(27)	1.30(1)
C(4)	C(42)	1.53(1)	C(27)	C(49)	1.89(1)
C(5)	C(6)	1.32(1)	C(29)	C(30)	1.51(1)
C(6)	C(43)	1.48(1)	C(29)	C(34)	1.534(9)
C(8)	C(9)	1.58(1)	C(30)	C(31)	1.53(1)
C(8)	C(13)	1.52(1)	C(31)	C(32)	1.49(2)
C(9)	C(10)	1.47(1)	C(32)	C(33)	1.54(1)
C(10)	C(11)	1.50(1)	C(33)	C(34)	1.52(1)
C(11)	C(12)	1.49(1)	C(35)	C(37)	1.46(1)
C(12)	C(13)	1.41(1)	C(36)	C(37)	1.51(1)
C(14)	C(16)	1.36(1)	C(36)	C(41)	1.33(1)
C(15)	C(16)	1.47(1)	C(37)	C(38)	1.36(1)
C(15)	C(20)	1.43(1)	C(38)	C(39)	1.41(1)
C(16)	C(17)	1.39(1)	C(39)	C(40)	1.41(1)
C(17)	C(18)	1.31(1)	C(39)	C(42)	1.48(1)
C(18)	C(19)	1.43(1)	C(40)	C(41)	1.47(1)
C(18)	C(21)	1.52(1)	C(41)	C(52)	1.43(1)
C(19)	C(20)	1.45(1)	C(43)	C(44)	1.39(2)
C(20)	C(46)	1.55(1)	C(43)	C(45)	1.55(2)
C(21)	C(25)	1.56(1)	C(46)	C(47)	1.37(1)
C(22)	C(23)	1.31(1)	C(46)	C(48)	1.60(1)
C(22)	C(27)	1.50(1)	C(49)	C(50)	1.50(1)
C(49)	C(51)	1.65(1)	C(52)	C(53)	1.43(1)
C(52)	C(54)	1.45(2)	C(55C)	C(55B)	1.2011(1)
C(55C)	C(55)	1.4133(1)	C(55C)	C(55A)	0.672
C(55B)	C(55)	0.961	C(55B)	C(55A)	1.011
C(55)	C(55A)	1.4348(1)			

Distances are in angstroms. Estimated standard in the least significant figure are given in parentheses.

Table A5.5 Intramolecular bond angles involving nonhydrogen atoms

atom	atom	atom	angle	atom	atom	atom	angle
O(1)	Cu(1)	O(2)	94.8(2)	Cl(2B)	Cl(2)	Cl(2D)	40.6714(8)
O(1)	Cu(1)	N(1)	91.2(2)	Cl(2B)	Cl(2)	C(55C)	62.168(2)
O(1)	Cu(1)	N(2)	168.4(2)	Cl(2B)	Cl(2)	C(55B)	77.934(3)
O(2)	Cu(1)	N(1)	163.9(2)	Cl(2B)	Cl(2)	C(55)	49.156(3)
O(2)	Cu(1)	N(2)	89.8(2)	Cl(2B)	Cl(2)	C(55A)	77.3521(5)
N(1)	Cu(1)	N(2)	81.7(2)	Cl(2C)	Cl(2)	Cl(2D)	86.659(3)
O(3)	Cu(2)	O(4)	96.3(2)	Cl(2C)	Cl(2)	C(55C)	86.744(3)
O(3)	Cu(2)	N(3)	90.6(2)	Cl(2C)	Cl(2)	C(55B)	65.059(4)
O(3)	Cu(2)	N(4)	170.2(2)	Cl(2C)	Cl(2)	C(55)	36.848(5)
O(4)	Cu(2)	N(3)	165.2(2)	Cl(2C)	Cl(2)	C(55A)	98.816(1)
O(4)	Cu(2)	N(4)	89.0(2)	Cl(2D)	Cl(2)	C(55C)	43.5539(7)
N(3)	Cu(2)	N(4)	82.5(2)	Cl(2D)	Cl(2)	C(55B)	85.181(5)
C(55C)	Cl(1)	C(55B)	47.4(1)	Cl(2D)	Cl(2)	C(55)	71.616(4)
C(55C)	Cl(1)	C(55)	49.0(1)	Cl(2D)	Cl(2)	C(55A)	54.157(2)
C(55C)	Cl(1)	C(55A)	18.67(8)	C(55C)	Cl(2)	C(55B)	46.349(5)
C(55B)	Cl(1)	C(55)	27.52(9)	C(55C)	Cl(2)	C(55)	52.472(2)
C(55B)	Cl(1)	C(55A)	33.3(1)	C(55C)	Cl(2)	C(55A)	15.229(2)
C(55)	Cl(1)	C(55A)	45.7(1)	C(55B)	Cl(2)	C(55)	33.0363(7)
Cl(2A)	Cl(2)	Cl(2B)	44.459(2)	C(55B)	Cl(2)	C(55A)	46.817(5)
Cl(2A)	Cl(2)	Cl(2C)	78.145(3)	C(55)	Cl(2)	C(55A)	62.597(4)
Cl(2A)	Cl(2)	Cl(2D)	47.603(6)	Cl(2)	Cl(2A)	Cl(2B)	76.732(4)
Cl(2A)	Cl(2)	C(55C)	90.262(6)	Cl(2)	Cl(2A)	Cl(2C)	44.618(3)
Cl(2A)	Cl(2)	C(55B)	121.660(3)	Cl(2)	Cl(2A)	Cl(2D)	57.991(1)
Cl(2A)	Cl(2)	C(55)	92.441(4)	Cl(2)	Cl(2A)	C(55A)	31.843(1)
Cl(2A)	Cl(2)	C(55A)	101.759(4)	Cl(2B)	Cl(2A)	Cl(2C)	45.8697(3)
Cl(2B)	Cl(2)	Cl(2C)	47.080(3)	Cl(2B)	Cl(2A)	Cl(2D)	55.669(4)
Cl(2B)	Cl(2A)	C(55A)	62.103(5)	C(55C)	Cl(2B)	C(55B)	38.555(2)
Cl(2C)	Cl(2A)	Cl(2D)	71.8698(9)	C(55C)	Cl(2B)	C(55)	54.818(2)
Cl(2C)	Cl(2A)	C(55A)	55.935(2)	C(55C)	Cl(2B)	C(55A)	22.6403(4)
Cl(2D)	Cl(2A)	C(55A)	26.148(3)	C(55B)	Cl(2B)	C(55)	22.783(1)
Cl(2)	Cl(2B)	Cl(2A)	58.810(3)	C(55B)	Cl(2B)	C(55A)	31.870(1)
Cl(2)	Cl(2B)	Cl(2C)	47.0707(7)	C(55)	Cl(2B)	C(55A)	54.163(2)
Cl(2)	Cl(2B)	Cl(2D)	50.674(4)	Cl(2)	Cl(2C)	Cl(2A)	57.237(1)
Cl(2)	Cl(2B)	C(55C)	58.629(5)	Cl(2)	Cl(2C)	Cl(2B)	65.850(3)

Table A5.5 (cont.)

atom	atom	atom	angle	atom	atom	atom	angle
Cl(2A)	Cl(2B)	C(55A)	81.143(7)	Cl(2A)	Cl(2C)	C(55B)	106.364(2)
Cl(2C)	Cl(2B)	Cl(2D)	96.440(3)	Cl(2A)	Cl(2C)	C(55)	109.4383(9
Cl(2C)	Cl(2B)	C(55C)	84.118(4)	Cl(2A)	Cl(2C)	C(55A)	70.117(4)
Cl(2C)	Cl(2B)	C(55B)	46.949(5)	Cl(2B)	Cl(2C)	Cl(2D)	38.742(3)
Cl(2C)	Cl(2B)	C(55)	44.149(5)	Cl(2B)	Cl(2C)	C(55C)	59.453(2)
Cl(2C)	Cl(2B)	C(55A)	68.357(4)	Cl(2B)	Cl(2C)	C(55B)	94.211(5)
Cl(2D)	Cl(2B)	C(55C)	41.007(1)	Cl(2B)	Cl(2C)	C(55)	74.224(2)
Cl(2D)	Cl(2B)	C(55B)	67.513(3)	Cl(2B)	Cl(2C)	C(55A)	70.893(3)
Cl(2D)	Cl(2B)	C(55)	89.559(3)	Cl(2D)	Cl(2C)	C(55C)	34.7697(4)
Cl(2D)	Cl(2B)	C(55A)	35.644(2)	Cl(2D)	Cl(2C)	C(55B)	70.289(4)
Cl(2D)	Cl(2C)	C(55)	73.215(4)	Cl(2C)	Cl(2D)	C(55C)	85.995(7)
Cl(2D)	Cl(2C)	C(55A)	36.6708(9)	Cl(2C)	Cl(2D)	C(55B)	47.172(5)
C(55C)	Cl(2C)	C(55B)	37.428(4)	Cl(2C)	Cl(2D)	C(55)	32.686(4)
C(55C)	Cl(2C)	C(55)	42.506(5)	Cl(2C)	Cl(2D)	C(55A)	72.530(5)
C(55C)	Cl(2C)	C(55A)	19.584(1)	C(55C)	Cl(2D)	C(55B)	41.227(2)
C(55B)	Cl(2C)	C(55)	37.354(5)	C(55C)	Cl(2D)	C(55)	56.488(2)
C(55B)	Cl(2C)	C(55A)	36.400(3)	C(55C)	Cl(2D)	C(55A)	35.667(1)
C(55)	Cl(2C)	C(55A)	57.342(6)	C(55B)	Cl(2D)	C(55)	28.519(2)
Cl(2)	Cl(2D)	Cl(2A)	74.406(5)	C(55B)	Cl(2D)	C(55A)	29.659(2)
Cl(2)	Cl(2D)	Cl(2B)	68.855(4)	C(55)	Cl(2D)	C(55A)	57.984(4)
Cl(2)	Cl(2D)	Cl(2C)	45.074(3)	Cu(1)	O(1)	C(1)	124.6(5)
Cl(2)	Cl(2D)	C(55C)	85.542(7)	Cu(1)	O(2)	C(15)	116.2(5)
Cl(2)	Cl(2D)	C(55B)	50.223(5)	Cu(2)	O(3)	C(22)	118.7(4)
Cl(2)	Cl(2D)	C(55)	62.937(4)	Cu(2)	O(4)	C(36)	123.2(4)
Cl(2)	Cl(2D)	C(55A)	52.467(6)	Cu(1)	N(1)	C(7)	121.6(6)
Cl(2A)	Cl(2D)	Cl(2B)	65.722(2)	Cu(1)	N(1)	C(8)	114.4(4)
Cl(2A)	Cl(2D)	Cl(2C)	69.909(4)	C(7)	N(1)	C(8)	119.5(7)
Cl(2A)	Cl(2D)	C(55C)	155.490(3)	Cu(1)	N(2)	C(13)	110.7(4)
Cl(2A)	Cl(2D)	C(55B)	114.392(1)	Cu(1)	N(2)	C(14)	123.1(6)
Cl(2A)	Cl(2D)	C(55)	100.9573(7	C(13)	N(2)	C(14)	124.0(7)
Cl(2A)	Cl(2D)	C(55A)	126.972(2)	Cu(2)	N(3)	C(28)	124.7(5)
Cl(2B)	Cl(2D)	Cl(2C)	44.818(1)	Cu(2)	N(3)	C(29)	113.8(4)
Cl(2B)	Cl(2D)	C(55C)	100.484(4)	C(28)	N(3)	C(29)	118.1(6)

Table A5.5 (cont)

atom	atom	atom	angle	atom	atom	atom	angle
Cl(2B)	Cl(2D)	C(55B)	79.225(2)	Cu(2)	N(4)	C(34)	110.7(4)
Cl(2B)	Cl(2D)	C(55)	51.197(2)	Cu(2)	N(4)	C(35)	125.2(5)
Cl(2B)	Cl(2D)	C(55A)	108.881(3)	C(34)	N(4)	C(35)	123.0(6)
C(1)	C(1)	C(2)	119.5(8)	O(2)	C(15)	C(16)	125.7(7)
O(1)	C(1)	C(6)	119.5(9)	O(2)	C(15)	C(20)	117.9(7)
C(2)	C(1)	C(6)	120.9(7)	C(16)	C(15)	C(20)	116.3(7)
C(1)	C(2)	C(3)	118.8(8)	C(14)	C(16)	C(15)	121.9(7)
C(1)	C(2)	C(7)	123.7(7)	C(14)	C(16)	C(17)	118.2(8)
C(3)	C(2)	C(7)	117.3(8)	C(15)	C(16)	C(17)	119.5(8)
C(2)	C(3)	C(4)	120.6(8)	C(16)	C(17)	C(18)	126.1(8)
C(3)	C(4)	C(5)	118.3(7)	C(17)	C(18)	C(19)	116.8(7)
C(3)	C(4)	C(42)	114.5(8)	C(17)	C(18)	C(21)	129.0(8)
C(5)	C(4)	C(42)	128.6(8)	C(19)	C(18)	C(21)	114.2(7)
C(4)	C(5)	C(6)	126.4(9)	C(18)	C(19)	C(20)	121.8(7)
C(1)	C(6)	C(5)	118.0(8)	C(15)	C(20)	C(19)	118.9(8)
C(1)	C(6)	C(43)	119.5(7)	C(15)	C(20)	C(46)	118.2(7)
C(5)	C(6)	C(43)	122.2(8)	C(19)	C(20)	C(46)	122.8(8)
N(1)	C(7)	C(2)	128.7(8)	C(18)	C(21)	C(25)	106.0(6)
N(1)	C(8)	C(9)	118.3(6)	O(3)	C(22)	C(23)	125.4(7)
N(1)	C(8)	C(13)	111.4(6)	O(3)	C(22)	C(27)	116.0(6)
C(9)	C(8)	C(13)	110.6(6)	C(23)	C(22)	C(27)	118.6(6)
C(8)	C(9)	C(10)	110.9(7)	C(22)	C(23)	C(24)	119.8(7)
C(9)	C(10)	C(11)	120.8(8)	C(22)	C(23)	C(28)	123.8(7)
C(10)	C(11)	C(12)	112.9(8)	C(24)	C(23)	C(28)	116.4(6)
C(11)	C(12)	C(13)	115.9(7)	C(23)	C(24)	C(25)	121.8(7)
N(2)	C(13)	C(8)	103.5(5)	C(21)	C(25)	C(24)	123.6(7)
N(2)	C(13)	C(12)	121.2(6)	C(21)	C(25)	C(26)	117.4(7)
C(8)	C(13)	C(12)	115.3(7)	C(24)	C(25)	C(26)	118.3(7)
N(2)	C(14)	C(16)	125.1(9)	C(25)	C(26)	C(27)	124.6(8)
C(22)	C(27)	C(26)	117.8(7)	C(36)	C(41)	C(40)	119.9(7)
C(22)	C(27)	C(49)	116.2(6)	C(36)	C(41)	C(52)	123.0(7)
C(26)	C(27)	C(49)	126.0(7)	C(40)	C(41)	C(52)	116.6(7)
N(3)	C(28)	C(23)	125.9(7)	C(4)	C(42)	C(39)	109.9(6)
N(3)	C(29)	C(30)	117.9(5)	C(6)	C(43)	C(44)	116(1)
N(3)	C(29)	C(34)	108.0(5)	C(6)	C(43)	C(45)	114.1(8)

Table A5.5 (cont)

atom	atom	atom	angle	atom	atom	atom	angle
C(30)	C(29)	C(34)	109.9(6)	C(44)	C(43)	C(45)	104(1)
C(29)	C(30)	C(31)	109.6(7)	C(20)	C(46)	C(47)	111.1(8)
C(30)	C(31)	C(32)	109.2(8)	C(20)	C(46)	C(48)	109.8(7)
C(31)	C(32)	C(33)	116.0(8)	C(47)	C(46)	C(48)	112.5(8)
C(32)	C(33)	C(34)	106.4(6)	C(27)	C(49)	C(50)	107.6(8)
N(4)	C(34)	C(29)	107.7(5)	C(27)	C(49)	C(51)	107.0(7)
N(4)	C(34)	C(33)	118.9(6)	C(50)	C(49)	C(51)	106.4(8)
N(4)	C(35)	C(37)	122.3(6)	C(41)	C(52)	C(54)	123.1(8)
O(4)	C(36)	C(37)	119.6(6)	C(53)	C(52)	C(54)	97.3(8)
O(4)	C(36)	C(41)	122.9(7)	Cl(1)	C(55C)	Cl(2)	127.6(1)
C(37)	C(36)	C(41)	117.5(6)	Cl(1)	C(55C)	Cl(2B)	122.1(3)
C(35)	C(37)	C(36)	122.8(6)	Cl(1)	C(55C)	Cl(2C)	106.9(2)
C(35)	C(37)	C(38)	117.1(7)	Cl(1)	C(55C)	Cl(2D)	160.5(3)
C(36)	C(37)	C(38)	120.1(7)	Cl(1)	C(55C)	C(55B)	71.8(1)
C(37)	C(38)	C(39)	123.4(7)	Cl(1)	C(55C)	C(55)	81.5(2)
C(38)	C(39)	C(40)	115.0(6)	Cl(1)	C(55C)	C(55A)	118.5(2)
C(38)	C(39)	C(42)	118.5(7)	Cl(2)	C(55C)	Cl(2B)	59.203(7)
C(40)	C(39)	C(42)	126.4(8)	Cl(2)	C(55C)	Cl(2C)	37.584(5)
C(39)	C(40)	C(41)	122.9(7)	Cl(2)	C(55C)	Cl(2D)	50.904(6)
Cl(2)	C(55C)	C(55B)	56.260(1)	Cl(2)	C(55B)	Cl(2C)	51.094(6)
Cl(2)	C(55C)	C(55)	62.162(5)	Cl(2)	C(55B)	Cl(2D)	44.5957(9)
Cl(2)	C(55C)	C(55A)	24.096(1)	Cl(2)	C(55B)	C(55C)	77.391(6)
Cl(2B)	C(55C)	Cl(2C)	37.430(4)	Cl(2)	C(55B)	C(55)	86.053(5)
Cl(2B)	C(55C)	Cl(2D)	38.510(4)	Cl(2)	C(55B)	C(55A)	48.800(4)
Cl(2B)	C(55C)	C(55B)	80.910(4)	Cl(2B)	C(55B)	Cl(2C)	35.839(1)
Cl(2B)	C(55C)	C(55)	49.187(3)	Cl(2B)	C(55B)	Cl(2D)	33.263(2)
Cl(2B)	C(55C)	C(55A)	83.232(8)	Cl(2B)	C(55B)	C(55C)	60.535(5)
Cl(2C)	C(55C)	Cl(2D)	59.235(7)	Cl(2B)	C(55B)	C(55)	36.0512(9)
Cl(2C)	C(55C)	C(55B)	44.8720(3)	Cl(2B)	C(55B)	C(55A)	64.724(4)
Cl(2C)	C(55C)	C(55)	26.9267(2)	Cl(2C)	C(55B)	Cl(2D)	62.540(1)
Cl(2C)	C(55C)	C(55A)	58.276(6)	Cl(2C)	C(55B)	C(55C)	97.700(4)
Cl(2D)	C(55C)	C(55B)	100.869(7)	Cl(2C)	C(55B)	C(55)	41.8658(5)
Cl(2D)	C(55C)	C(55)	82.176(6)	Cl(2C)	C(55B)	C(55A)	88.707(2)
Cl(2D)	C(55C)	C(55A)	67.876(6)	Cl(2D)	C(55B)	C(55C)	37.903(5)
C(55B)	C(55C)	C(55)	37.361(2)	Cl(2D)	C(55B)	C(55)	68.602(2)
C(55B)	C(55C)	C(55A)	57.336(2)	Cl(2D)	C(55B)	C(55A)	31.463(2)

Table A5.5 (cont.)

atom	atom	atom	angle	atom	atom	atom	angle
C(55)	C(55C)	C(55A)	79.152(6)	C(55C)	C(55B)	C(55)	84.822(3)
Cl(1)	C(55B)	Cl(2D)	97.1(1)	Cl(1)	C(55)	Cl(2B)	117.56(9)
Cl(1)	C(55B)	C(55C)	60.9(1)	Cl(1)	C(55)	Cl(2C)	154.4(2)
Cl(1)	C(55B)	C(55)	96.2(2)	Cl(1)	C(55)	Cl(2D)	90.4(1)
Cl(1)	C(55B)	C(55A)	89.5(2)	Cl(1)	C(55)	C(55C)	49.3(2)
Cl(2)	C(55B)	Cl(2B)	56.981(4)	Cl(1)	C(55)	C(55B)	56.3(2)
Cl(1)	C(55)	C(55A)	66.9(2)	Cl(1)	C(55A)	Cl(2D)	116.6(2)
Cl(2)	C(55)	Cl(2B)	68.076(3)	Cl(1)	C(55A)	C(55C)	42.8(1)
Cl(2)	C(55)	Cl(2C)	49.239(2)	Cl(1)	C(55A)	C(55B)	57.2(1)
Cl(2)	C(55)	Cl(2D)	45.447(1)	Cl(1)	C(55A)	C(55)	67.5(2)
Cl(2)	C(55)	C(55C)	65.366(6)	Cl(2)	C(55A)	Cl(2A)	46.397(5)
Cl(2)	C(55)	C(55B)	60.911(6)	Cl(2)	C(55A)	Cl(2B)	66.641(4)
Cl(2)	C(55)	C(55A)	40.222(5)	Cl(2)	C(55A)	Cl(2C)	43.937(4)
Cl(2B)	C(55)	Cl(2C)	61.627(3)	Cl(2)	C(55A)	Cl(2D)	73.376(5)
Cl(2B)	C(55)	Cl(2D)	39.245(3)	Cl(2)	C(55A)	C(55C)	140.675(3)
Cl(2B)	C(55)	C(55C)	75.996(5)	Cl(2)	C(55A)	C(55B)	84.383(1)
Cl(2B)	C(55)	C(55B)	121.166(2)	Cl(2)	C(55A)	C(55)	77.182(2)
Cl(2B)	C(55)	C(55A)	78.152(3)	Cl(2A)	C(55A)	Cl(2B)	86.754(1)
Cl(2C)	C(55)	Cl(2D)	74.099(1)6	Cl(2A)	C(55A)	Cl(2C)	54.049(5)
Cl(2C)	C(55)	C(55C)	110.568(5)	Cl(2A)	C(55A)	Cl(2D)	26.9799(6)
Cl(2C)	C(55)	C(55B)	100.791(4)	Cl(2A)	C(55A)	C(55C)	100.996(7)
Cl(2C)	C(55)	C(55A)	88.891(3)	Cl(2A)	C(55A)	C(55B)	109.759(3)
Cl(2D)	C(55)	C(55C)	41.336(4)	Cl(2A)	C(55A)	C(55)	79.779(3)
Cl(2D)	C(55)	C(55B)	82.979(3)	Cl(2B)	C(55A)	Cl(2C)	40.750(3)
Cl(2D)	C(55)	C(55A)	39.089(1)	Cl(2B)	C(55A)	Cl(2D)	35.475(1)
C(55C)	C(55)	C(55B)	57.818(3)	Cl(2B)	C(55A)	C(55C)	74.129(8)
C(55C)	C(55)	C(55A)	27.259(1)	Cl(2B)	C(55A)	C(55B)	83.406(3)
C(55B)	C(55)	C(55A)	44.010(3)	Cl(2B)	C(55A)	C(55)	47.685(3)
Cl(1)	C(55A)	Cl(2)	140.9(1)	Cl(2C)	C(55A)	Cl(2D)	70.799(4)
Cl(1)	C(55A)	Cl(2A)	135.0(2)	Cl(2C)	C(55A)	C(55C)	102.140(7)
Cl(1)	C(55A)	Cl(2B)	98.9(2)	Cl(2C)	C(55A)	C(55B)	54.693(3)
Cl(1)	C(55A)	Cl(2C)	101.0(2)	Cl(2C)	C(55A)	C(55)	33.767(3)
Cl(2D)	C(55A)	C(55C)	76.457(7)	Cl(2D)	C(55A)	C(55B)	119.879(4)
Cl(2D)	C(55A)	C(55)	82.934(4)	C(55C)	C(55A)	C(55B)	86.684(3)
C(55C)	C(55A)	C(55)	74.589(5)	C(55B)	C(55A)	C(55)	36.2690(6)

Table A5.6 Torsion or conformation angles in the binuclear copper complex

(1)	(2)	(3)	(4)	angle	(1)	(2)	(3)	(4)	angle
Cu(1)	O(1)	C(1)	C(2)	31.0(9)	Cu(1)	O(1)	C(1)	C(6)	-144.9(6)
Cu(1)	O(2)	C(15)	C(16)	-40.6(9)	Cu(1)	O(2)	C(15)	C(20)	142.6(6)
Cu(1)	N(1)	C(7)	C(2)	-6(1)	Cu(1)	N(1)	C(8)	C(9)	145.5(6)
Cu(1)	N(1)	C(8)	C(13)	15.8(7)	Cu(1)	N(2)	C(13)	C(8)	45.6(6)
Cu(1)	N(2)	C(13)	C(12)	176.5(6)	Cu(1)	N(2)	C(14)	C(16)	15(1)
Cu(2)	O(3)	C(22)	C(23)	32.2(9)	Cu(2)	O(3)	C(22)	C(27)	-147.4(5)
Cu(2)	O(4)	C(36)	C(37)	-35.4(8)	Cu(2)	O(4)	C(36)	C(41)	147.2(6)
Cu(2)	N(3)	C(28)	C(23)	-10(1)	Cu(2)	N(3)	C(29)	C(30)	135.5(6)
Cu(2)	N(3)	C(29)	C(34)	10.4(6)	Cu(2)	N(4)	C(34)	C(29)	45.7(6)
Cu(2)	N(4)	C(34)	C(33)	171.7(5)	Cu(2)	N(4)	C(35)	C(37)	8(1)
O(1)	Cu(1)	O(2)	C(15)	-124.8(5)	O(1)	Cu(1)	N(1)	C(7)	23.2(7)
O(1)	Cu(1)	N(1)	C(8)	179.2(5)	O(1)	Cu(1)	N(2)	C(13)	-84(1)
O(1)	Cu(1)	N(2)	C(14)	79(1)	O(1)	C(1)	C(2)	C(3)	-177.8(6)
O(1)	C(1)	C(2)	C(7)	-3(1)	O(1)	C(1)	C(6)	C(5)	177.3(7)
O(1)	C(1)	C(6)	C(43)	4(1)	O(4)	C(36)	C(41)	C(40)	-172.7(6)
O(2)	Cu(1)	O(1)	C(1)	128.6(6)	O(4)	C(36)	C(41)	C(52)	-1(1)
O(2)	Cu(1)	N(1)	C(7)	-89(1)	N(1)	Cu(1)	O(1)	C(1)	-36.4(6)
O(2)	Cu(1)	N(1)	C(8)	67(1)	N(1)	Cu(1)	O(2)	C(15)	-13(1)
O(2)	Cu(1)	N(2)	C(13)	162.4(5)	N(1)	Cu(1)	N(2)	C(13)	-31.4(4)
O(2)	Cu(1)	N(2)	C(14)	-34.0(7)	N(1)	Cu(1)	N(2)	C(14)	132.3(7)
O(2)	C(15)	C(16)	C(14)	10(1)	N(1)	C(7)	C(2)	C(1)	-11(1)
O(2)	C(15)	C(16)	C(17)	-177.7(7)	N(1)	C(7)	C(2)	C(3)	164.7(8)
O(2)	C(15)	C(20)	C(19)	179.3(6)	N(1)	C(8)	C(9)	C(10)	-175.0(7)
O(2)	C(15)	C(20)	C(46)	-1(1)	N(1)	C(8)	C(13)	N(2)	-38.5(7)
O(3)	Cu(2)	O(4)	C(36)	-125.6(5)	N(1)	C(8)	C(13)	C(12)	-173.0(6)
O(3)	Cu(2)	N(3)	C(28)	25.5(6)	N(2)	Cu(1)	O(1)	C(1)	16(1)
O(3)	Cu(2)	N(3)	C(29)	-176.0(4)	N(2)	Cu(1)	O(2)	C(15)	44.5(5)
O(3)	Cu(2)	N(4)	C(34)	-79(1)	N(2)	Cu(1)	N(1)	C(7)	-147.6(7)
O(3)	Cu(2)	N(4)	C(35)	91(1)	N(2)	Cu(1)	N(1)	C(8)	8.5(5)
O(3)	C(22)	C(23)	C(24)	-175.5(6)	N(2)	C(13)	C(8)	C(9)	-172.1(6)
O(3)	C(22)	C(23)	C(28)	-7(1)	N(2)	C(13)	C(12)	C(11)	-178.2(7)
O(3)	C(22)	C(27)	C(26)	175.9(6)	N(2)	C(14)	C(16)	C(15)	6(1)
O(3)	C(22)	C(27)	C(49)	-6.8(9)	N(2)	C(14)	C(16)	C(17)	-166.8(8)

Table A5.6 Torsion or conformation angles (cont.)

(1)	(2)	(3)	(4)	angle	(1)	(2)	(3)	(4)	angle
O(4)	Cu(2)	O(3)	C(22)	132.1(5)	N(3)	Cu(2)	O(3)	C(22)	-34.8(5)
O(4)	Cu(2)	N(3)	C(28)	-92(1)	N(3)	Cu(2)	O(4)	C(36)	-8(1)
O(4)	Cu(2)	N(3)	C(29)	66(1)	N(3)	Cu(2)	N(4)	C(34)	-32.6(4)
O(4)	Cu(2)	N(4)	C(34)	159.5(4)	N(3)	Cu(2)	N(4)	C(35)	135.8(6)
O(4)	Cu(2)	N(4)	C(35)	-32.1(6)	N(3)	C(29)	C(23)	C(22)	-6(1)
O(4)	C(36)	C(37)	C(35)	-3(1)	N(3)	C(29)	C(23)	C(24)	162.3(7)
O(4)	C(36)	C(37)	C(38)	177.9(6)	N(3)	C(29)	C(30)	C(31)	174.8(7)
N(3)	C(29)	C(34)	N(4)	-35.5(6)	C(5)	C(4)	C(42)	C(39)	79(1)
N(3)	C(29)	C(34)	C(33)	-166.6(5)	C(5)	C(6)	C(43)	C(44)	-59(1)
N(4)	Cu(2)	O(3)	C(22)	10(2)	C(5)	C(6)	C(43)	C(45)	61(1)
N(4)	Cu(2)	O(4)	C(36)	46.1(5)	C(6)	C(1)	C(2)	C(7)	173.2(7)
N(4)	Cu(2)	N(3)	C(28)	-147.7(6)	C(6)	C(5)	C(4)	C(42)	-167.1(8)
N(4)	Cu(2)	N(3)	C(29)	10.9(4)	C(7)	N(1)	C(8)	C(9)	-58(1)
N(4)	C(34)	C(29)	C(30)	-165.2(6)	C(7)	N(1)	C(8)	C(13)	170.4(7)
N(4)	C(34)	C(33)	C(32)	177.7(6)	C(8)	C(9)	C(10)	C(11)	40(1)
N(4)	C(35)	C(37)	C(36)	17(1)	C(8)	C(13)	N(2)	C(14)	-117.9(8)
N(4)	C(35)	C(37)	C(38)	-163.7(7)	C(8)	C(13)	C(12)	C(11)	-52(1)
C(1)	C(2)	C(3)	C(4)	0(1)	C(9)	C(8)	C(13)	C(12)	53.4(9)
C(1)	C(6)	C(5)	C(4)	1(1)	C(9)	C(10)	C(11)	C(12)	-37(1)
C(1)	C(6)	C(43)	C(44)	114(1)	C(10)	C(9)	C(8)	C(13)	-45(1)
C(1)	C(6)	C(43)	C(45)	-126(1)	C(10)	C(11)	C(12)	C(13)	42(1)
C(2)	C(1)	C(6)	C(5)	1(1)	C(12)	C(13)	N(2)	C(14)	13(1)
C(2)	C(1)	C(6)	C(43)	-172.3(8)	C(13)	N(2)	C(14)	C(16)	176.5(8)
C(2)	C(3)	C(4)	C(5)	2(1)	C(14)	C(16)	C(15)	C(20)	-173.2(8)
C(2)	C(3)	C(4)	C(42)	168.7(6)	C(14)	C(16)	C(17)	C(18)	168.2(8)
C(2)	C(7)	N(1)	C(8)	-160.5(8)	C(15)	C(16)	C(17)	C(18)	-4(1)
C(3)	C(2)	C(1)	C(6)	-2(1)	C(15)	C(20)	C(19)	C(18)	3(1)
C(3)	C(4)	C(5)	C(6)	-2(1)	C(15)	C(20)	C(46)	C(47)	102.6(9)
C(3)	C(4)	C(42)	C(39)	-85.5(9)	C(15)	C(20)	C(46)	C(48)	-132.3(8)
C(4)	C(3)	C(2)	C(7)	-175.2(6)	C(16)	C(15)	C(20)	C(19)	1(1)
C(4)	C(5)	C(6)	C(43)	174.5(8)	C(16)	C(15)	C(20)	C(46)	-178.6(7)
C(4)	C(42)	C(39)	C(38)	91.7(9)	C(16)	C(17)	C(18)	C(19)	9(1)
C(4)	C(42)	C(39)	C(40)	-84.4(9)	C(16)	C(17)	C(18)	C(21)	-169.9(7)

Table A5.6 (cont)

(1) (2) (3) (4)	angle	(1) (2) (3) (4)	angle
C(17)C(16)C(15)C(20)	-1(1)	C(27)C(22)C(23)C(28)	172.5(6)
C(17)C(18)C(19)C(20)	-8(1)	C(28)N(3) C(29)C(30)	-64.4(9)
C(17)C(18)C(21)C(25)	95.0(9)	C(28)N(3) C(29)C(34)	170.5(6)
C(18)C(19)C(20)C(46)	-177.1(7)	C(29)C(30)C(31)C(32)	56(1)
C(18)C(21)C(25)C(24)	-74.3(9)	C(29)C(34)N(4) C(35)	-123.0(7)
C(19)C(21)C(25)C(26)	95.7(8)	C(29)C(34)C(33)C(32)	-57.4(8)
C(19)C(18)C(21)C(25)	-93.5(8)	C(30)C(29)C(34)C(33)	63.7(7)
C(19)C(20)C(46)C(47)	-77(1)	C(30)C(31)C(32)C(33)	-55(1)
C(19)C(20)C(46)C(48)	46(1)	C(31)C(30)C(29)C(34)	-61.0(9)
C(20)C(19)C(18)C(21)	170.9(6)	C(31)C(32)C(33)C(34)	56(1)
C(21)C(25)C(24)C(23)	170.0(6)	C(33)C(34)N(4) C(35)	3.0(9)
C(21)C(25)C(26)C(27)	-170.2(7)	C(34)N(4) C(35)C(37)	175.1(6)
C(22)C(23)C(24)C(25)	-3(1)	C(35)C(37)C(36)C(41)	174.4(7)
C(22)C(27)C(26)C(25)	1(1)	C(35)C(37)C(38)C(39)	174.6(6)
C(22)C(27)C(49)C(50)	161.9(7)	C(36)C(37)C(38)C(39)	-6(1)
C(22)C(27)C(49)C(51)	-84.1(8)	C(36)C(41)C(40)C(39)	-5(1)
C(23)C(22)C(27)C(26)	-4(1)	C(36)C(41)C(52)C(53)	-71(1)
C(23)C(22)C(27)C(49)	173.5(7)	C(36)C(41)C(52)C(54)	176.8(9)
C(23)C(24)C(25)C(26)	0(1)	C(37)C(36)C(41)C(40)	10(1)
C(23)C(28)N(3) C(29)	-167.4(6)	C(37)C(36)C(41)C(52)	-178.5(7)
C(24)C(23)C(22)C(27)	4(1)	C(37)C(38)C(39)C(40)	11(1)
C(24)C(25)C(26)C(27)	0(1)	C(37)C(38)C(39)C(42)	-165.6(7)
C(25)C(24)C(23)C(28)	-171.7(7)	C(38)C(37)C(36)C(41)	-5(1)
C(25)C(26)C(27)C(49)	-176.5(7)	C(38)C(39)C(40)C(41)	-5(1)
C(26)C(27)C(49)C(50)	-21(1)	C(39)C(40)C(41)C(52)	-177.4(7)
C(26)C(27)C(49)C(51)	92.9(9)	C(40)C(41)C(52)C(53)	100.7(8)
C(40)C(41)C(52)C(54)	-9(1)	C(41)C(40)C(39)C(42)	170.9(7)

References for X-ray studies

1. a) Sheldrick, G. M. In *Crystallographic Computing 3*. Sheldrick, G. M.; Kruger, C.; Goddard, R. Eds.: Oxford University Press. **1985**. b) Walker, N.; Stuart, A. *Acta Cryst.* **1983**. A39, 158.

2. Admiraal, P. T.; Beurskens, G.; Bosman, G.; de Gelder, W. P.; Israel, R.; Smits, J. M. M. *The DIRDIF-94 Program System* In *Technical Report of the Crystallography Laboratory* **1994**. University of Nijmegen, The Netherlands.

3. Least Squares function minimized:

$\Sigma w(|F_o|-|F_c|)^2$ where $w = 1/[\sigma^2(Fo)] = [\sigma^2_c(Fo) + p^2Fo^2/4]^{-1}$, $s_c(Fo)$ = e.s.d. based on counting statistics. p = p-factor

4. Standard deviation of an observation of unit weight:

$[\Sigma w(|F_o|-|F_c|)^2/(N_o-N_v)]^{1/2}$

where N_o = number of observations, N_v = number of variables

5. Cromer, D. T.; Waber, J. T. *International Tables for X-ray Crystallography*, Vol. IV, Table 2.2 A: The Kynoch Press: Birmingham. **1974**.

6. Ibers, J. A.; Hamilton, W. C. *Acta Cryst.* **1964**. *17*, 781.

7. Creagh, D. C.; McAuley, W. J. *International Tables for Crystallography*, Vol. C, Table 4.2.6.8, p. 219-222, Wilson, A. J. C. Ed.: Kluwer Academic Publishers: Boston. **1992**.

8. Creagh, D. C.; Hubbell, J. H. *International Tables for Crystallography*, Vol. C, Table 4.2.4.3, p.200-206. Wilson, A. J. C., Ed.: Kluwer Academic Publishers: Boston. **1992**.

9. TeXsan for Windows *Crystal Structure Analysis Package*, Molecular Structure Corporation. **1997**.

Appendix 6

Selected ^{1}H. ^{13}C NMR and ESMS spectra

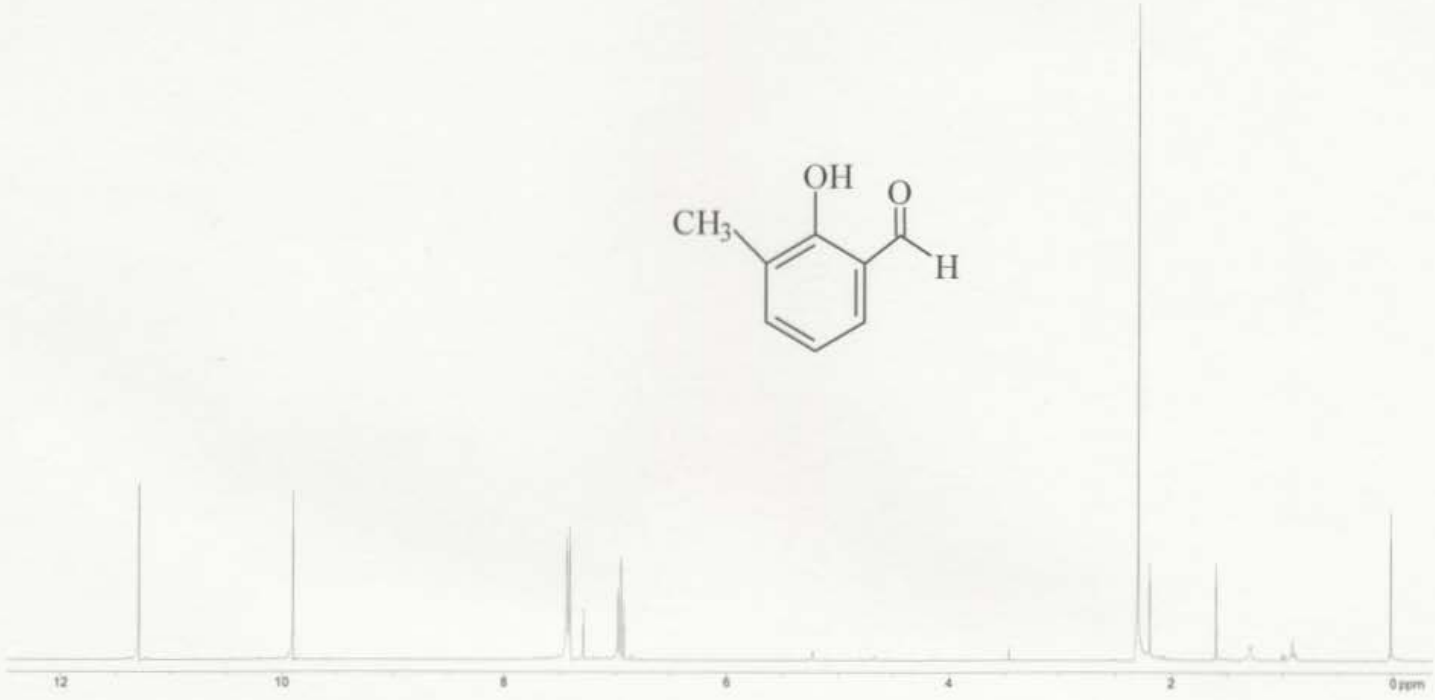

Figure A2.1 ^{1}H NMR spectrum of the salicylaldehyde **2b** in $CDCl_3$

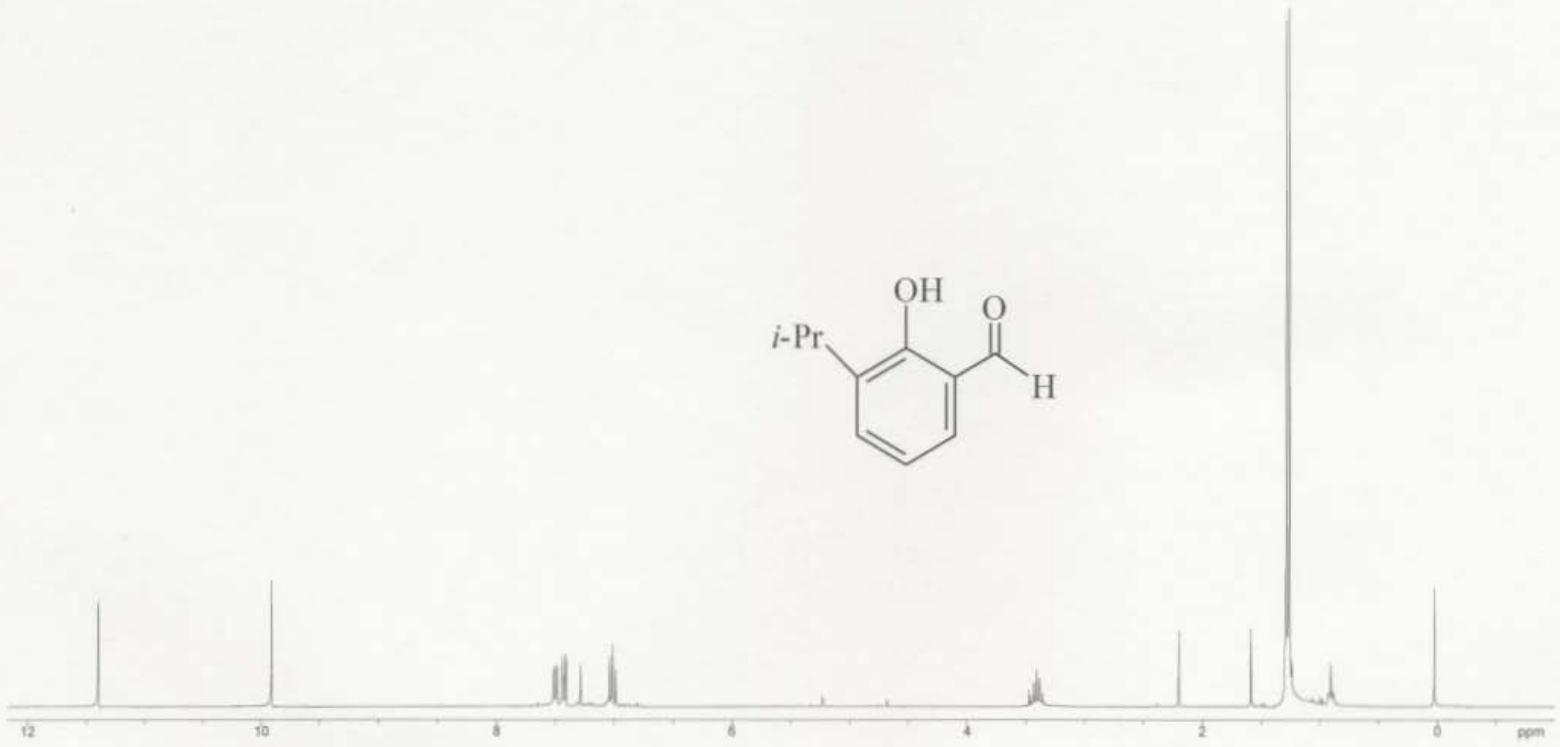

Figure A2.2 ^{1}H NMR spectrum of the salicylaldehyde **2c** in $CDCl_3$

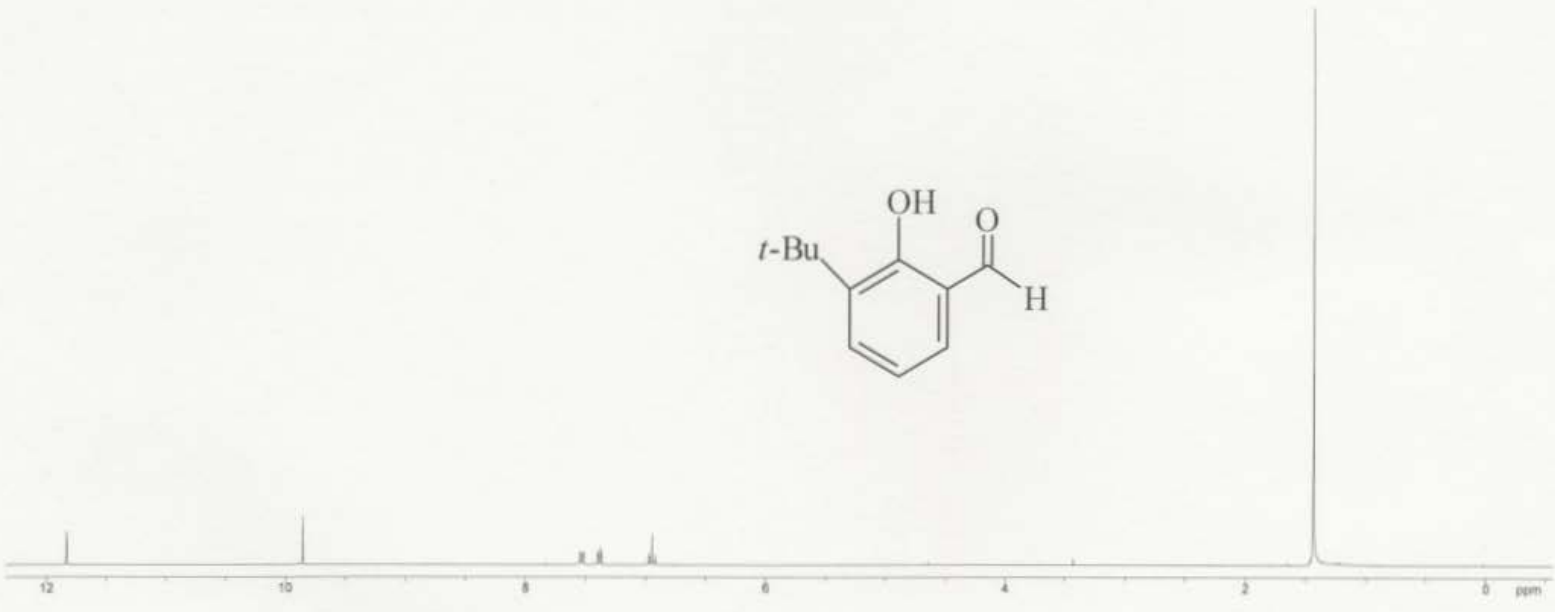

Figure A2.3 ^{1}H NMR spectrum of the salicylaldehyde **2d** in $CDCl_3$

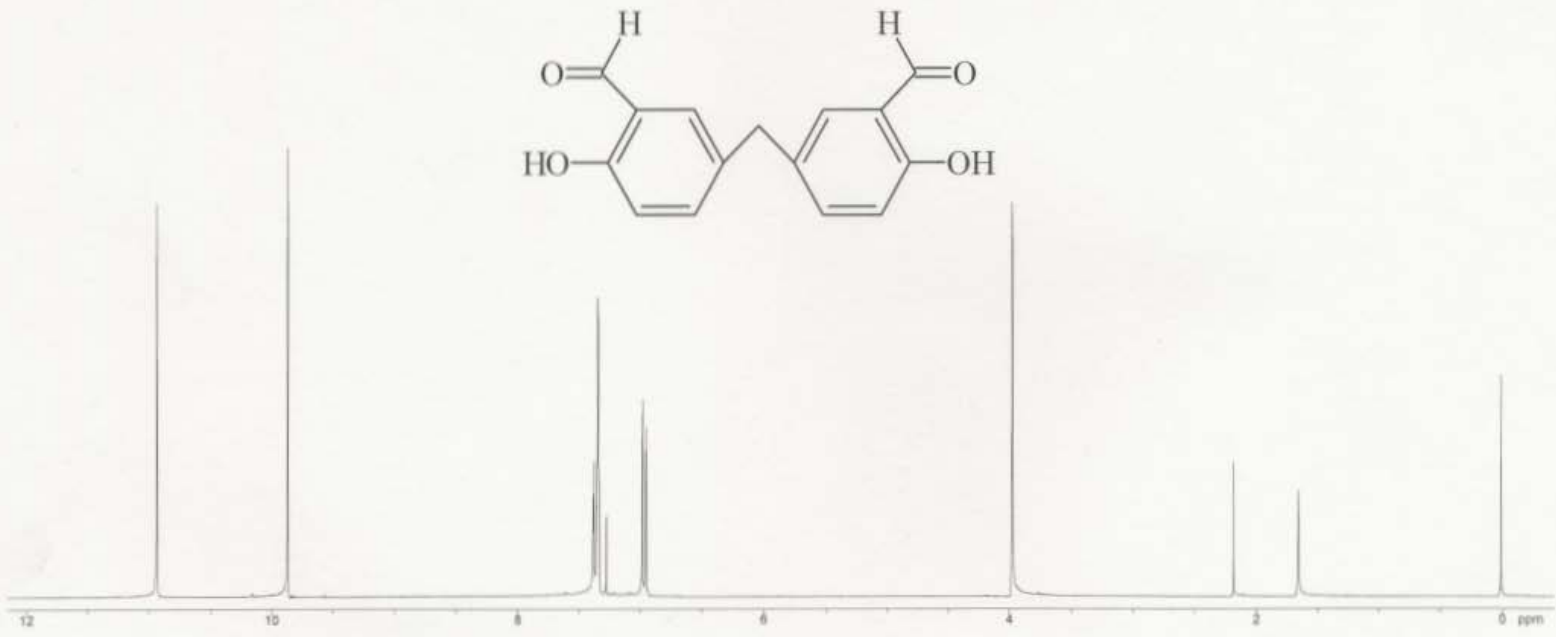

Figure A2.4 ^{1}H NMR spectrum of the dialdehyde **3a** in $CDCl_3$

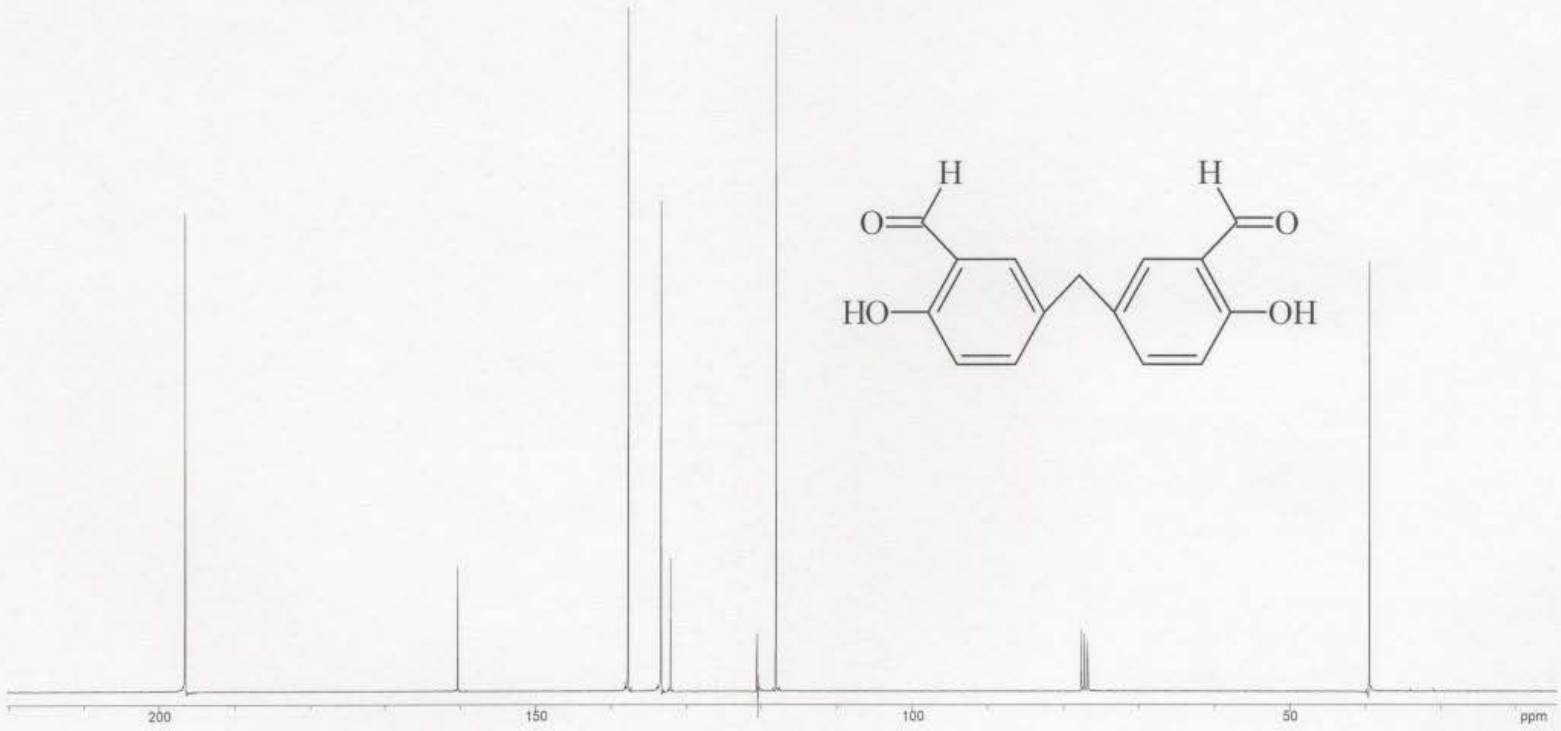

Figure A2.5 ^{13}C NMR spectra of the dialdehyde **3a** in $CDCl_3$

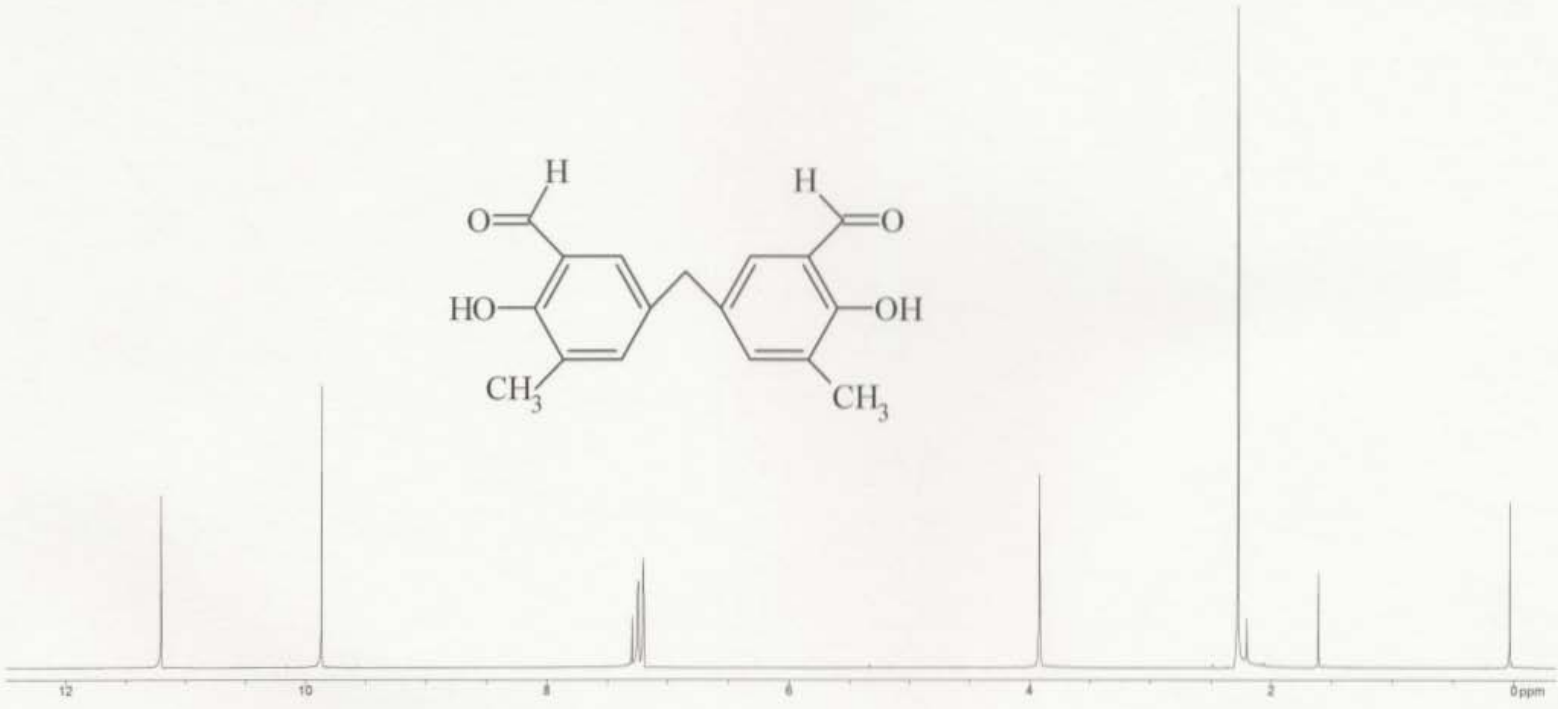

Figure A2.6 ^{1}H NMR spectrum of the dialdehyde **3b** in $CDCl_3$

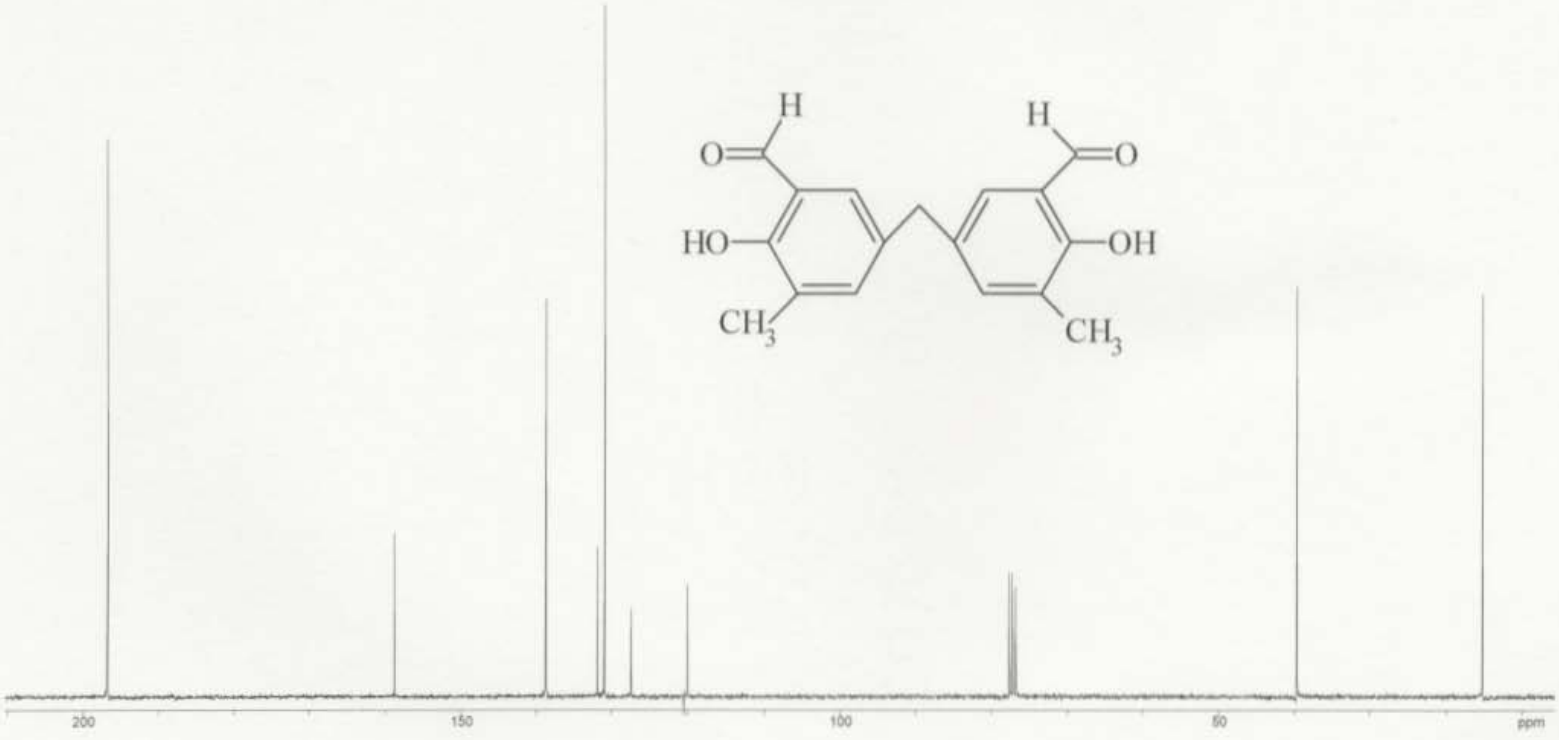

Figure A2.7 ^{13}C NMR spectrum of the salicylaldehyde **3b** in $CDCl_3$

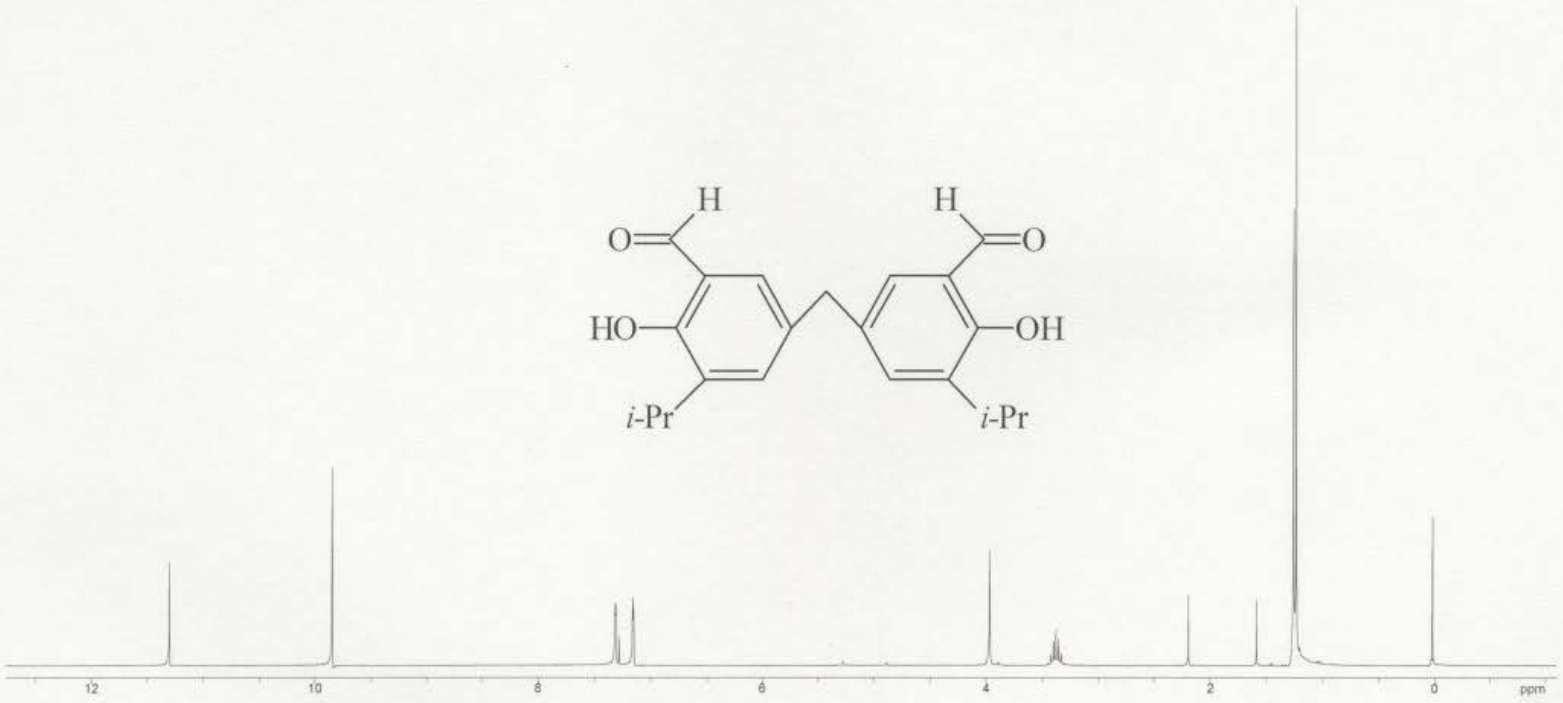

Figure A2.8 ^{1}H NMR spectrum of the dialdehyde **3c** in $CDCl_3$

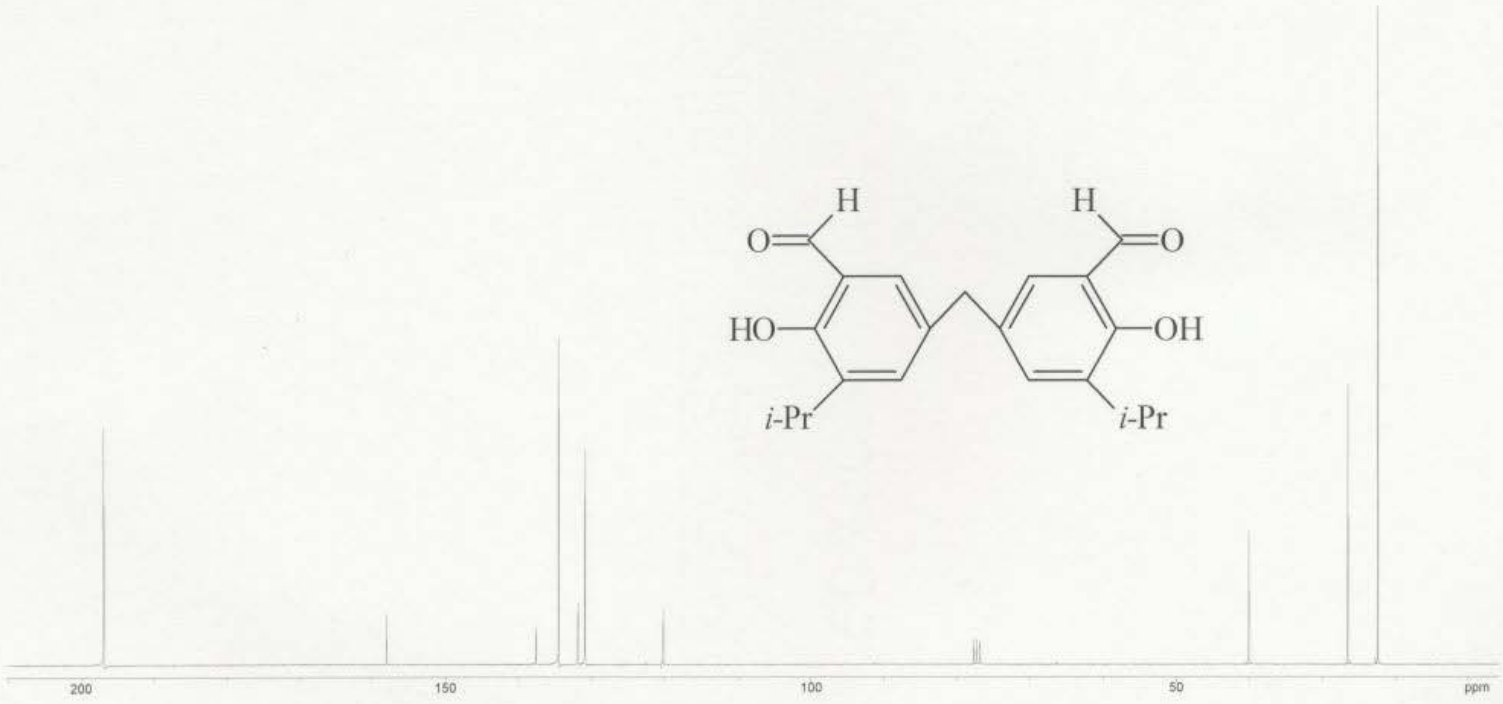

Figure A2.9 ^{13}C NMR spectrum of the dialdehyde **3c** in $CDCl_3$

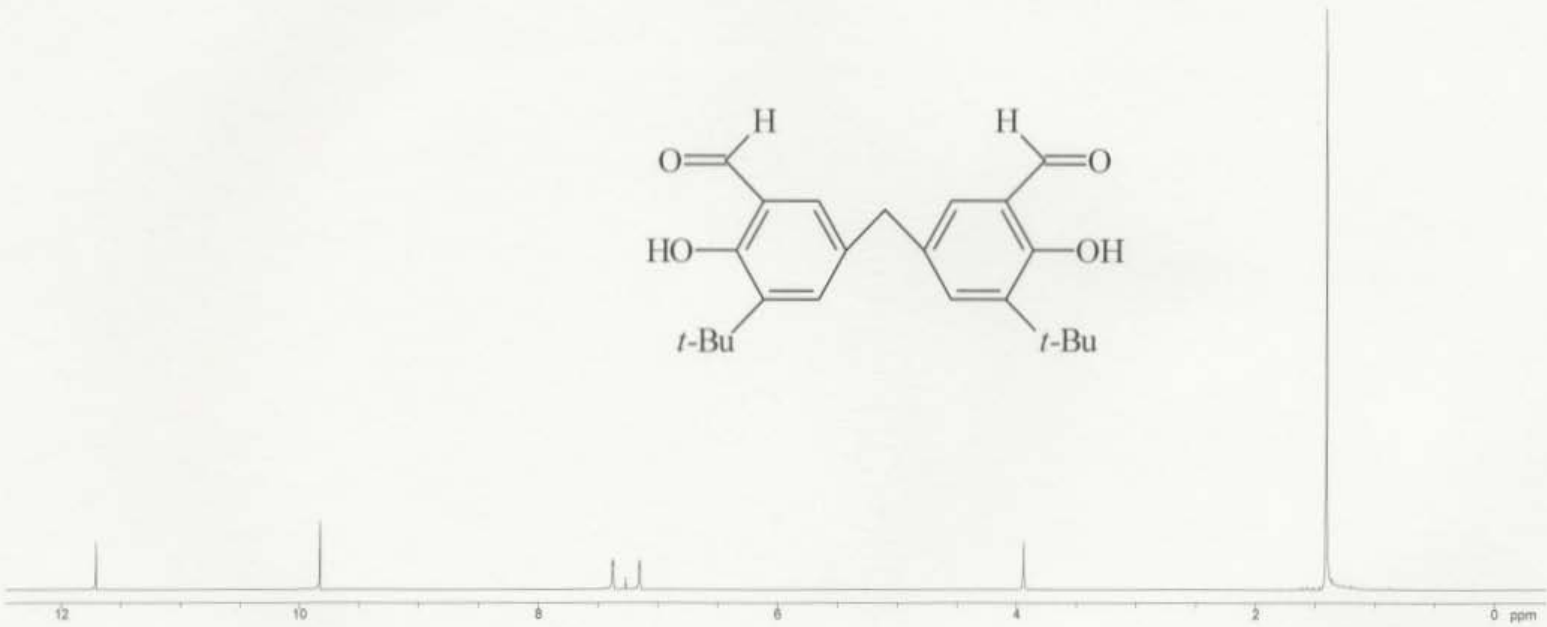

Figure A2.10 ^{1}H NMR spectrum of the dialdehyde **3d** in $CDCl_3$

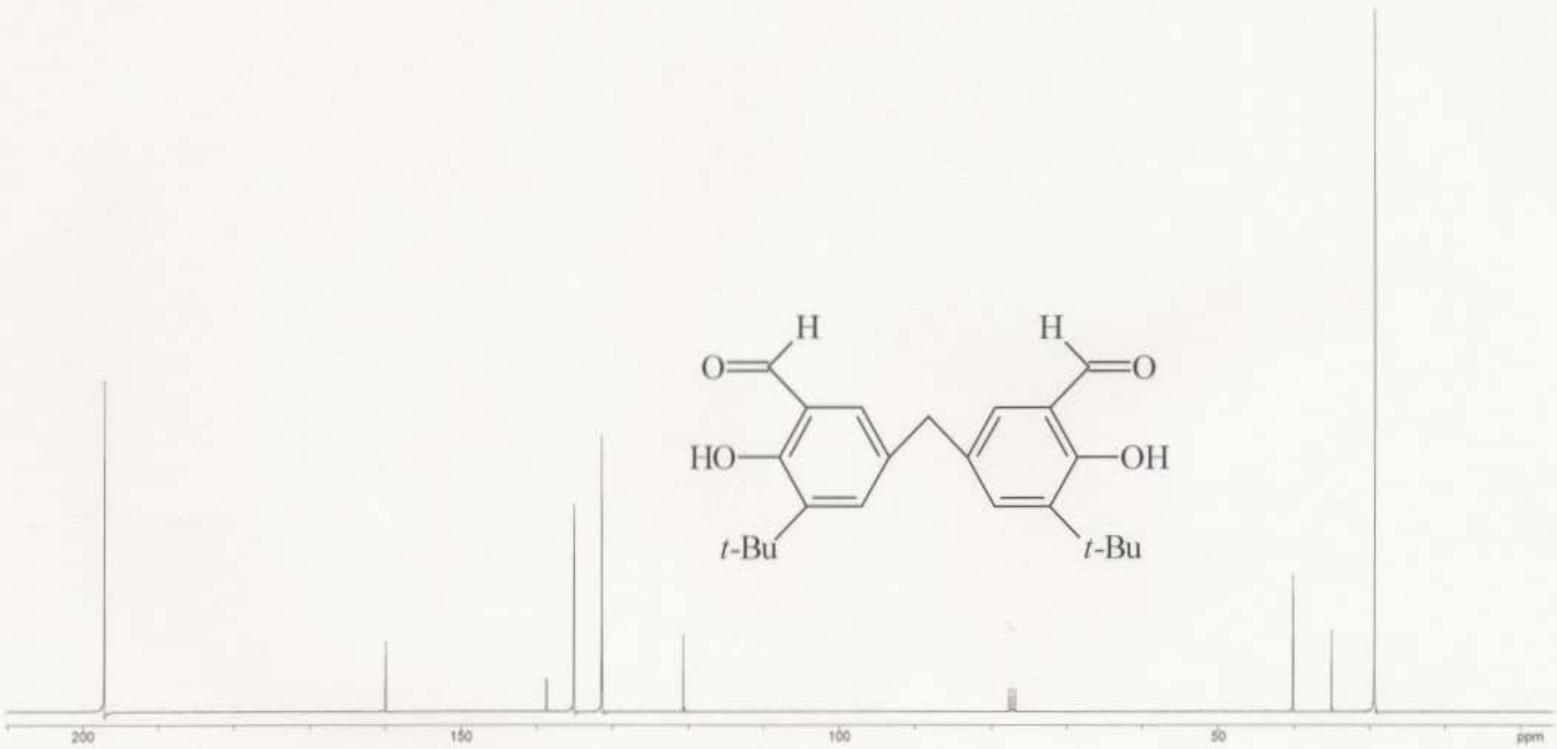

Figure A2.11 ^{13}C NMR spectrum of the dialdehyde **3d** in $CDCl_3$

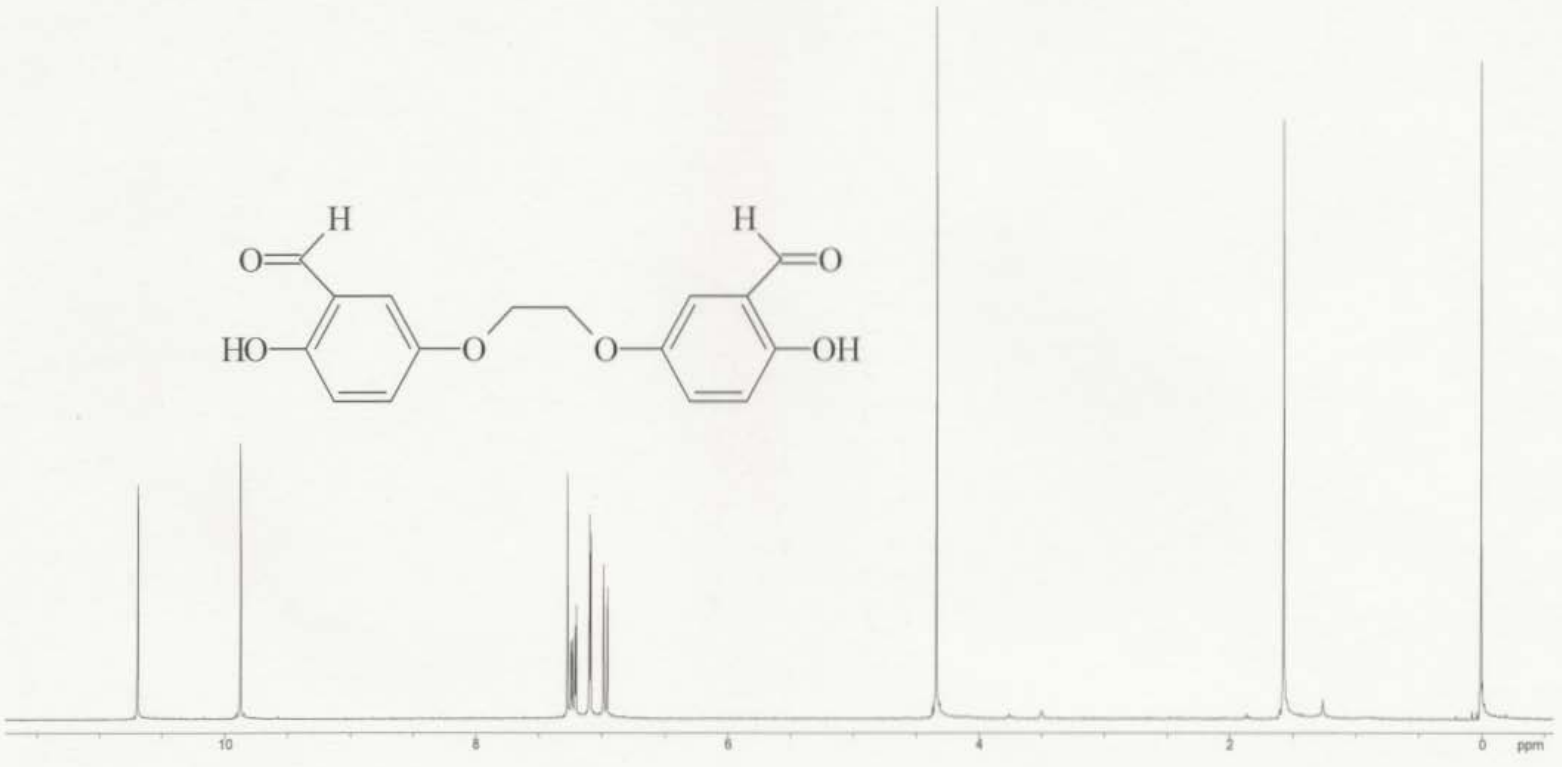

Figure A2.12 ^{1}H NMR spectrum of the dialdehyde **6** in $CDCl_3$

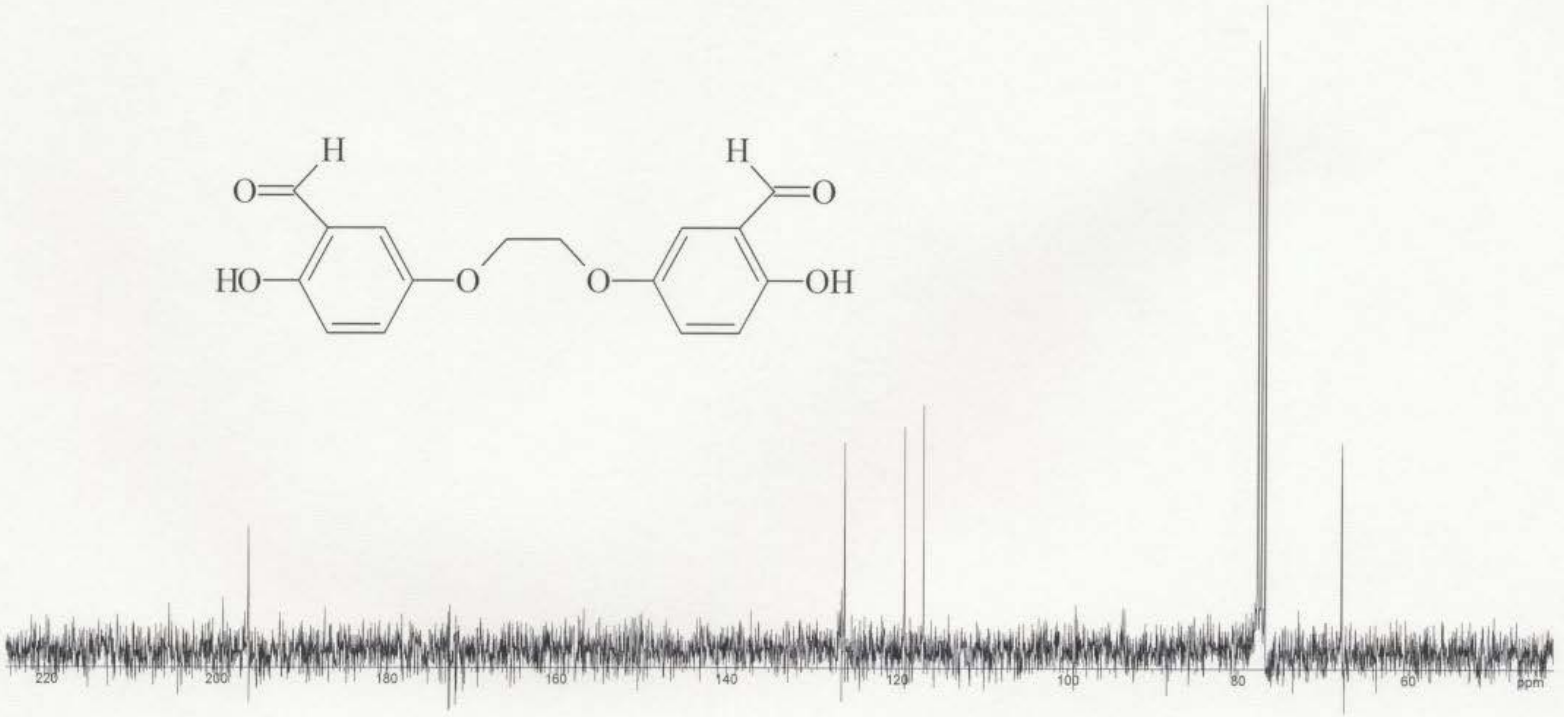

Figure A2.13 ^{13}C NMR spectrum of the dialdehyde **6** in $CDCl_3$

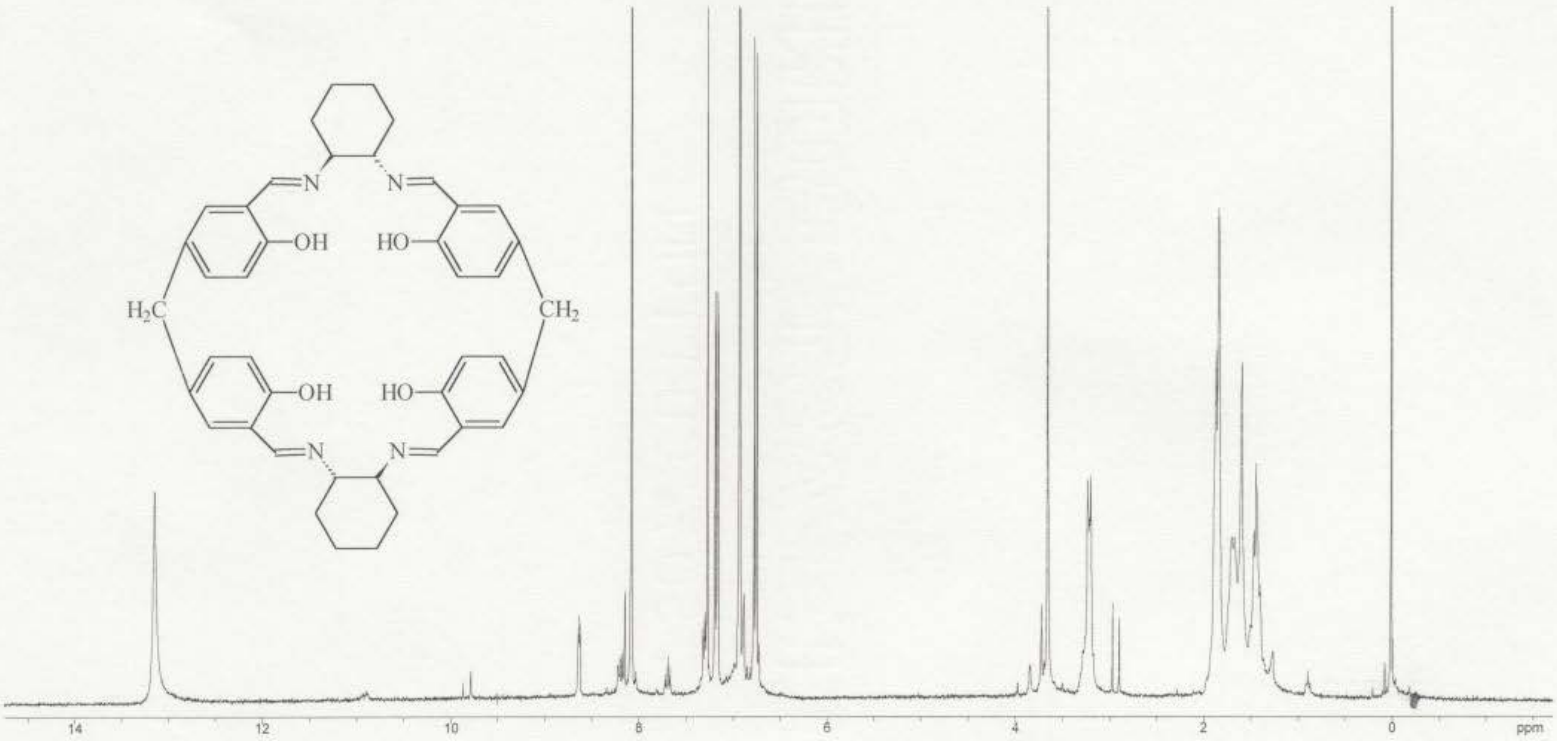

Figure A2.14 ^{1}H NMR spectrum of the calixsalen **14a** in $CDCl_3$

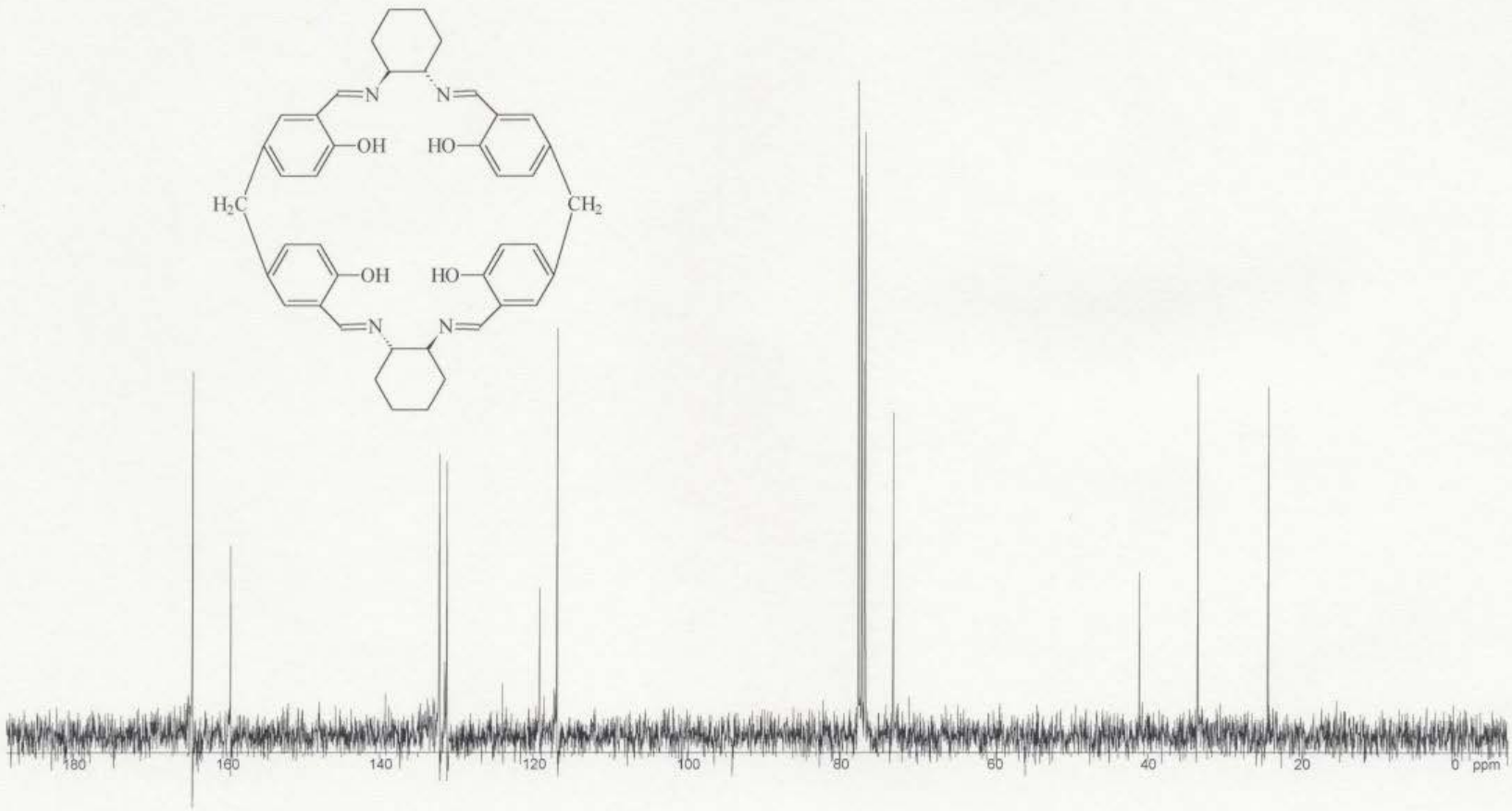

Figure A2.15 ^{13}C NMR spectrum of the calixsalen **14a** in $CDCl_3$

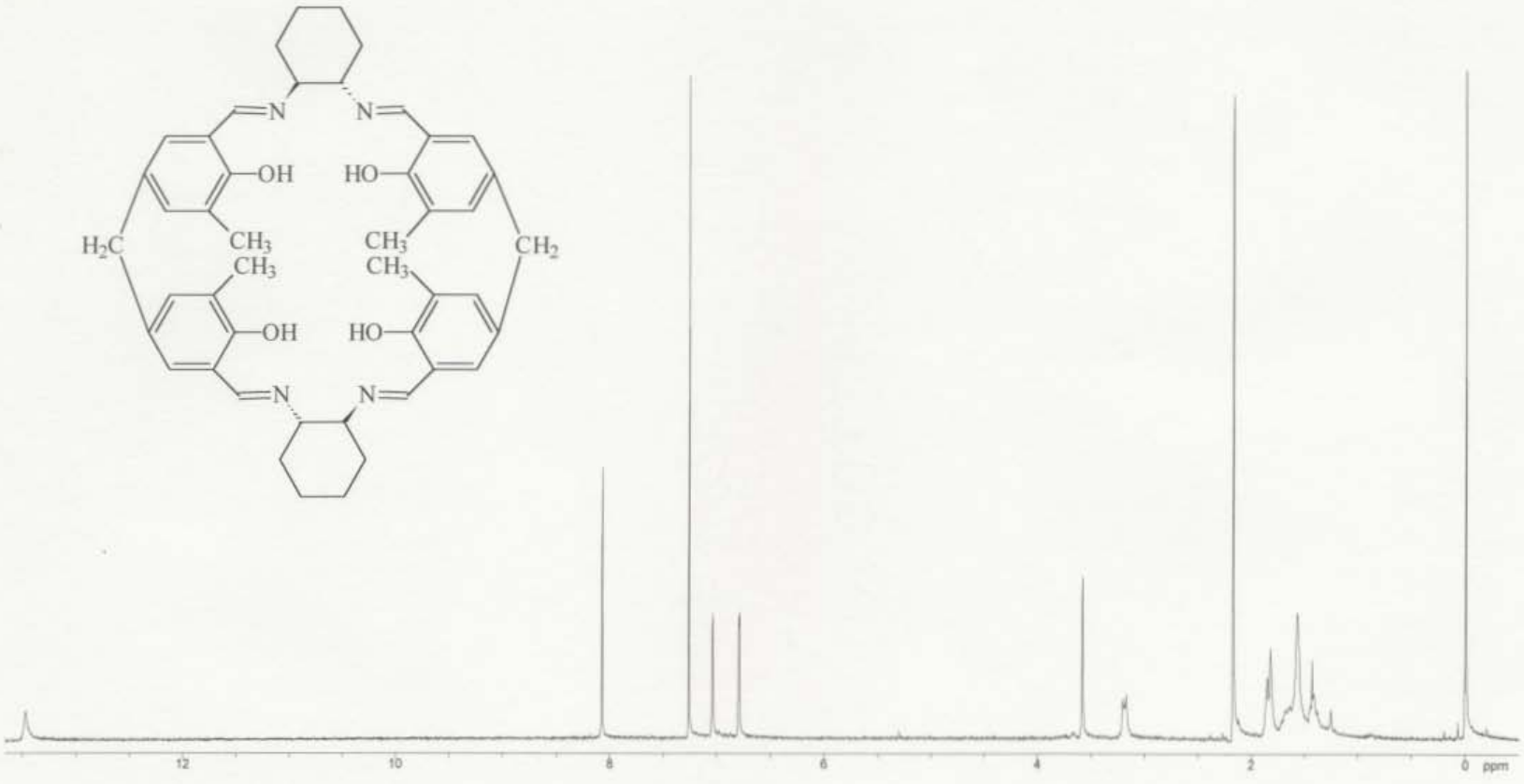

Figure A2.16 ^{1}H NMR spectrum of the calixsalen **14b** in $CDCl_3$

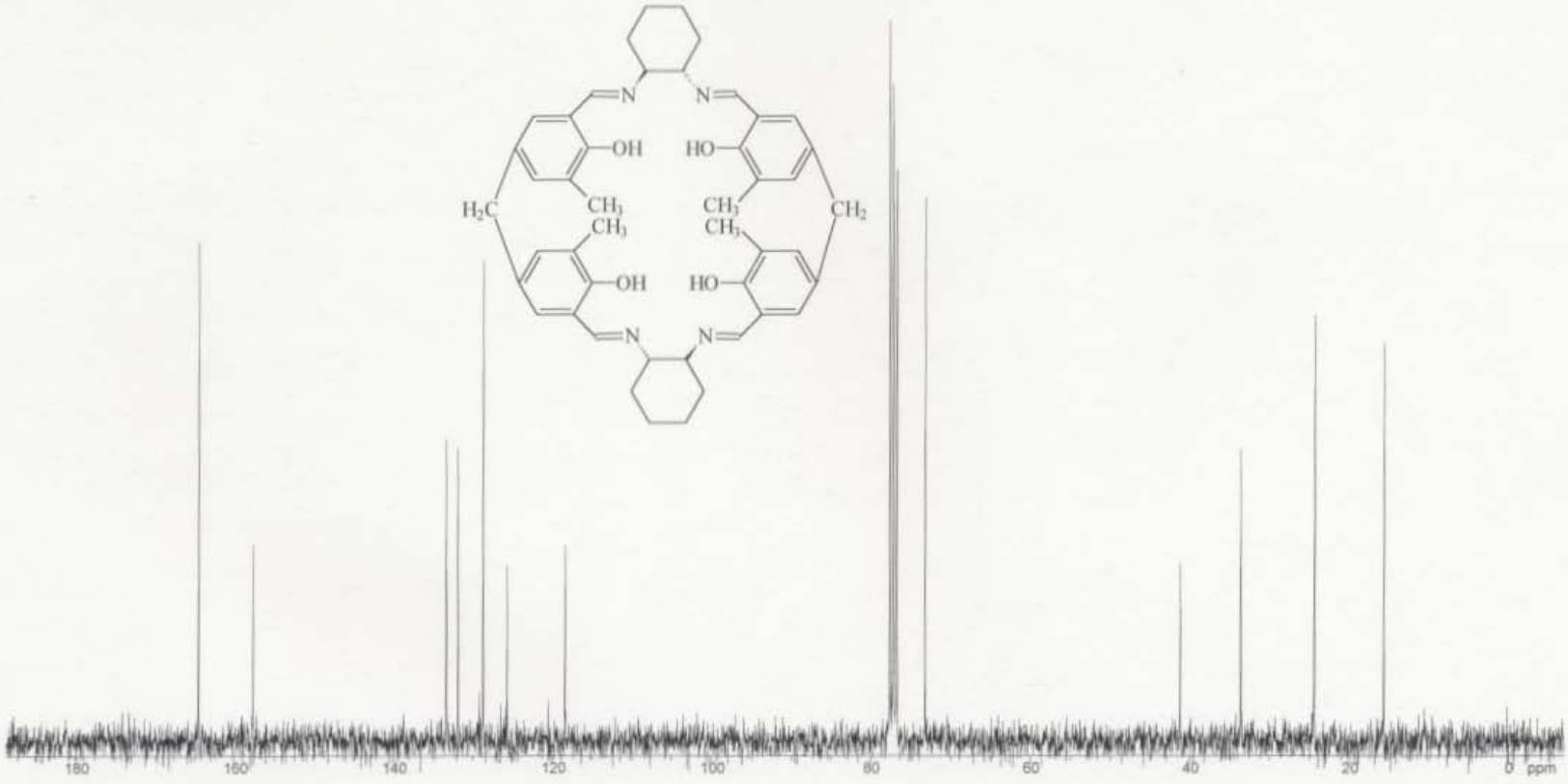

Figure A2.17 ^{13}C NMR spectrum of the calixsalen **14b** in $CDCl_3$

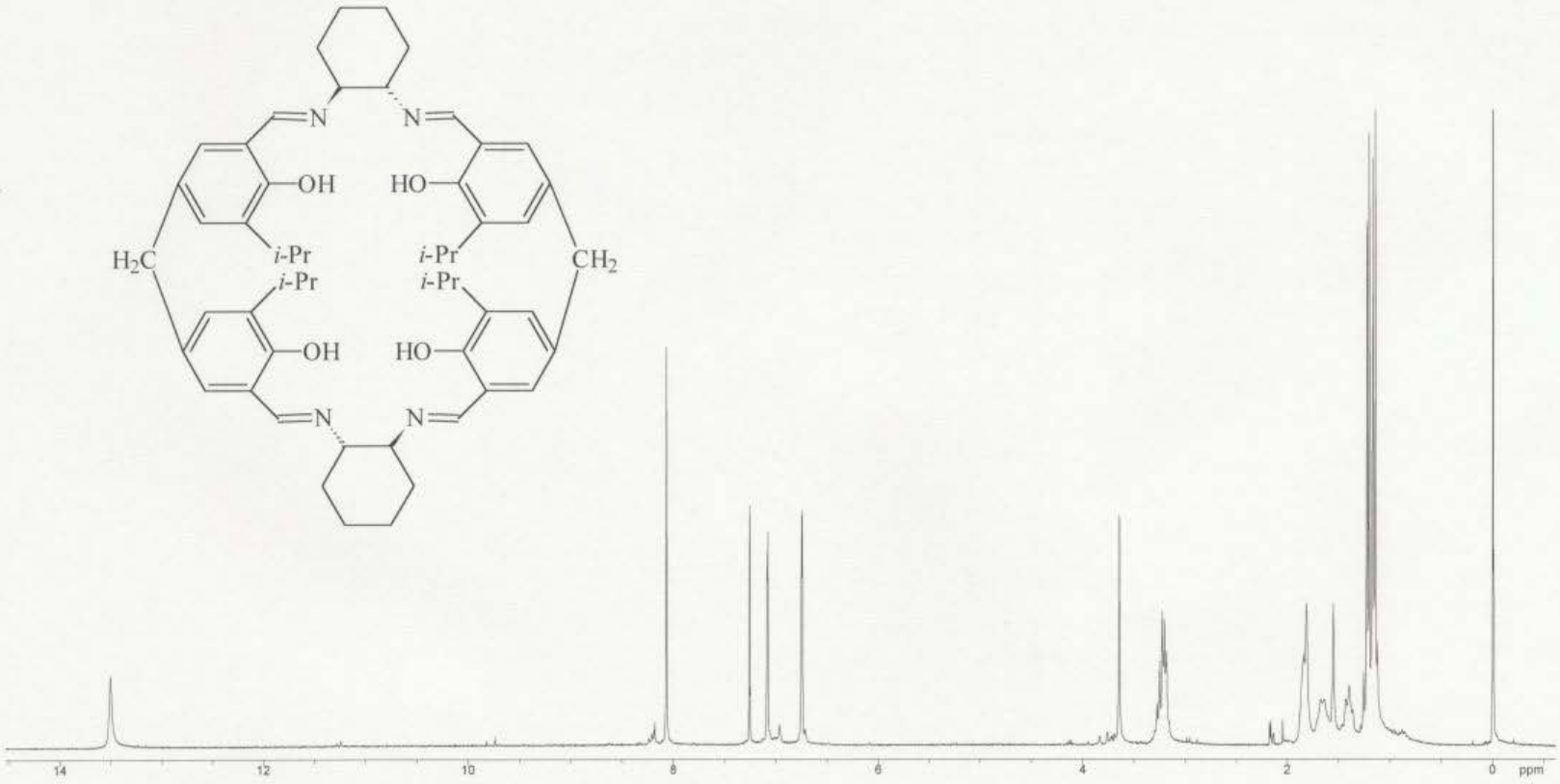

Figure A2.18 ^{1}H NMR spectrum of the calixsalen **14c** in $CDCl_3$

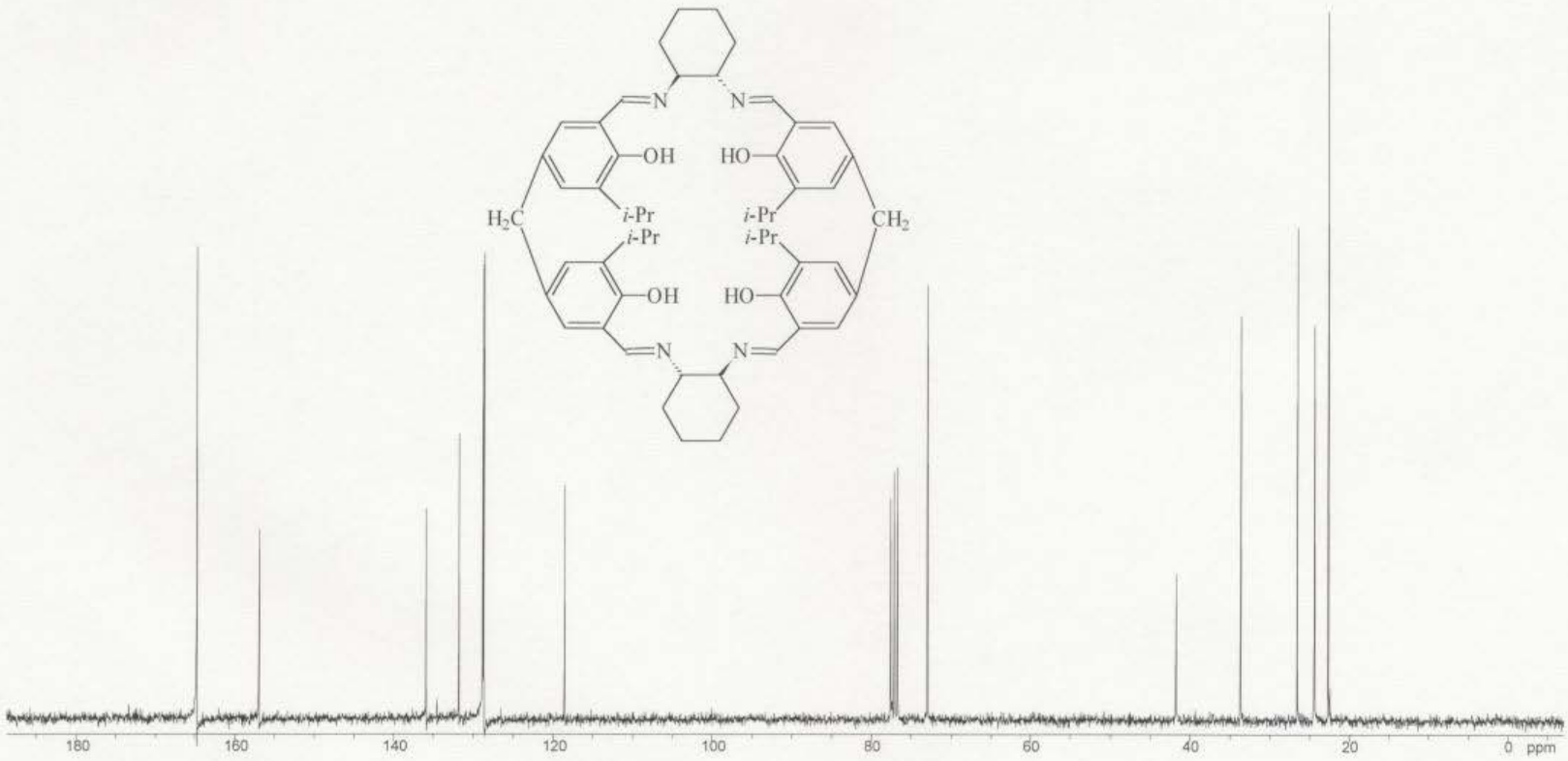

Figure A2.19 ^{13}C NMR spectrum of the calixsalen **14c** in $CDCl_3$

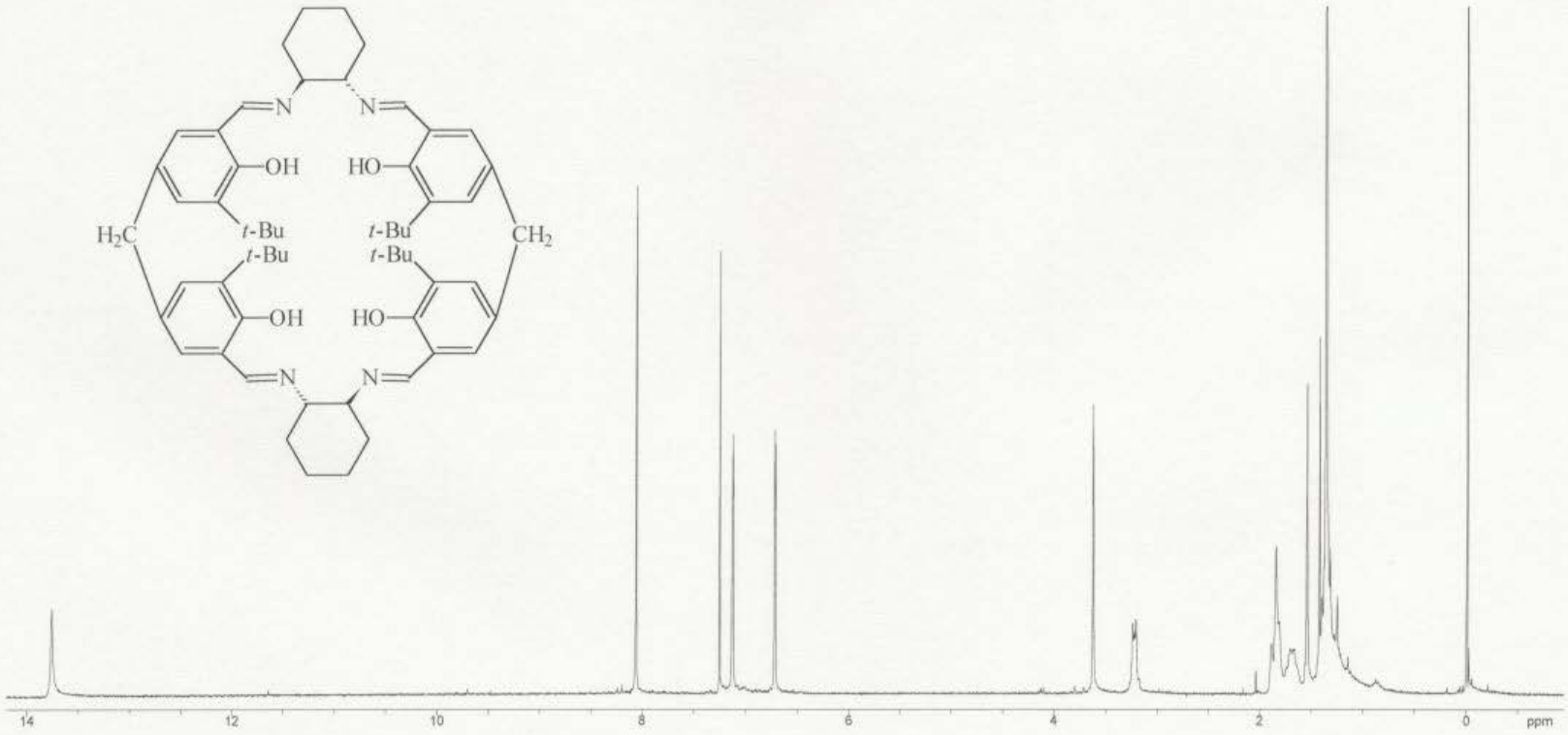

A2.20 ^{1}H NMR spectrum of the calixsalen **14d** in $CDCl_3$

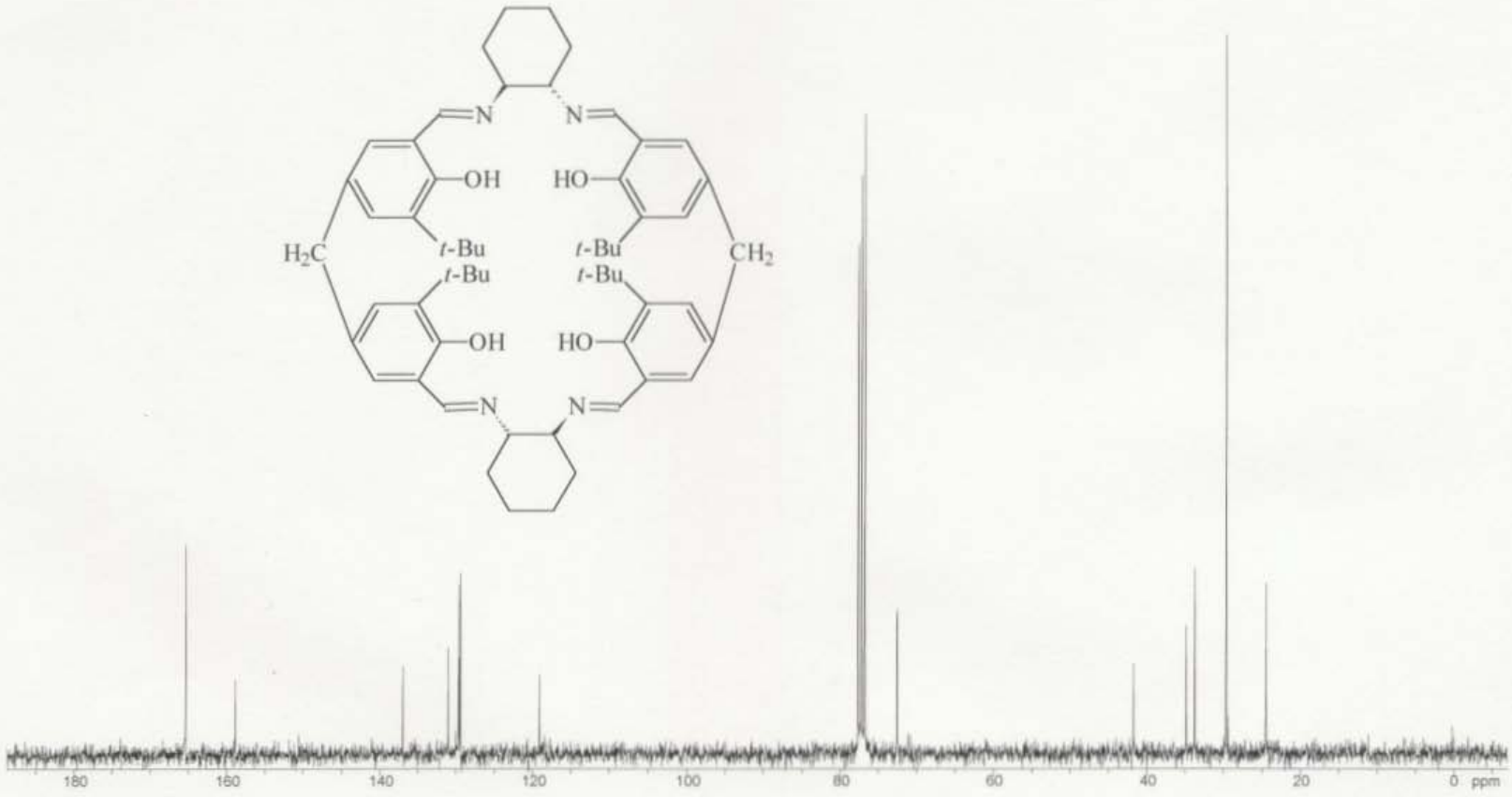

Figure A2.21 ^{13}C NMR spectrum of the calixsalen **14d** in $CDCl_3$

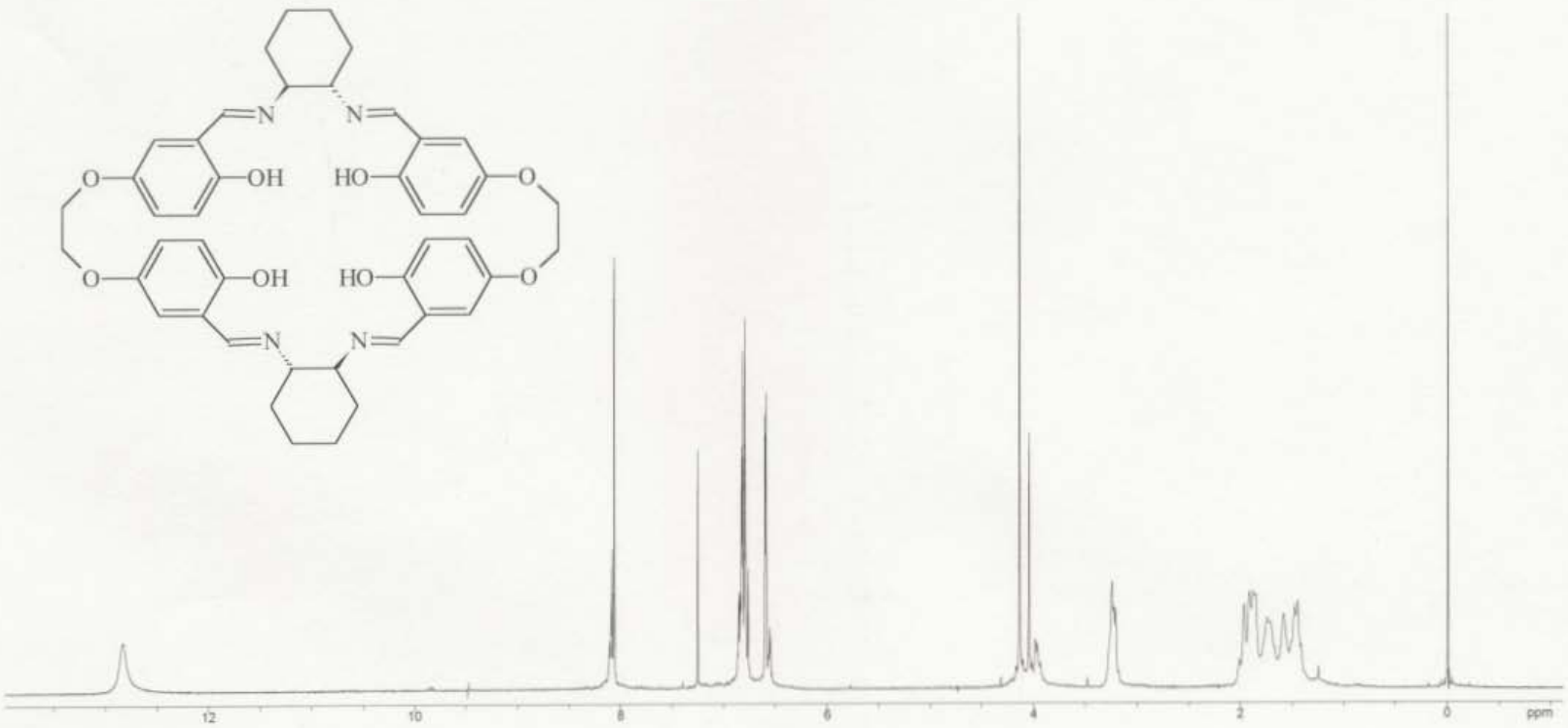

Figure A2.22 ^{1}H NMR spectrum of the calixsalen **17** in CDCl3

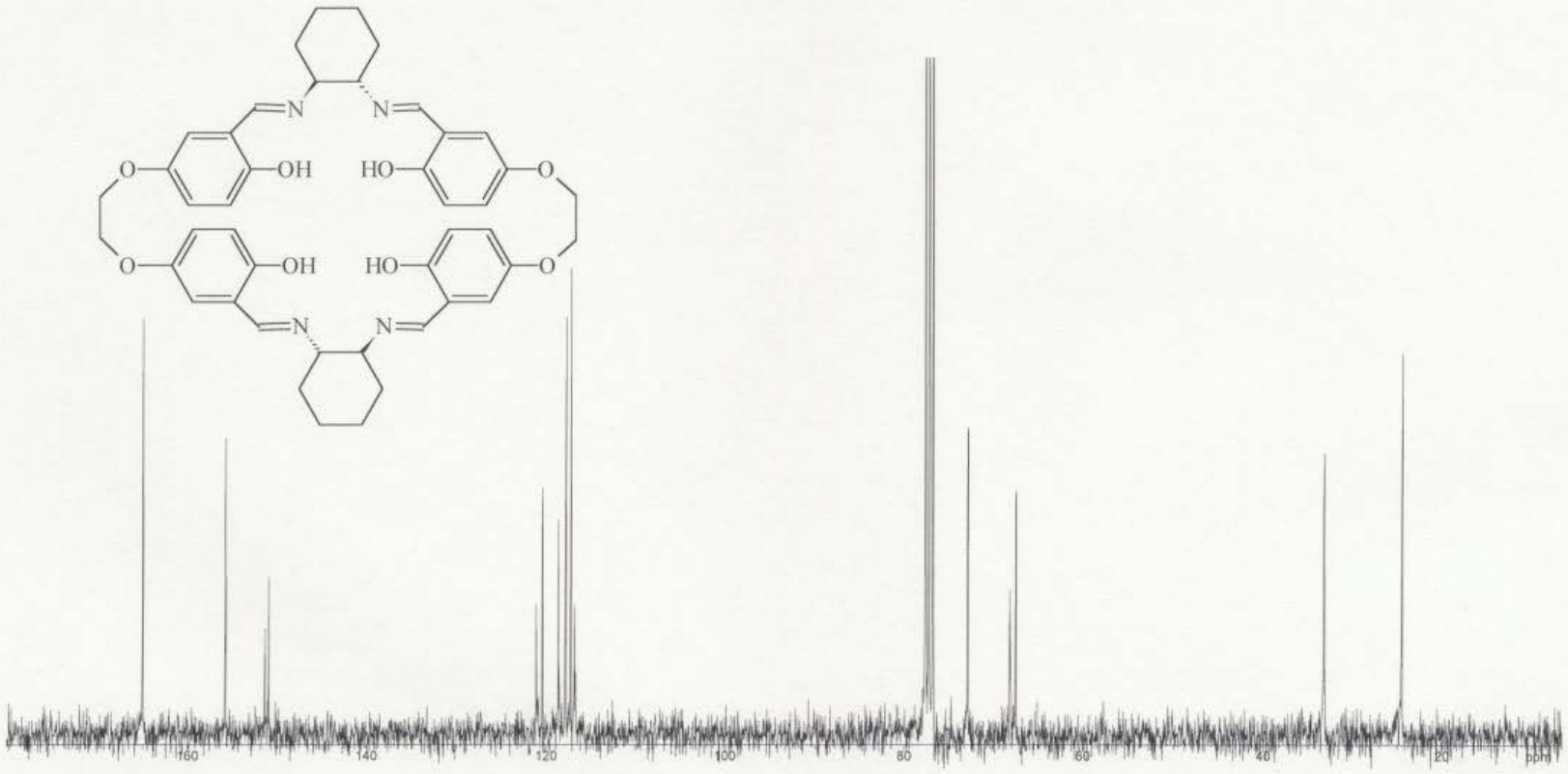

Figure A2.23 ^{13}C NMR spectrum of the calixsalen **17** at 50^0C in $CDCl_3$

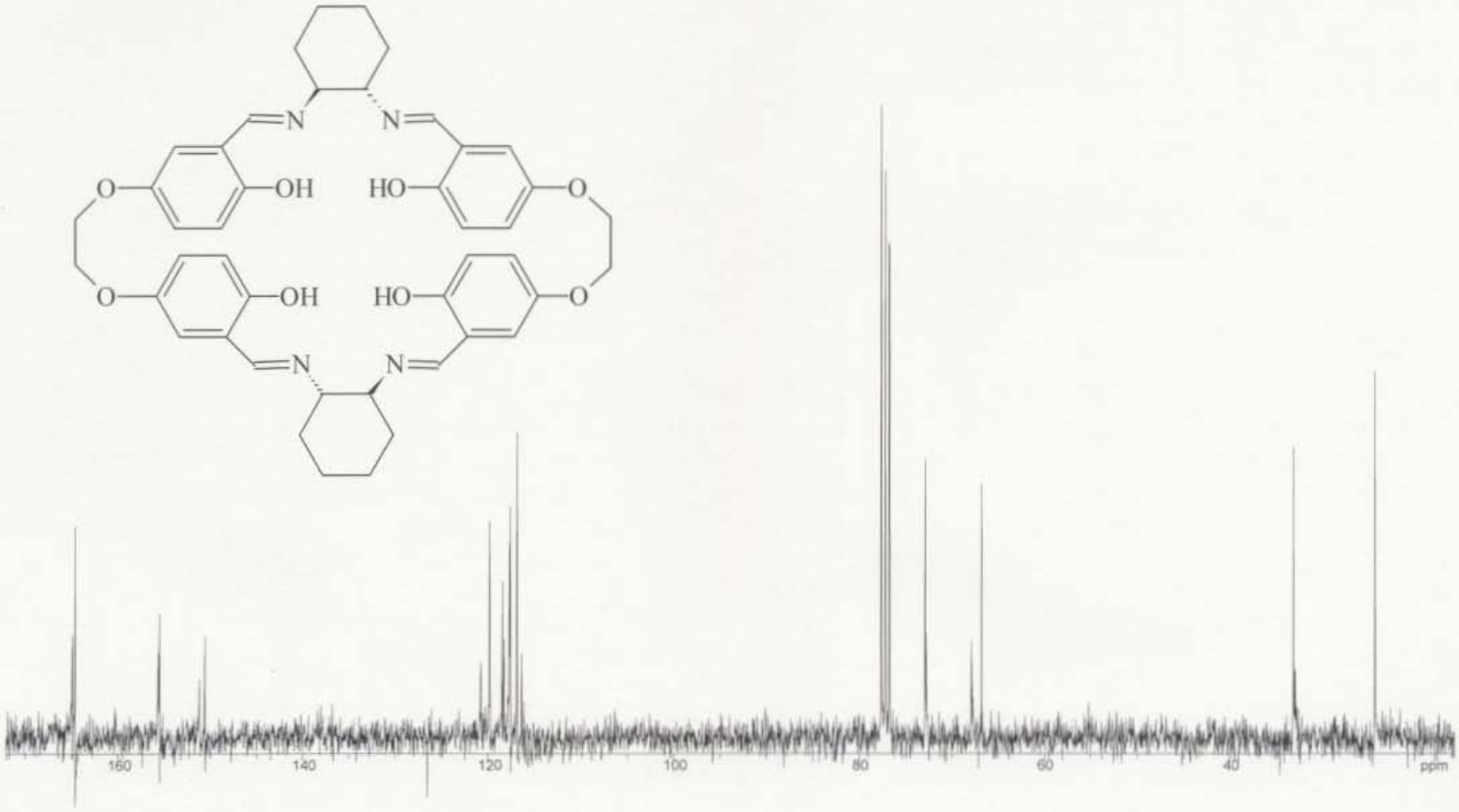

Figure A2.24 ^{13}C NMR spectrum of the calixsalen **17** at RT in $CDCl_3$

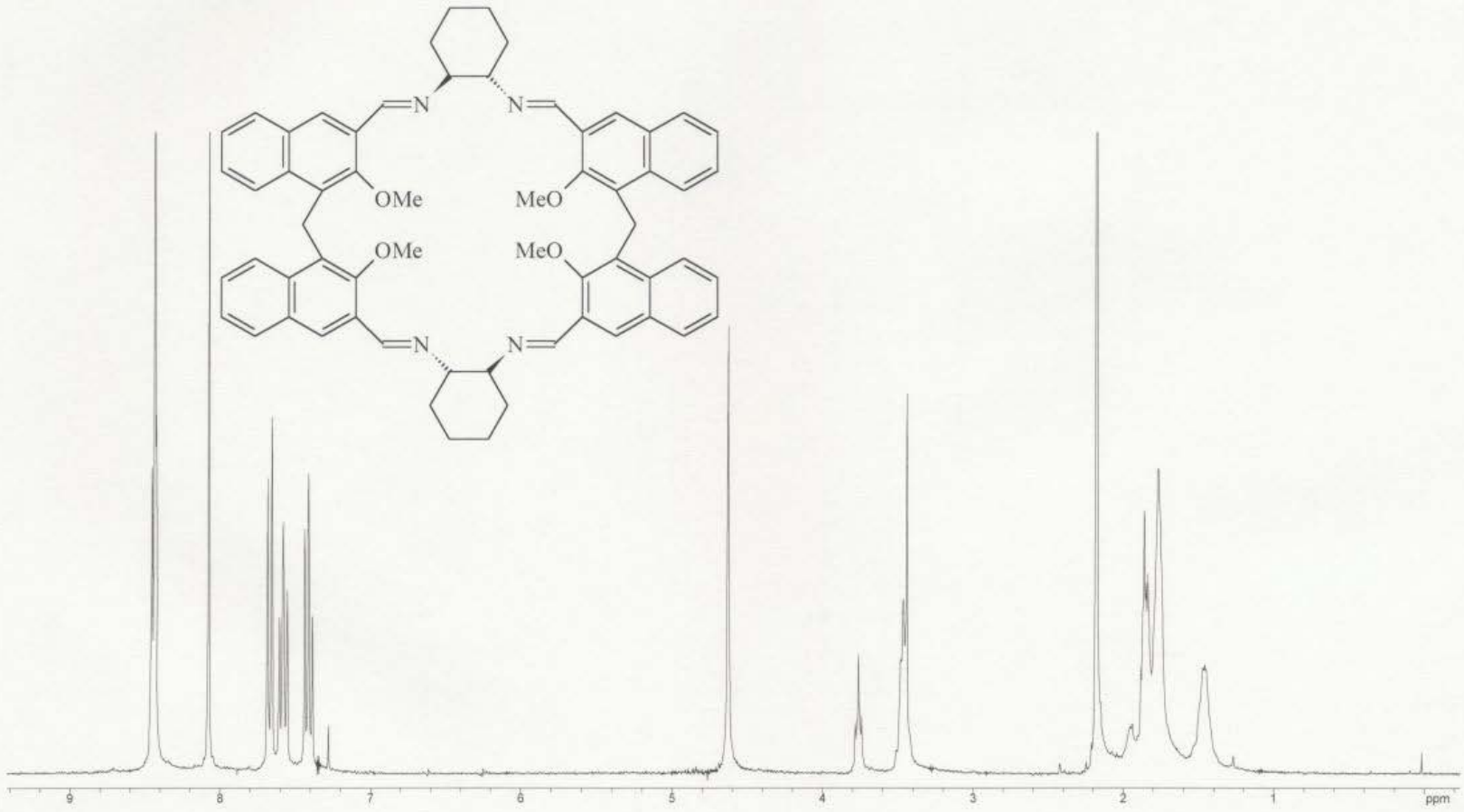

Figure A2.25 ^{1}H NMR spectrum of the macrocyclic dimer **18** in $CDCl_3$

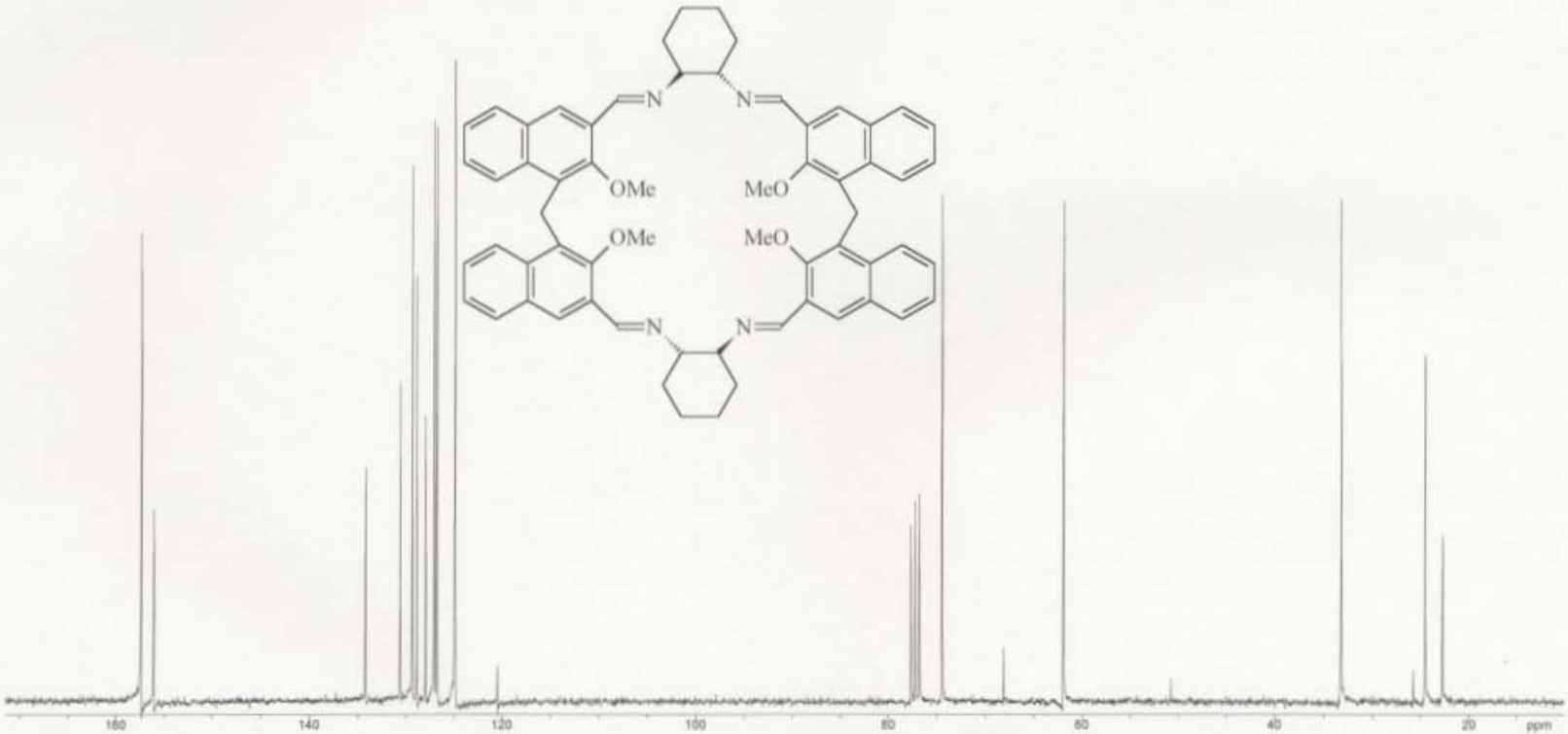

Figure A2.26 ^{13}C NMR spectrum of the macrocyclic dimer **18** in $CDCl_3$

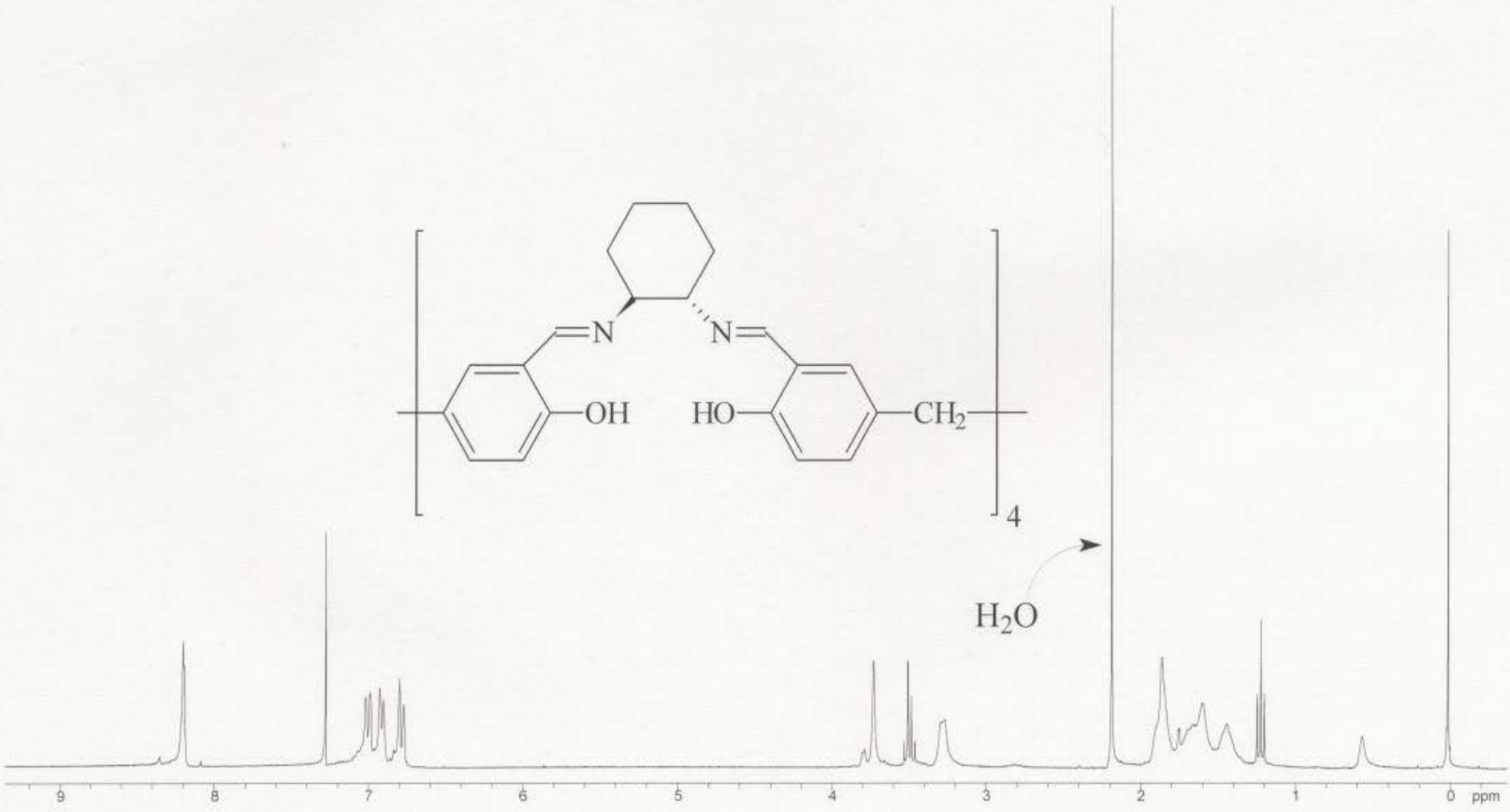

Figure A2.27 ^{1}H NMR spectrum of the macrocyclic tetramer **21a** in $CDCl_3$

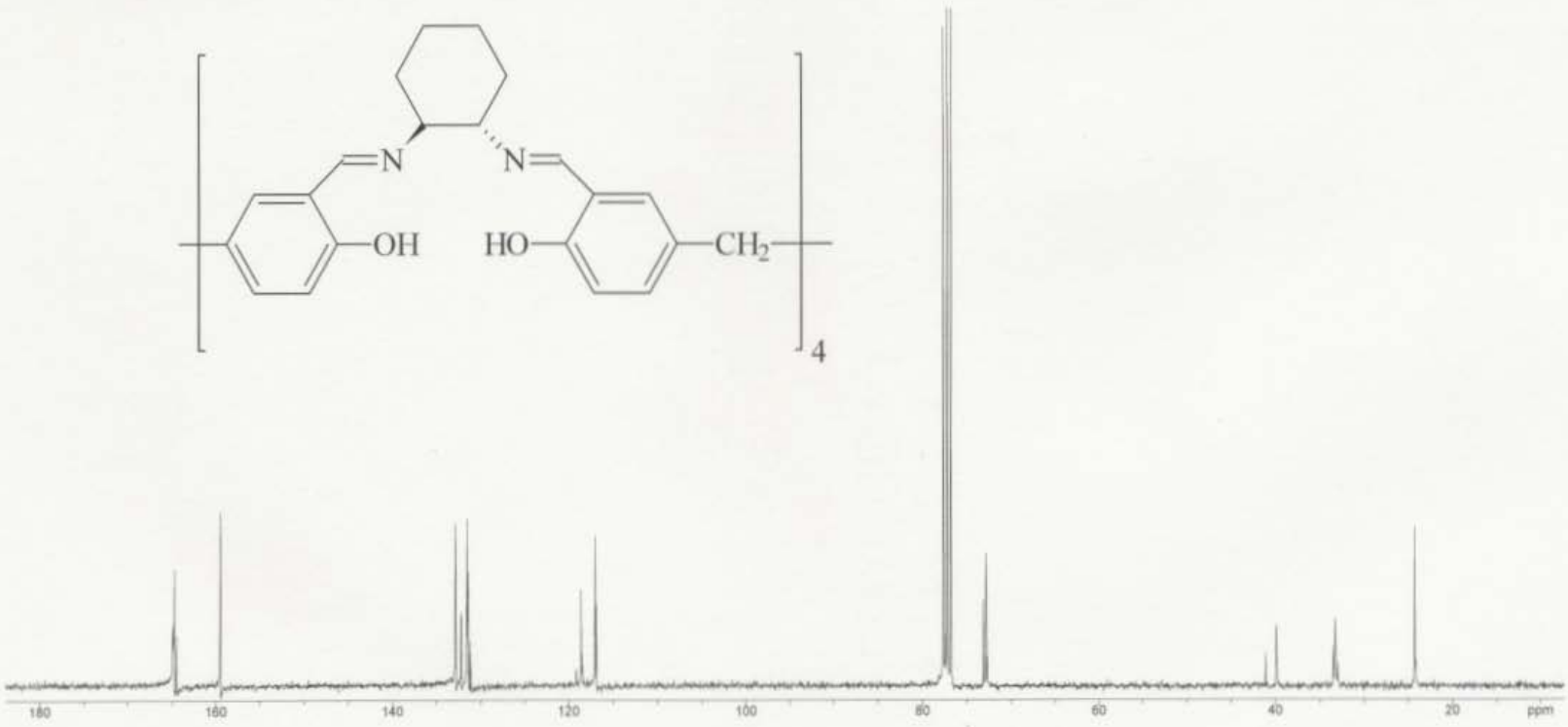

Figure A2.28 ^{13}C NMR spectrum of the macrocyclic tetramer **21a** in $CDCl_3$

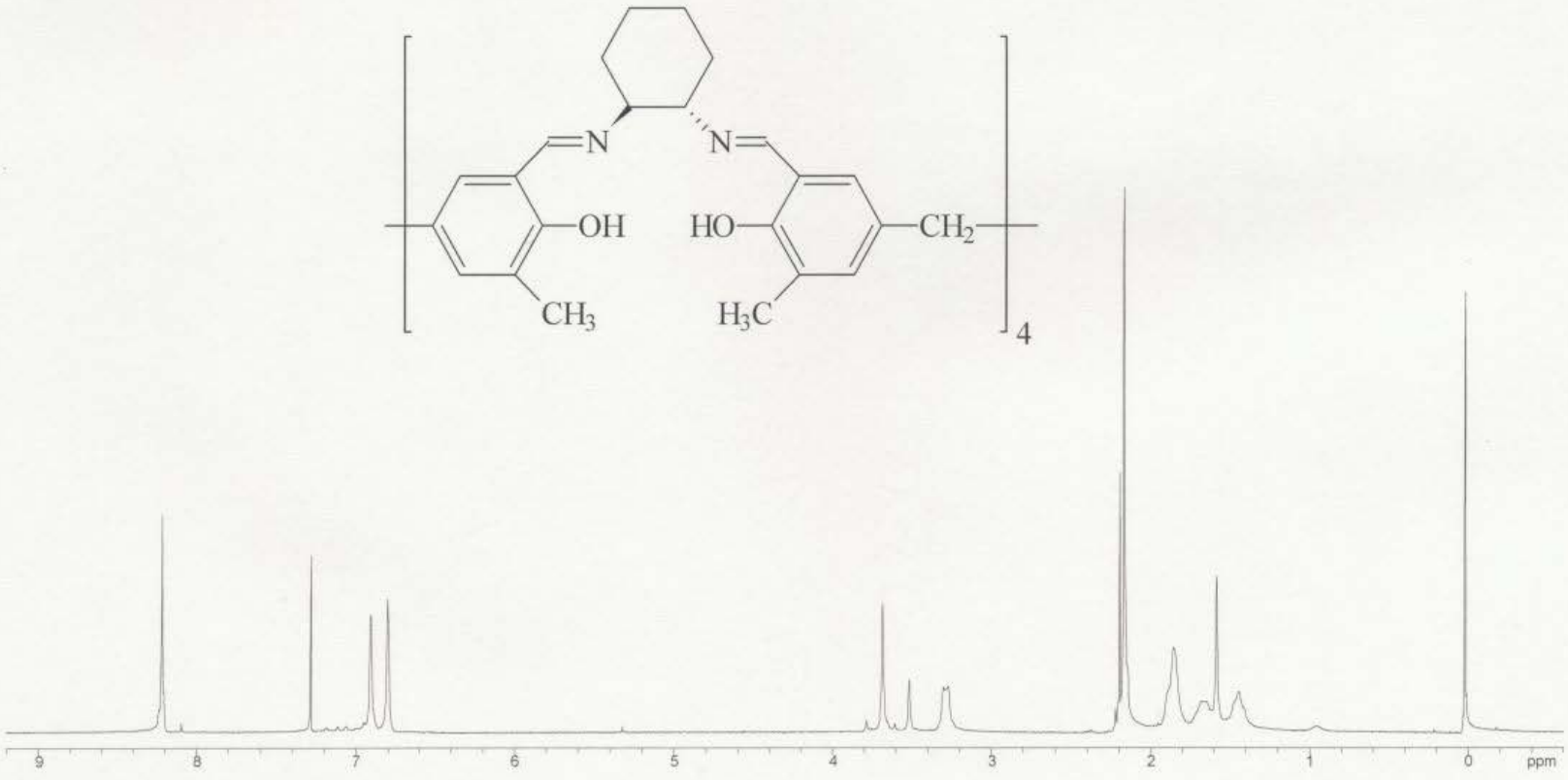

Figure A2.29 ^{1}H NMR spectrum of the macrocyclic tetramer **21b** in $CDCl_3$

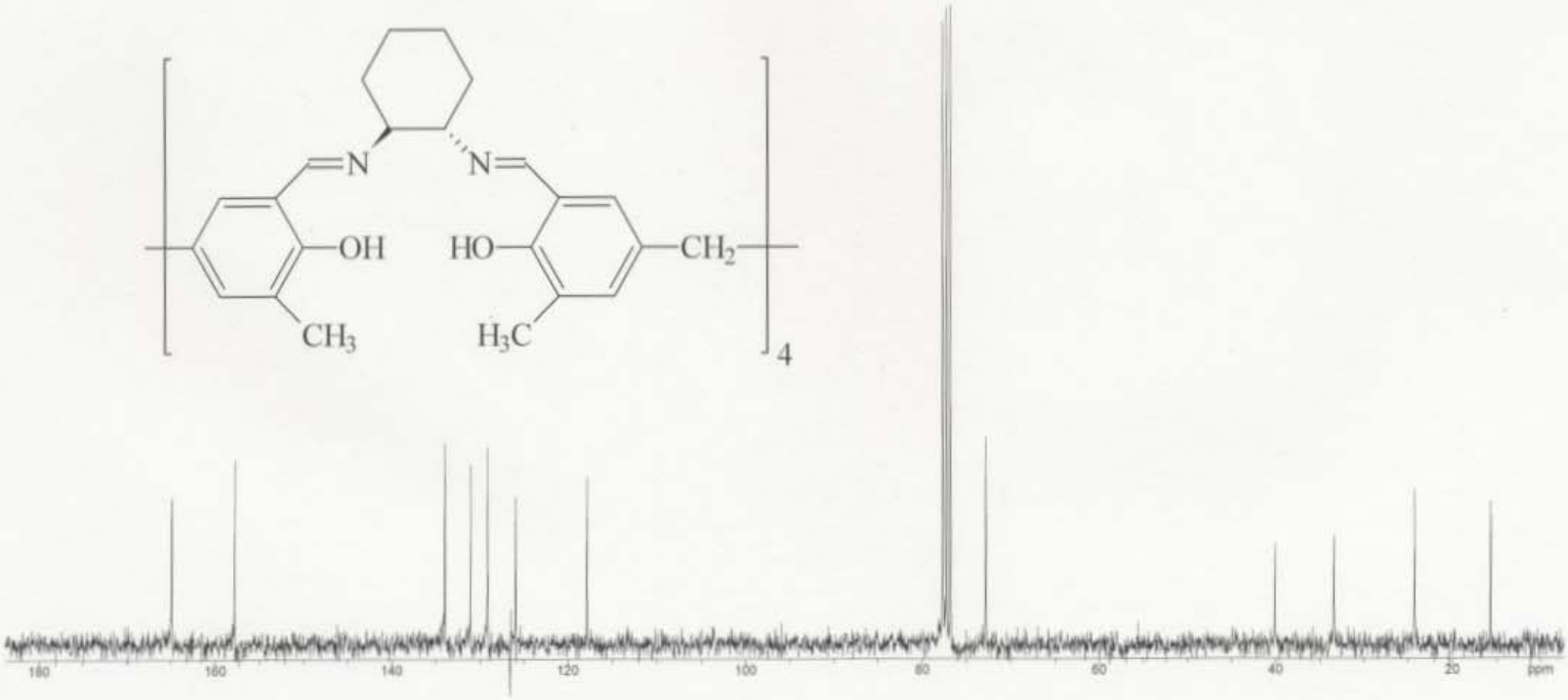

Figure A2.30 ^{13}C NMR spectrum of the macrocyclic salen tetramer **21b** in $CDCl_3$

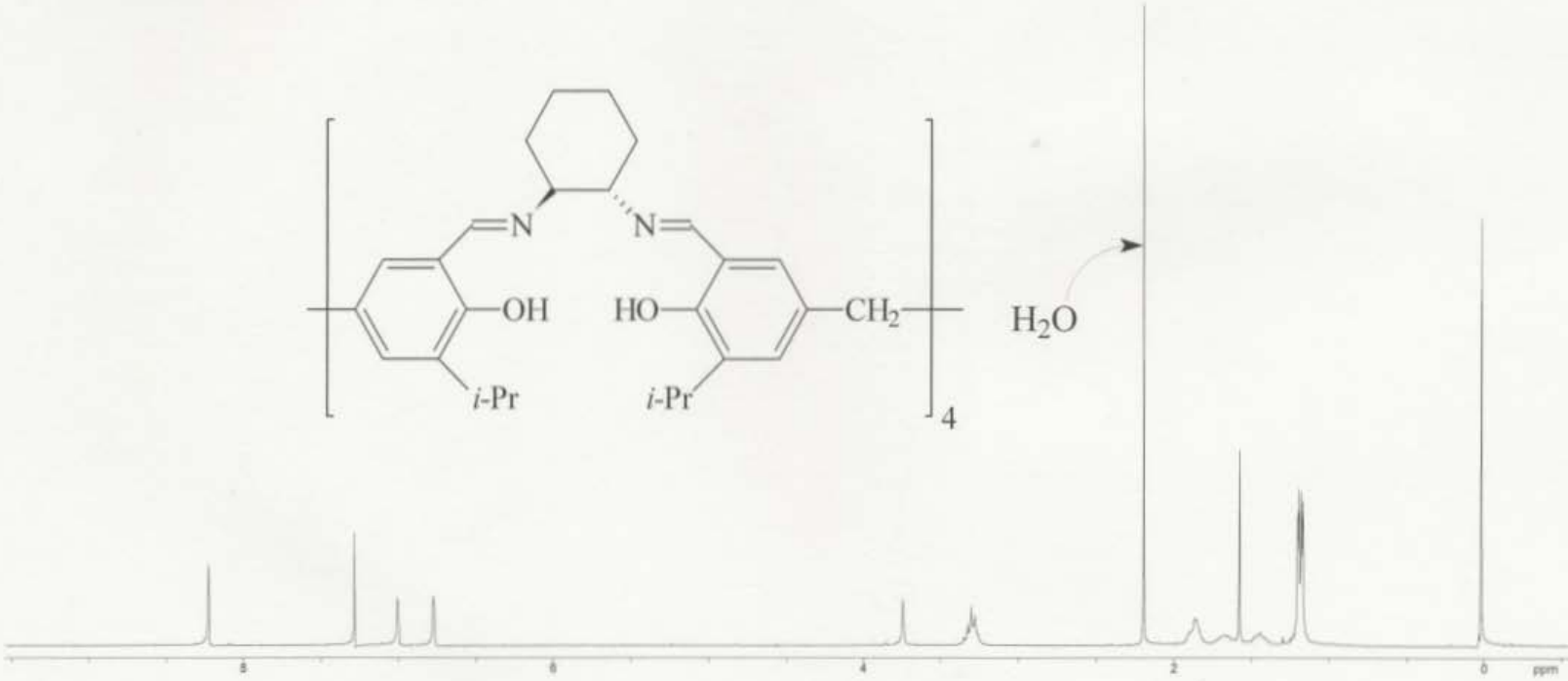

Figure A2.31 ^{1}H NMR spectrum of the macrocyclic tetramer of **21c** in $CDCl_3$

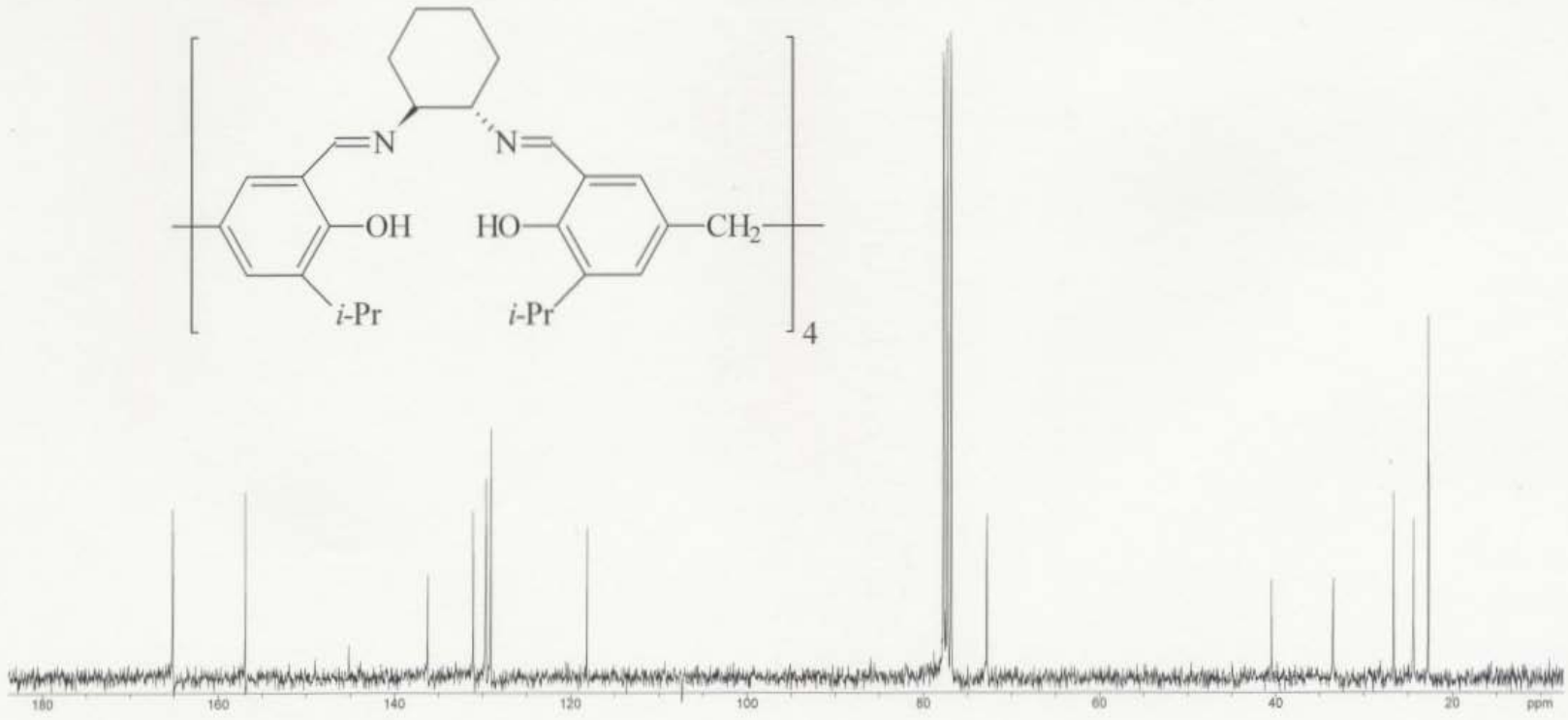

Figure A2.32 ^{13}C NMR spectrum of the macrocyclic dimer **21c** in $CDCl_3$

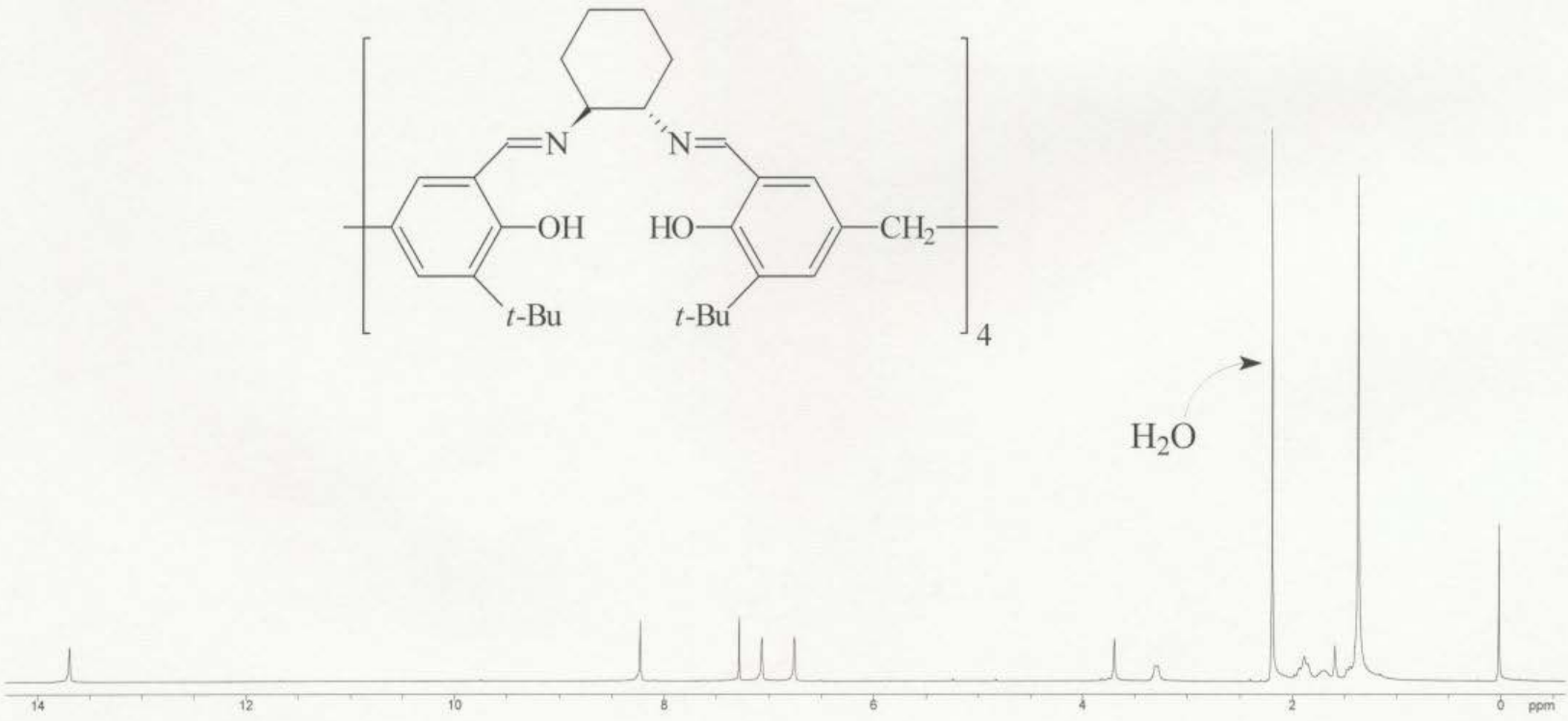

Figure A2.33 ^{1}H NMR spectrum of the macrocyclic tetramer **21d** in $CDCl_3$

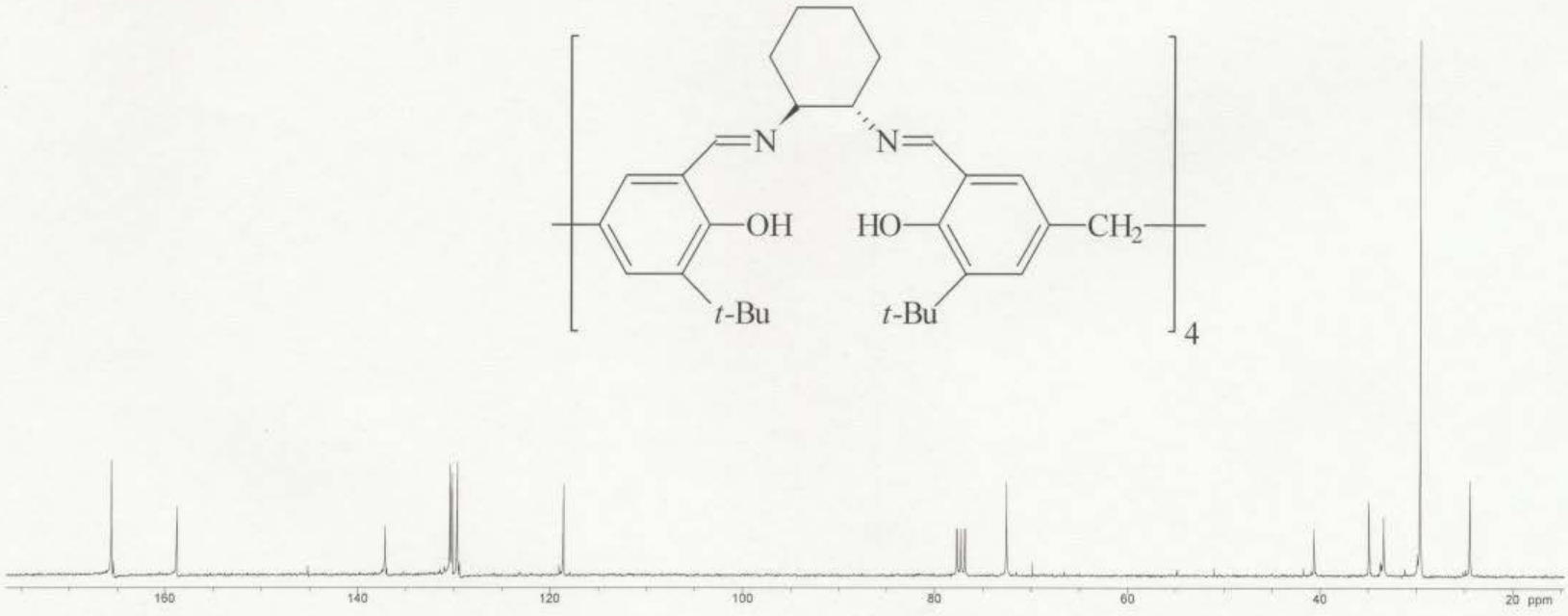

Figure A2.34 ^{13}C NMR spectrum of the macrocyclic salen dimer **21d** in $CDCl_3$

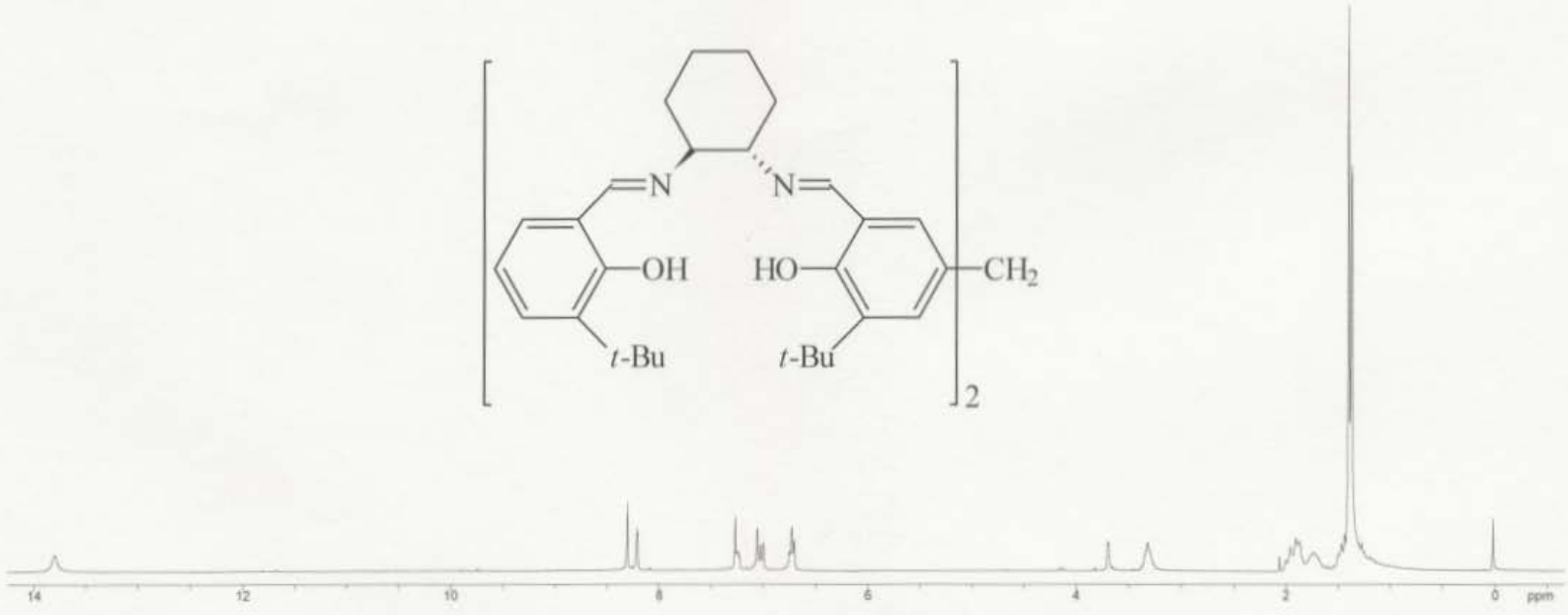

Figure A2.35 ^{1}H NMR spectrum of the linear salen dimer **20** in $CDCl_3$

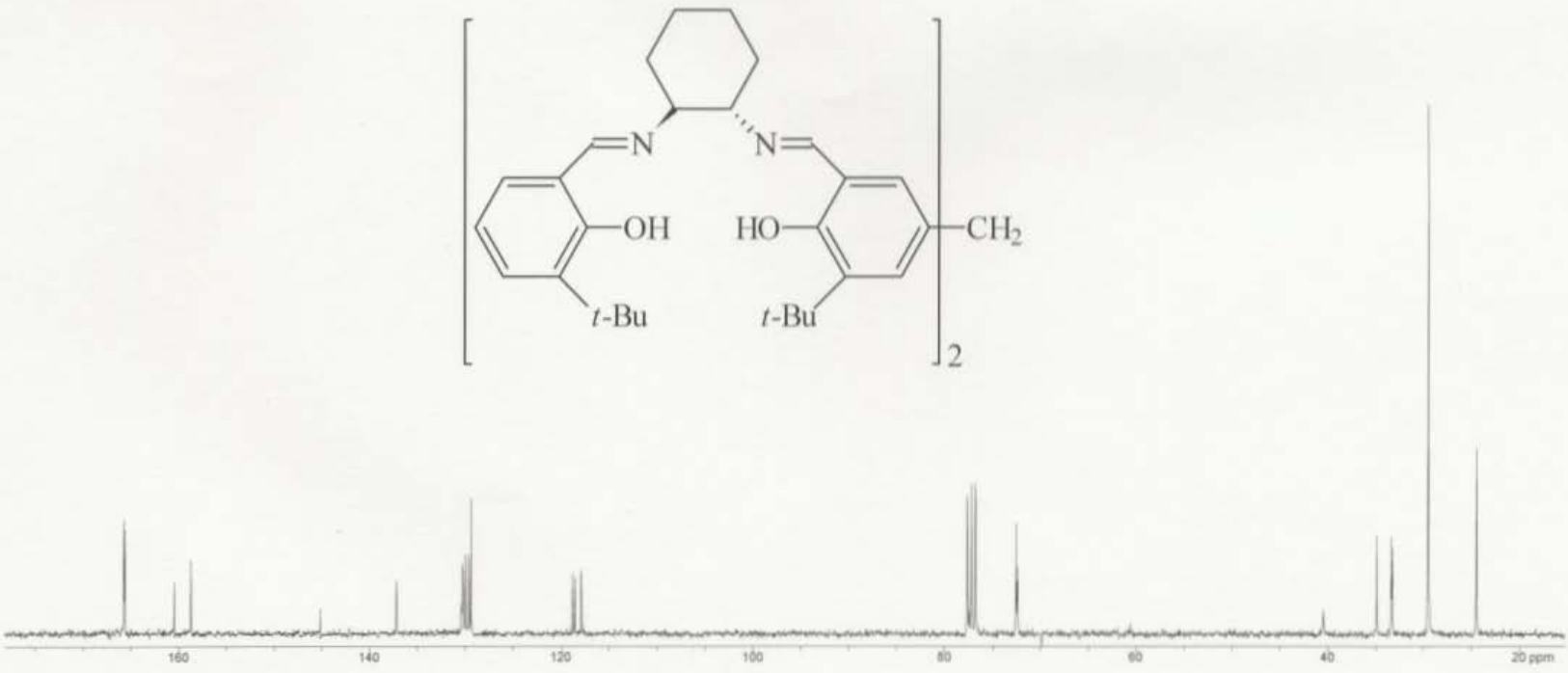

Figure A2.36 ^{13}C NMR spectrum of the linear salen dimer **20** in $CDCl_3$

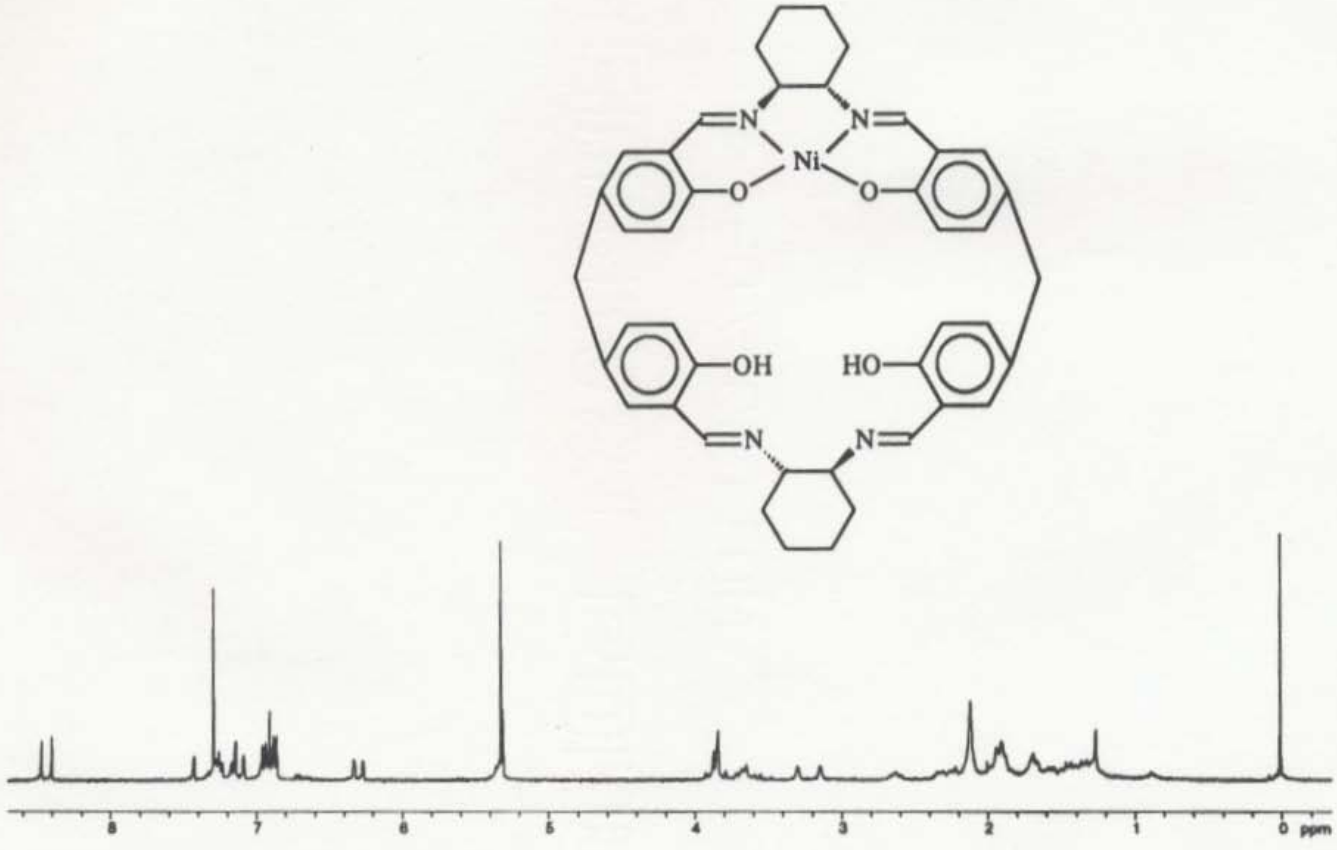

Figure A3.1 ^{1}H NMR spectrum of the momonuclear chiral complex **3.1** in $CDCl_3$ and CD_2Cl_2

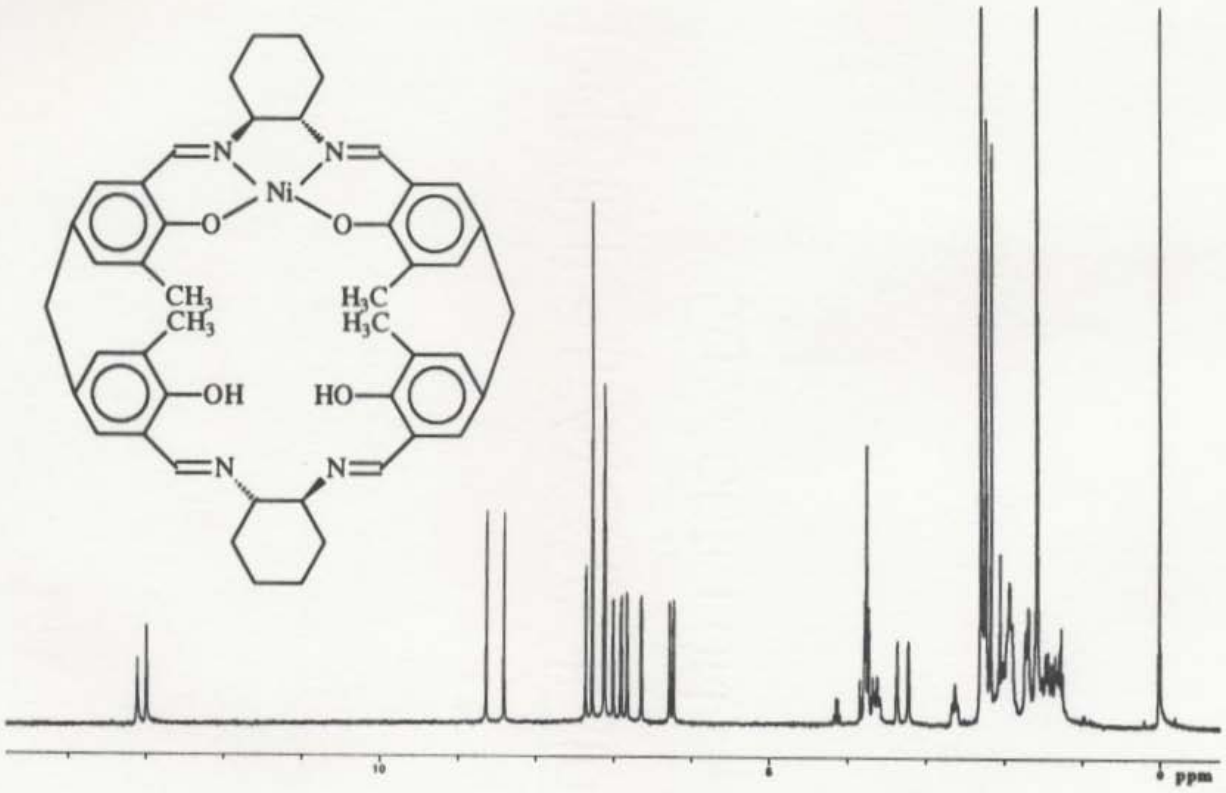

Figure A3.2-1 ^{1}H NMR spectrum of the mononuclear nickel complex **3.2** in $CDCl_3$

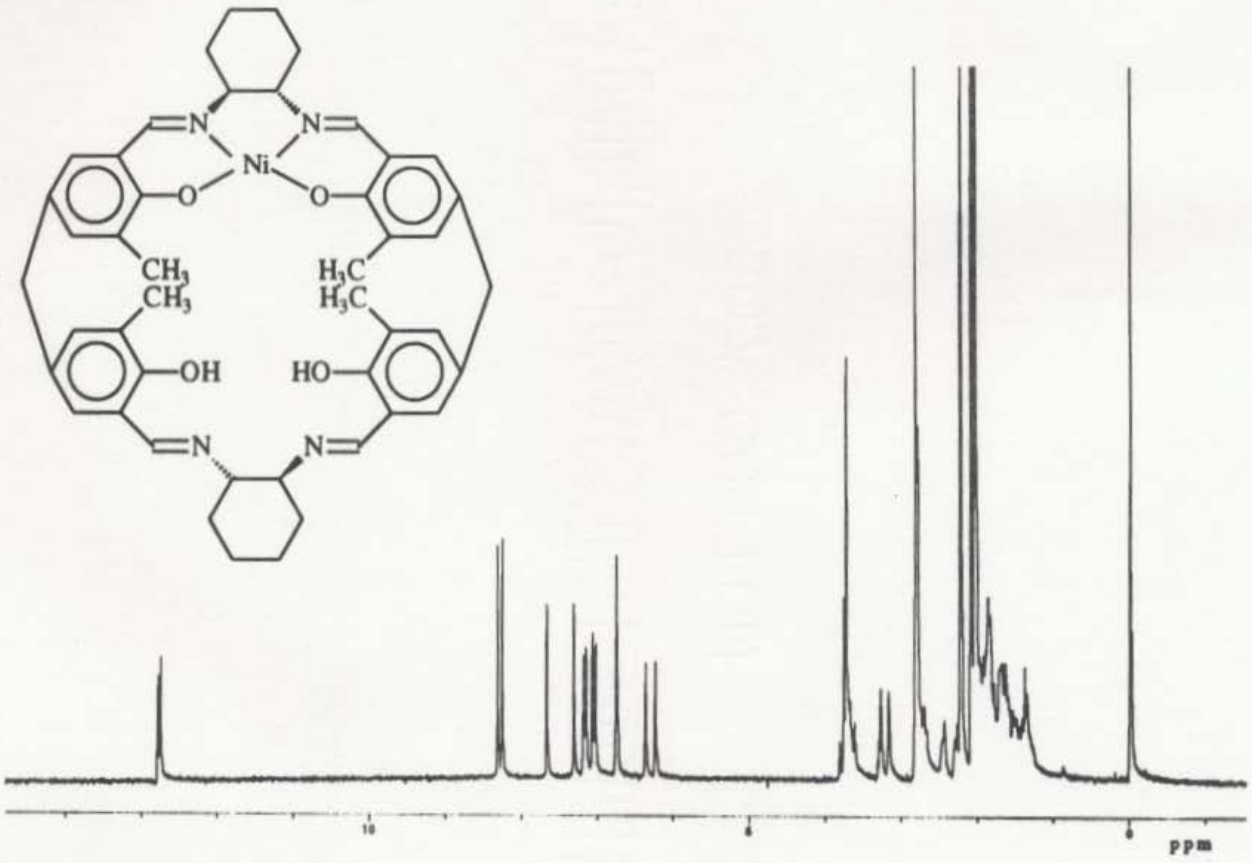

Figure A3.2-2 ^{1}H NMR spectrum of the mononuclear nickel complex **3.2** in CD_3COCD_3

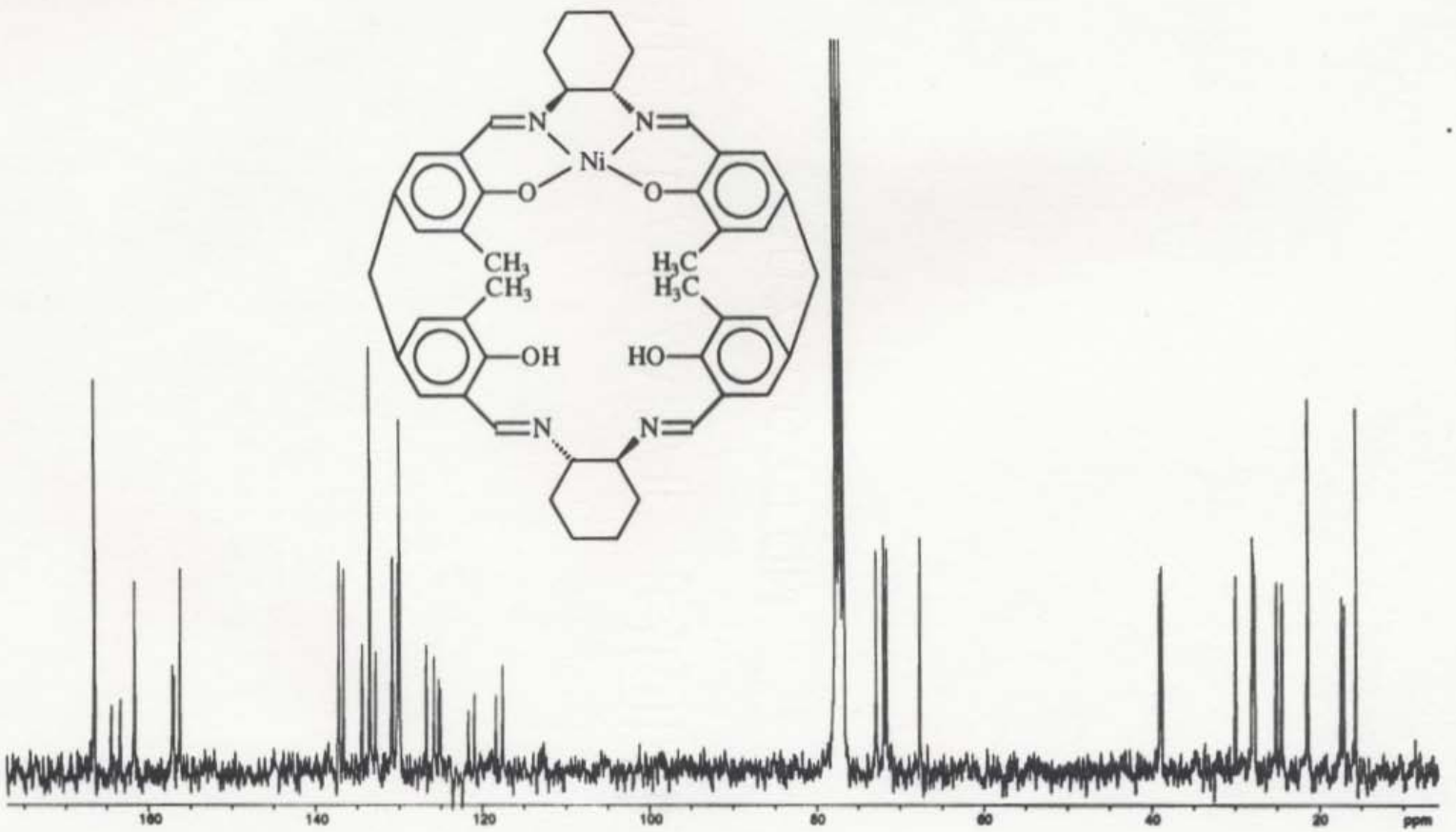

Figure A3.3 ^{13}C NMR spectrum of the mononuclear nickel complex **3.2** in $CDCl_3$

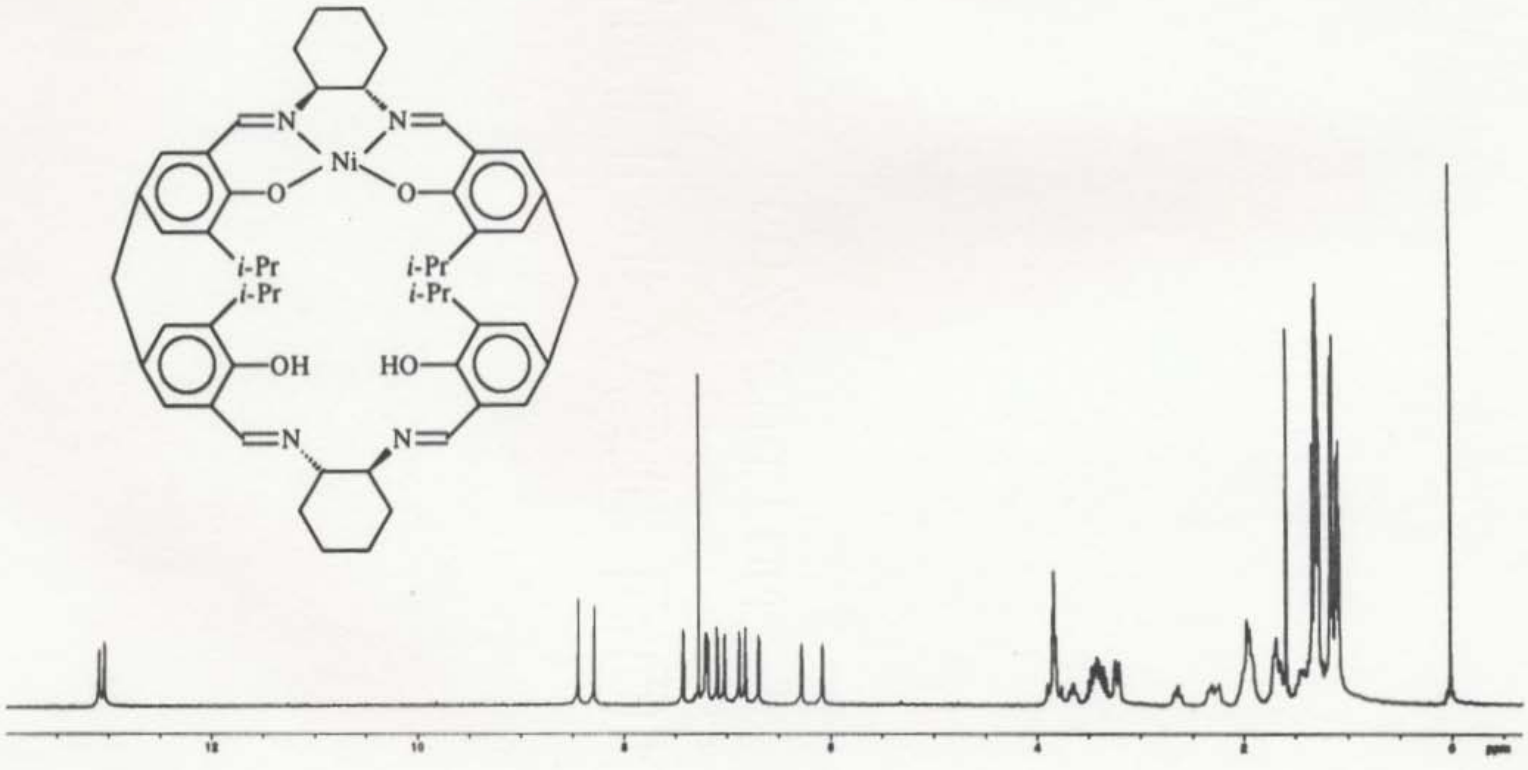

Figure A3.4 ^{1}H NMR spectrum of the mononuclear complex **3.3** in $CDCl_3$

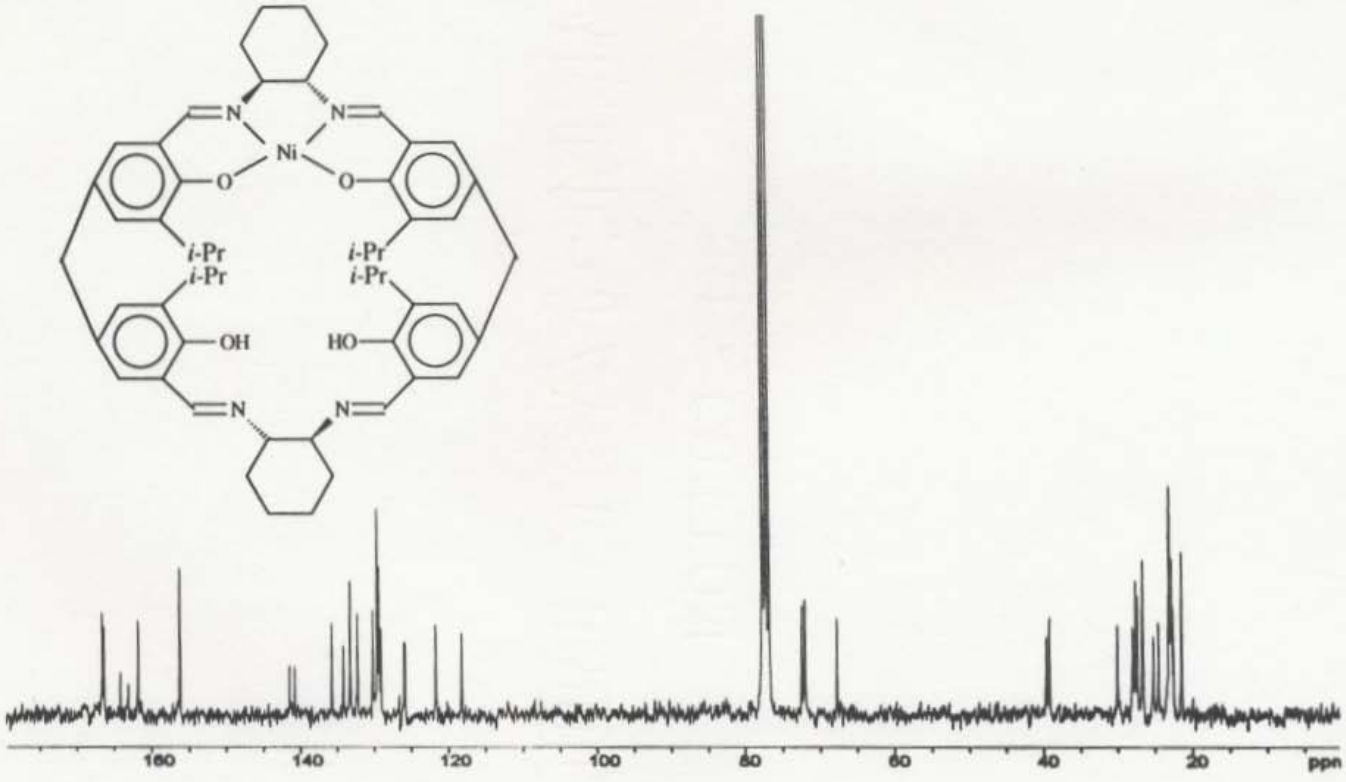

Figure A3.5 ^{13}C NMR spectrum of the mononuclear nickel complex **3.3** in $CDCl_3$

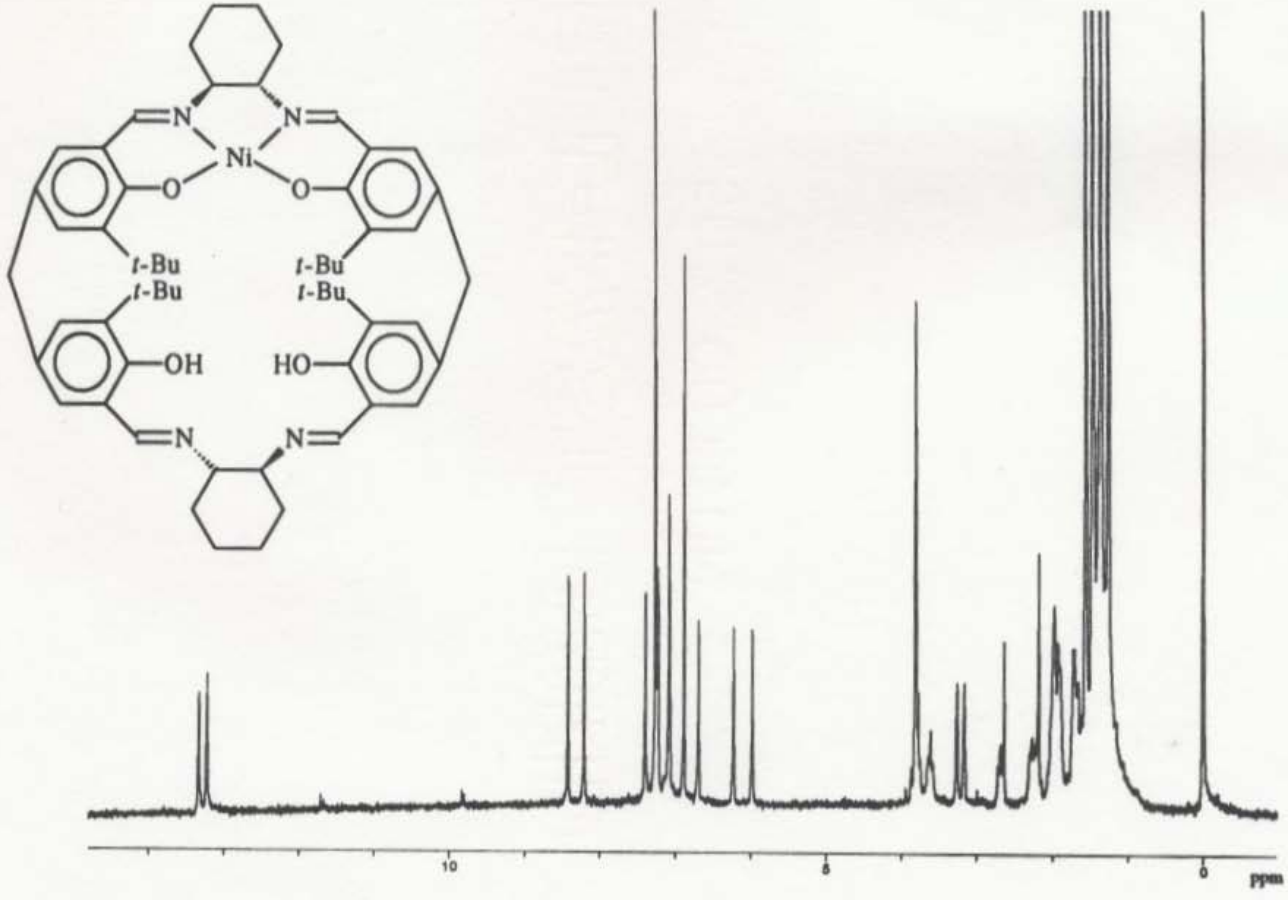

Figure A3.6-1 ^{1}H NMR spectrum of the mononuclear nickel complex **3.4** in $CDCl_3$

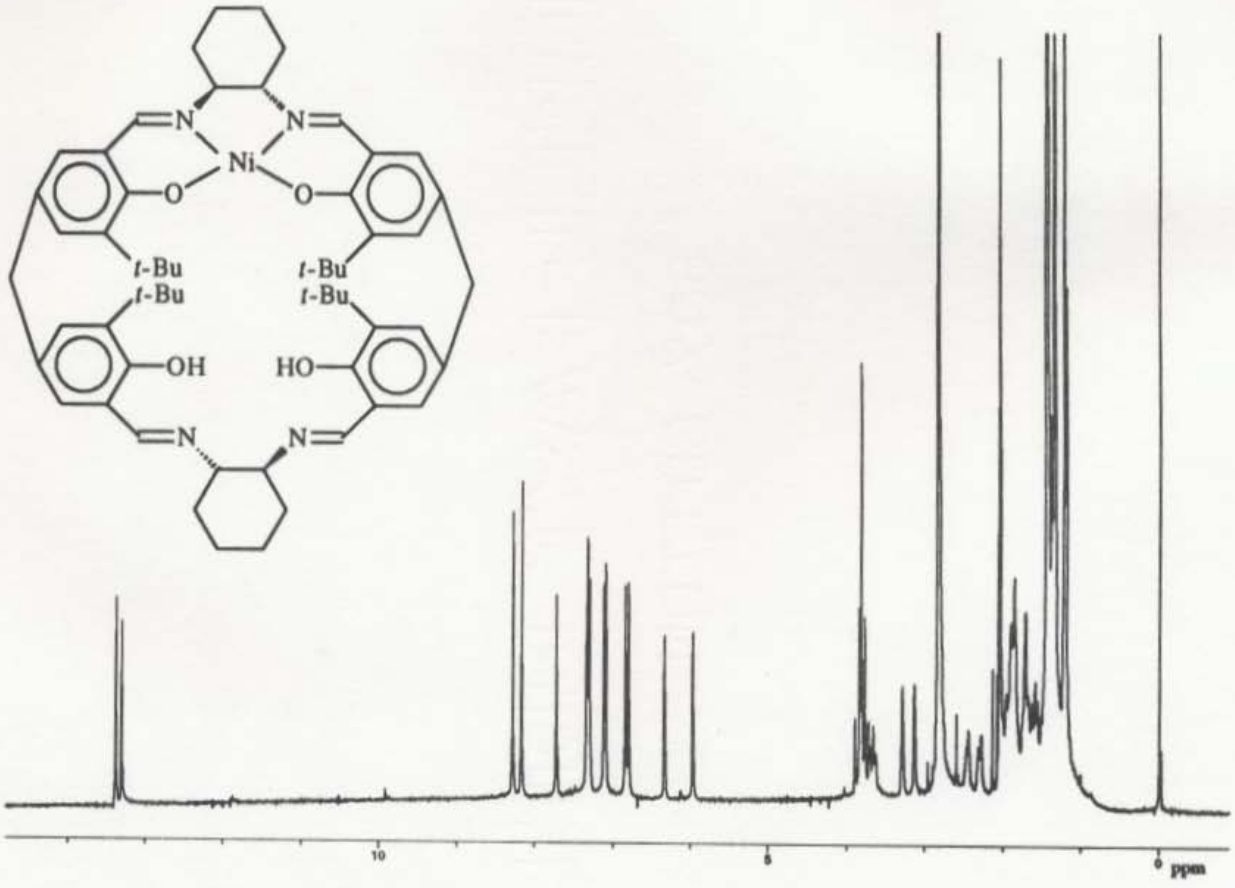

Figure A3.6-2 ^{1}H NMR spectrum of the mononuclear nickel complex **3.4** in CD_3COCD_3

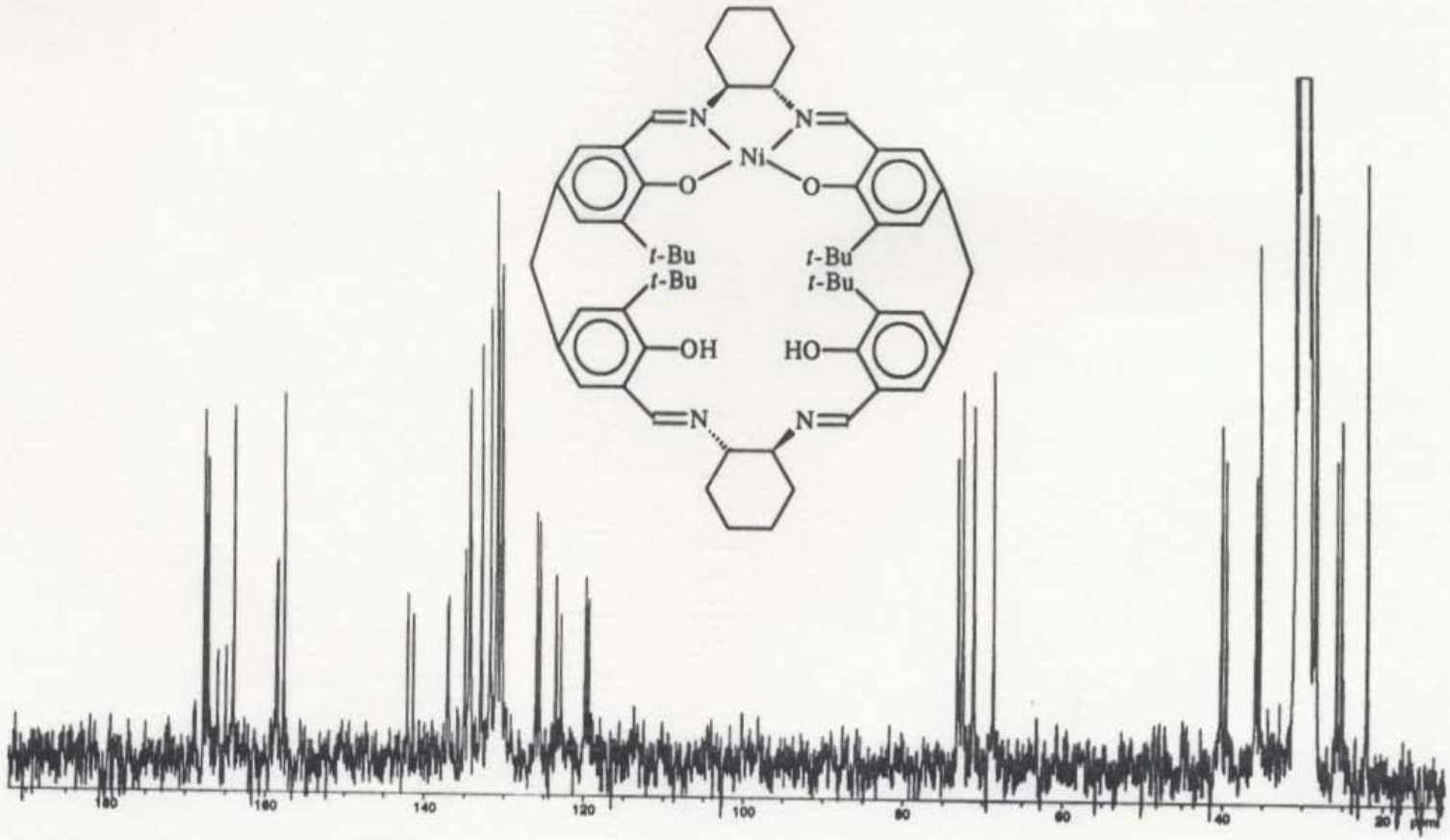

Figure A3.7 ^{13}C NMR of the mononuclear nickel complex **3.4** in CD_3COCD_3

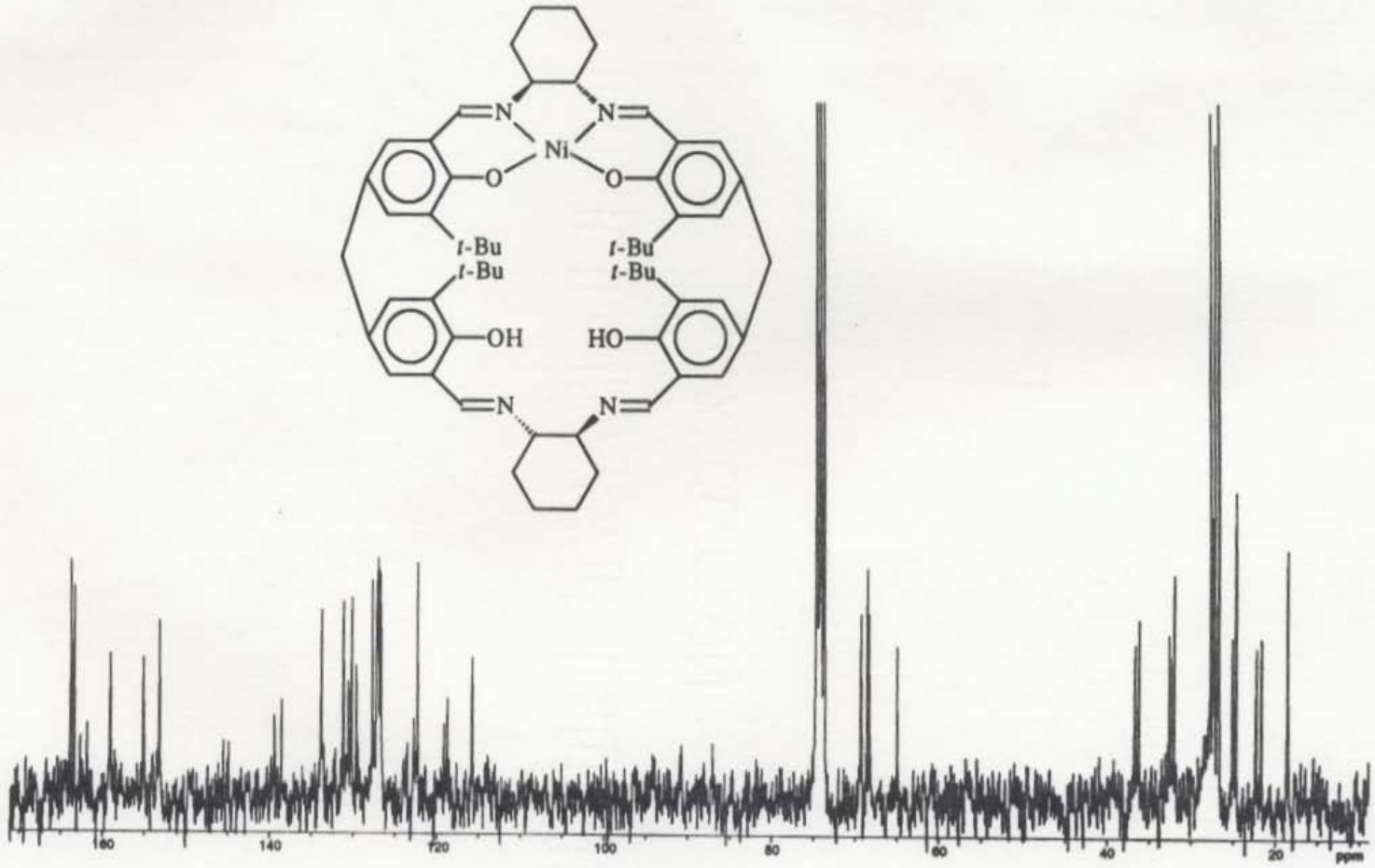

Figure A3.8 ^{13}C NMR of the mononuclear nickel complex **3.4** in $CDCl_3$

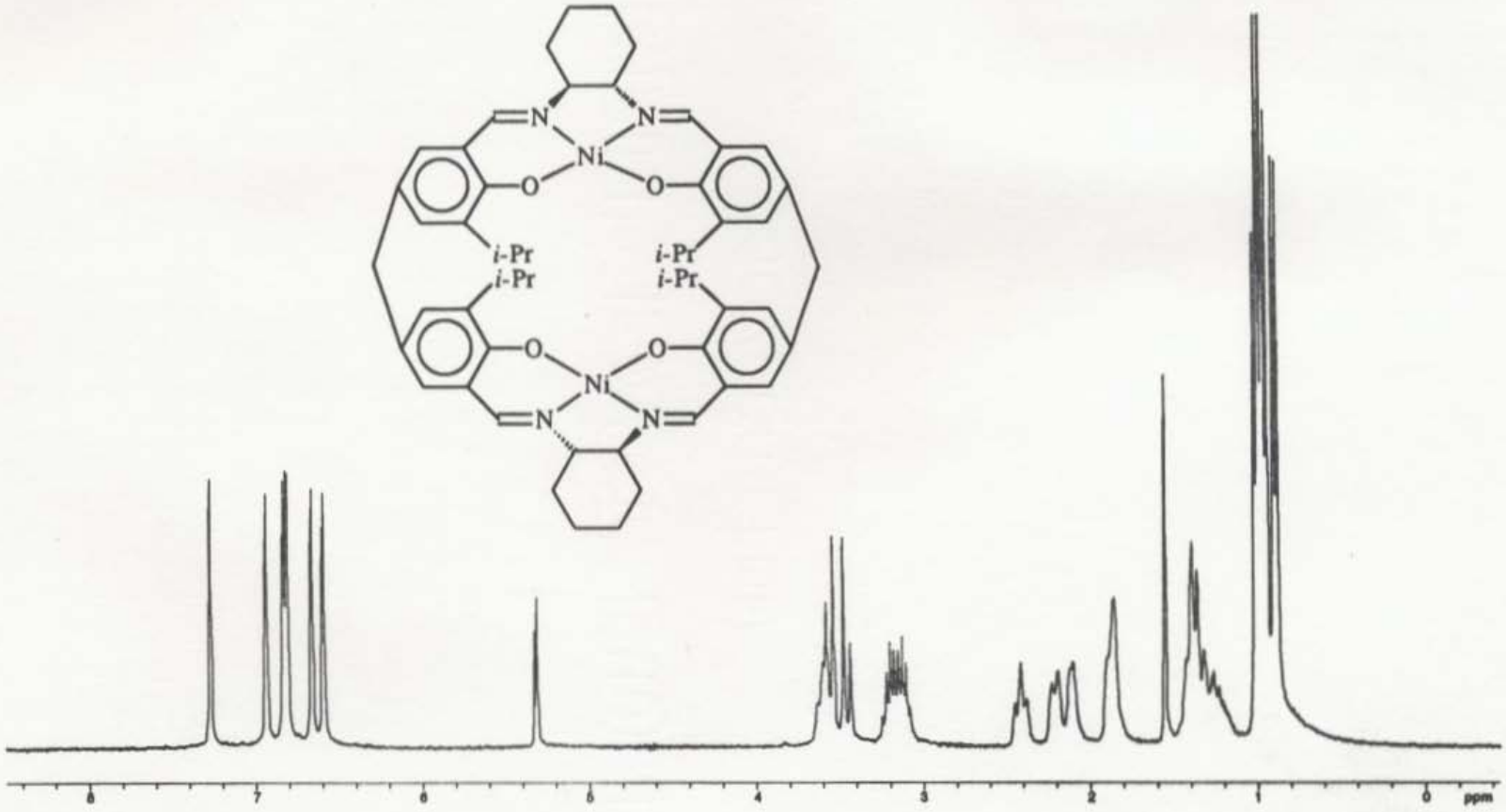

Figure A3.9 ^{1}H NMR spectrum of the (*R*,*R*)-binuclear nickel complex **3.7** in CD_2Cl_2

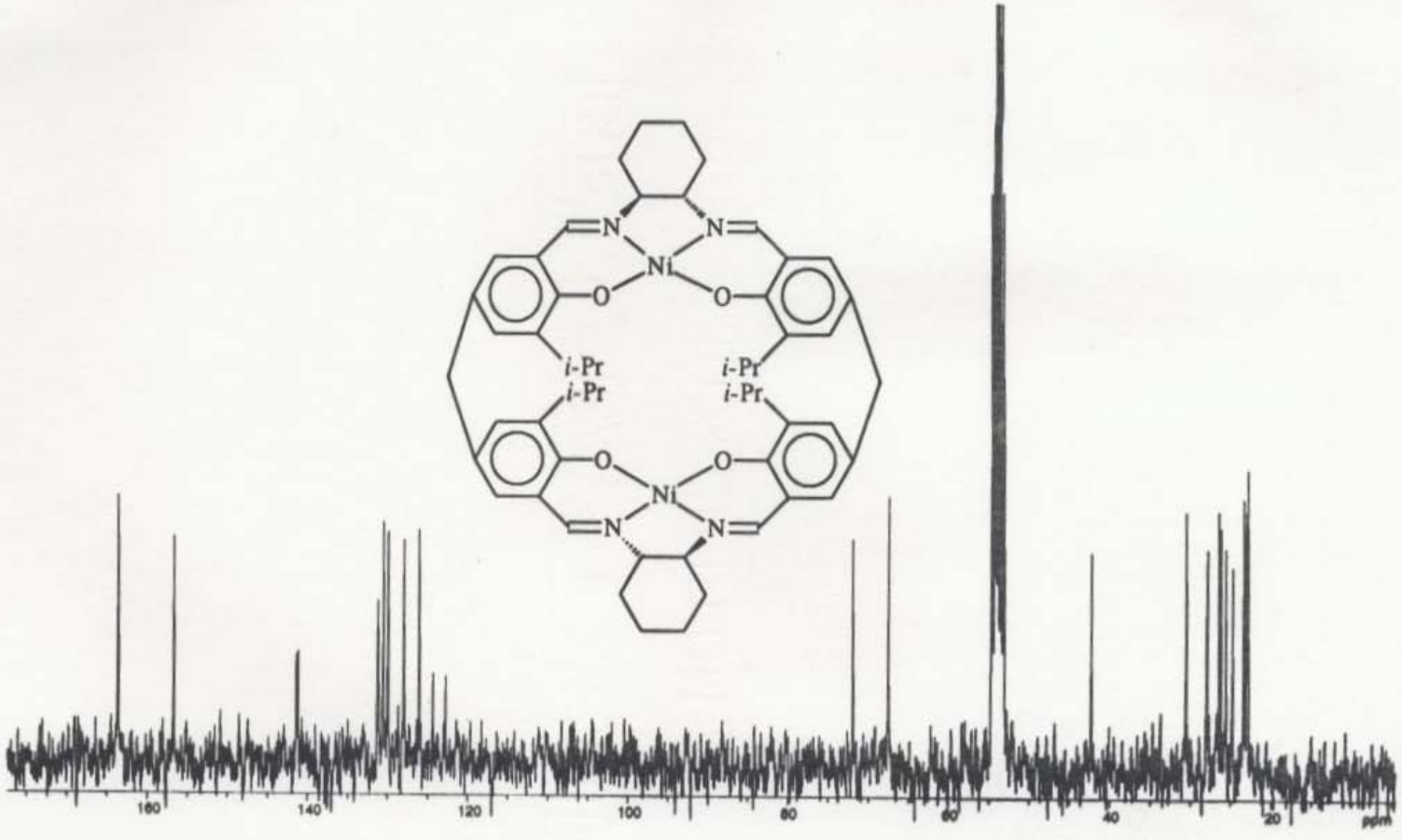

Figure A3.10 ^{13}C NMR of the binuclear nickel complex **3.7** in CD_2Cl_2

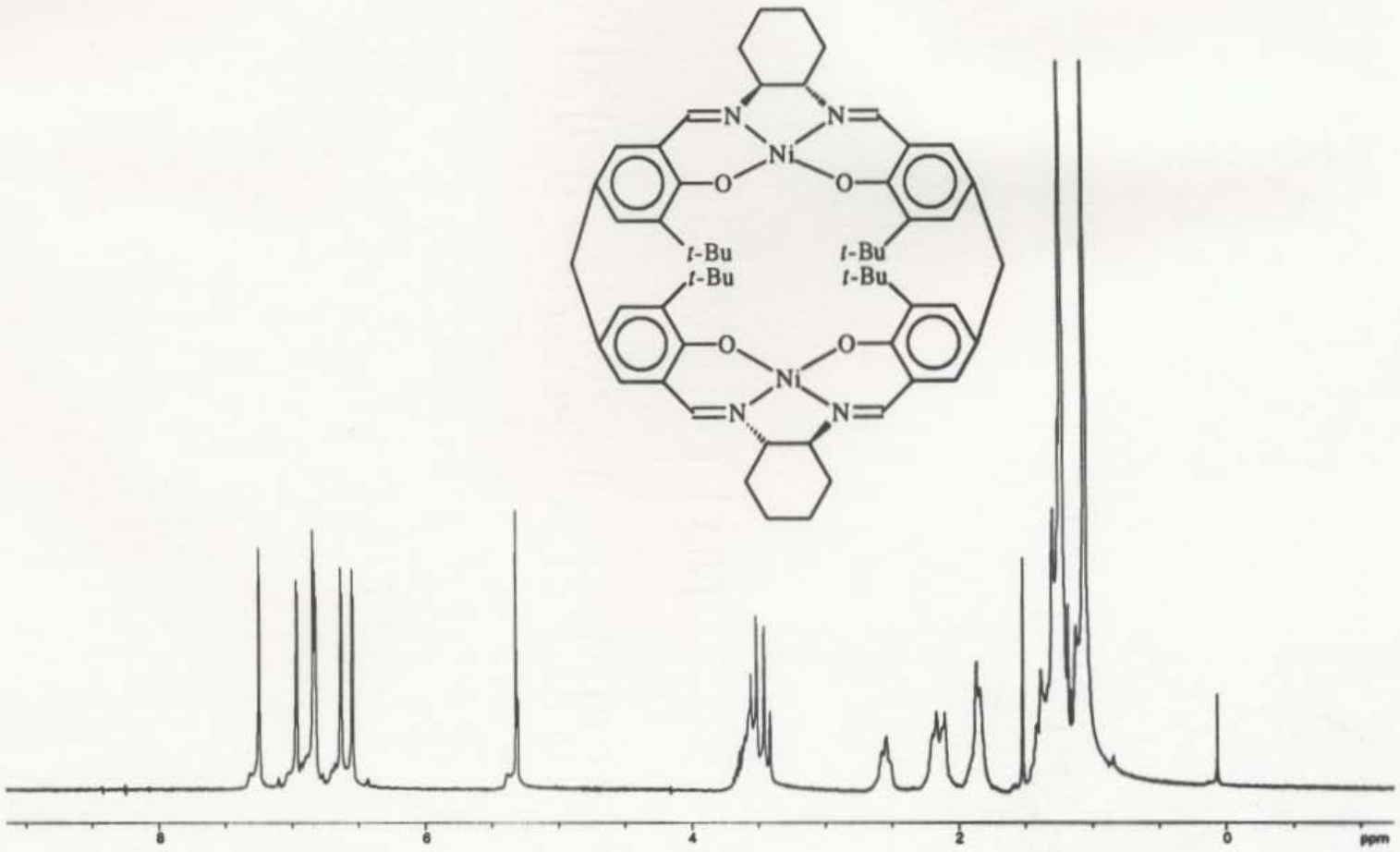

Figure A3.11 ^{1}H NMR spectrum of the binuclear complex of (*R*,*R*)-**3.8** in CD_2Cl_2

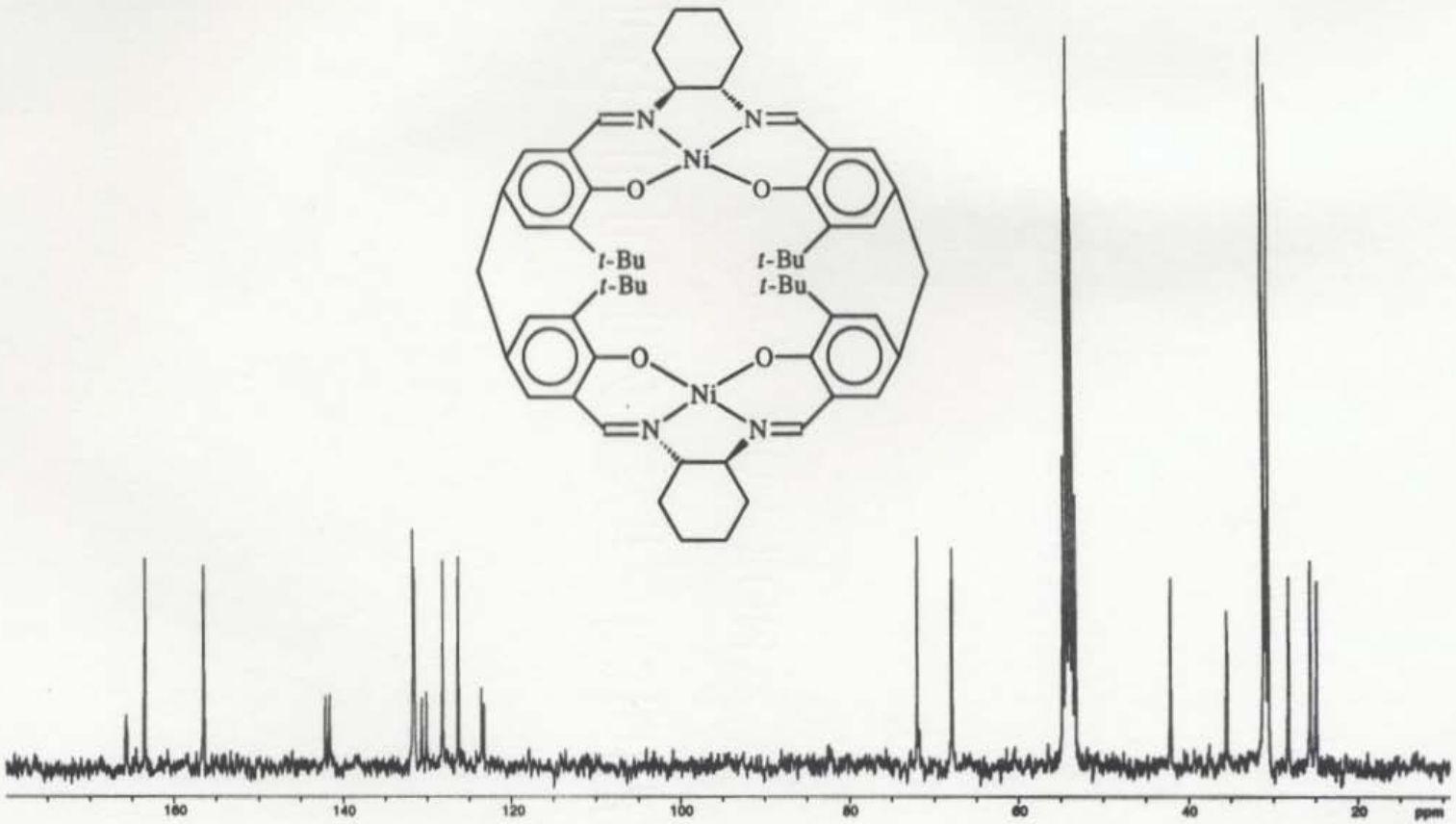

Figure A3.12 ^{13}C NMR spectrum of the binuclear complex of (*R,R*)-**3.8** in CD_2Cl_2

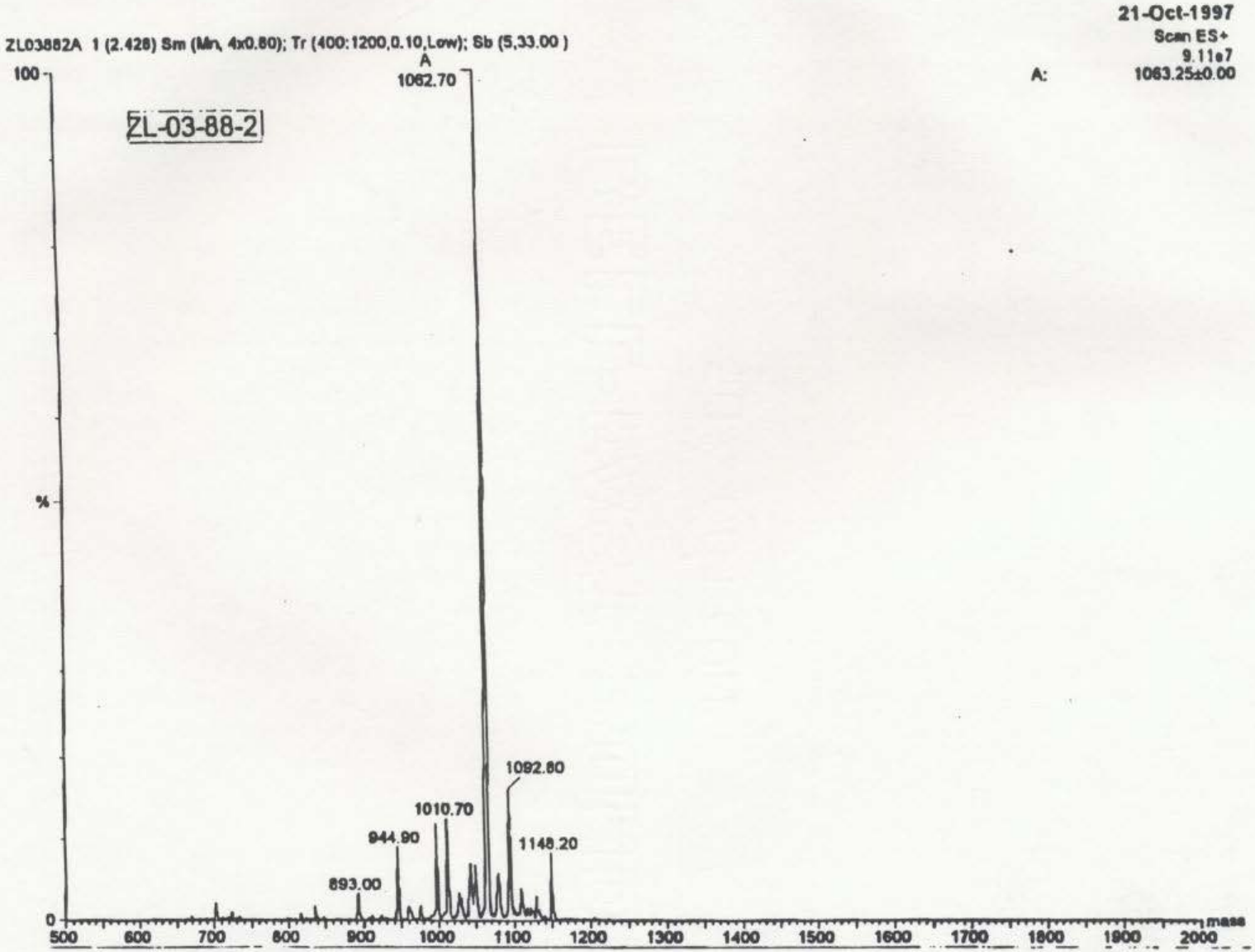

Figure A5.1 ESMS spectrum of the bis-manganese calixsalen complex **5d**

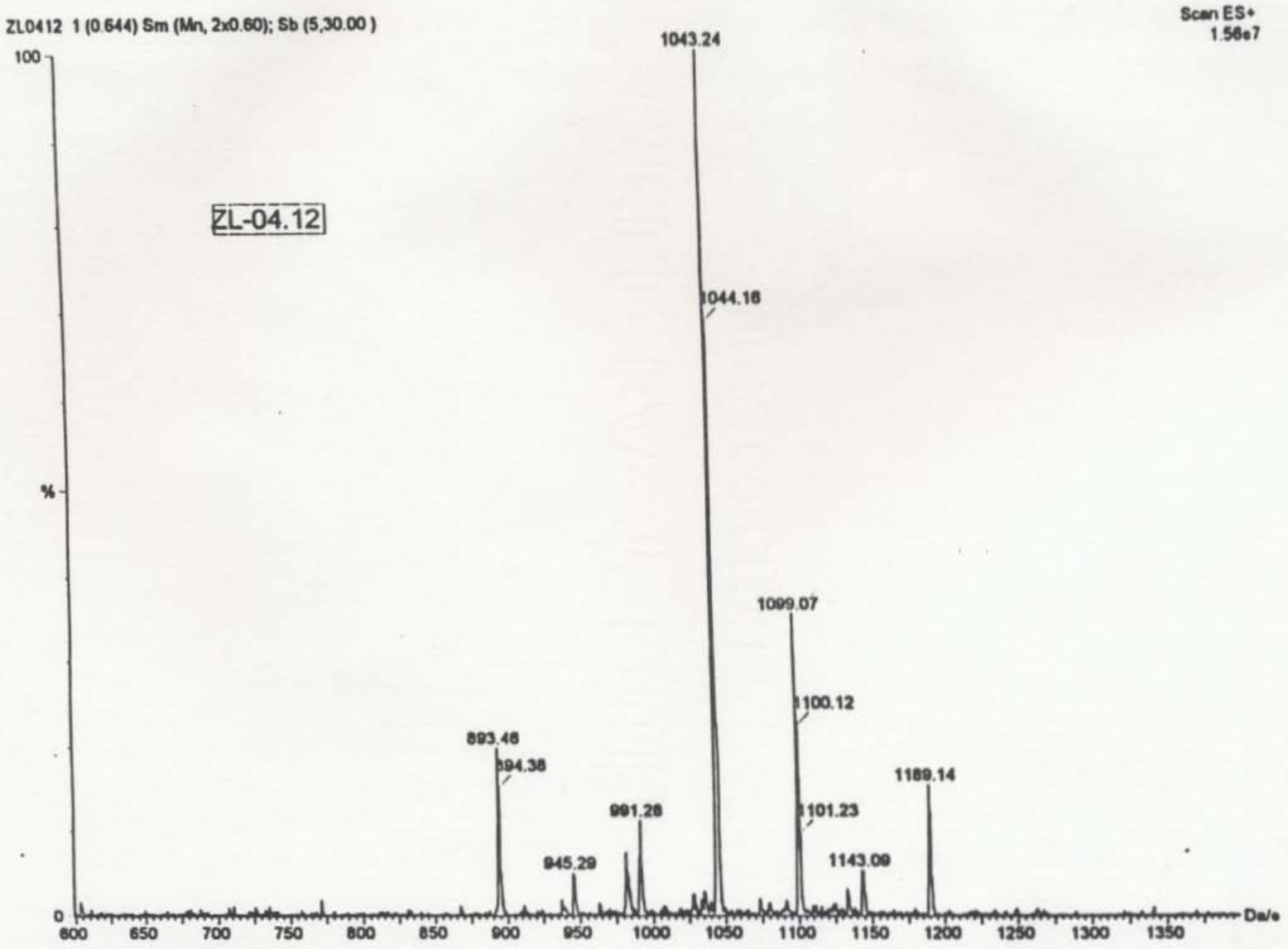

Figure A5.2 ESMS spectrum of the bis-manganese calixsalen complex **5e**

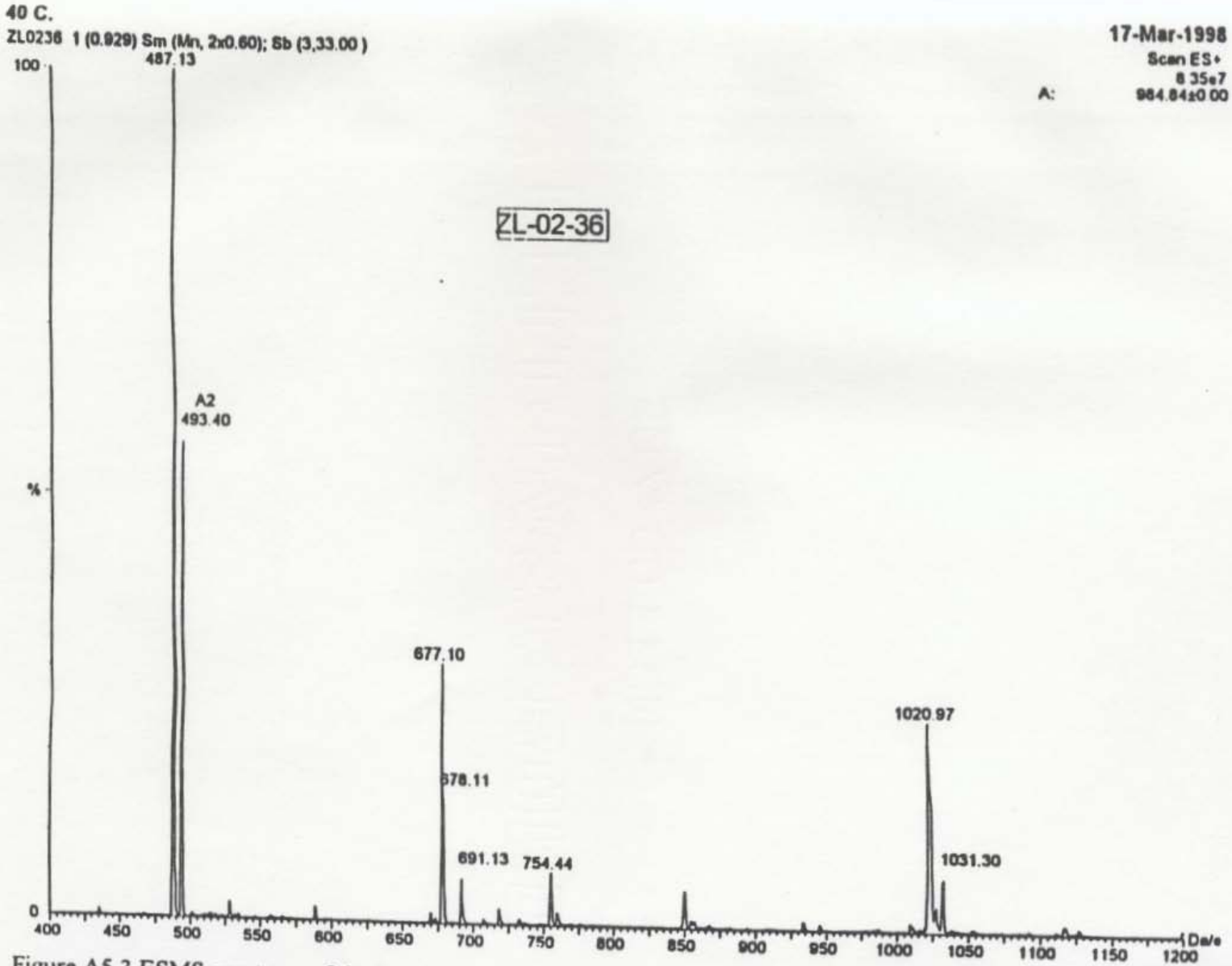

Figure A5.3 ESMS spectrum of the linear salen bis-manganese complex **5h**